DESIGN STUDIES AND MODEL TESTS OF THE STOWED TILT ROTOR CONCEPT

Volume VIII. Summary of Structural Design Criteria and Aerodynamic Prediction Techniques

Robin W. Sandford
Francis J. McHugh
Leon N. Delarm
Edward B. Schagrin
John P. Magee

FOREWORD

This report was prepared by The Boeing Company, Vertol Division, Philadelphia, Pennsylvania, for the Air Force Flight Dynamics Laboratory, Wright-Patterson Air Force Base, Ohio, under Phase II of Contract F33615-69-C-1577. The contract objective is to develop design criteria and aerodynamic prediction techniques for the folding tilt rotor concept through a program of model testing and analysis.

The contract was administered by the Air Force Flight Dynamics Laboratory with Mr. Daniel E. Fraga (FV) as Project Engineer.

This report covers the period from December 1970 to July 1971.

The reports published under this contract for Design Studies and Model Tests of the Stowed Tilt Rotor Concept are:

Volume I	Parametric Design Studies
Volume II	Component Design Studies
Volume III	Performance Data for Parametric Study
Volume IV	Wind Tunnel Test of the Conversion Process of a Folding Tilt Rotor Aircraft Using a Semi-Span Unpowered Model
Volume V	Wind Tunnel Test of a Powered Tilt Rotor Performance Model
Volume VI	Wind Tunnel Test of a Powered Tilt Rotor Dynamic Model on a Simulated Free Flight Suspension System
Volume VII	Wind Tunnel Test of the Dynamics and Aerodynamics of Rotor Spinup, Stopping and Folding on a Semi-Span Folding Tilt Rotor Model
Volume VIII	Summary of Structural Design Criteria and Aerodynamic Prediction Techniques
Volume IX	Value Engineering Report

This report has been reviewed and is approved.

Ernest J. Cross, Jr.
Lt. Colonel, USAF
Chief, Prototype Division

ABSTRACT

This report presents a summary of the technical data from four wind tunnel tests on tilt and stowed rotor performance and fully dynamic models. Blade loads, dynamic stability, performance, rotor/wing interactions and stability and control data are presented. The impact of the tests on stowed rotor aircraft design are discussed and recommendations for further technical and design work are provided.

TABLE OF CONTENTS

LIST OF FIGURES

LIST OF TABLES

LIST OF SYMBOLS

SYMBOL		UNITS
A	Rotor Disc Area πR^2	FT^2
A/C	Aircraft	-
b	Wing span - number of rotor blades	FT
c	Wing chord - rotor blade chord	FT
C_D	Airframe drag - $\frac{D}{qS}$	-
C_{D_D}	Hover download drag coefficient (See Page 105)	-
C_L	Aircraft lift coefficient $\frac{L}{qS}$	-
C_{L_s}	Aircraft slipstream lift coefficient $\frac{L}{q_s S}$	-
C_{L_T}	Tail lift coefficient	-
C_M	Rotor hub moment/$\rho AV_T^2 R$	-
C_N	Rotor normal force coefficient $\frac{NF}{\rho AV_T^2}$	-
C_p	Rotor power coefficient $\frac{HPx\ 550}{\rho AV_T^3} = \frac{Q}{\rho AV_T^2 R}$	-
$C_{p_{A/C}}$	Aircraft power coefficient $\frac{HP}{2\rho AV_T^3}$	-
ΔC_{P_M}	Aircraft pitch control moment (about wing quarter chord) $\frac{PM}{qSc}$	-
C_{SF}	Rotor side force coefficient $\frac{SF}{\rho AV_T^2}$	-
C_{PM}	Rotor pitching moment coefficient $\frac{PM}{\rho AV_T^2 R}$	-

LIST OF SYMBOLS

SYMBOL		UNITS
C_{PM_s}	Aircraft slipstream pitching moment coefficient $\frac{PM}{q_s S}$	-
$C_{PM_{c/4}}$	Aircraft pitching moment coefficient about wing quarter chord $\frac{PM}{qSc}$	-
i_N	Nacelle incidence	DEG
i_t	Horizontal tail incidence	DEG
IGE	In ground effect	-
L	Lift	LB
n	Aircraft maximum gust load factor at V_H	LB
NF	Normal force	LB
PM	Pitching moment	FT-LB
q	Dynamic pressure $1/2\rho V^2$	LB/FT^2
Q	Rotor torque	FT-LB
q_s	Slipstream dynamic pressure qxT/A	LB/FT^2
R	Rotor radius	FT
RM	Rolling moment	FT-LB
r	Radial location to a blade station	IN
SF	Side force	LB
S	Wing area	FT^2
T	Rotor thrust	LB
V_o	Ideal induced velocity from rotor	FT/SEC

LIST OF SYMBOLS

SYMBOL		UNITS
V	Freestream velocity	FT/SEC
V_L	Aircraft limit speed	KNOTS
V_G	Aircraft gust calculation speed $=\sqrt{n}V_S$	KNOTS
V_H	Aircraft maximum level flight speed	KNOTS
V_T	Rotor tip speed	FT/SEC
V_S	Aircraft stall speed	KNOTS
X	Aircraft propulsive force	LB
YM	Yawing moment	FT-LB
α	Fuselage angle of attack	DEG
γ	Blade Locke number	DEG
δ_F	Trailing edge flap deflection	DEG
δ_u	Umbrella deflection	DEG
ξ	Lag angle	DEG
$\theta_{.75}$	Rotor blade collective pitch at the three quarter radius	DEG
μ	Advance ratio V/V_T	-
ψ	Fuselage yaw angle (rotor azimuth angle)	DEG
ρ	Density of air	$LB/SEC^2/FT$
σ	Rotor solidity $\frac{bCR}{\pi R^2}$	-
ϕ	Roll angle	DEG
Ω	Rotor angular velocity	RAD/SEC

LIST OF SYMBOLS

SYMBOL		UNIT
ω_n	nth coupled blade natural frequency where n = 1, 2, 3------n	RAD/SEC
ω_β	First mode, flapwise blade natural frequency	RAD/SEC
ω_L	First mode, inplane blade natural frequency	RAD/SEC

1.0 INTRODUCTION

Recent design studies have indicated that the stoppable rotor aircraft concept offers a very effective solution for satisfying V/STOL missions requiring a combination of relatively low downwash characteristics, good hover efficiency, and relatively high cruise speeds and cruise efficiency. In particular, the stowed-tilt-rotor stoppable rotor concept offers great potential for three missions: 1) high-speed long-range rescue, 2) capsule recovery, and 3) VTOL medium transport.

The Boeing Company, under USAF Flight Dynamics Laboratory Contract F33615-69-C-1577, has conducted a two phase program of parametric design, analysis, and wind-tunnel testing to establish design criteria for the stowed-tilt-rotor stoppable-rotor concept.

Parametric Design Studies

Phase I covered parametric design studies to provide information on the size and configuration of aircraft required to fulfill three basic mission requirements and two multimission requirements. The missions and the design aircraft are:

Mission	Aircraft
o High-speed long-range rescue	Design Point I
o Capsule recovery	Design Point II
o V/STOL medium transport	Design Point IV
o High-speed long-range rescue and capsule recovery (multimission)	Design Point III
o High-speed long-range rescue, capsule recovery, and V/STOL medium transport (multimission)	Design Point V

The intent of the analysis was to determine the degree of compatibility between aircraft designed to the three missions, and the compromise necessary to combine these mission capabilities in substantially common airframes. As a minimum, this commonality was extended to the lift/propulsion system comprising the wing, engines, drive system, and rotors. The relative numbers of production aircraft which might be required for each mission was considered in determining the degree of commonality. The technology level used in these studies is appropriate to a 1976 IOC date time frame.

The results from the above studies are presented in Reference 1.1 with additional details in Reference 1.3.

Because the multimission aircraft designed to accomplish all three basic roles turned out to weigh more than 100,000 pounds, a further study was made of a compromise aircraft based on the Design Point I rescue aircraft. This design point lift/propulsion system was combined with a transport type fuselage based on a CH-47 helicopter box size widened to 96 inches at the floor line to accommodate 463L system pallets. This aircraft is capable of carrying the full 88 x 108 inch pallet and air-dropping the 88 x 54 inch half-pallet. Pallet loading is restricted to 72 inches in height. Although this aircraft does not have the unrestricted 463L system pallet loading capability of the Design Point IV transport aircraft (i.e., maximum pallet height for air dropping of full pallets), it can nevertheless meet most of the transport mission requirements.

It was, therefore, decided that the baseline aircraft would be the Design Point I rescue aircraft, with a slightly increased span to permit the alternate installation of a wider transport fuselage. The baseline is, therefore, in reality two aircraft with common lift/propulsion systems.

This baseline aircraft approach is illustrated in Figure 1.1. A basic lift propulsion system is used with two different fuselages: one to fulfill the complete rescue mission (See Figure 1.2 for artist's concept) and the other to provide an aircraft which meets most of the mission requirements for the medium transport role.

Component Design Studies

Preliminary design studies of the critical or unique components of the selected baseline aircraft were carried out during the latter portion of the Phase I Study and are reported in Reference 1.2. These included the rotor blade, hub, and blade fold mechanism, drive system, rotor nacelle and tilting mechanism and the wing. Unique design features of these critical components are:

Rotor Blade - hingeless, soft inplane with an inplane frequency less than 1/rev, fiberglass construction.

Hub - flatwise folding along nacelle to minimize airplane drag and nacelle complexity.

Drive System- cross-shafting to minimize impact of engine out flight.

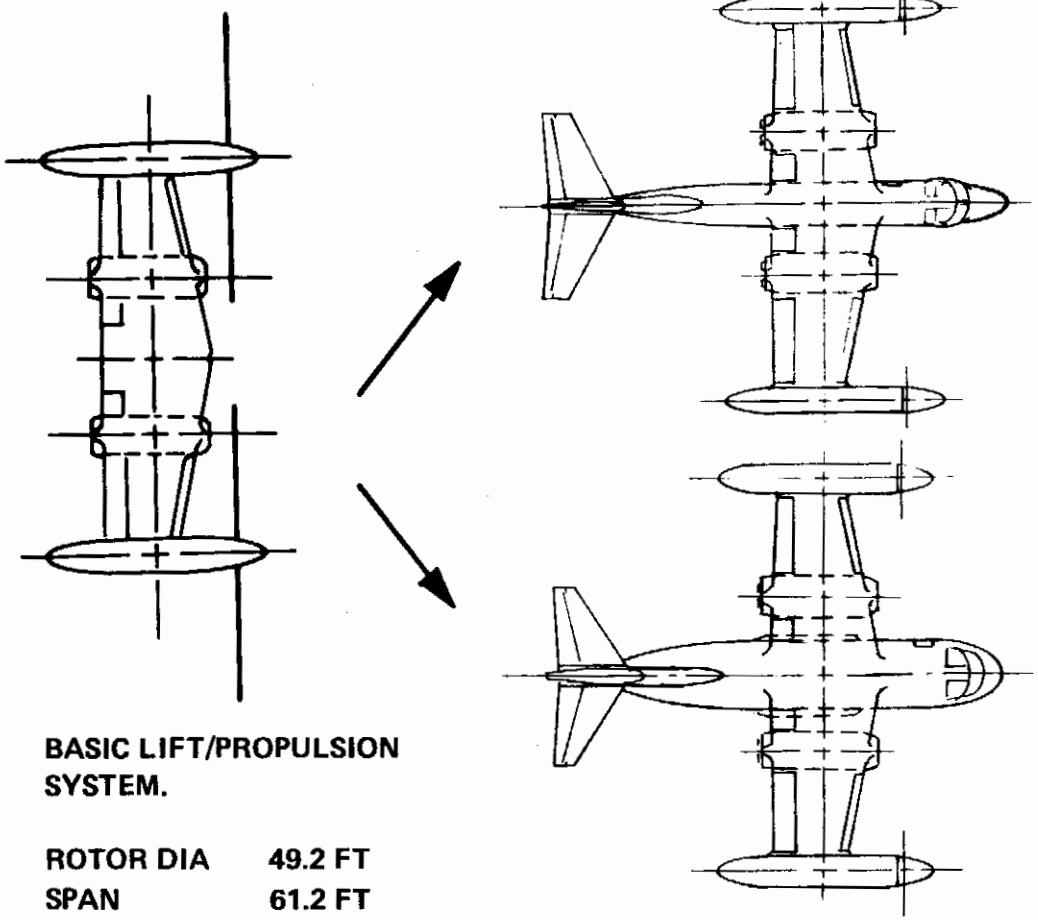

BASIC LIFT/PROPULSION SYSTEM.

ROTOR DIA	49.2 FT
SPAN	61.2 FT
POWER	4 x 4350 SHP.

RESCUE VERSION

MEETS ALL RESCUE MISSION REQUIREMENTS

CRUISE SPEED 400 KTS	AT	20,000 FT
DESIGN GROSS WEIGHT		67000 LB
MIDPOINT GROSS WEIGHT		57000 LB
MIDPOINT DISC LOADING		I5 PSF

TRANSPORT VERSION

TAKEOFF AT D.G.W. 67000 LB
5 TONS PAYLOAD OVER 260 N.M. RADIUS
AT 350 KTS, 100 N.M. INBOUND AND
OUTBOUND AT 3000 FT.

TAKEOFF AT MAX. TAKEOFF G.W. 80,000 LB
8½ TONS PAYLOAD OVER 375 N.M. RADIUS.
AT 350 KTS, 150 N.M. INBOUND AND
OUTBOUND AT 3000 FT.

MAX SPEED AT N.R.P. 380 KTS AT 2000 FT
CARGO BOX: 7.75 x 7.1 FT x 30 FT

FIGURE 1.1 SUGGESTED BASELINE APPROACH

FIGURE 1.2 STOWED TILT ROTOR RESCUE AIRCRAFT

The geometry, mass distribution, and stiffness characteristics of the aircraft and its components, as well as identification of areas that require research provided the planning for the Phase II program of wind tunnel testing and analysis.

Wind Tunnel Testing and Analysis

The test and analysis program of Phase II consisted of a redundant array of models, each providing somewhat different aeroelastic modeling. The objective was to prepare verified methodology for ensuring that the stowed rotor aircraft is stable and controllable through all phases of operation, i.e., takeoff, hover, transition to forward flight, conversion, and the reverse sequence through landing.

The program consisted of tests on four separate models. The models are designed to provide data demonstrating the validity of methodology and solutions to the dynamics, blade stress, and flying qualities problems indicated by Phase I studies and initial company sponsored Wind Tunnel tests.

Test Program I used the 1/16-scale folding tilt rotor semispan conversion model (Figure 1.3) with dynamically representative blades and was used to measure the dynamics of the start, stop and windmilling performance. This test was performed in the Princeton Forrestal Laboratories Wind Tunnel and results are presented in Reference 1.4.

Test Program II used the Boeing 1/10-scale powered performance wind tunnel model (Figure 1.4) to demonstrate the aerodynamics of the aircraft and its control system mixing and phasing from hover through transition and in tilt rotor cruise flight. Data were obtained for static stability; longitudinal, lateral, and directional stability derivatives; destabilizing effects of prop/rotors, and the force polars of the aircraft through transition. This test was performed in the Boeing-Vertol 20 x 20 foot V/STOL wind tunnel and results are presented in Reference 1.5.

Test Program III used the Boeing 1/9-scale semispan, non-powered conversion model (Figure 1.5), with full dynamic similarity to Model 213 to measure the dynamics and aerodynamics of conversion including spin-up, spin-down, stopping, folding and deployment. This test was performed in the Boeing-Vertol 20 x 20 foot V/STOL wind tunnel and results are presented in Reference 1.6.

Test Program IV used the Boeing 1/10-scale dynamic full-span powered model (Figure 1.6) to measure steady state and dynamic blade and wing loads throughout the flight envelope. This model incorporated shakers for exciting the aeroelastic modes to measure model damping response. This test was performed in the Boeing-Vertol 20 x 20 foot wind tunnel and results are presented in Reference 1.7.

From these four tests, programs covering all of the aspects of the non-fixed-wing aircraft flight conditions, an accumulation of loads, aerodynamic and dynamic information was made available for identification of key problems to use in developing programs for solution.

This summary report consolidates the data from the four test programs and the preliminary design work in order to define the state-of-the-art and to recommend the next steps for Stowed Rotor Aircraft Development. The report is divided into three major sections, Structural Design Criteria, Section 3 which includes structural and dynamic considerations of the design, Aerodynamic Prediction Techniques, Section 4, which includes performance and Section 5 which includes stability and control. The impact of the tests on the design and recommendations for further work are also presented.

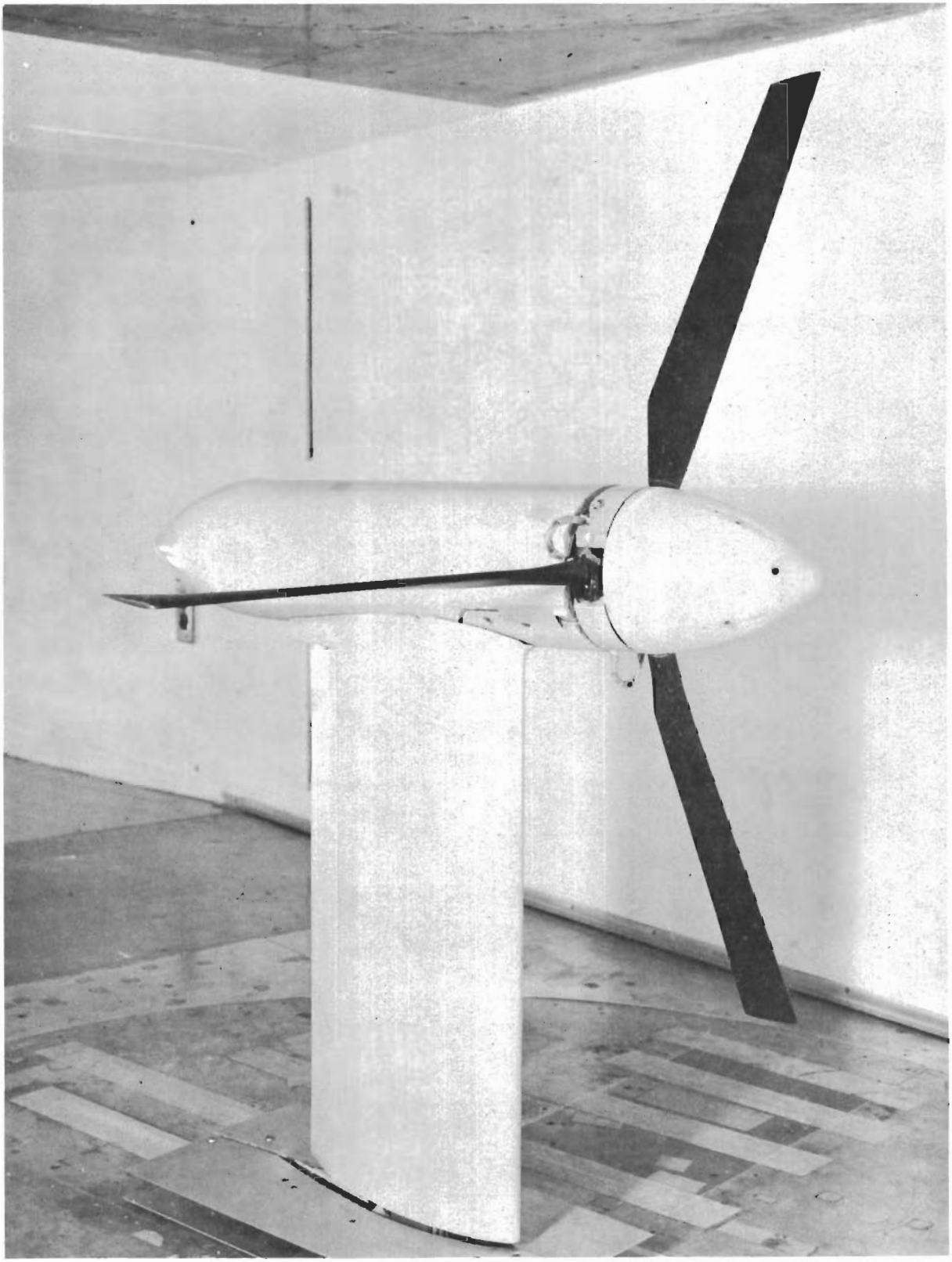

FIGURE 1.3 1/16 SCALE UNPOWERED STOWED ROTOR SPINUP AND FEATHER MODEL

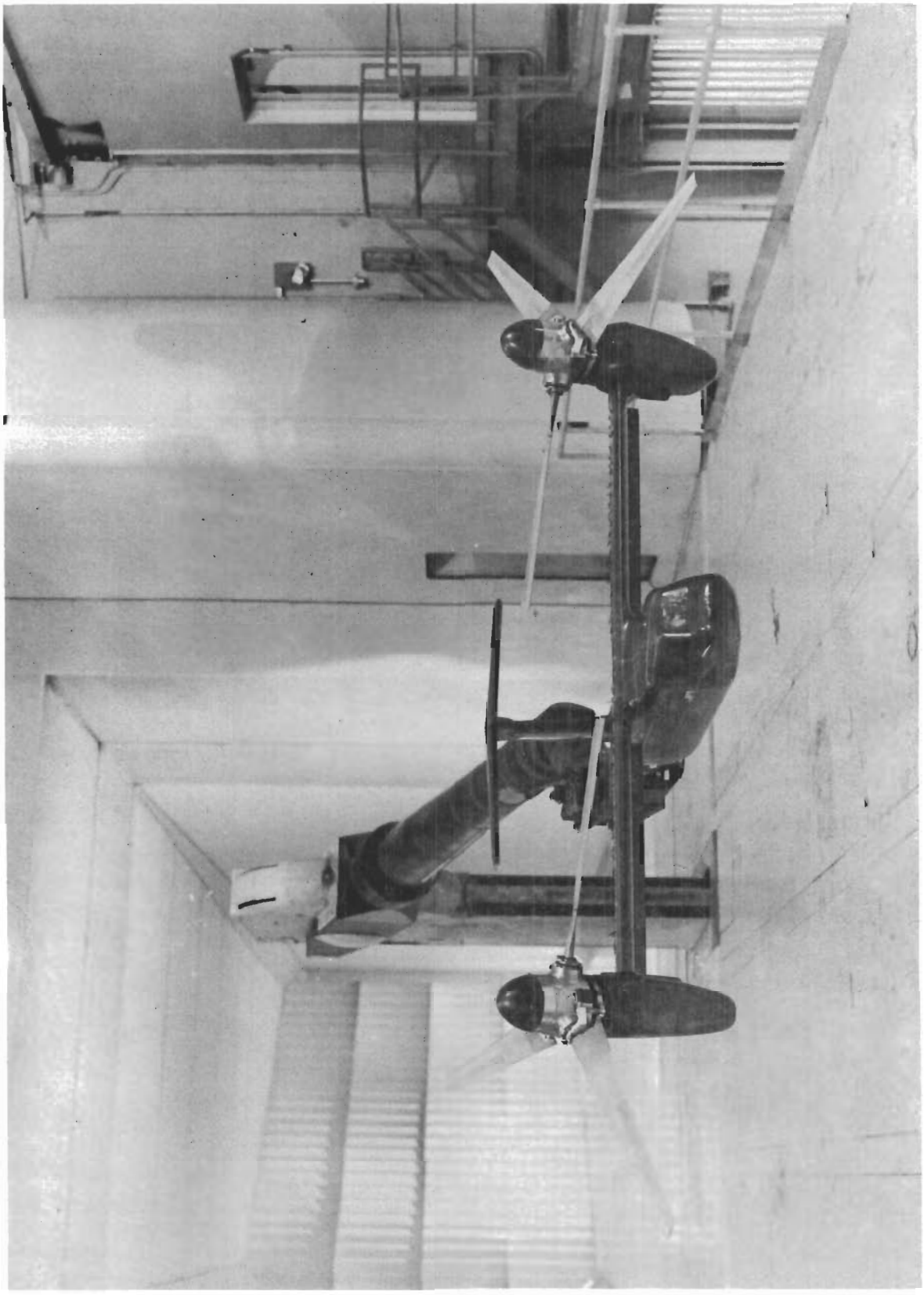

FIGURE 1.4 1/10 SCALE TILT ROTOR POWERED PERFORMANCE MODEL

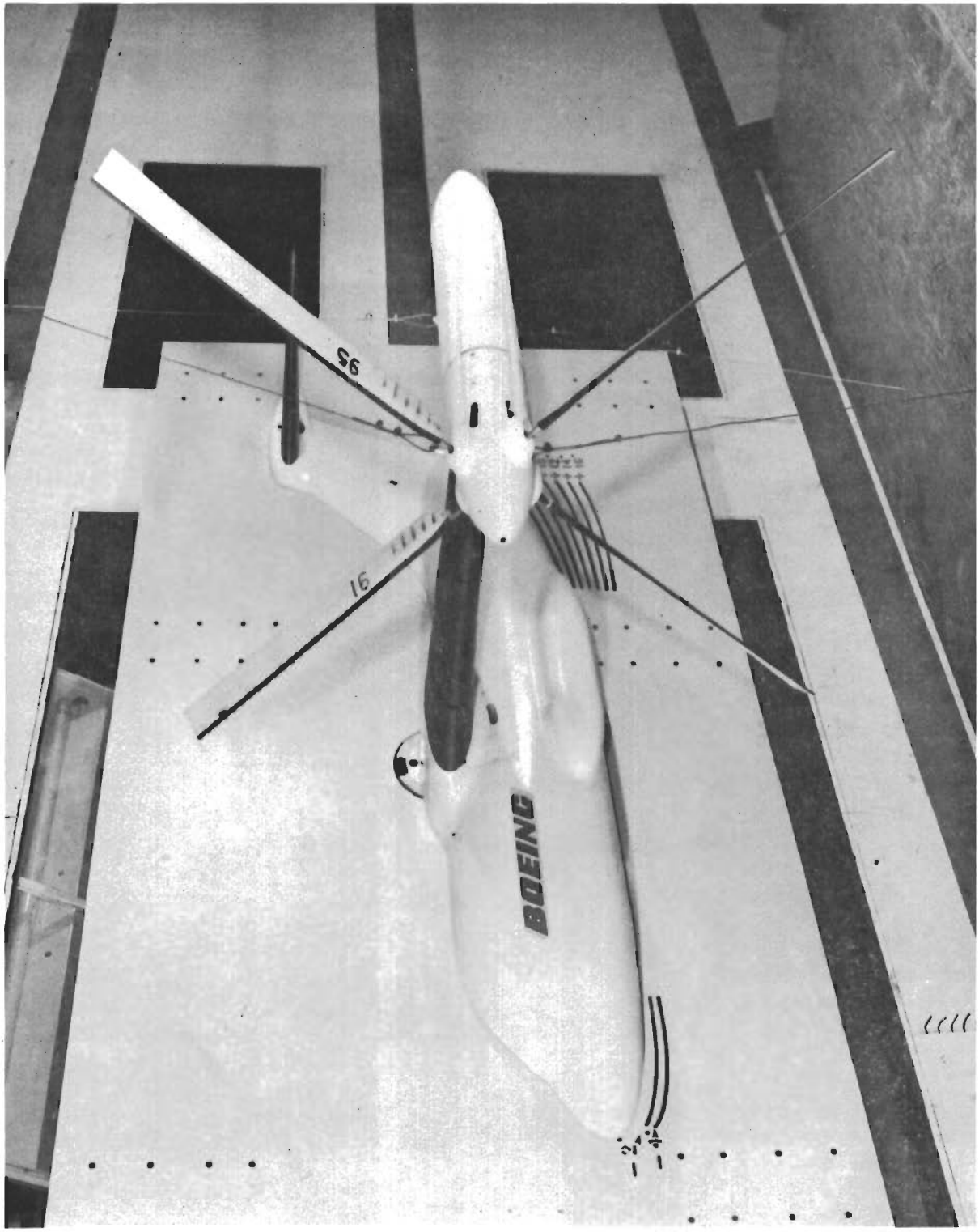

FIGURE 1.5 1/9 SCALE STOWED ROTOR DYNAMIC CONVERSION MODEL

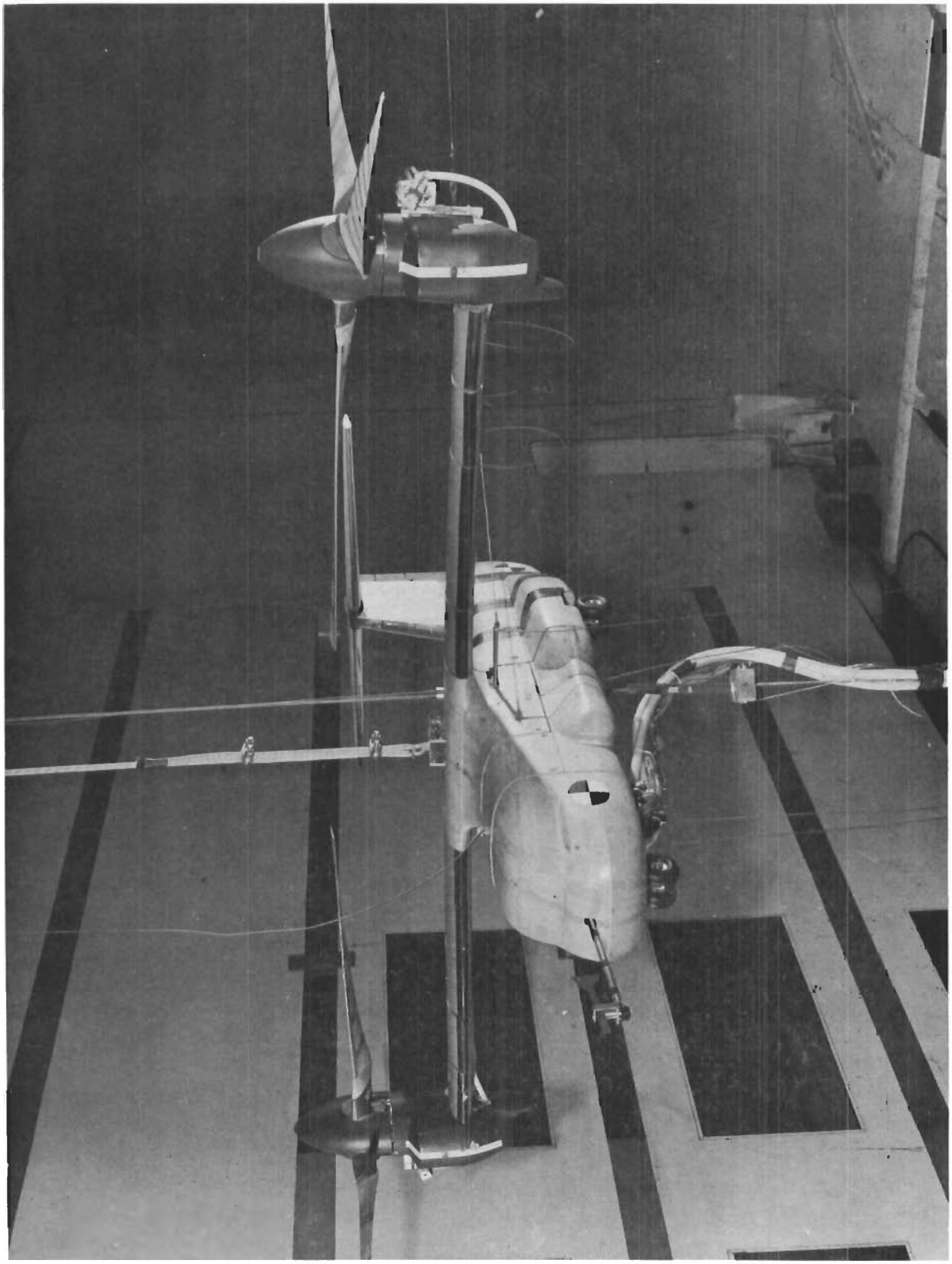

FIGURE 1.6 1/10 SCALE TILT ROTOR POWERED DYNAMIC MODEL

2.0 SUMMARY AND RECOMMENDATIONS

In this section the most significant results from the four test programs are summarized to provide a state-of-the-art review. Recommendations are presented for additional needed technical work. No program stoppers for the stowed tilt rotor aircraft have been found during these investigations.

Structures

A combination of current helicopter and airplane specifications is generally adequate for design of a stowed rotor aircraft.

A soft inplane hingeless rotor is recommended to reduce system complexities, improve flying qualities and minimize susceptibility to whirl flutter.

Critical design conditions for loads in the rotor system are the use of cyclic pitch for control in hover and transition. Prediction capability in these flight conditions is only fair. Boeing is developing improved analytical methods under USAF contract. The stowed rotor tests will be a prime data base for correlation.

Blade loads during the spinup, feather, fold and deploy cycles are not critical.

Rotor/Airframe Dynamics

The limited test data available on aeroelastic stability boundaries correlates well with predictions using current methodology.

An aircraft such as the Model 213 can be designed to be free from aeroelastic instabilities throughout its flight envelope without paying any appreciable penalties.

To minimize blade and wing loads and airframe vibration during feather and spinup, simultaneous coalescences of airframe and rotor natural frequencies with integer rotor harmonics should be avoided.

Aero Prediction Techniques

Rotor/aircraft performance is well predicted by current methodology.

Provision of leading edge umbrella flaps and high angle trailing edge flaps can reduce hover download by 60%.

Rotor spinup and feather can be performed in 10 seconds with less than 0.1g acceleration or deceleration of the aircraft.

Airplane drag for high speed cruise is minimized by folding the blades flatwise rather than edgewise.

Stability and Control

A combination of current airplane and helicopter specifications is generally adequate for design of stowed rotor aircraft.

The recommended hover control power criteria are:

Pitch	0.6 rad/sec^2
Roll	1.0 rad/sec^2
Yaw	0.5 rad/sec^2

The 0.5 rad/sec^2 yaw recommendation is less than Reference 5.1.

Skittishness in hover in ground effect was investigated and found by a dynamic model test. It was readily stabilized by attitude stabilization.

A force feel system which is variable between the hover and cruise modes is recommended.

Spinup, feather, fold and deploy cycles cause no stability or control problems.

In the tilt rotor cruise mode the soft inplane rotor has substantially less destabilizing effect than a stiff inplane rotor.

RECOMMENDATIONS FOR ADDITIONAL WORK

The total flight control system needs further study particularly in the following areas:

1. Feedback controls for gust alleviation and blade load reduction.

2. Flight simulation.

3. System mechanization.

Descent boundaries, including autorotation, should be investigated by analysis and additional model testing.

Development of a convertible fan engine and integration of the power plant with the aircraft system should be initiated early in the aircraft development cycle.

Additional model testing is needed to provide more data for correlation of aeroelastic stability boundaries.

The benefits which can be derived from the application of other advanced technologies to the stowed rotor aircraft should be evaluated. These would include:

1. Use of advanced airfoils to improve rotor performance.

2. Use of advanced composite materials in the airframe.

3.0 STRUCTURAL DESIGN CRITERIA

The folding tilt rotor vehicle is a composite, fixed/rotary-wing aircraft which is capable of flight in either the fixed wing or helicopter mode. The hingeless prop/rotor which is used as a helicopter rotor and as an airplane propeller, and is mounted at the wing tips, presents many unique structural problems. Of primary importance are the predictions of the rotor loads for strength considerations and the rotor/airframe dynamics for aircraft aeroelastic response considerations.

In this section, the structural specifications and the design criteria are presented; and the analytical methods used to ensure compatibility with requirements are described. Also, the rotor/airframe system structural loads and dynamic stability measured on the four wind tunnel models, described in Section 1, are summarized and correlated with analyses.

3.1 STRUCTURAL SPECIFICATIONS

A review of applicable military specifications has been performed to determine how these specifications apply to the folding tilt rotor aircraft. The results are contained in Reference 1.3. Generally, the available specifications are found to be adequate and only relatively minor interpretations or deviations are required. The folding tilt rotor vehicle is a composite, fixed/rotary-wing aircraft which is capable of flight in either the fixed wing or helicopter mode. Consequently, the composite vehicle must show compliance, where appropriate, with the requirements currently specified for both fixed wing and rotary wing aircraft. The extent to which the various requirements of these two types of aircraft are applied to the vehicle will be largely dependent upon the vehicle mission requirements and configuration. The folding tilt rotor aircraft will operate in five modes of flight:

a. Hover or helicopter mode (speeds less than 35 knots)
b. Transition mode
c. Tilt rotor airplane mode
d. Conversion mode (the rotor stopping and folding process)
e. Airplane with stowed rotors mode

The design requirements for this type of vehicle will be in general accord with those specifications which are most appropriate for the means of lift used in the various flight

modes. With rotor lift, the helicopter specifications should apply. For the transition mode, where lift is shared between the rotor system and the wing, the aircraft starts as a compound (winged) helicopter and approaches the end of transition as an airplane with upward inclined propellers. Blade folding is essentially the same function as wing sweep changes of a variable sweep airplane. With this approach, the existing specifications are generally applicable, with minor exceptions. The pertinent structural specification for the helicopter mode is MIL-S-8698 (ASG), Structural Design Requirements, Helicopters. The pertinent structural specifications for the fixed wing modes are:

a. MIL-A-8860 (ASG), Airplane Strength and Rigidity, General Specification for

b. MIL-A-8861 (ASG), Airplane Strength and Rigidity Flight Loads

c. MIL-A-8862 (ASG), Airplane Strength and Rigidity Landplane Landing and Ground Handling Loads

d. MIL-A-8865 (ASG), Airplane Strength and Rigidity Miscellaneous Loads

e. MIL-A-8866 (ASG), Airplane Strength and Rigidity Reliability Requirements, Repeated Loads, and Fatigue

f. MIL-A-8870 (ASG), Airplane Strength and Rigidity Vibration, Flutter and Divergence

3.2 DESIGN CRITERIA

General preliminary design criteria are developed from proposed and existing military specifications. A number of potentially critical design conditions are specified for the purpose of preliminary component design and evaluation. These criteria are used for determination of component concepts and their evaluation with respect to critical loading conditions, critical design areas such as space envelopes and mechanical complexity, and the determination of problem areas peculiar to the stowed-tilt-rotor vehicle concept.

3.2.1 Flight Mode Definition

The aircraft flight modes are defined as follows:

(1) Helicopter Flight

All the lift is provided by the rotors, and the airspeed is less than 35 knots in any direction.

(2) Transition Flight

Lift is provided by both the wing and rotors. The airspeed is between 35 knots and 170 knots. When the nacelle has reached the horizontal position, the transition flight mode is considered complete.

(3) Conversion Flight

All the lift is provided by the wing. The blades are either being folded, unfolded, or rotated at less than 70 percent hover rpm.

(4) Airplane Flight

All the lift is provided by the wing. When the blades are in the extended position, the limiting speed V_L is 250 knots.

(5) Airplane with Stowed Rotors

The blades are stowed and the limiting speed is V_L.

3.2.2 Factor of Safety

The yield factor of safety shall be 1.0. The ultimate factor of safety shall be 1.5.

3.2.3 Design Speeds

(1) For helicopter flight, the maximum forward, sideward, and rearward speed shall be 35 knots.

(2) For transition flight, the speed varies from 35 to 170 knots.

(3) For conversion flight, the speed range is from 1.2 V_S flaps down to 50 knots above this speed, or 1.2 V_S flaps up, whichever is greater.

(4) For airplane flight, the maximum speed is 250 knots with the blades unfolded and V_L when the blades are stowed. Maximum level flight speed (V_H) is 340 knots. Maximum design limit speed (V_L) is 390 knots. The speed for application of maximum gust intensity shall be $V_G = \sqrt{n}\ V_S$, where n is the maximum gust load factor at V_H: V_S is stalling speed for level flight at sea level in the basic configuration with power off.

3.2.4 V-N Diagram

Composite V-N diagrams for the flight modes at the basic flight design gross weight and minimum flying weights are shown in Figures 3.1 and 3.2. The airplane flight (solid lines) diagrams were constructed as specified in MIL-A-8861 for maneuver and gust load factors. Limit load factor for helicopter and transition flight (dashed lines) is shown as the sum of the helicopter load factor (2.5) and the airplane load factor at a given speed, the maximum being +3.0 and -1.0.

3.2.5 Limit Load Design Conditions

(1) Limit load design conditions are summarized in Tables 3.1, 3.2, 3.3, and 3.4. The conditions listed have been selected for investigation during preliminary design. Ground conditions to be considered are contained in Table 3.5.

(2) The maximum design gross weight is the gross weight at which limit load factor is 2.0.

3.2.6 Limit Load Factors

The limit maneuvering load factor at basic design gross weight for the various flight modes shall be as follows:

	Mode	Limit Load Factor
(1)	Helicopter flight	+2.5, -1.0
(2)	Transition flight	+3.0, -1.0
(3)	Conversion flight	+1.5, +0.5
(4)	Airplane flight	+3.0, -1.0

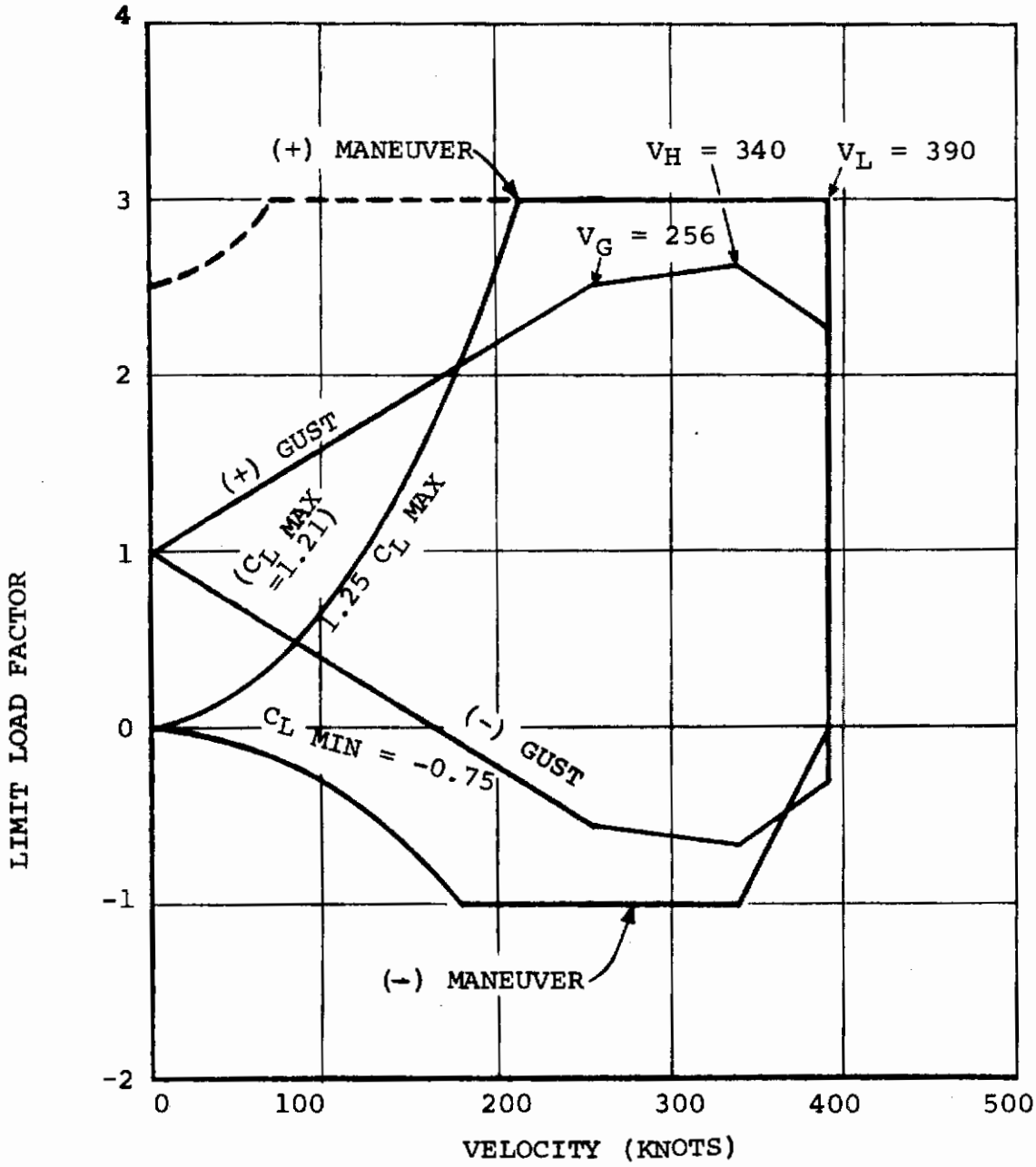

FIGURE 3.1 V-N DIAGRAM FOR SEA LEVEL BASIC FLIGHT DESIGN GROSS WEIGHT OF 67,000 POUNDS

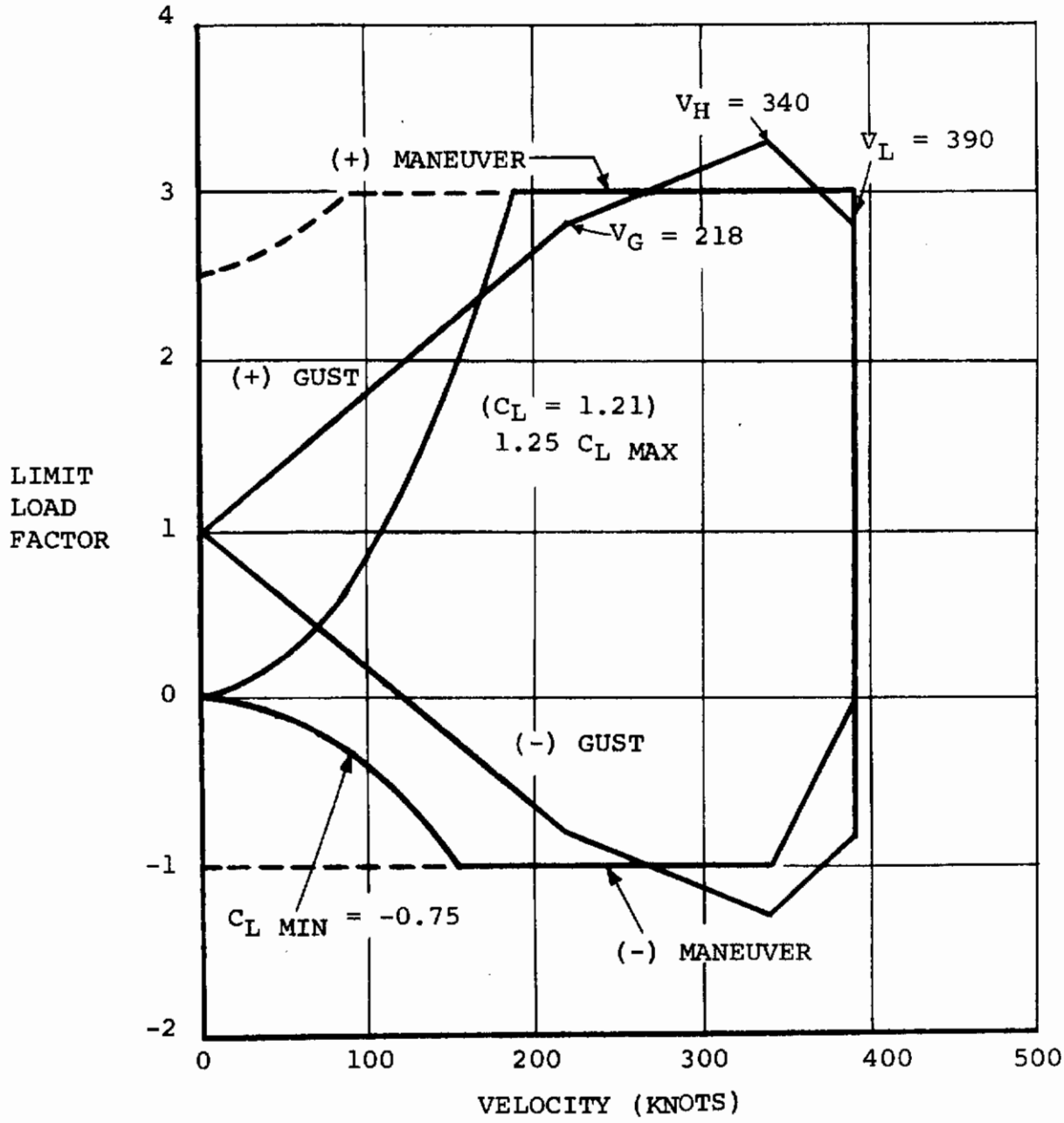

FIGURE 3.2 V-N DIAGRAM FOR SEA LEVEL MINIMUM FLYING WEIGHT OF 45,046 POUNDS

TABLE 3.1. LIMIT DESIGN CONDITIONS FOR HELICOPTER FLIGHT

Condition No.	Description	Gross Weight (lb)	Limit Load Factor	Air Speed (kn)	Acceleration (rad/sec^2)
1	Rolling	67,000	2.0	0	1.0
2	Yawing	67,000	1.0	0	0.5
3	Pull-up plus Pitch	67,000	2.5	0	0.6
4	Maximum Cyclic	67,000	1.0	0	Note (1)
5	Vertical Takeoff Note (2)	67,000	2.5	0	0
6	Pushdown (Collective Dump) Note(2)	67,000	-1.0	0	0

NOTES: (1) Maximum cyclic requirements of Condition 2 plus 1/2 of the cyclic requirement of Condition 3.

(2) Cyclic control applied to balance pitch

TABLE 3.2. LIMIT DESIGN CONDITIONS FOR TRANSITION FLIGHT				
Condition Number	Description	Gross Weight (lbs)	Limit Load Factor	Accelerations (rad/sec^2)
1	Symmetrical Pull-Out	67,000	3.0	0.6
2	Rolling Pull-Out	67,000	2.4	1.0
3	Yawing	67,000	1.0	0.5
NOTE: (1) The rotor speed for the above conditions shall be the limit rotor speed				

TABLE 3.3 LIMIT DESIGN CONDITIONS FOR CONVERSION FLIGHT				
Condition Number	Description	Gross Weight (lbs)	Limit Load Factor	Special Conditions
1	Gust Response	45,046	Due to 66 fps vertical gust	180 knots
2	Gust Response	67,000	Due to 66 fps vertical gust	180 knots

TABLE 3.4. LIMIT DESIGN CONDITIONS FOR AIRPLANE FLIGHT

Condition Number	Description	Gross Weight (lb)	Limit Load Factor	Air Speed (knots)
1	Balanced Symmetrical Maneuver	67,000	+3.0	215
			+3.0	V_L
			-1.0	180
			-1.0	V_H
			0	V_L
2	Symmetrical Maneuver with Pitch	67,000	Control displacement as per MIL-A-8861, Para. 3.2.2.2	
3	Rolling Pull Out	67,000	Control displacement as per MIL-A-8861, Para. 3.3.1 and 3.3.1.1	
4	Vertical Gust	67,000	As specified in MIL-A-8861, Para 3.5	
		45,046		

TABLE 3.5. GROUND CONDITIONS

Condition Number	Description	Remarks
1	Rotor Acceleration	Condition as specified in MIL-S-8698, Para. 3.3.1
2	Landing	Landing conditions as specified in Section 3.2.7 of this report.

3.2.7 Landing Sinking Speed

(1) The maximum landing sinking speed shall be 15 fps for the basic design gross weight for the transport aircraft. Limit landing load factors shall be +3.0g at the center of gravity of the airplane and 2.0g at the gear.

(2) The maximum landing sinking speed shall be 8 fps for the basic design gross weight for the rescue aircraft and rotor lift equal to two-thirds of the basic design gross weight.

3.2.8 Rotor Speed

(1) The design limit rotor speed factor shall be 1.25 for both helicopter and transition flight modes.

(2) The normal maximum operating rpm for helicopter and transition flight modes shall be 388 rpm with power on.

(3) The normal maximum operating rpm for airplane flight mode shall be 262 rpm.

3.2.9 Fatigue Design Conditions

3.2.9.1 Basic Fatigue Schedule

The stowed-tilt-rotor aircraft is exposed to fatigue damage both as a fixed-wing and a rotary-wing aircraft. Fatigue damage shall be evaluated as specified in MIL-S-7698, and ASD-TR-66-57.

The basic fatigue schedule shall be based on aircraft usage as defined by the mission profiles. Damage assessment shall be based on a cumulative damage theory. The significant conditions affecting the fatigue performance of the wing are the repeated maneuvers and atmospheric turbulence at low altitudes and the relatively large number of ground-air-ground cycles. The significant conditions affecting the fatigue performance of the nacelle structure are repeated maneuvers with the vehicle in the airplane mode, ground-air-ground cycles and rotor loads. The significant conditions affecting the fatigue performance of the dynamic system are the prop/rotor cyclic control and airplane flight and inclination of the prop/rotor

axis. The dynamic system is considered to include the prop/rotor blade, hub, controls and drive and drive system.

Rotor Hub and Blade Loads for Preliminary Design

The most significant hub and blade design loads are the alternating fatigue loads due to the application of rotor cyclic pitch in the helicopter mode. In this flight mode rotor cyclic pitch provides for the aircraft yaw and pitch control. The rotor blade component design study considered the primary design loads for unlimited life corresponding to application of cyclic pitch to achieve 25% of the maximum yaw acceleration plus aircraft trim at the most adverse center of gravity position. Blade loads occurring from other conditions such as airplane maneuvers, gusts, and transition mode are anticipated to be no higher than the cyclic pitch loads. The frequency spectrum of cyclic pitch control inputs greater than the design case is highly dependent on aircraft flying qualities and requires further study. This single fatigue design condition serves as a base reference by which all other flight loads can be evaluated including blade loads from model tests.

Service Life

The service life of the wing and nacelle structure shall be 10,000 hours. The service life on dynamic system components shall be 3,600 hours, except as indicated below.

Airplane integrity shall be established along the guidelines of ASD-TR-66-57, "Air Force Structural Integrity Program Requirements."

The B-10 design life for the individual drive system bearings shall be established based on the mean time between removal (MTBR) of the desired transmission. This means that the total bearing system life, when combined with other critical component lives, will result in the desired transmission MTBR.

Gearbox cases shall be designed for a service life of 10,000 hours, considering drive train and rotor loads. All drive system gears and splines shall be designed for unrestricted fatigue life under maximum rated power at normal operation rpm.

3.3 ROTOR ANALYTICAL METHODS

3.3.1 Rotor Blade Natural Frequencies

The analytical programs used to calculate the rotor blade natural frequencies are designated L-01 for torsion and L-21 for bending.

The L-01 program calculates the natural frequencies and mode shapes for the uncoupled flap bending, chord bending and torsional free vibrations of stationary and rotating wings. Only the torsional analysis is used for prop/rotor analysis.

The theoretical basis of this program is the lumped parameter method of analysis employing finite difference equations to relate the dynamic aeroelastic quantities of adjacent wing stations, whose maximum number is fifty (50). Trial and error tabular calculations are employed in search of the wing natural frequencies, these being attained by satisfaction of the root boundary conditions, including the pinned and cantilever conditions. Having found the natural frequencies, the program proceeds to calculate the deflection, slope, moment, shear, and loading distributions for each natural mode. In addition, the program calculates the critical aerodynamic damping ratios, the damped natural frequencies, damped amplification factors, and phase angles, the latter two for twelve harmonics of exciting frequencies, for each natural mode. Following the solutions for the natural modes, a classical flutter analysis is made for the coupled flap bending and torsion flutter vibrations of the stationary or rotating wing, for all combinations of the natural modes found earlier. The analysis employs generalized coordinate theory with the Theodorsen unsteady aerodynamic theory, wherein the complex circulation function is made unity. The program output includes natural frequencies, mode shapes, amplification factors and flutter parameters.

The L-21 program calculates the coupled flap/chord bending natural frequencies and normal modes of a twisted propeller by means of transfer equations written in matrix form. Non-uniform blade properties are read into the program which proceeds to divide each distribution into forty uniform sections. Matrix transfers are based on simple beam theory (Reference: 3.1) using a mass, elastic, twist and spring matrix in a series from blade tip to root station. Boundary conditions are imposed on the product of the matrix series to

yield a determinant whose zero's define the natural frequencies of the system. A tip modal column of shear, moment, slope and deflection is computed and used in the matrix series to complete the modal print-out. The output provides natural frequencies, the associated normal mode of shear, moment, slope and deflection normalized to unit vertical tip deflection; mode integrals, damped amplification factors, centrifugal force; static droop under 1g loading and also under unit pressure loading. Program results are based on propeller flap and chord motions only. The rotor hub has no degree of freedom.

3.3.2 Rotor Blade Loads Analysis

The analytical program used to calculate rotor blade loads is D-88.

The D-88 program calculates rotor blade flap, lag and pitch deflections and loads together with control system forces, vibratory hub loads and rotor performance. Articulated and hingeless rotors with from 2 to 9 blades may be analyzed. The analysis is limited to calculations involving steady state flight at constant rotor tip speeds. The blades may be of arbitrary planform, twist, and radial variation in airfoil characteristics.

The analysis considers coupled flap-pitch and uncoupled lag flexibility of the rotor blades. The blade is represented by fifteen (15) lumped masses, interconnected in series by elastic elements. Boundary conditions for either articulated or hingeless rotors are applied and the solution obtained by expanding the variables in a ten harmonic fourier series.

Airload calculations include the effects of airfoil section geometry, compressibility, stall, 3-dimensional flow, unsteady aerodynamics and non-uniform inflow. The solution for the non-linear aerodynamic forces and the coupled flap-pitch dynamic response are performed in series and an iteration technique is used to obtain the final solution.

Non-uniform downwash field, airloads (in both wind and disc axis systems), non-dimensional aerodynamic performance, blade loads and displacements (in both blade and disc axis systems), hub loads, rotating pitch link loads, and fixed system control loads are provided.

3.4 ROTOR BLADE DYNAMICS

3.4.1 Blade Design Criteria

The hingeless rotor design is fundamentally controlled by blade frequency requirements. The use of the rotor for hover yaw control dictates a "flexible" blade to provide the required thrust vector tilt with minimum complexity of the rotor and nacelle systems. The hingeless rotor with a low chordwise stiffness of the inboard portion of the blade provides a soft in-plane feature with the first lag bending frequency ratio less than one. A typical rotor frequency chart is shown in Figure 3.3. This feature results in low lag bending moments and minimizes the weight of the blade root structure. The blade dynamic requirements are defined by the blade natural frequencies and are specified as follows:

(a) The first coupled rotating bending frequency ratio ($\frac{\omega}{\Omega}$) shall be 0.70 to 0.80 for helicopter, transition and airplane flight at normal rotor speeds for each condition. The predominant bending mode shall be in the plane of the rotor (lag).

(b) The second coupled rotating bending frequency ratio shall be 1.15 to 1.25 for helicopter and transition flight at normal rotor speed for each condition. The predominant bending mode shall be out of plane of the rotor (flap).

(c) The third and fourth coupled bending frequencies shall be displaced $\pm$ 10% of rotor speed and .15/rev from any integer harmonic for both helicopter, transition and airplane flight. Additionally, the frequencies shall not occur within the frequency band of n$\pm$0.25/rev where n is the number of blades per rotor.

(d) The first torsional natural frequency shall be displaced at least $\pm$ 10% of rotor RPM and 0.25/rev from any integer harmonic for both helicopter and airplane flights.

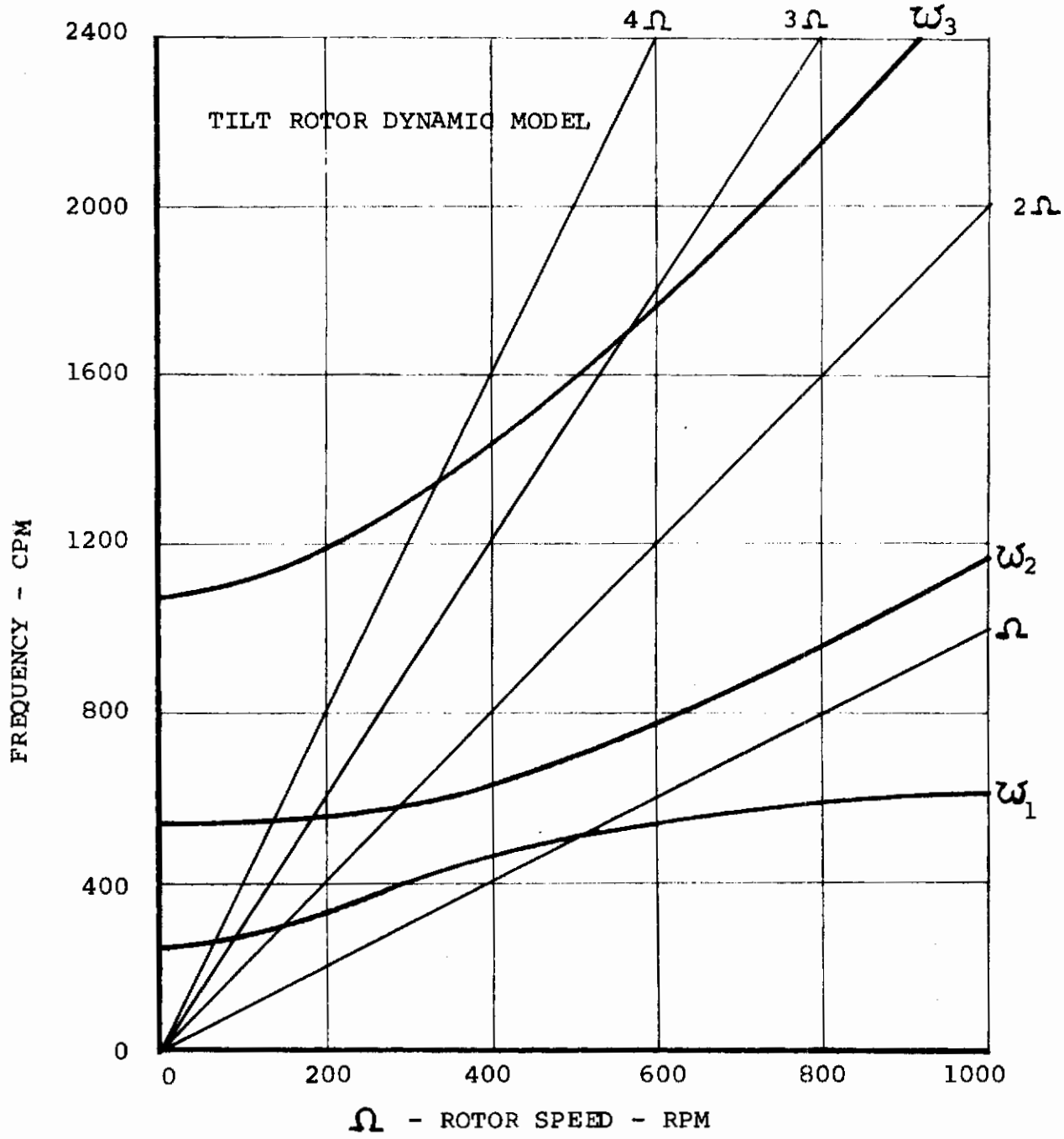

FIGURE 3.3 TYPICAL CALCULATED BLADE FREQUENCY SPECTRUM FOR HOVER

(e) The coupled bending frequencies and the first torsional frequency shall be displaced by at least 0.5/rev.

(f) There shall be no resonance crossings of any integer harmonic up to n/per rev within the normal operating RPM range; i.e., from cruise to hover RPM.

3.4.1.2 Stall Flutter

The rotor shall be free of stall flutter in hover within the normal operating envelope for a rotor thrust for 1.15 vertical load factor.

3.4.1.3 Classical Flutter

The rotor blades shall be free of aeroelastic instabilities (such as but not limited to classical flutter, divergence, pitch-lag and pitch-flap instabilities at all rotor speeds up to 1.25 times the design limit speed with and without power and including the zero RPM feathered propeller condition, at all thrust conditions from maximum design negative thrust to the maximum positive thrust condition including the effects of control power requirements, for all environmental conditions encompassed by the design flight envelope, for all design conditions of gusts and maneuvers, and for all aircraft speeds up to 1.15 the maximum design speed.

3.4.2 Blade Frequency Variation Within the Operating Envelope

The blade bending frequencies are affected by variation in rotor speed and collective pitch (Figure 3.4). These parameters can vary considerably for the helicopter, transition and airplane flight modes. The first two bending mode natural frequencies for the rotor blade design considered are controlled by the blade spar structure inboard of 30 percent radius. The resulting blade spar has different root flap and chord stiffness. It is important that the blade natural frequencies can be predicted accurately. A correlation study was conducted to demonstrate the prediction capability.

3.4.3 Results of Prop/Rotor Frequency Correlation

3.4.3.1 Frequency Measurements

A primary objective of the model tests was to measure the

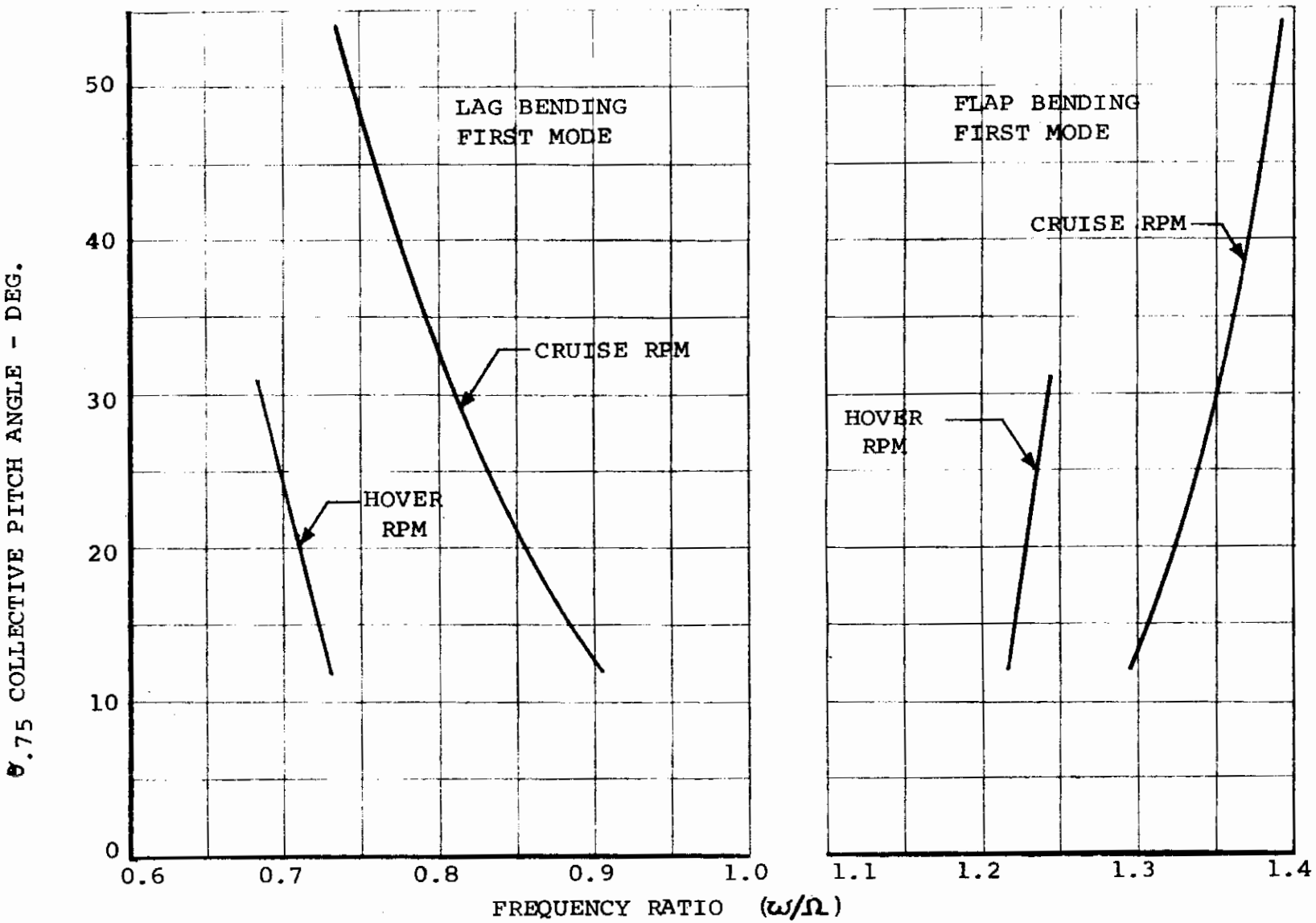

FIGURE 3.4 EFFECT OF COLLECTIVE PITCH ON BLADE BENDING FREQUENCIES

blade rotating frequencies for correlation with calculated values. During the rotor startup to operating rotor speed several integer harmonic frequency crossings are encountered. The blade bending moments respond predominantly at those frequencies. Test programs I, II and IV included frequency measurements using baffles placed under the rotor disc plane to provide 1,2,3 and 4 per rev excitation. The baffles excite the blades by restricting the downwash as each blade passes over a baffle. Since the rotor wake is subsonic, any downwash restriction in the wake will immediately influence the flow field in the disc plane. A description of the baffle arrangement is shown in the respective test and reports.

3.4.3.3 Correlation of Measured and Predicted Blade Frequencies

Blade bending frequencies are calculated by the Program L-21 described in paragraph 3.3. Correlation with frequency spectrum is shown in Figures 3.5 and 3.6. Correlation of measured and predicted blade frequencies for each model tested is shown in Figures 3.7 to 3.9. These figures show the analysis to be good. The deviations shown are due to differences between the calculated and actual mass and stiffness properties of the model blades. Any deviations are important to the blade load predictions because the first two bending modes produce the dominant alternating bending moments.

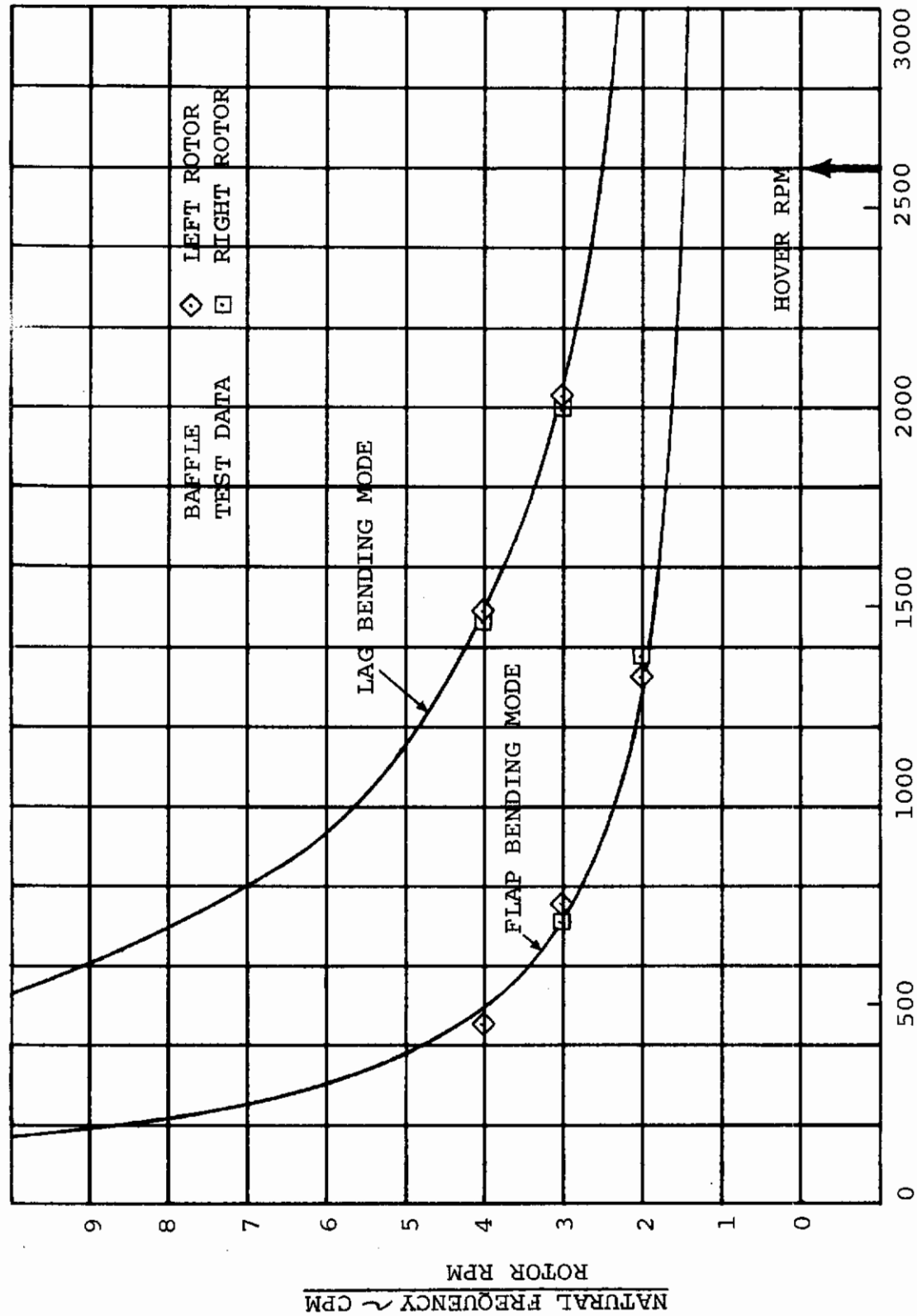

FIGURE 3.5 PREDICTED AND MEASURED ROTOR BLADE NATURAL FREQUENCIES FOR $\theta_{.75} = 15°$ TILT ROTOR PERFORMANCE MODEL

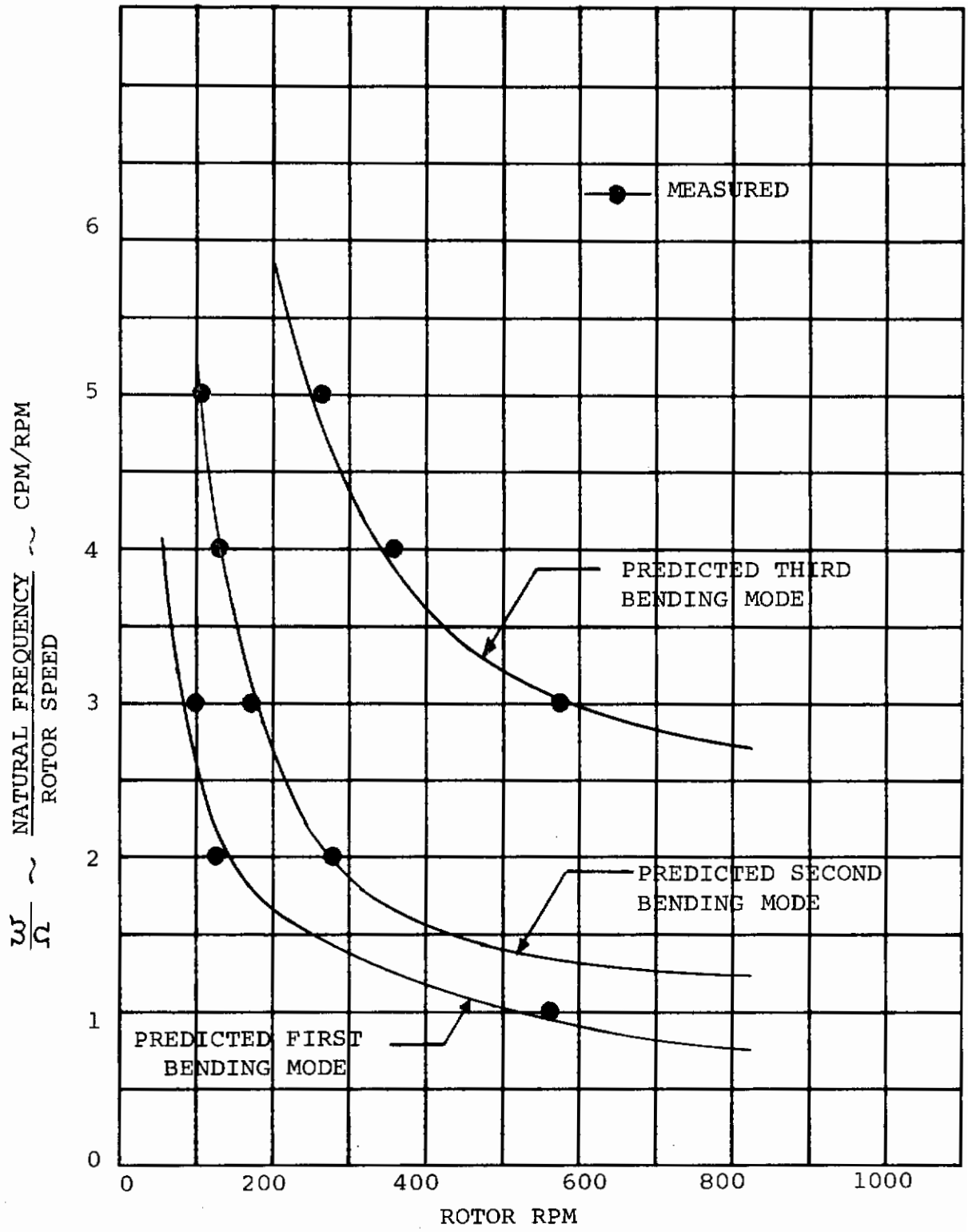

FIGURE 3.6 PREDICTED AND MEASURED ROTOR BLADE NATURAL FREQUENCIES FOR $\theta_{.75}$ = 3 DEG.
TILT ROTOR DYNAMIC MODEL

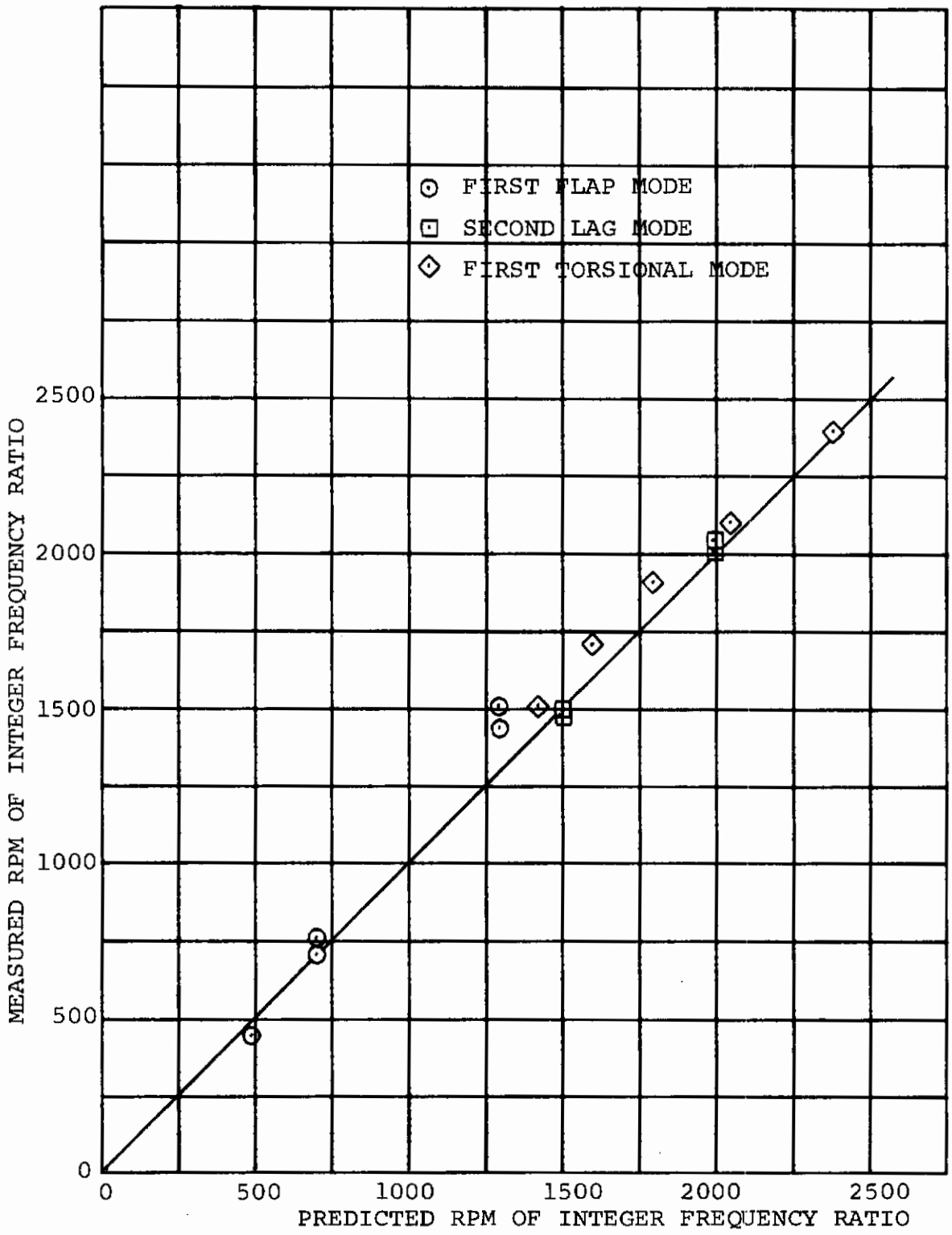

FIGURE 3.7 CORRELATION OF MEASURED AND PREDICTED BLADE FREQUENCIES
TILT ROTOR PERFORMANCE MODEL

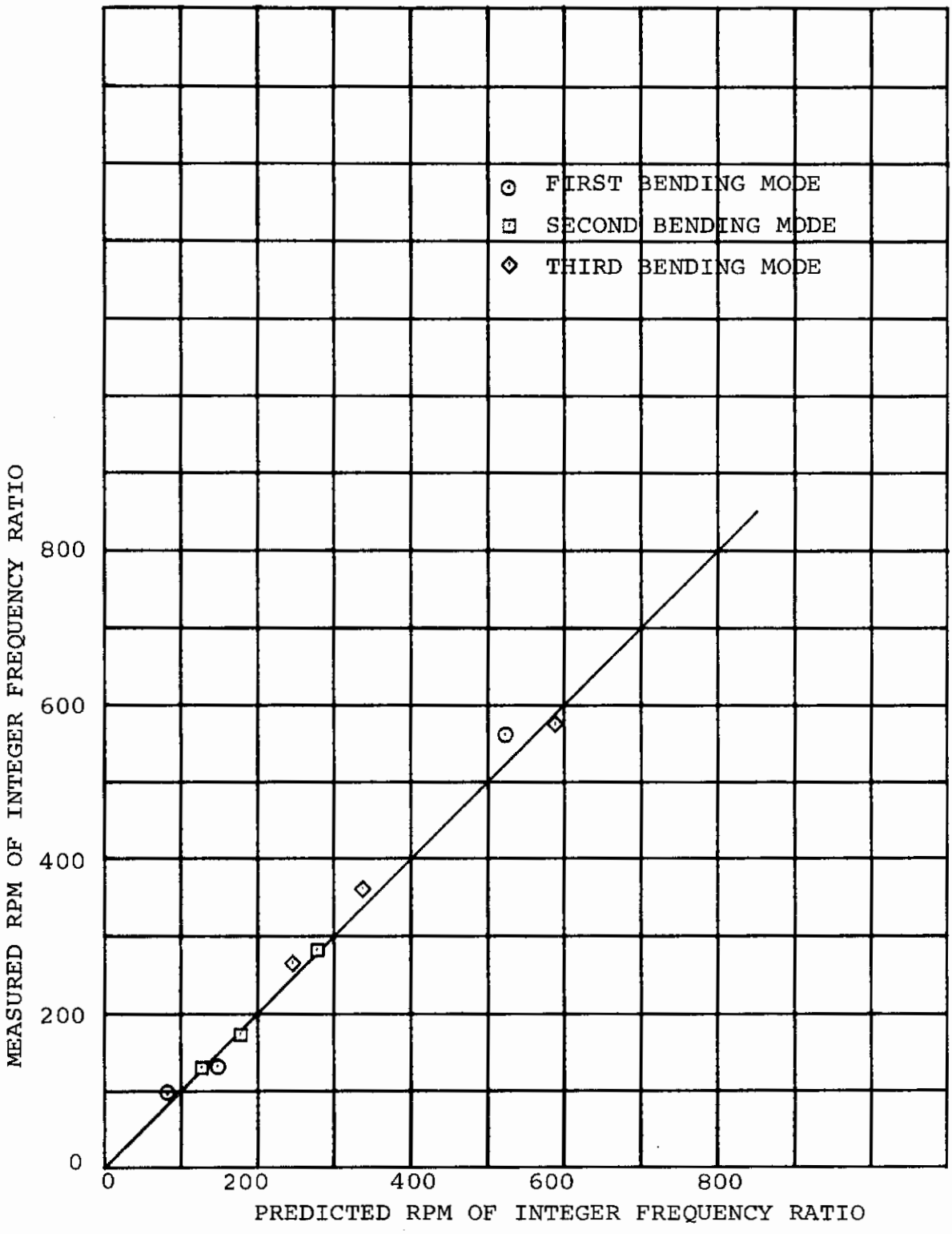

FIGURE 3.8 CORRELATION OF MEASURED AND PREDICTED BLADE FREQUENCIES
TILT ROTOR DYNAMIC MODEL

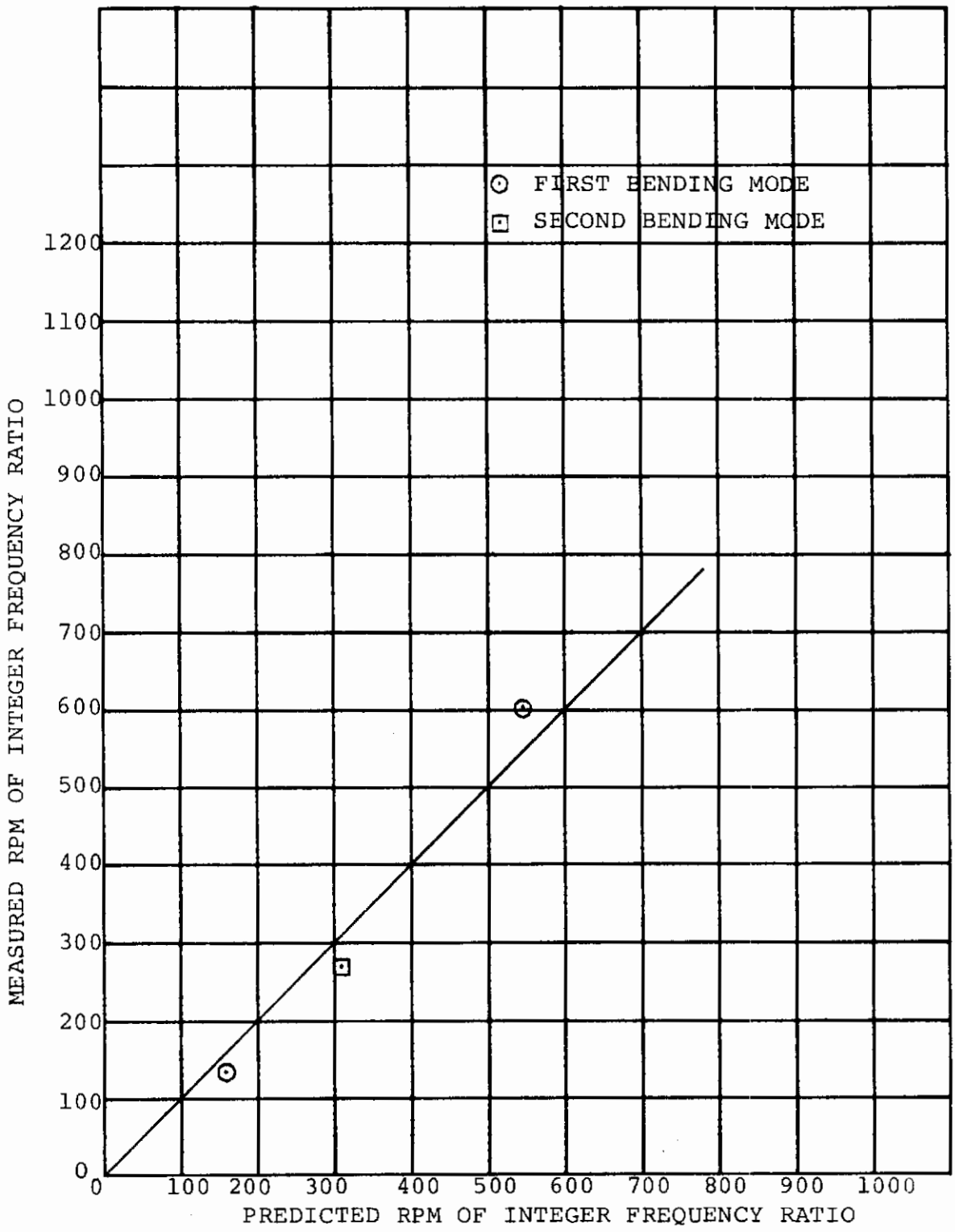

FIGURE 3.9 CORRELATION OF MEASURED AND PREDICTED BLADE FREQUENCIES 1/9 SCALE CONVERSION MODEL

3.5 MODEL ROTOR BLADE TEST LOADS

The four model tests (References 1.4 through 1.7) provided blade load data for hover, tilt transition and cruise attitudes and for the conversion process including windmilling, feathering and stowing. Parameters varied were collective pitch, cyclic pitch, rotor speed, nacelle tilt, model pitch and yaw and dynamic pressure. Blade flap and chord bending moments were measured by strain gages placed close to the blade root and limited to one flap and one chord bending gage for the tilt rotor dynamic and performance models and two flap and two chord bending gages for the conversion models. A summary discussion of the trends of the results is given in the following paragraphs. These trends are from the blade loads sections of References 1.4, Section 8.2; 1.5, Section 6.0; 1.6, Section 7.0; 1.7 Section 6.0. Only some of the figures will be repeated here to avoid repetition.

It should be noted that only the 1/9 scale stowed rotor model and the 1/10 scale dynamic tilt rotor model (test programs III and IV) have a dynamically scaled wing, nacelle and rotor system. The 1/16 scale conversion model of test program I has dynamically scaled rotor blades but a stiff wing. The 1/10 scale performance model of test program II had heavy blades that were designed mainly for pumping air over the model to obtain airframe/rotor interference data. The blades however are representative of stiff-in-plane rotor blades and trend data are included here to show parametric effects.

3.5.1 Hover

Some of the questions that the model test programs were designed to answer for hover flight are presented below:

(1) What are the effects of cyclic pitch and collective pitch on blade loads?

(2) Are these loads affected by ground height?

(3) What are the blade loads during rotor start up?

(4) What are the blade loads due to rotor interference?

(5) What are the control moments due to cyclic pitch in hover?

(6) Are stall flutter inception and loads in hover and transition predictable?

One of the primary objectives was to determine the effect of cyclic pitch on blade loads in hover. The tilt rotor dynamic and performance models both had the capability of cyclic pitch control and typical results are shown in Figure 3.10. The blade bending moments are linear with cyclic pitch variation; however, the moments at zero cyclic pitch are finite. The source of these loads is harmonics higher than 1/rev and they are caused by ground effects, model mounting or rotor balance. The high chordwise loads for the performance model at zero cyclic are caused by operation on the 3/rev resonance point at 2000 RPM, see Figure 3.5. Other conclusions drawn from the hover results, (but not shown here), are that the sensitivity of blade loads to cyclic pitch is not affected by ground effect, but ground effect does increase the minimum blade load at zero cyclic. Increased collective pitch increased the blade load sensitivity to cyclic pitch. The blade alternating loads were essentially unaffected by differential collective between the two rotors corresponding to that required for roll control power in hover. Stall flutter as illustrated by the rate of change of the blade torsion amplitude at its natural frequency was encountered on the tilt rotor dynamic model. However, even at the highest thrust tested, producing a thrust coefficient C_T/σ equal to 0.118, the absolute value of alternating torsion moment is low. A comparison of the blade loads measured on the two tilt rotor models for various conditions is shown in Table 3.6.

3.5.2 Transition

Tests on the tilt rotor dynamic and performance models investigated the transition mode. Test results show that for each nacelle tilt, collective pitch and dynamic pressure, there is a value of cyclic pitch at which alternating blade bending moments are minimized. This effect of cyclic pitch is shown in Figure 3.11. The blade loads are primarily of one per rev response although some higher harmonic response does exist. With correct phasing of the cyclic pitch, the one per rev loading should be eliminated. For a constant nacelle tilt with collective and cyclic adjusted for minimum loads, increased dynamic pressure increases the minimum value of alternating bending moments, as shown on Figure 3.11.

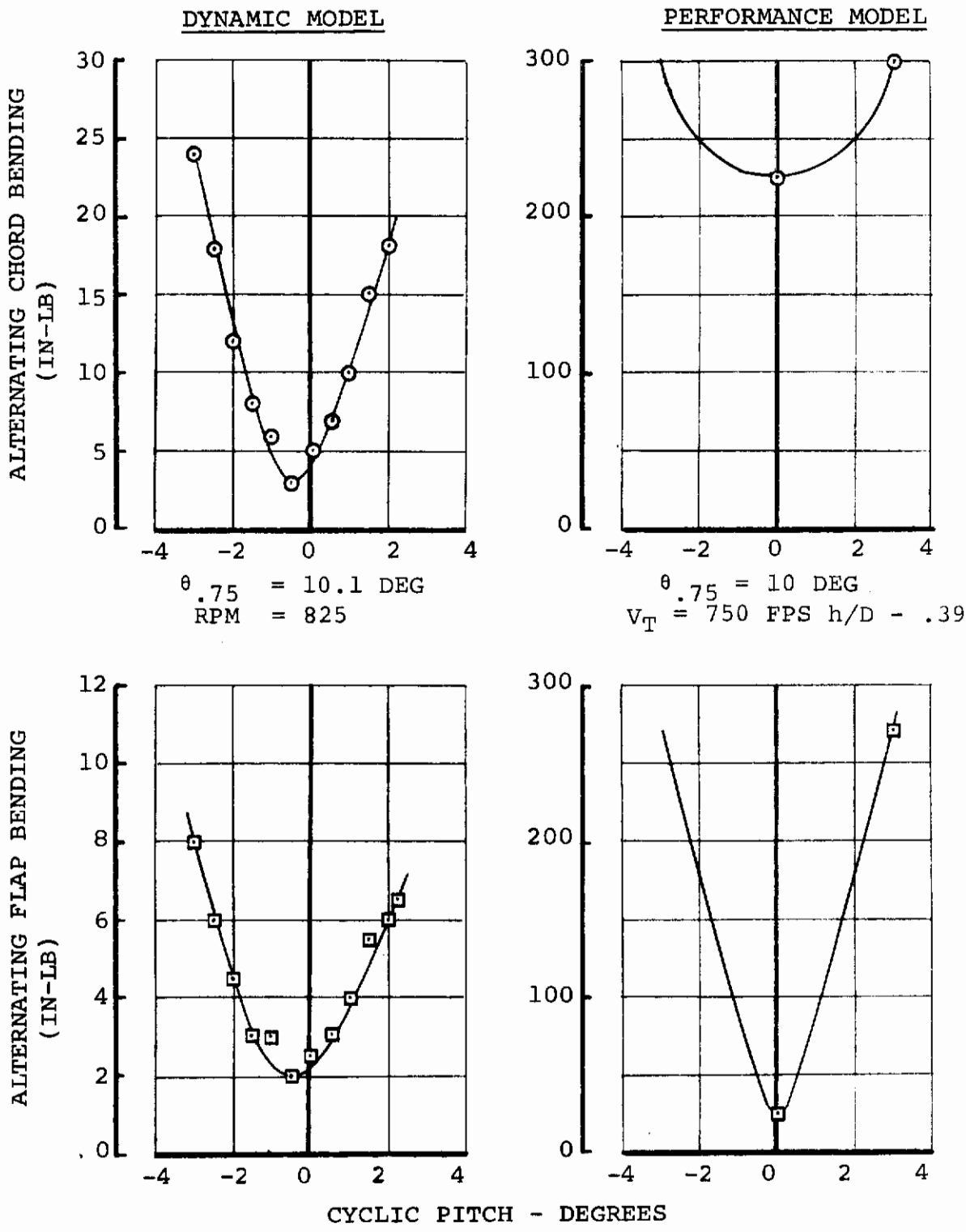

FIGURE 3.10 EFFECT OF CYCLIC PITCH ON BLADE ROOT BENDING MOMENTS IN HOVER

TABLE 3.6

SUMMARY OF MEASURED BLADE LOADS FOR TILT ROTOR MODELS

CONDITION	ALTERNATING BENDING MOMENT IN-LB			
	DYNAMIC MODEL		PERFORMANCE MODEL	
	CHORD	FLAP	CHORD	FLAP
ROTOR START	16.	3.2	-	-
ROTOR SHUT DOWN	11.	3.2	-	-
HOVER MOMENT/DEG CYCLIC	7.	3.2	25.	63.
HOVER MINIMUM LOAD	3.	2.	225.*	25.
TRANSITION MOMENT/DEG CYCLIC	7.	2.	-	-
TRANSITION MOMENT/DEG PITCH	5.	1.	8.	9.
TRANSITION MOMENT/DEG YAW	.9	.1	NEGLI-GIBLE	NEGLI-GIBLE
CRUISE STEADY	5.	2.5	150.	20.
MOMENT/DEG CYCLIC	16.	0.	-	-
MOMENT/DEG PITCH	6.5	.5	16.	22.
MOMENT/DEG YAW	1.4	.2	NEGLI-GIBLE	NEGLI-GIBLE

*Rotor is operating at 2000 RPM. This corresponds to coincidence of the second lag mode and 3 per rev as shown on Figure 3.7.

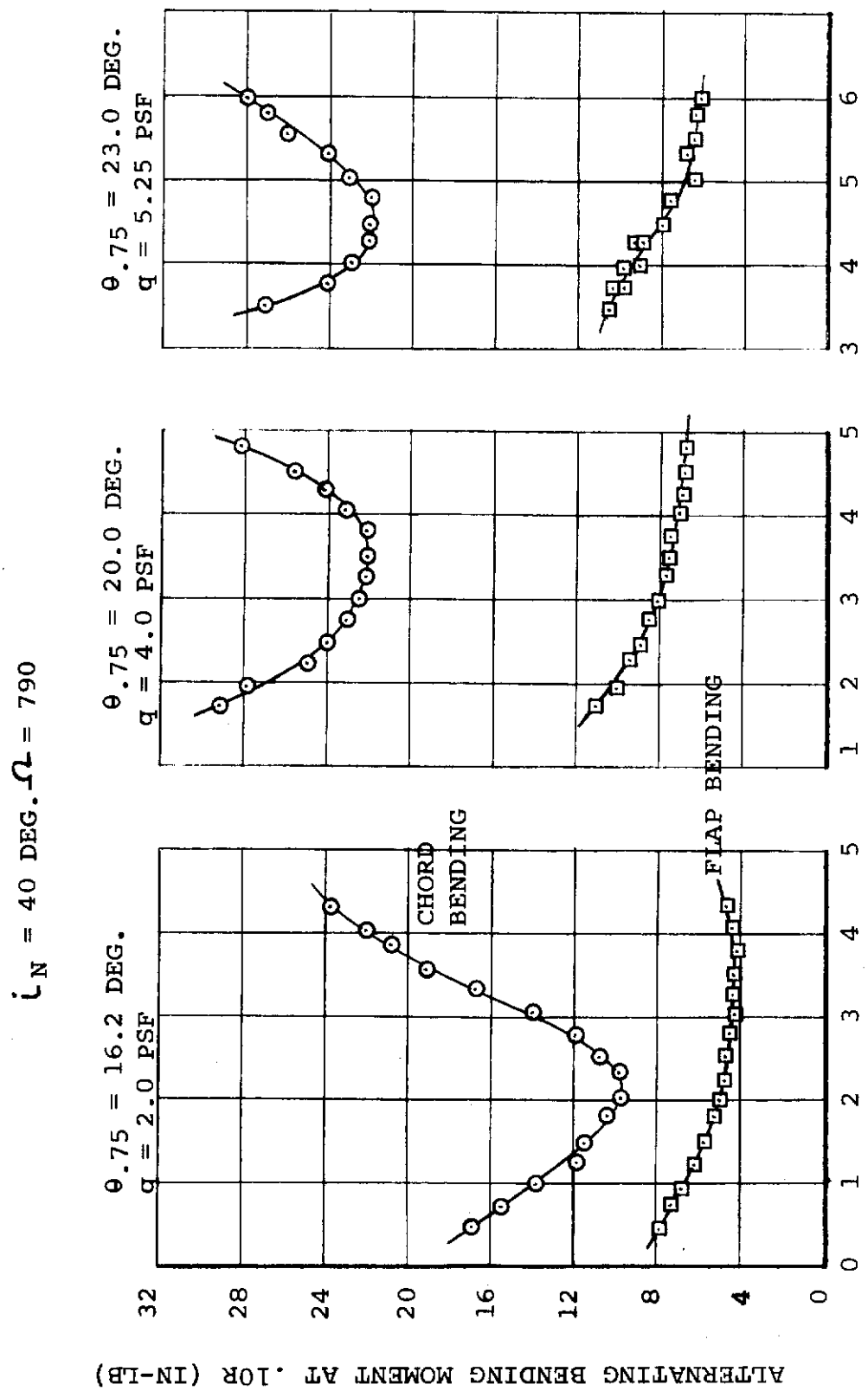

FIGURE 3.11 EFFECT OF CYCLIC PITCH ON BLADE LOADS IN TRANSITION TILT ROTOR DYNAMIC MODEL

3.5.3 Tilt Rotor Airplane

Tests on the tilt rotor dynamic and performance models in the cruise or tilt rotor airplane mode investigated the effects of aircraft angle of attack, wing flap incidence, aircraft yaw and cyclic pitch on alternating blade bending moments. The results show a near-linear increase in blade loads as the aircraft angle of attack is varied from zero. This effect of aircraft pitch on alternating bending moments is shown in Figure 3.12. This trend is expected since a change in rotor angle of attack from zero introduces the rotor to cross flow and results in a once-per-rev sinusoidal variation of blade section angle of attack around the azimuth. Wing circulation also produces alternating blade moments when the wing is producing lift. The circulation due to wing lift alters the velocity flow-field in the rotor disc plane and this results in a change in blade section angle of attack around the azimuth. This change in local blade angle due to wing interference is not sinusoidal and it is additive to the once-per-rev change in blade angle due to inflow. Both rotor inflow and wing circulation increase the blade angle on the advancing side of disc when the aircraft angle of attack is increased from zero. Rotor inflow and wing circulation effects on blade loads are also additive when the aircraft angle of attack is negative and the wing is producing negative lift since rotor inflow and wing circulation decrease the blade angle on the advancing side of the disc.

Wing interference effects can cause approximately 20 percent of the alternating bending moments when the aircraft is pitched but no effect when the aircraft is yawed, since wing circulation changes are small with aircraft yaw.

3.5.4 Rotor Windmilling, Spin-Up and Feathering

The blade alternating loads measured during steady windmilling, spin-up and feathering show that there is no significant difference for these conditions and that the collective schedule for rotor spin-up and feathering will not be constrained by blade loads. Typical bending moments are shown in Figures 3.13 and 3.14. The effect of aircraft angle of attack change during steady windmilling on blade loads (Figure 3.15) was the same as for the tilt rotor models in airplane flight.

A summary of the measured loads for the conversion models for various conditions is contained in Table 3.7.

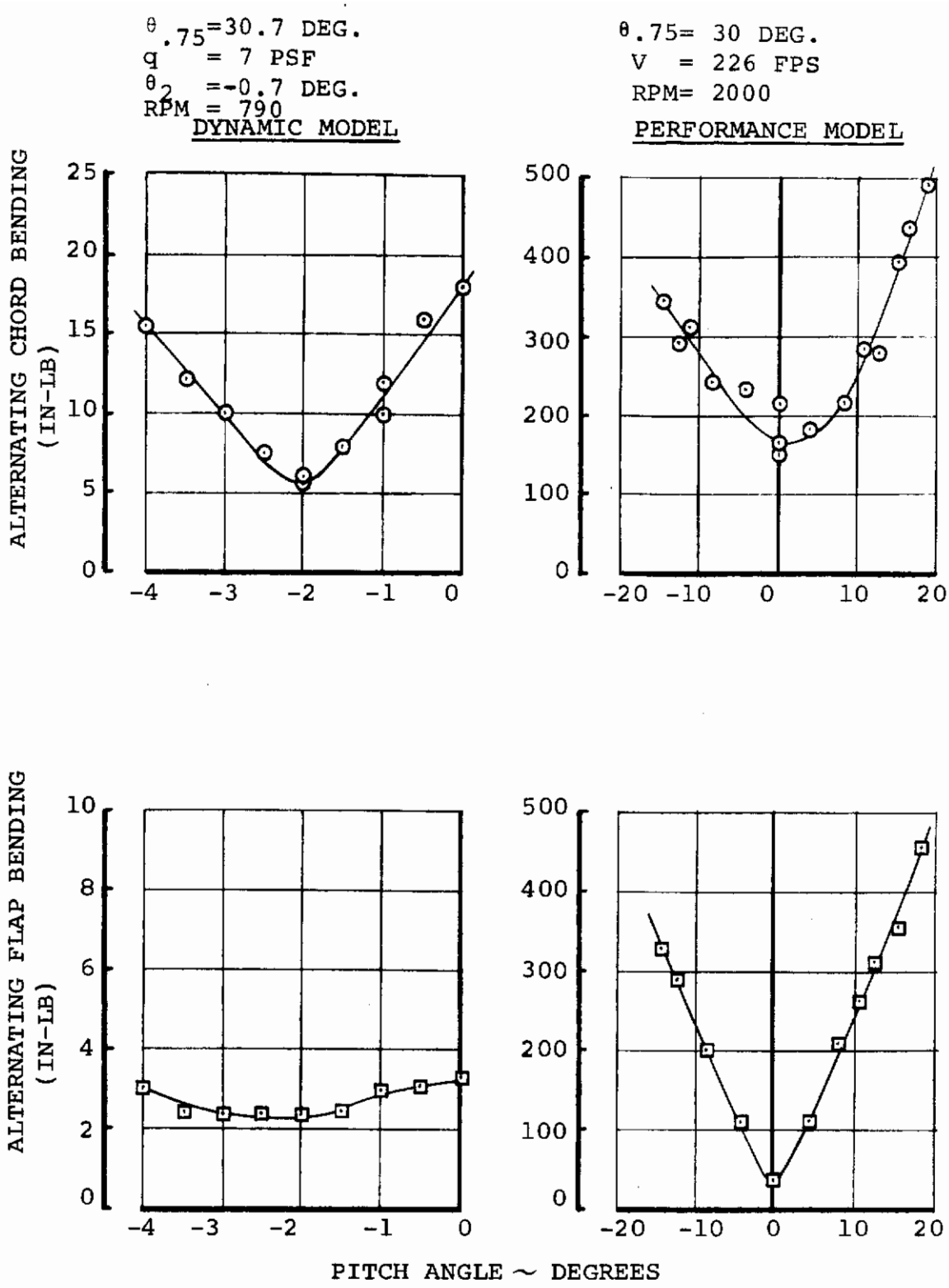

FIGURE 3.12 EFFECT OF AIRCRAFT PITCH ON BLADE ROOT BENDING MOMENTS IN CRUISE FLIGHT

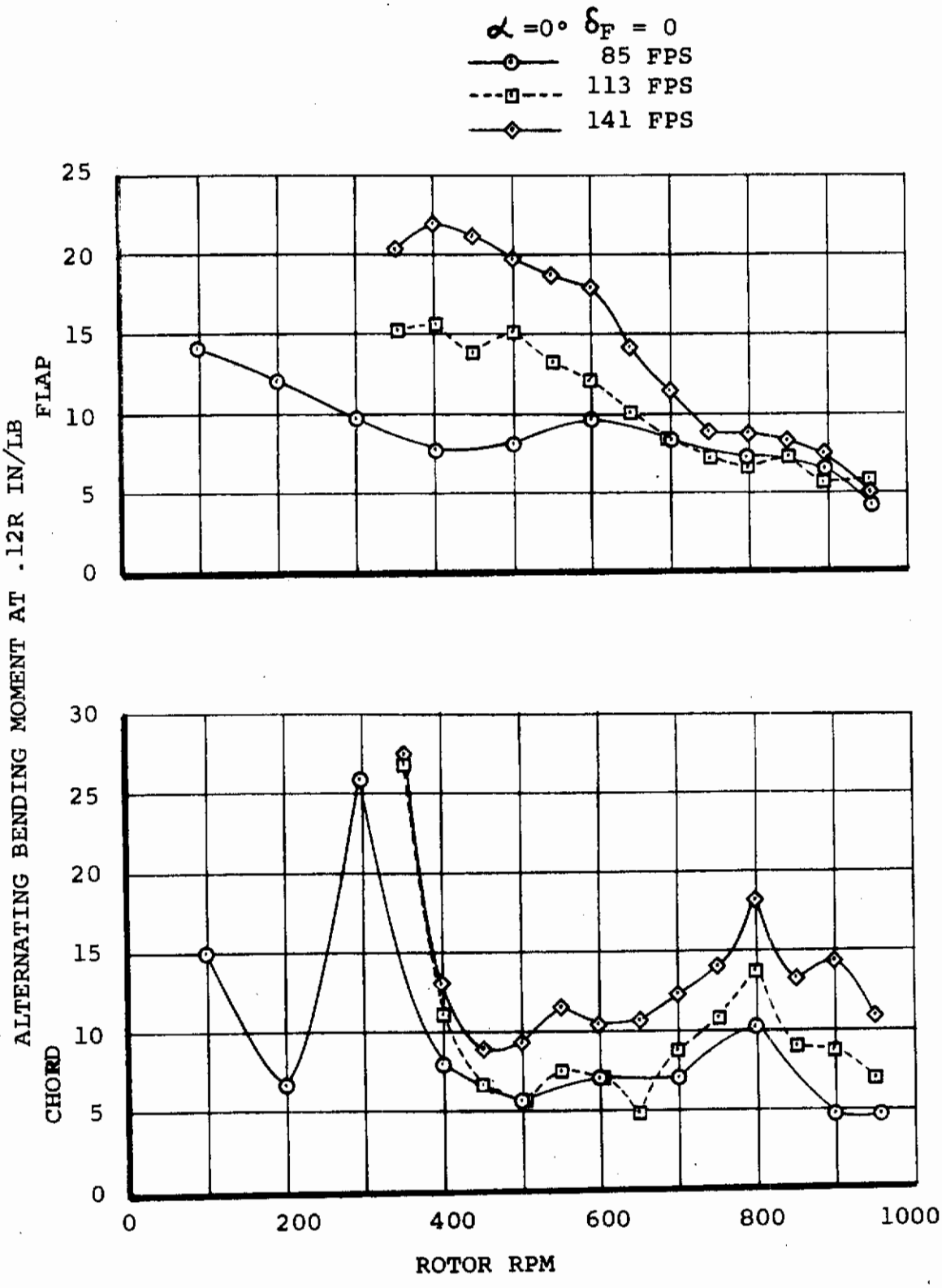

FIGURE 3.13 ALTERNATING BLADE BENDING MOMENTS FOR STEADY WINDMILLING 1/9 SCALE STOWED ROTOR MODEL

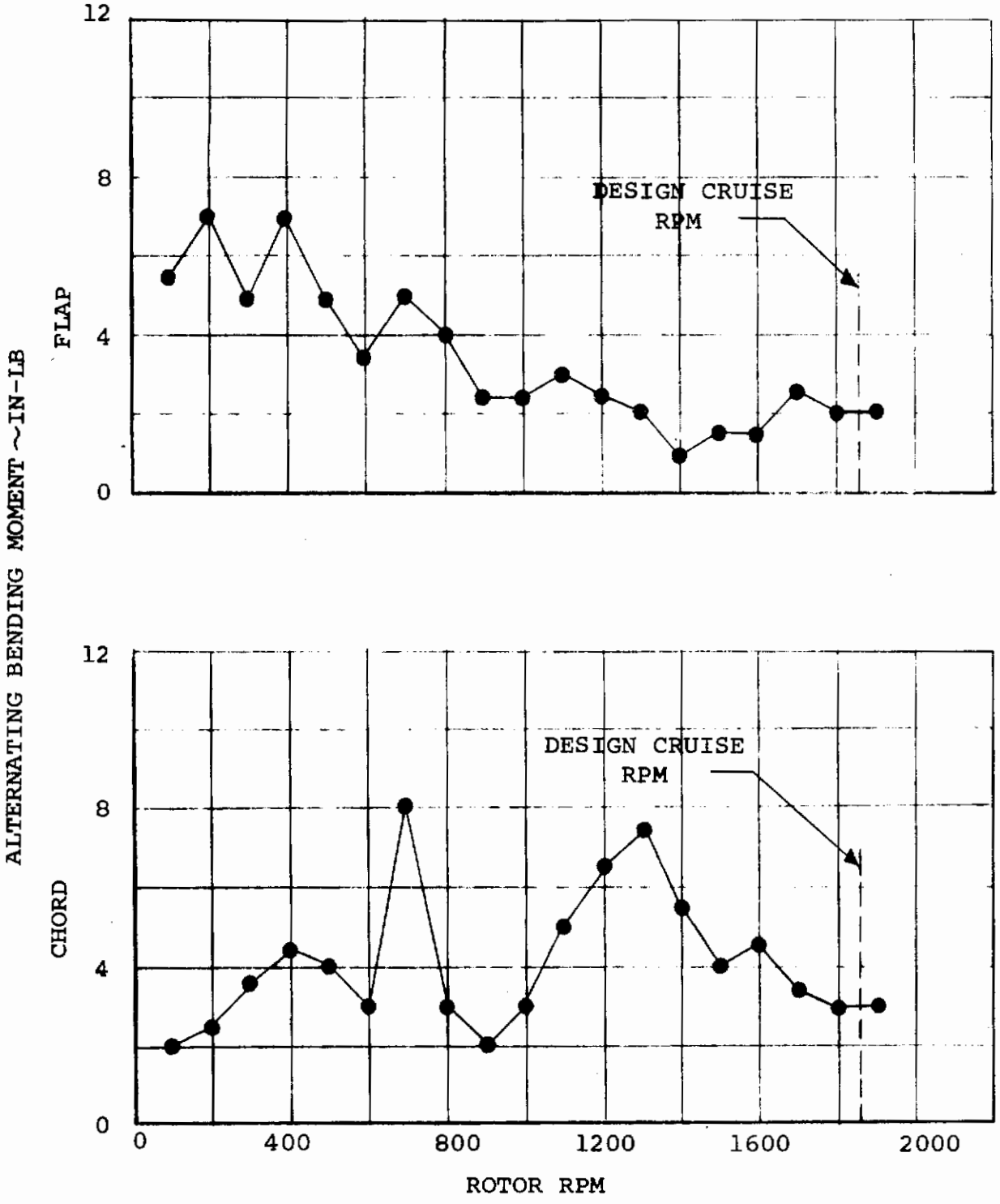

FIGURE 3.14 ALTERNATING BLADE BENDING MOMENTS FOR STEADY WINDMILLING
1/16 SCALE CONVERSION MODEL

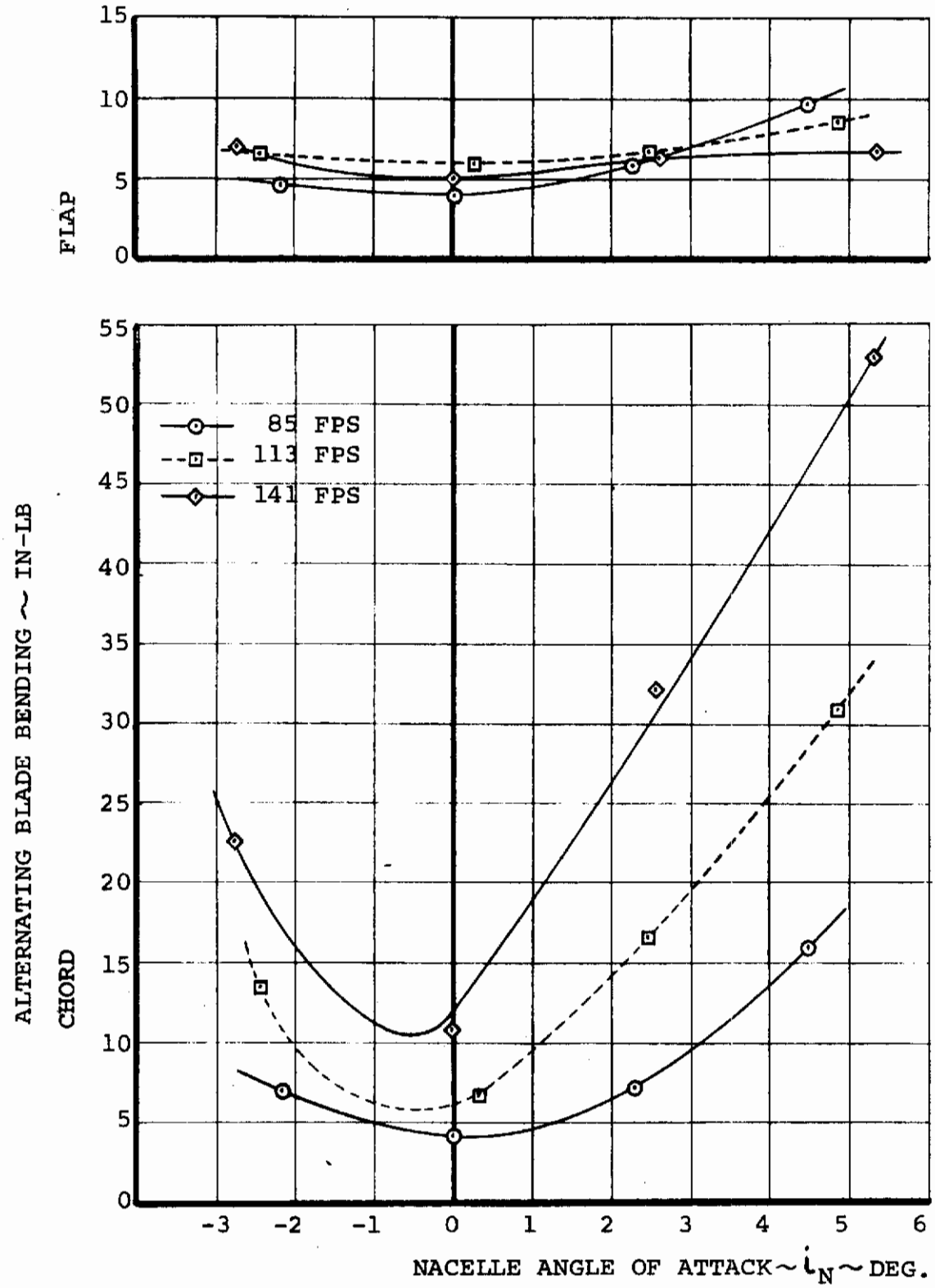

FIGURE 3.15 ALTERNATING BLADE BENDING FOR THREE TUNNEL SPEEDS AND VARIOUS NACELLE ANGLES AT 950 RPM

TABLE 3.7

SUMMARY OF MEASURED BLADE LOADS FOR CONVERSION MODELS

CONDITION	ALTERNATING BENDING MOMENT - IN-LB			
	1/16 SCALE MODEL		1/9 SCALE MODEL	
	CHORD	FLAP	CHORD	FLAP
MAXIMUM LOAD SPINUP AND SPINDOWN	8.	7.	26.	18.
LOAD AT CRUISE RPM	3.*	2.*	12.**	18.**
LOAD AT HOVER RPM	-	-	11.**	5.**
LOAD PER/DEG. PITCH CRUISE RPM	4.	1.	-	-
LOAD PER/DEG. PITCH HOVER RPM	-	-	8.	1.

* 135 FPS VELOCITY

** 141 FPS VELOCITY

3.5.5 Rotor Stowing and Deploying

Folding and deployment tests were performed using blade edgewise and flatwise methods. The blade steady bending moment measured during those cycles were no higher than those for the stopped or feathered rotor condition and did not result in any limitation to the folding method. Typical steady load trend with blade fold angle are shown from the 1/9 scale conversion model in Figures 3.16 and 3.17. The blade bending deflections observed for the 1/9 scale model with stopped rotor indicated that the maximum bending moments were at approximately the blade mid-span. The moments calculated for 40 percent radius considering air loads are 2.2 times higher than at 12.5 percent radius (blade strain gage radius). This essentially confirms the observed deflections.

The vibratory bending moments during all stowing and deploying tests were insignificant.

3.6 BLADE LOAD CORRELATION

Measured blade loads are correlated with analytical predictions for selected conditions showing the effect of cyclic pitch and rotor angle of attack for both pitch and yaw. The tilt rotor dynamic and performance model and the 1/9 scale conversion model test data are included. Most of the correlation is for alternating blade flap and chord bending moments. Blade alternating torsional moment due to stall flutter measured during testing of 5' diameter blades reported in reference 3.2 is correlated with D-88 predictions using unsteady aerodynamics.

3.6.1 Evaluation of Blade Load Prediction Capability

The successful design of a propeller/rotor blade depends to a large extent on the capability to predict the rotor blade loads and the identification of critical flight conditions. Correlation of predicted and measured blade bending moments using the Program D-88 is shown in Paragraph 3.6 for three structurally and dynamically different prop/rotor blades.

The tilt rotor performance model blade is of fiberglass construction with high bending stiffness. The tilt rotor dynamic model was constructed with an aluminum spar and titanium alloy root fittings. The flap bending frequency ratio for this blade was 1.2 and the chord bending ratio less than one (soft-in-plane). The 1/9 conversion model blade was constructed of a steel spar with matched flap and chord stiffness inboard of 30 percent radius.

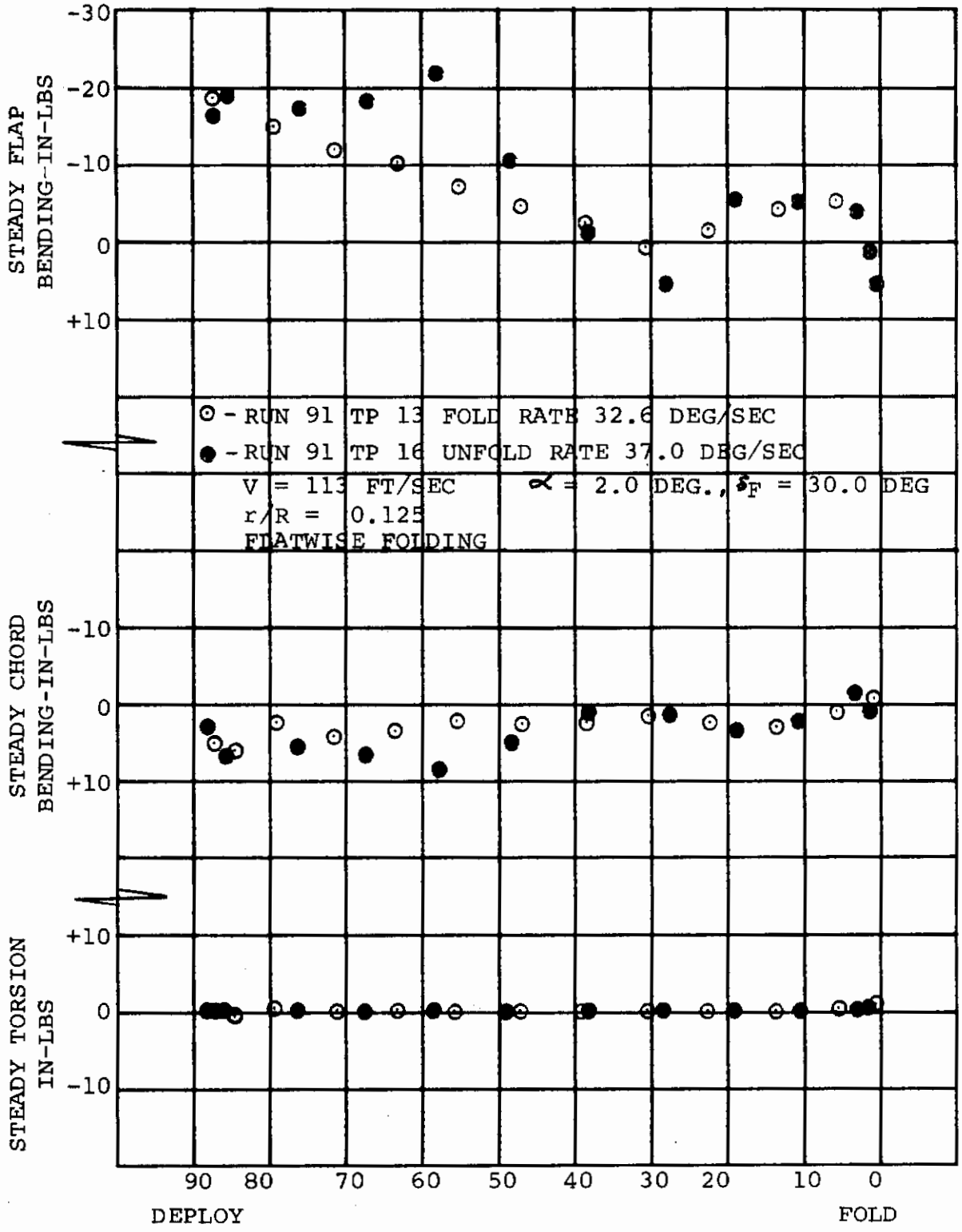

FIGURE 3.16 STEADY BLADE LOADS DURING DYNAMIC FOLD AND DEPLOYMENT, FLATWISE FOLDING

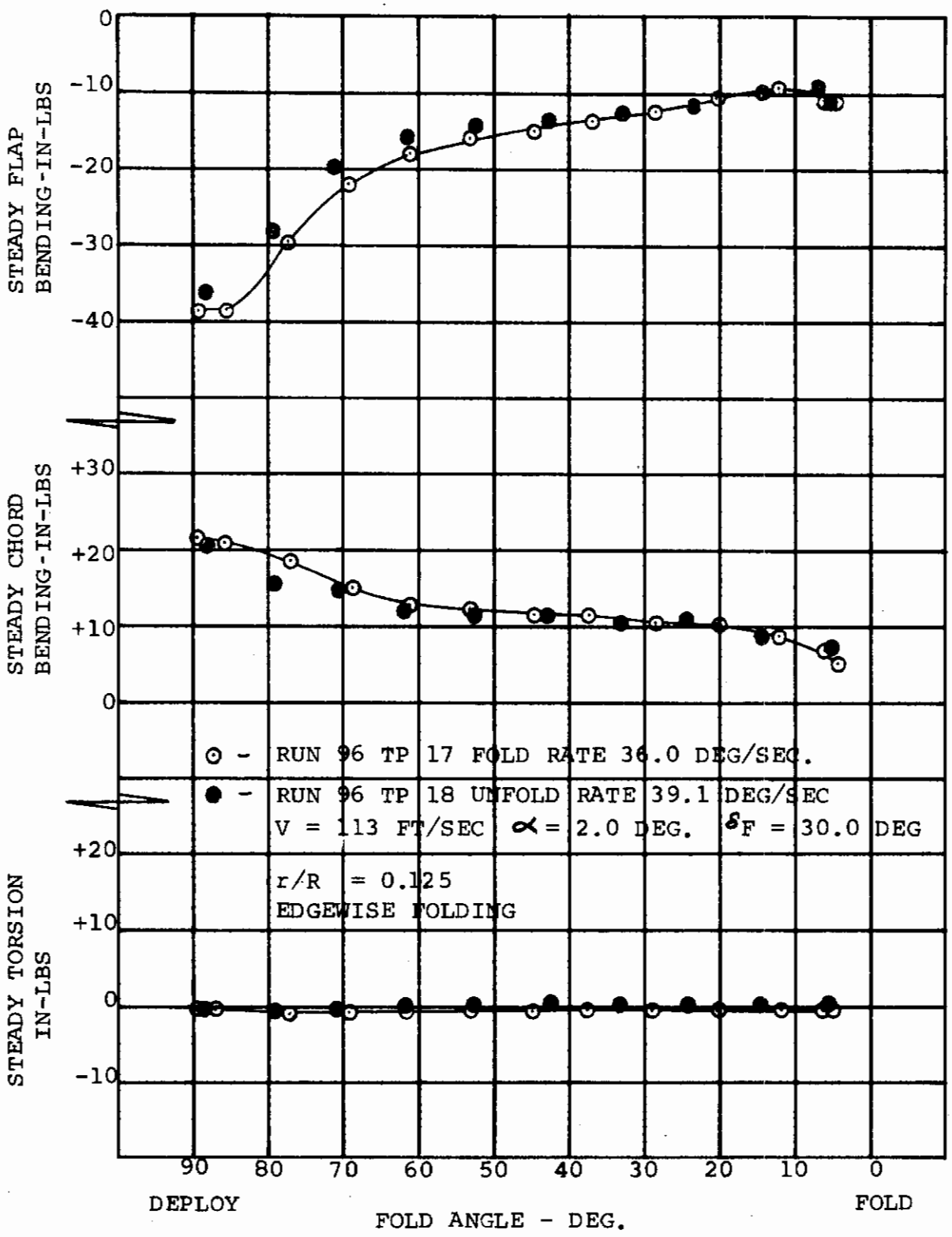

FIGURE 3.17 STEADY BLADE LOADS DURING DYNAMIC FOLD AND DEPLOYMENT, EDGEWISE FOLDING

The bending frequencies were similar to the tilt rotor dynamic blade. Both of the latter blades are dynamically similar to the soft-in-plane propeller/rotor designed in the component design phase, Reference 1.2.

The three models were also mounted by quite different methods. The performance model was sting-mounted, the dynamic model was freely suspended and the semi-span conversion model had a cantilevered wing. The analysis used in the correlation presented here didnot attempt to represent these various differences and the analysis assumed a rigidly mounted rotor isolated from the model dynamics or vibration.

The free suspension of the tilt rotor dynamic model resulted in questionable measurements of aircraft attitudes and angular velocities. For this model rotor unbalance, vibration and hub motions produced noticeable effects on blade load levels and slope of blade load with cyclic pitch and attitude variation. The vibrations, etc. present on other models primarily effected a change in load levels, but not the slope.

The D-88 program analysis was selected for the initial correlation study because of the following features:

a. It is fully operational.
b. It has been used over 10 years for helicopter rotor analysis.
c. It incorporates an unsteady aerodynamics capability
d. It has a wing interference effect capability.

The D-88 program was originated for helicopter rotor blades with relatively low twist, and intended for use in edgewise flight at low collective pitch angles. The program is an uncoupled flap/lag analysis and the blade stiffnesses are input in-plane and out-of-plane of the rotor without accounting for the twist. It is therefore seen that the stiffnesses cannot be truly represented in the program. For a flexible hingeless rotor the blade bending for the first in-plane and out-of-plane modes takes place over the inboard area of the spar. Providing the uncoupled and coupled frequencies are approximately the same, the D-88 program, although not exact, will perform a satisfactory analysis.

A summary of the prediction capability is presented in Table 3.8. Ratings of good, fair or poor for load level and slope are given to each one of the correlation figures. The predictions for the tilt rotor dynamic model in transition and cruise are poor compared to the other models due to the model problems previously discussed.

TABLE 3.8 SUMMARY OF BLADE LOAD PREDICTION CAPABILITY

MODEL	DIRECTION	CONDITION	PARAMETER	PROGRAM	FIG.NO.	RATING	
						SLOPE	LEVEL
DYNAMIC	FLAP	HOVER	CYCLIC	D88	3.18	FAIR	POOR
DYNAMIC	CHORD	HOVER	CYCLIC	D88	3.19	FAIR	BAD
DYNAMIC	CHORD	TRANSITION	CYCLIC	D88	3.24	BAD	POOR
DYNAMIC	FLAP	TRANSITION	CYCLIC	D88	3.25	BAD	POOR
DYNAMIC	FLAP	CRUISE	ψ	L22	3.28	GOOD	POOR
DYNAMIC	CHORD	CRUISE	ψ	L22	3.29	BAD	BAD
DYNAMIC	FLAP	CRUISE	α	D88	3.34	FAIR	GOOD
DYNAMIC	CHORD	CRUISE	α	D88	3.35	POOR	POOR
DYNAMIC	FLAP	CRUISE	CYCLIC	D88	3.36	GOOD	FAIR
DYNAMIC	CHORD	CRUISE	CYCLIC	D88	.37	BAD	BAD
PERFOR-MANCE	FLAP	HOVER	CYCLIC	D88	3.20	GOOD	GOOD
PERFOR-MANCE	CHORD	HOVER	CYCLIC	D88	3.20	GOOD	BAD
PERFOR-MANCE	FLAP	TRANSITION	α	D88	3.26	GOOD	FAIR
PERFOR-MANCE	CHORD	TRANSITION	α	D88	3.27	POOR	BAD
PERFOR-MANCE	FLAP	CRUISE	ψ	L22	3.30	GOOD	FAIR
PERFOR-MANCE	CHORD	CRUISE	ψ	L22	3.31	FAIR	POOR
PERFOR-MANCE	FLAP	CRUISE	α	D88	3.32	OOD	GOOD
PERFOR-MANCE	CHORD	CRUISE	α	D88	3.33	GOOD	POOR
PERFOR-MANCE	FLAP	CRUISE	FLAP SETTING	D88	3.38	GOOD	FAIR
PERFOR-MANCE	CHORD	CRUISE	FLAP SETTING	D88	3.39	POOR	POOR
1/9 SCALE	FLAP & CHORD	WINDMILL	α	D88	3.40	FAIR	FAIR
NASA PERFOR.	TORSION	HOVER	C_T/σ	D88	3.23	FAIR	FAIR

The analysis predicts the flap bending moments in hover due to cyclic pitch if consideration is given to the higher harmonic bending due to model vibration. However, the chord bending moments are underpredicted. This is attributed partially to the sensitivity of the blade in-plane bending to the in-plane frequency, the residual built-in cyclic in the small scale models and to difficulty in obtaining the correct frequency response in the load analysis.

The unsteady aerodynamics feature of the D-88 program identifies the occurrence and the characteristics of stall flutter. The program is being improved continuously by introduction of unsteady airloads data from airfoil and rotor tests. A very aggressive program is being pursued by The Boeing Company in this area.

For transition and cruise the analysis predicts the order and general trend of flap bending moments due to aircraft or rotor attitude and cyclic pitch. The chord bending moment parametric changes is predicted but at a lower level because of the residual cyclic and frequency effects.

Program L-22 is also operational but has had limited application to date. It was specifically designed to calculate the coupled flap/chord forced vibrations of highly twisted propeller blades. The analysis uses linear aerodynamics and at the present time the effect of wing interference is not included. Correlation with and improvements to this program are considered to be the next steps.

Recognizing the need for improved analytical methods for both blade load and stability, the USAF awarded a contract to Boeing in early 1971 for the development of improved methodology.

Program C-70 is being developed under this contract and will be operational by the end of 1971. It is designed specifically for propeller/rotor analysis and will include flap/lag/pitch coupling and unsteady aerodynamics. This program will basically combine the desirable features of D-88 and L-22 programs and is anticipated to provide a considerable technology advance and improved blade load prediction capability.

3.6.2 Hover

Measured alternating blade bending moments caused by rotor cyclic pitch in hover are correlated with program D-88. Data are shown in Figures 3.18 and 3.19 for the dynamic model (Test Program IV), and in Figure 3.20 for the performance model (Test Program II). The analyses are for an isolated rigidly mounted rotor and they predict zero bending moments for the zero cyclic case. The non-zero flap bending moment at zero cyclic for the dynamic model is caused by higher bending harmonics and residual cyclic pitch. The chord bending moment shift in load level is due to residual cyclic out of phase with the models monocyclic control and also rotor unbalance. The mismatch between test and theory is also discussed in Paragraph 3.6.1.

Figure 3.20 shows good correlation with flap bending test data. The shift in alternating chord bending moment between analysis and theory is caused by the 6th harmonic for which the analysis was not correctly modeled. This is shown in Figures 3.21 and 3.22 where the waveforms indicate that good chordwise correlation exists for the 1/rev components of the measured bending moments. The 6/rev is due to a third bending mode and/or torsional response of the blade.

Blade stall flutter was encountered during testing of the tilt rotor models. The conditions and test data have not been analyzed in sufficient detail for correlation with analytical predictions. However, the unsteady aerodynamic capability of the D-88 analysis program has been utilized to predict stall flutter for other prop/rotor model blades. Figure 3.23 shows the test and analytical results for the 5-foot diameter prop/rotor test reported in Reference 3.2. The analysis shows good correlation of the alternating root torsion with increase in rotor thrust coefficient C_T/σ. The growth in the alternating torsion predicted by the analysis is due to the increase of the sixth harmonic component which corresponds to the blade torsional frequency ratio of 5.67/rev at 2000 RPM rotor speed.

3.6.3 Transition

Correlation of measured and predicted blade bending moments is shown for transition flight for variation of cyclic pitch angle and aircraft angle of attack. The test data for the tilt rotor dynamic model shows the effect of cyclic pitch and the data for the tilt rotor performance model shows the effect of aircraft angle of attack. The nacelle tilt angles are 40 degrees and 45 degrees respectively.

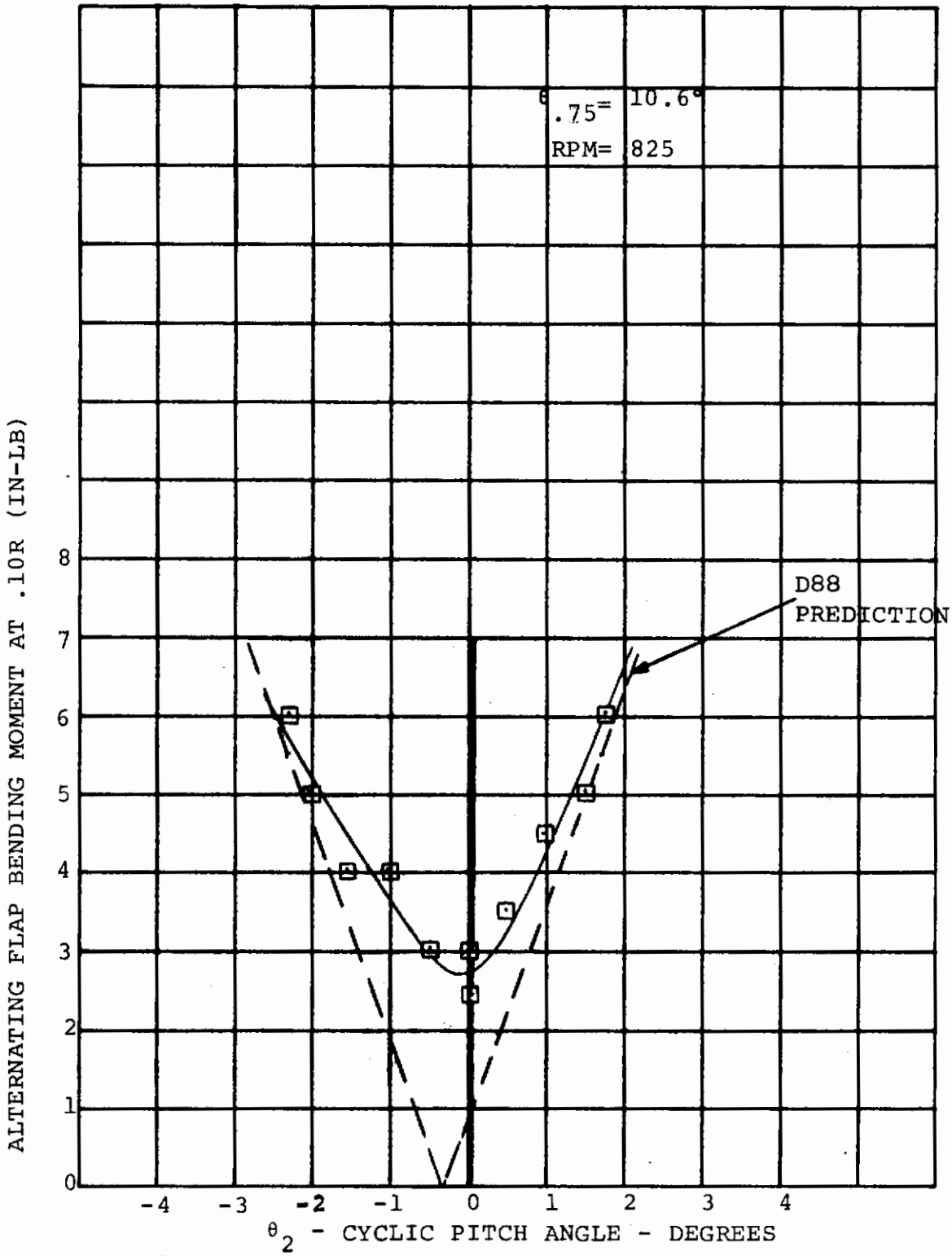

FIGURE 3.18 CORRELATION OF MEASURED AND PREDICTED ROTOR ALTERNATING FLAP BENDING MOMENT IN HOVER WITH CYCLIC PITCH VARIATION-TILT ROTOR DYNAMIC MODEL

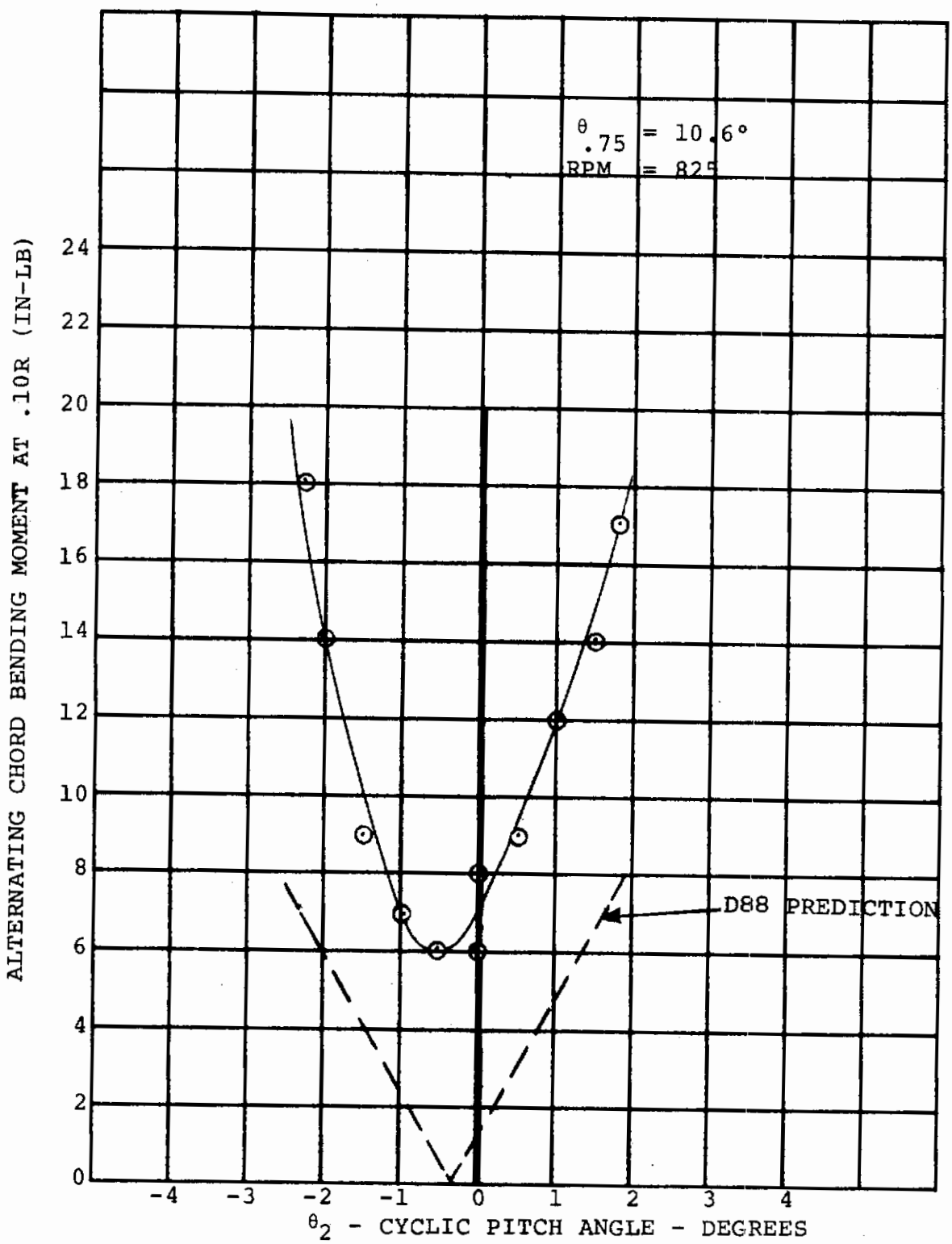

FIGURE 3.19 CORRELATION OF MEASURED AND PREDICTED ROTOR ALTERNATING CHORD BENDING MOMENT IN HOVER WITH CYCLIC PITCH VARIATION- TILT ROTOR DYNAMIC MODEL

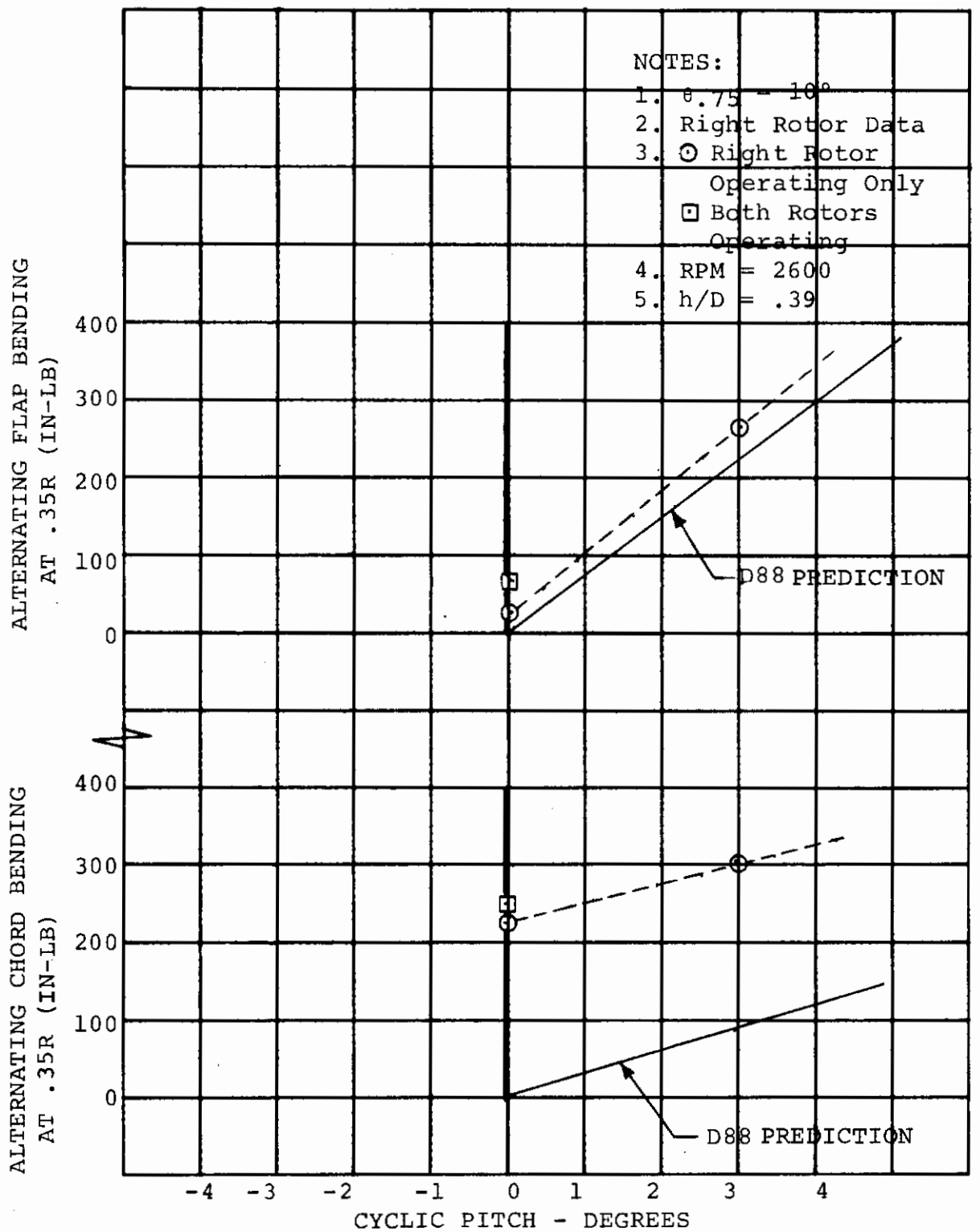

FIGURE 3.20 CORRELATION OF MEASURED AND PREDICTED BLADE LOADS PRODUCED BY CYCLIC PITCH IN HOVER TILT ROTOR PERFORMANCE MODEL

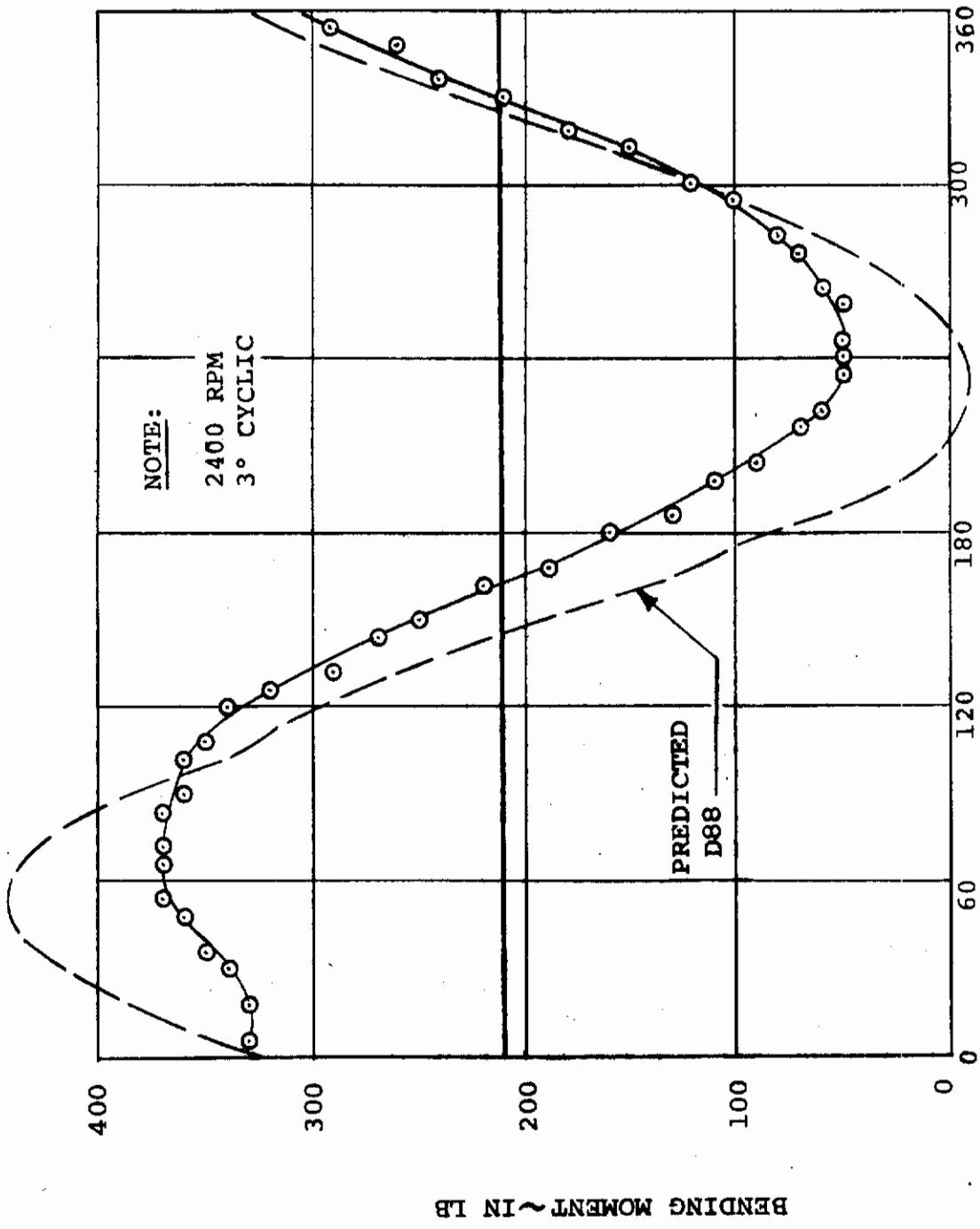

FIGURE 321 CORRELATION OF MEASURED AND PREDICTED ROTOR FLAP BENDING MOMENT WAVEFORM TILT ROTOR PERFORMANCE MODEL

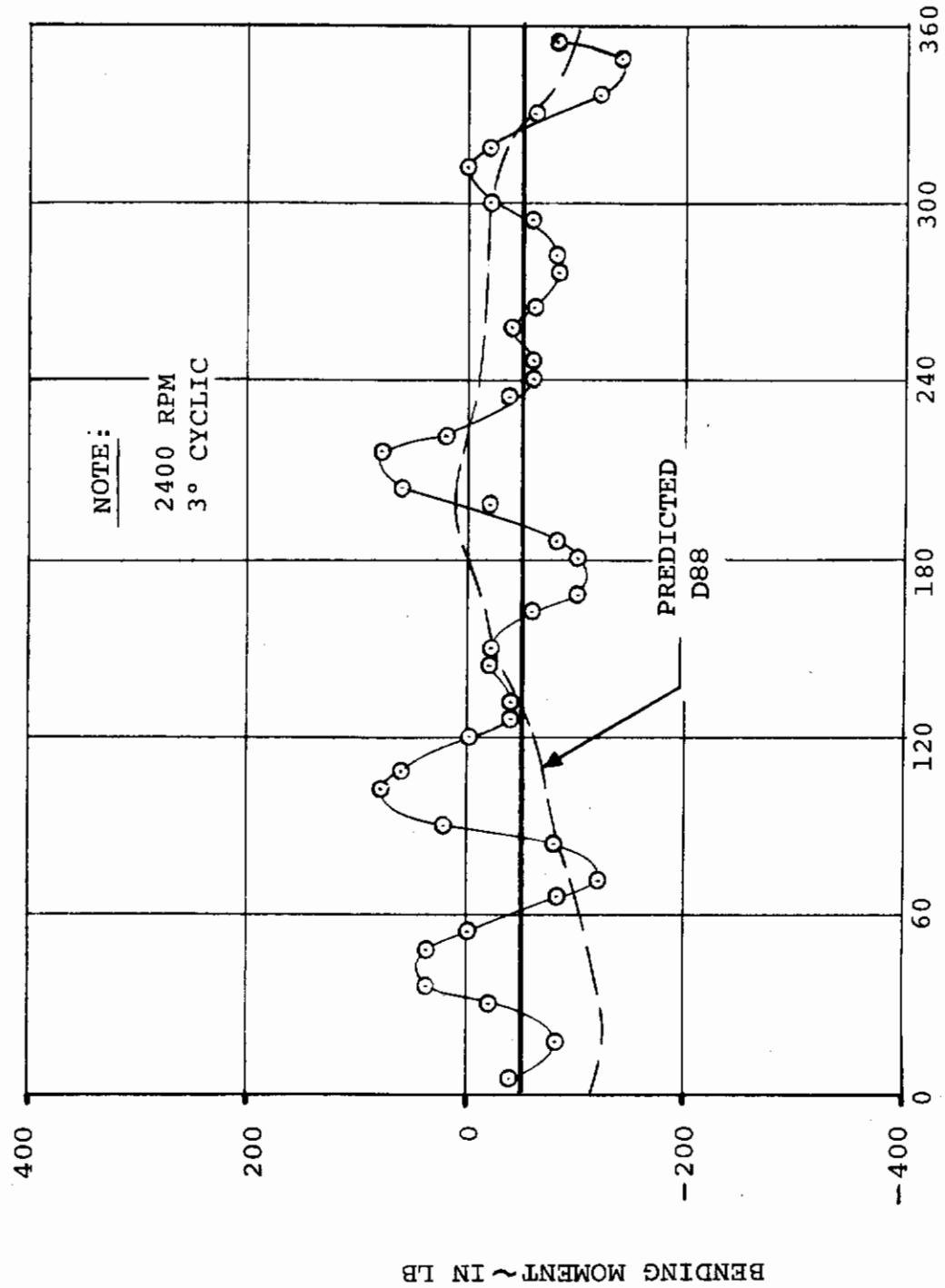

FIGURE 3.22 CORRELATION OF MEASURED AND PREDICTED ROTOR CHORD BENDING MOMENT WAVEFORM
TILT ROTOR PERFORMANCE MODEL

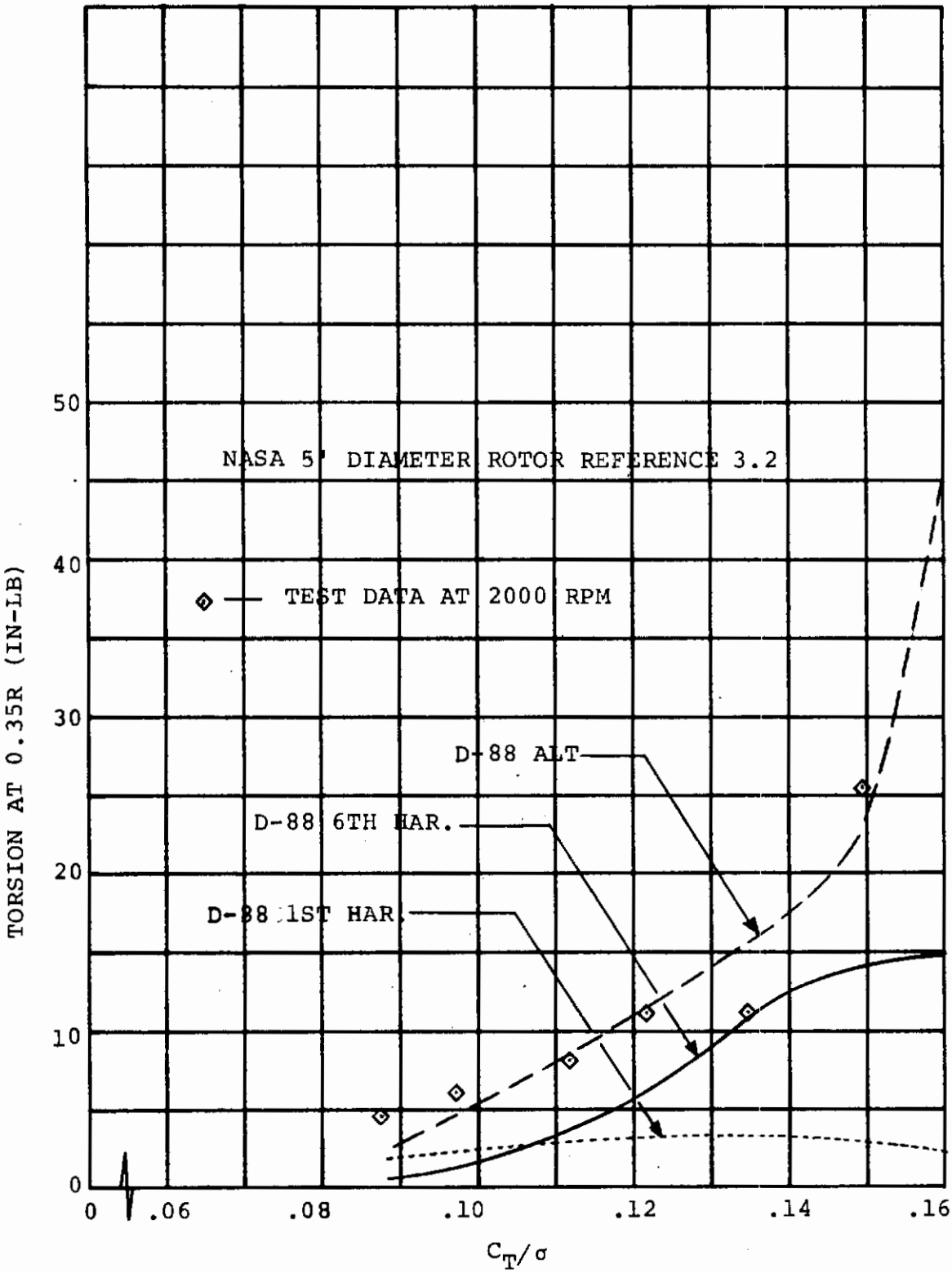

FIGURE 3.23 CORRELATION OF MEASURED AND PREDICTED BLADE ALTERNATING TORSION DUE TO STALL FLUTTER

The D-88 program analysis is used to predict the effect of cyclic pitch in Figures 3.24 and 3.25. The analysis overpredicts the measured flap and chord bending moments by approximately 40 percent. Cyclic pitch is used in transition flight to minimize the alternating bending moments due to the rotor angle of attack. Theoretically, the first harmonic moment can be reduced to zero by the correct cyclic pitch. The test data show that the models longitudinal cyclic pitch input is not correctly phased for minimum loads and that lateral cyclic pitch is required as well to reduce the alternating bending moments. The mismatch between test and theory is also discussed in Paragraph 3.6.1.

The effect of aircraft angle of attack is predicted by D-88 analysis in Figures 3.26 and 3.27 for the performance model. The predicted trend of flap bending moment with angle of attack matches the measured data. The chord bending moments are underpredicted. This is mainly due to the higher harmonic content of the measured data caused by the proximity of the three per rev integer harmonic crossing for the second or lag bending mode as shown in Figure 3.5.

3.6.4 Tilt Rotor Airplane

Correlation of predicted and measured blade alternating flap and chord bending moment for cruise flight with aircraft yaw angle. aircraft pitch angle, cyclic pitch and wing flap deflection is shown in Figures 3.28 through 3.39. The data are for the tilt rotor dynamic and performance models. The L-22 program analysis is used to predict the effect of yaw angle on both models as yaw angle input is not possible with D-88. (The L-22 program was designed for propeller load analysis and has had limited application.) For the dynamic model (Figures 3.28 and 3.29) the analysis predicts the sensitivity of chord versus flap bending to yaw angle variation. The flap bending moments are much lower than chord bending. The analysis greatly overpredicts the sensitivity of chord bending to yaw angle and underpredicts the flap bending. The mismatch between test and theory is also discussed in Paragraph 3.6.1. It is noted again that the L-22 program does not include the effect of wing interference and only includes the influence of gravity at zero yaw angle. For the performance model (Figures 3.30 and 3.31) the analysis closely predicts the flap bending moment trend with yaw angle. The chordwise moment is underpredicted which is mainly due to the proximity of higher harmonic integer crossings of the lag bending modes.

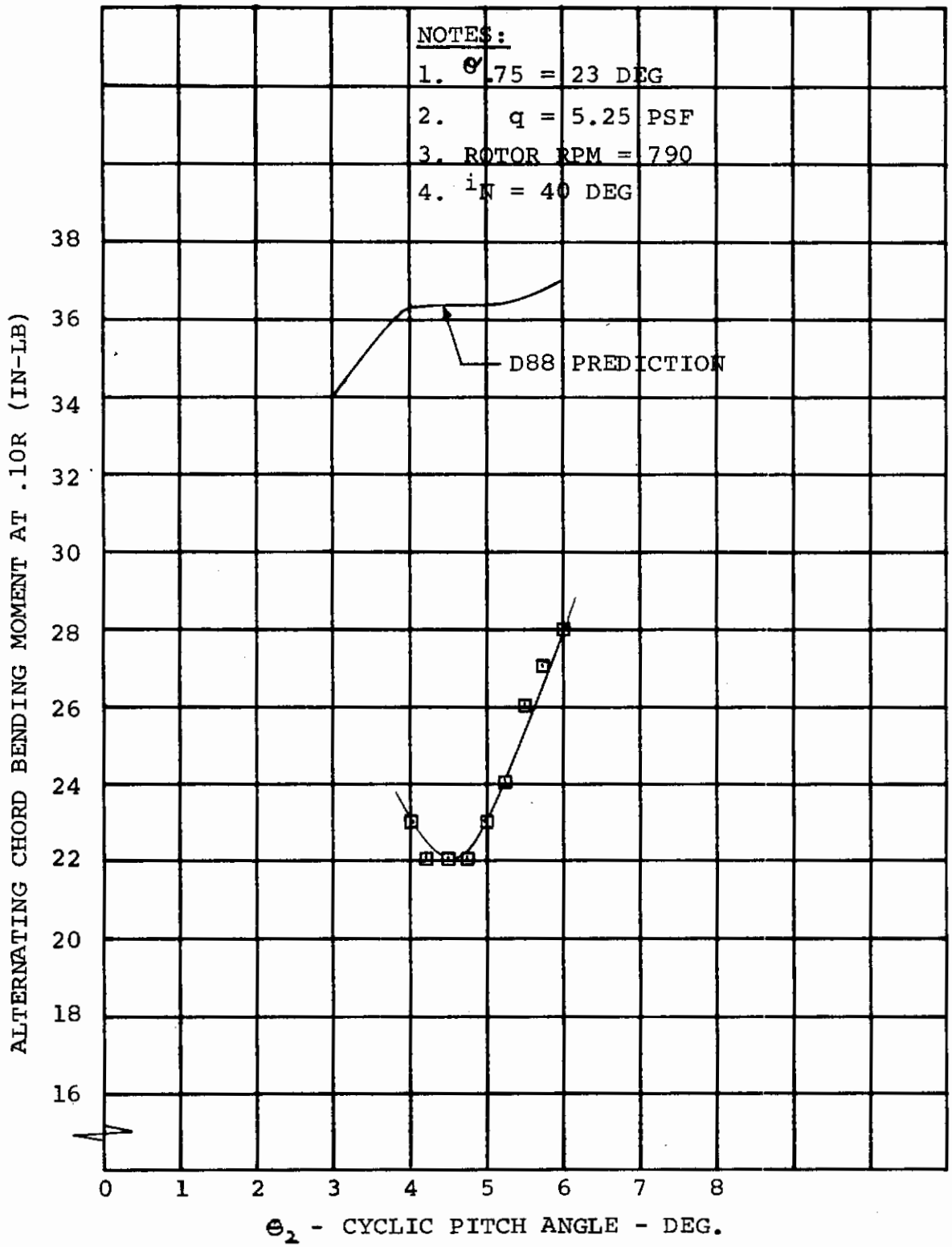

FIGURE 3.24 CORRELATION OF PREDICTED AND MEASURED BLADE ALTERNATING CHORD BENDING MOMENT WITH CYCLIC PITCH ANGLE FOR TRANSITION FLIGHT, TILT ROTOR DYNAMIC MODEL

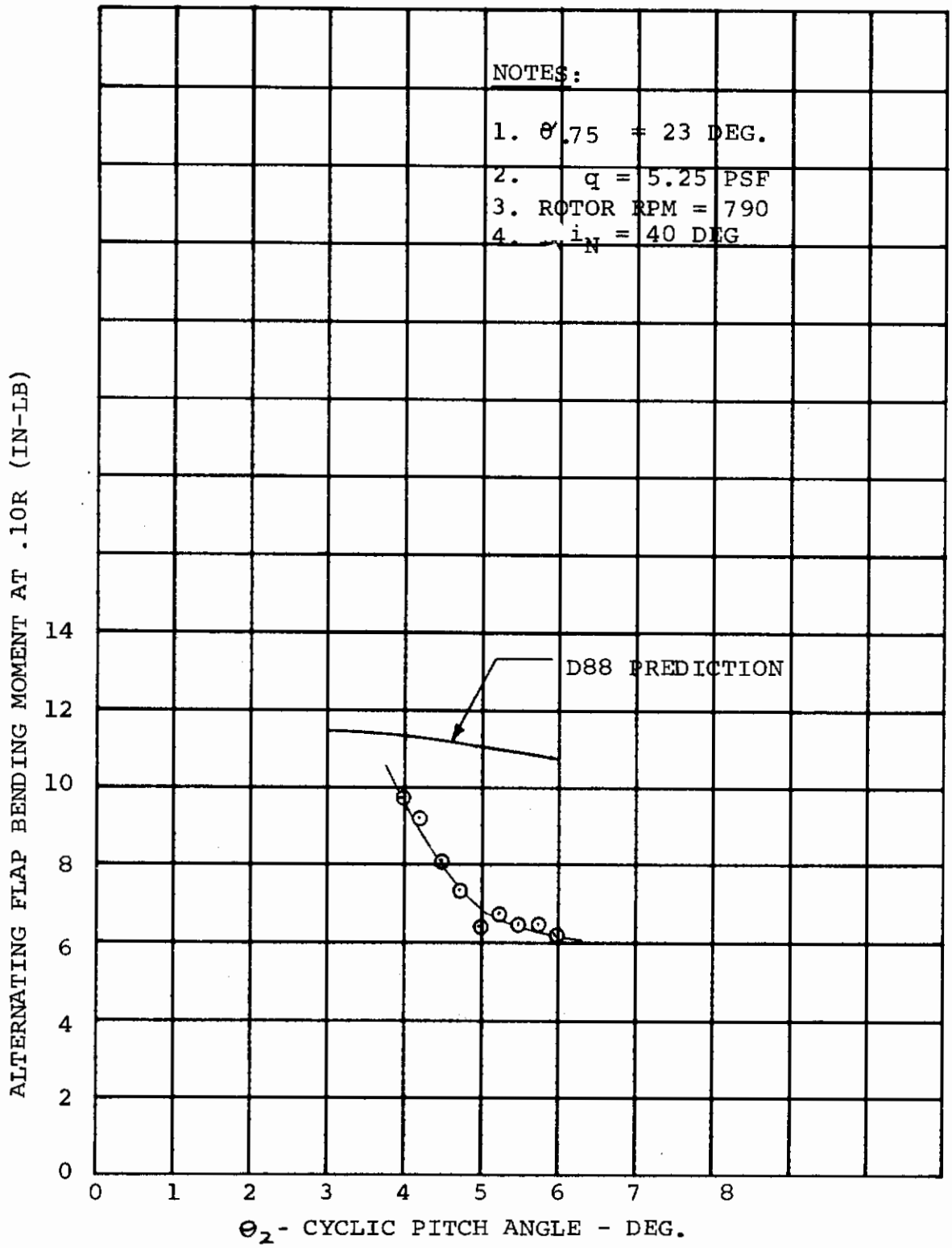

FIGURE 3.25 CORRELATION OF PREDICTED AND MEASURED BLADE ALTERNATING FLAP BENDING MOMENT WITH CYCLIC PITCH ANGLE FOR TRANSITION FLIGHT, TILT ROTOR DYNAMIC MODEL

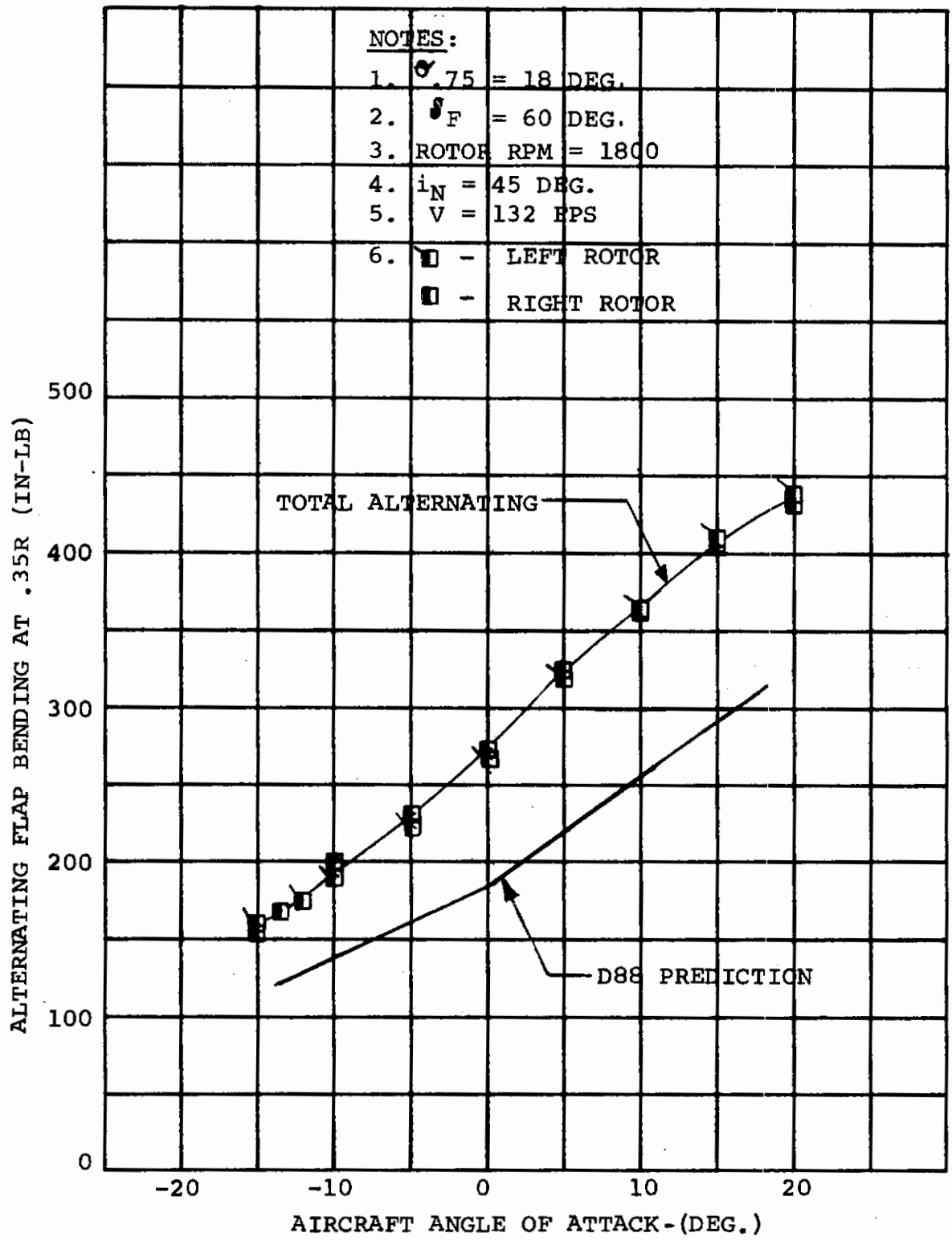

FIGURE 3.26 CORRELATION OF PREDICTED AND MEASURED BLADE ALTERNATING FLAP BENDING MOMENT WITH AIRCRAFT ANGLE OF ATTACK FOR TRANSITION FLIGHT, TILT ROTOR PERFORMANCE MODEL

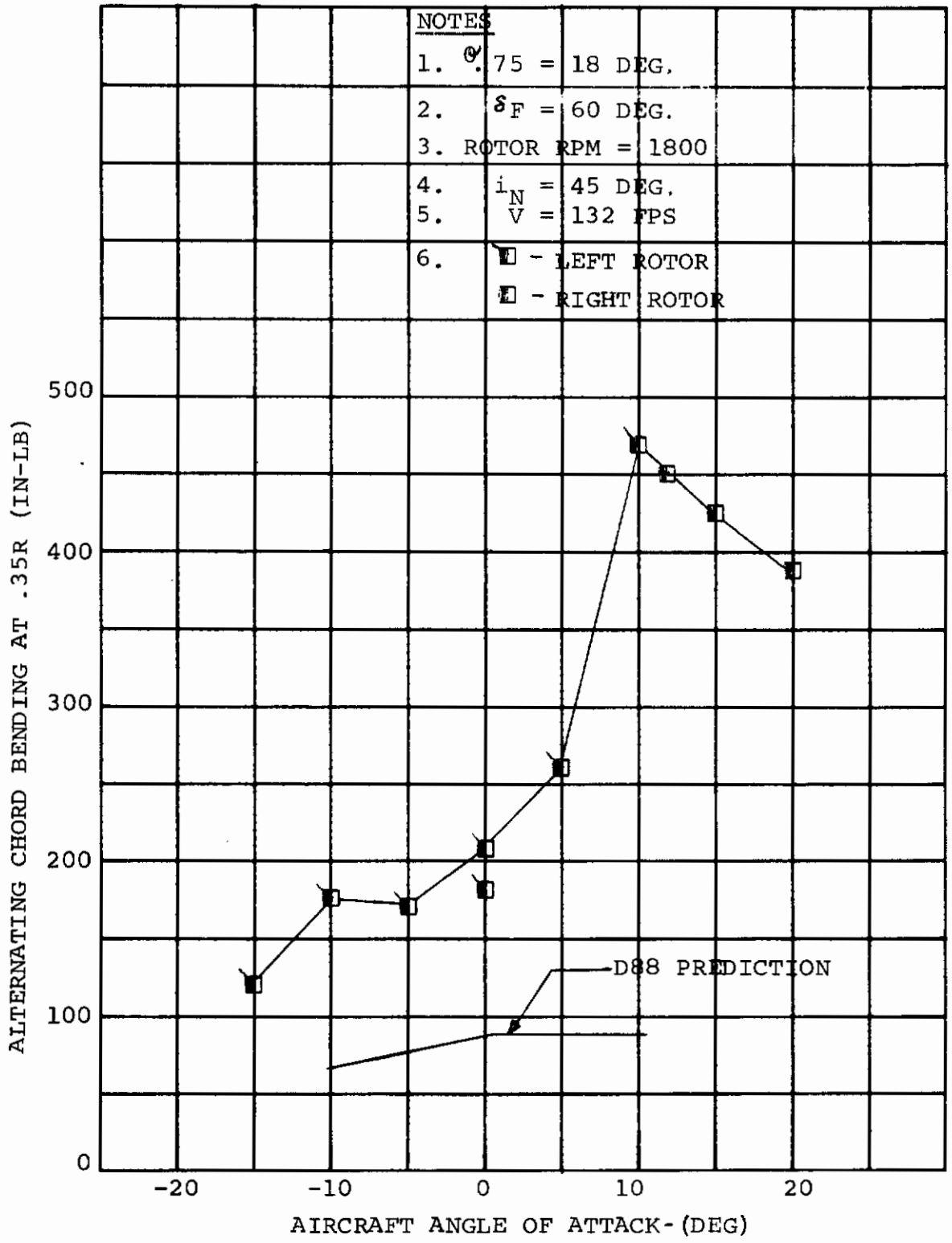

FIGURE 3.27 CORRELATION OF PREDICTED AND MEASURED BLADE ALTERNATING CHORD BENDING MOMENT WITH AIRCRAFT ANGLE OF ATTACK FOR TRANSITION FLIGHT, TILT ROTOR PERFORMANCE MODEL.

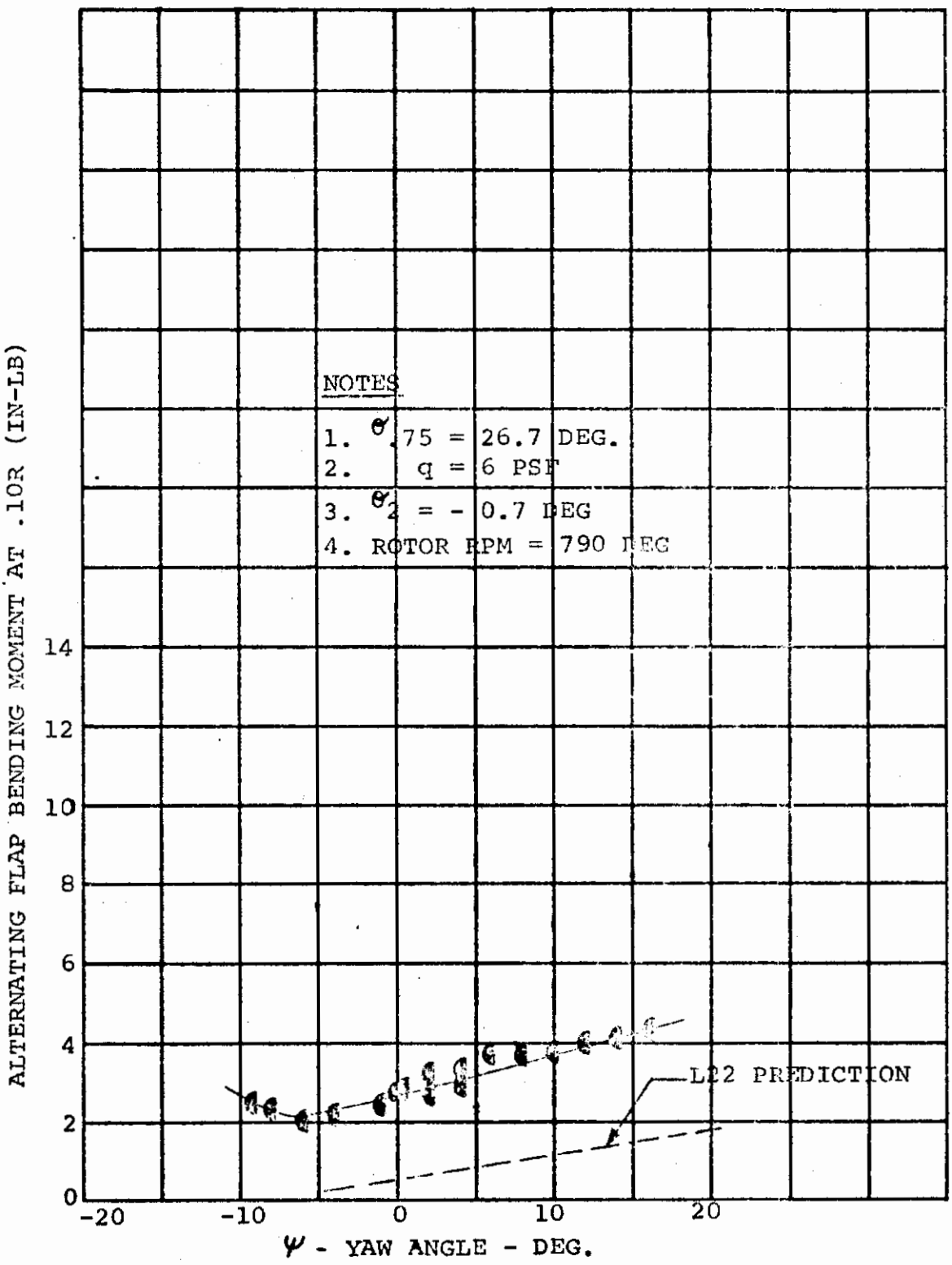

FIGURE 3.28 CORRELATION OF PREDICTED AND MEASURED BLADE ALTERNATING FLAP BENDING MOMENT WITH AIRCRAFT YAW ANGLE FOR CRUISE FLIGHT, TILT ROTOR DYNAMIC MODEL

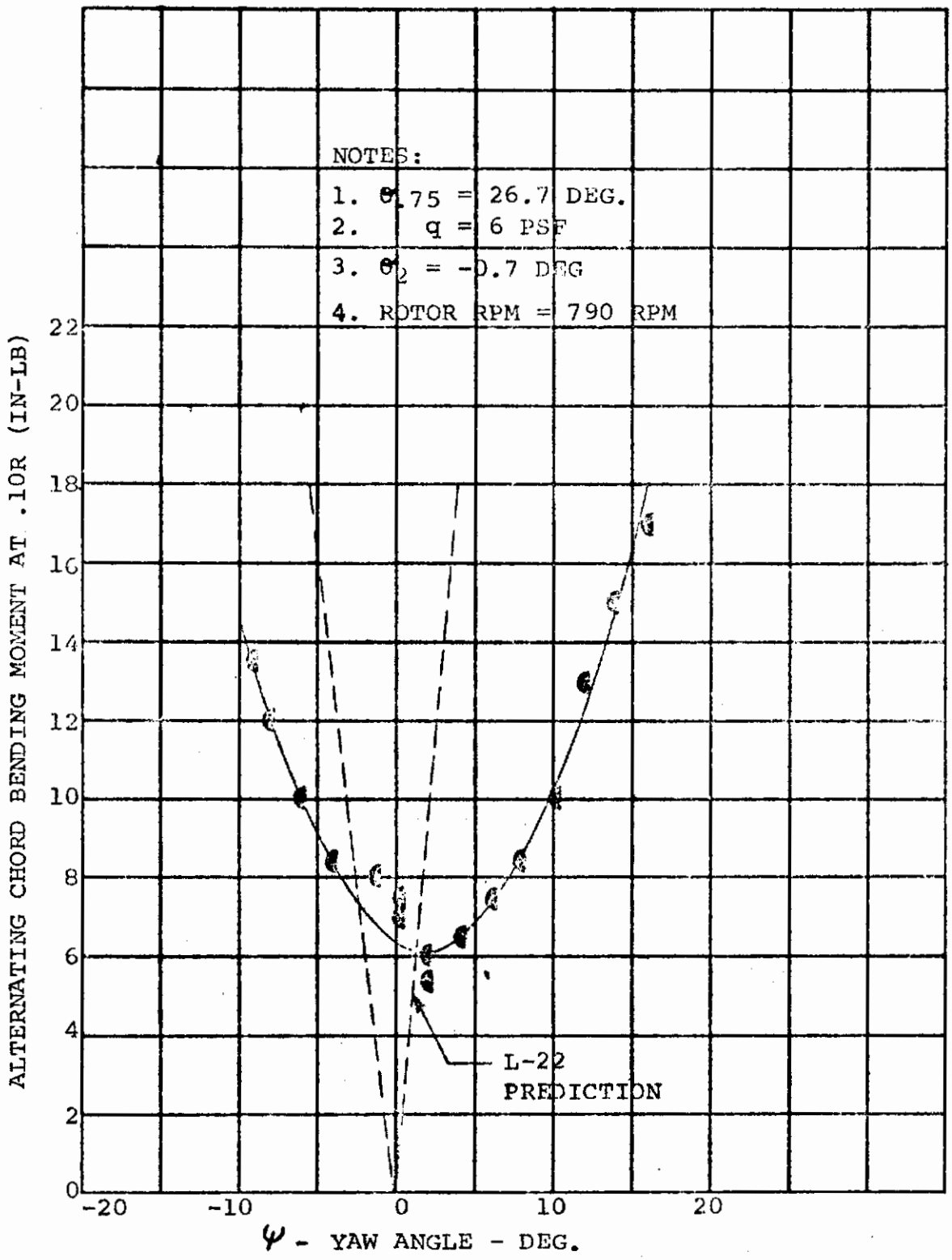

FIGURE 3.29 CORRELATION OF PREDICTED AND MEASURED BLADE ALTERNATING CHORD BENDING MOMENT WITH AIRCRAFT YAW ANGLE FOR CRUISE FLIGHT, TILT ROTOR DYNAMIC MODEL

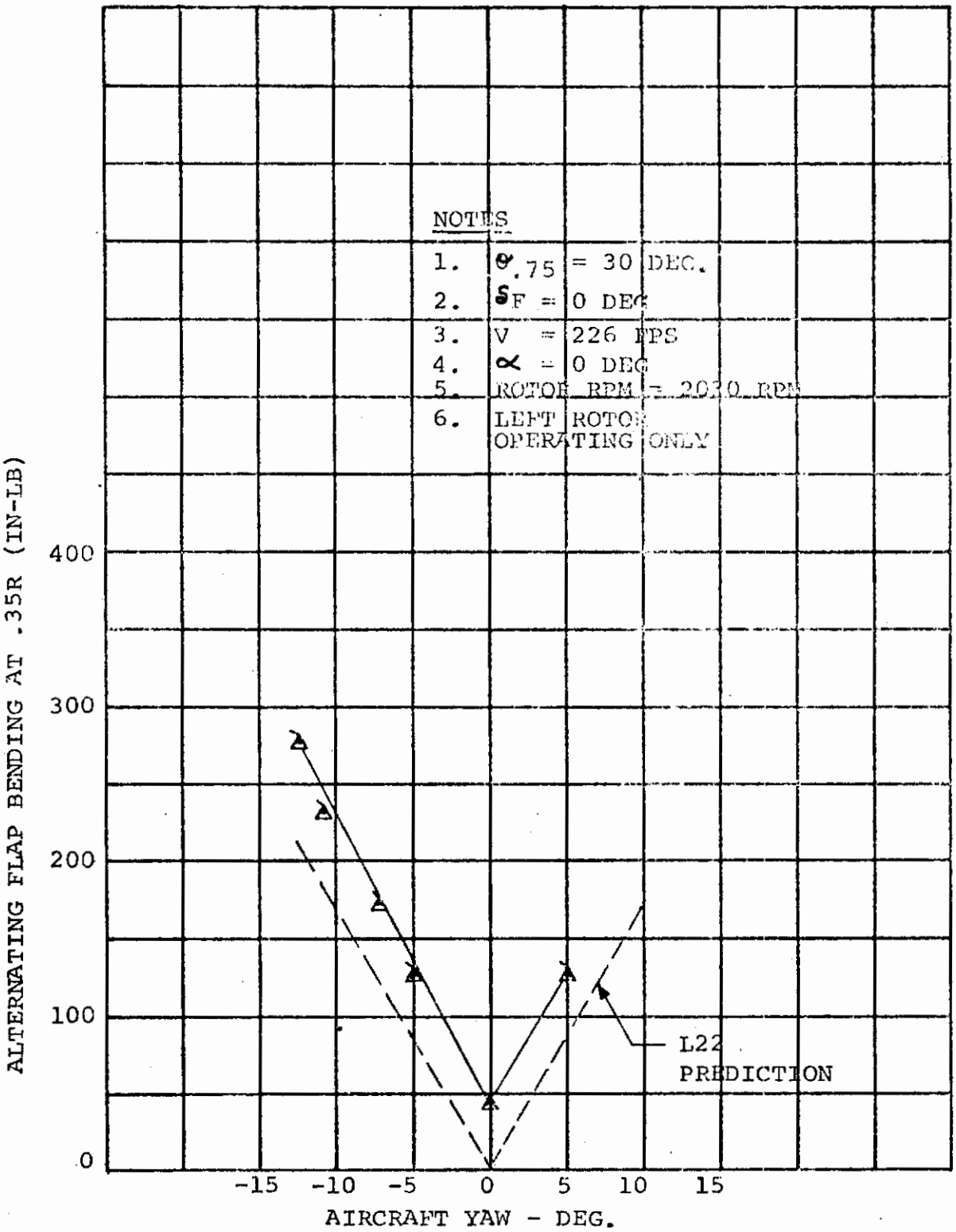

FIGURE 3.30 CORRELATION OF PREDICTED AND MEASURED ALTERNATING BLADE FLAP BENDING MOMENT WITH AIRCRAFT YAW ANGLE VARIATION FOR CRUISE FLIGHT, TILT ROTOR PERFORMANCE MODEL.

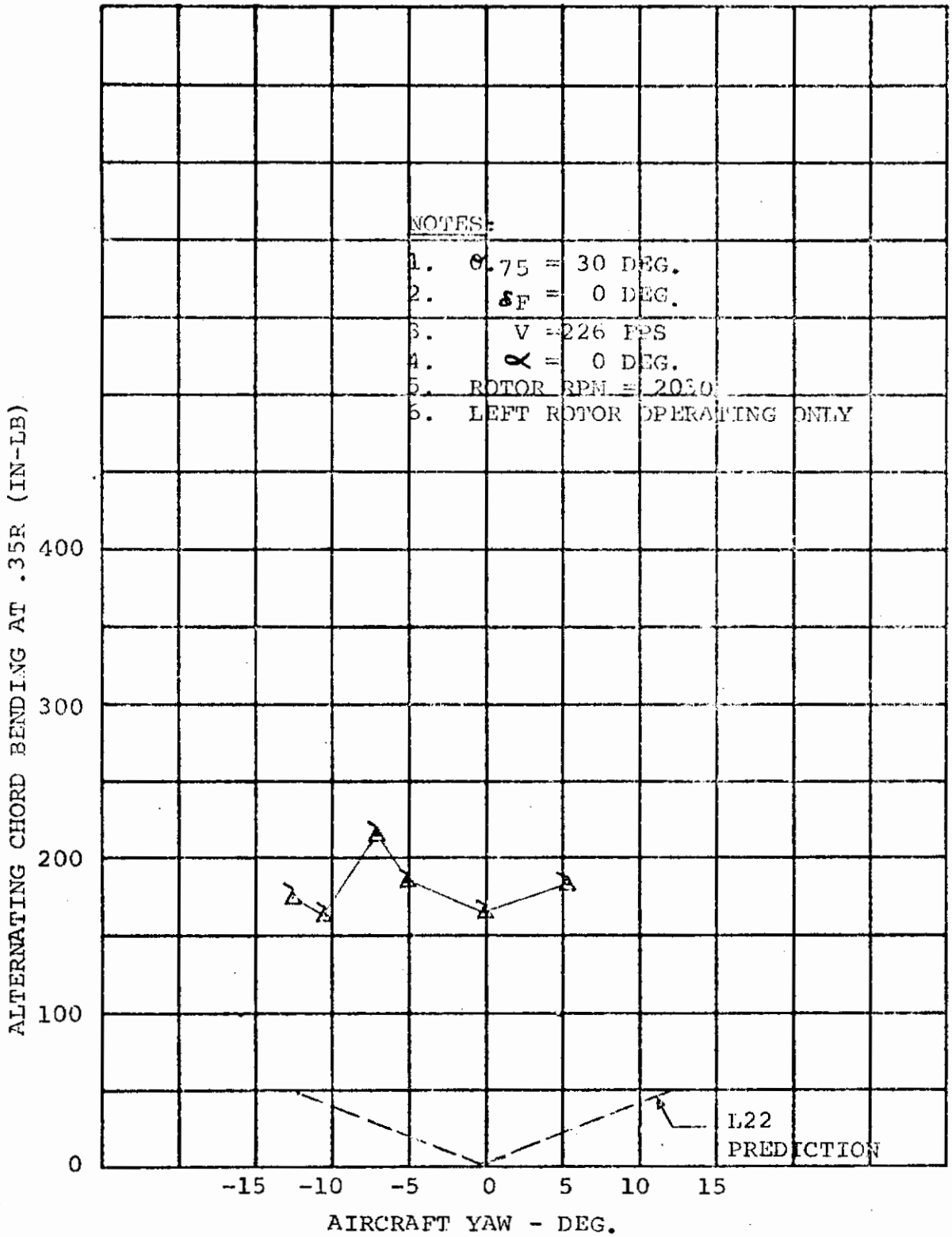

FIGURE 3.31 CORRELATION OF PREDICTED AND MEASURED ALTERNATING BLADE CHORD BENDING MOMENT WITH AIRCRAFT YAW ANGLE VARIATION FOR CRUISE FLIGHT, TILT ROTOR PERFORMANCE MODEL

The D-88 program is used to predict the effect of aircraft pitch angle for the tilt rotor performance model. The predicted trends in bending moments, Figures 3.32 and 3.33, are similar to those trends for yaw angle variation. The D-88 program includes the effect of wing interference and closely predicts the flap bending moments for the performance model. The chord bending moment data for the performance model again contains the unpredicted higher harmonic moments. The correlation of D-88 predicted and measured moments with variation of angle of attack for the dynamic model in Figures 3.34 and 3.35 is poor. This is believed to be due to the incorrect phasing of the cyclic pitch in the analysis due to the difficulty of accurately recording instantaneous values of cyclic on the model. The effect of cyclic pitch on blade bending moments is predicted for the dynamic model in Figures 3.36 and 3.37. The insensitivity of the flap bending to cyclic pitch is predicted. Chord bending moments increase rapidly with cyclic pitch as indicated by both measured and predicted data. The mismatch between test and theory is also discussed in Paragraph 3.6.1.

The influence of the wing flap deflection on blade bending moments is analyzed by the D-88 program in the same way as wing interference. Predictions for the performance model are contained in Figures 3.38 and 3.39. The predictions are fair in slope but not in magnitude. Rotor loads are relatively insensitive to flap deflection.

3.6.5 Windmilling Rotor

Correlation of measured and predicted blade bending moments for a windmilling rotor is shown in Figure 3.40. Alternating bending moments are shown for variation of aircraft pitch angle. The test data is for the 1/9 scale conversion model. This case represents a low negative rotor thrust flight condition. The blades for this model were of relatively simple construction and were easily represented in the program.

The predicted trend of bending moments with angle of attack matches the data for both flap and chord bending. The bending moments at zero angle of attack are closely predicted. The calculated loads for this condition are due to gravity and wing interference effects. The flap and chord moments at the higher angle of attack are underpredicted.

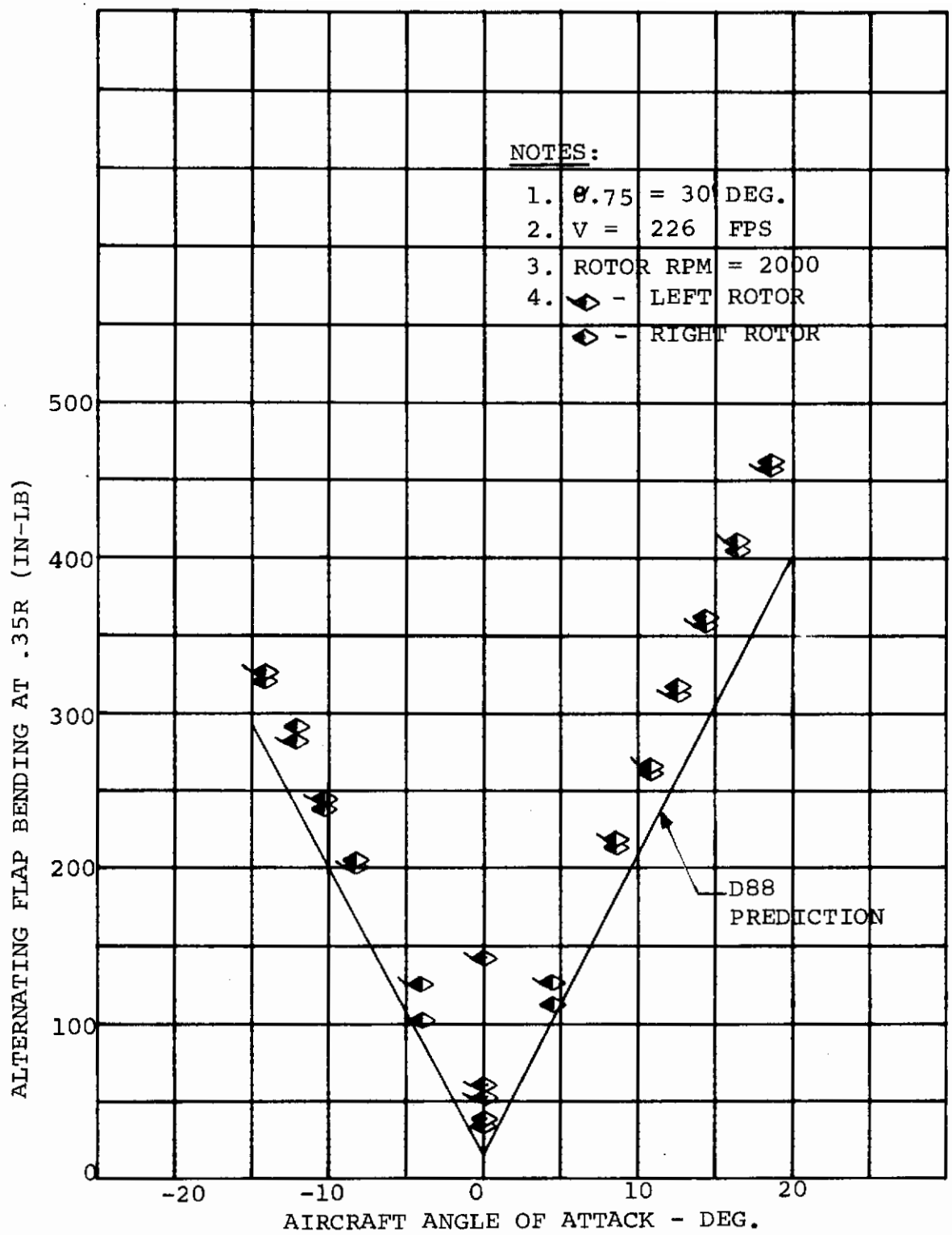

FIGURE 3.32 CORRELATION OF PREDICTED AND MEASURED ALTERNATING BLADE FLAP BENDING MOMENT WITH ANGLE OF ATTACK VARIATION FOR CRUISE FLIGHT, TILT ROTOR PERFORMANCE MODEL.

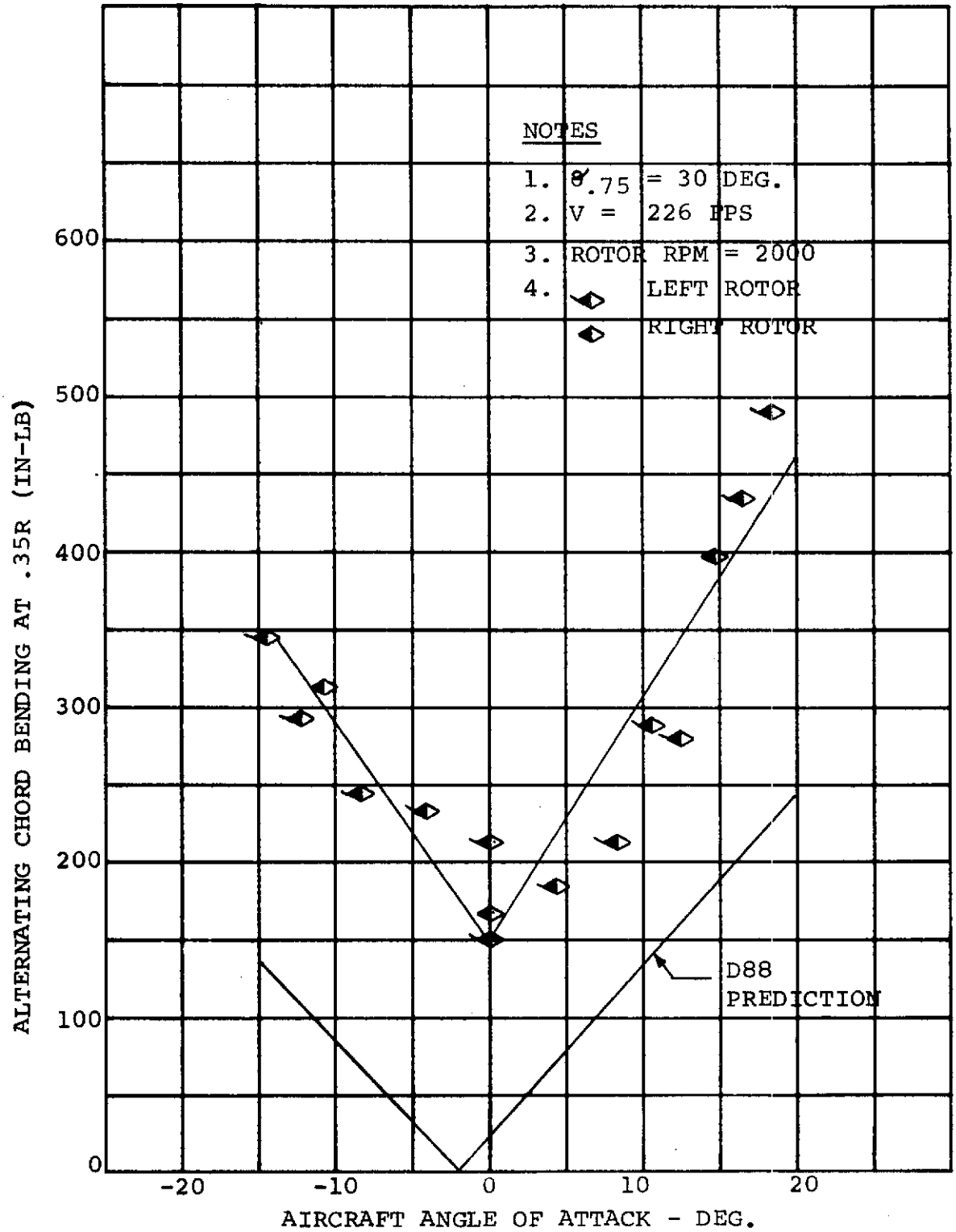

FIGURE 3.33 CORRELATION OF PREDICTED AND MEASURED ALTERNATING BLADE CHORD BENDING MOMENT WITH ANGLE OF ATTACK VARIATION FOR CRUISE FLIGHT, TILT ROTOR PERFORMANCE MODEL.

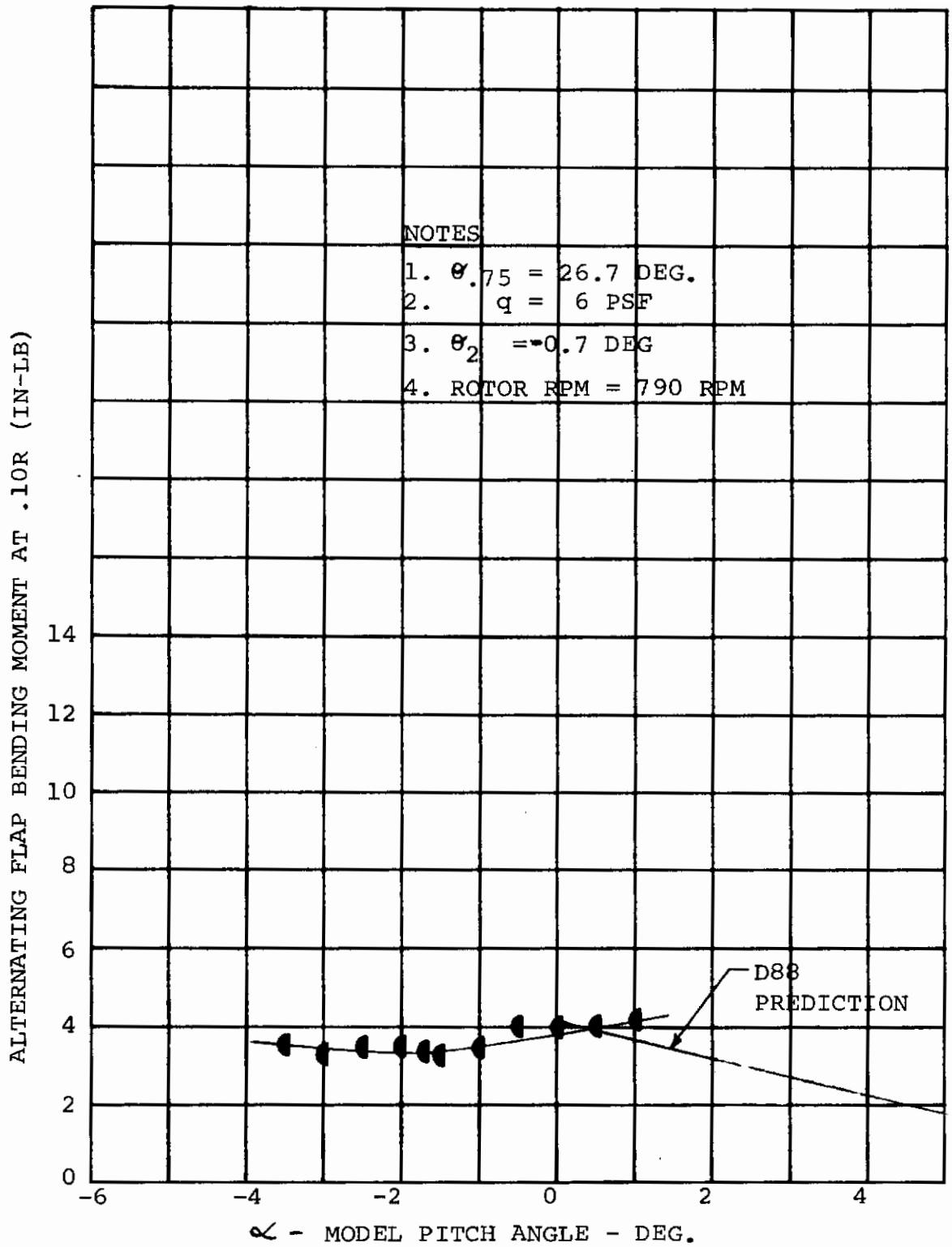

FIGURE 3.34 CORRELATION OF PREDICTED AND MEASURED BLADE ALTERNATING FLAP BENDING MOMENT WITH MODEL PITCH ANGLE FOR CRUISE FLIGHT, TILT ROTOR DYNAMIC MODEL

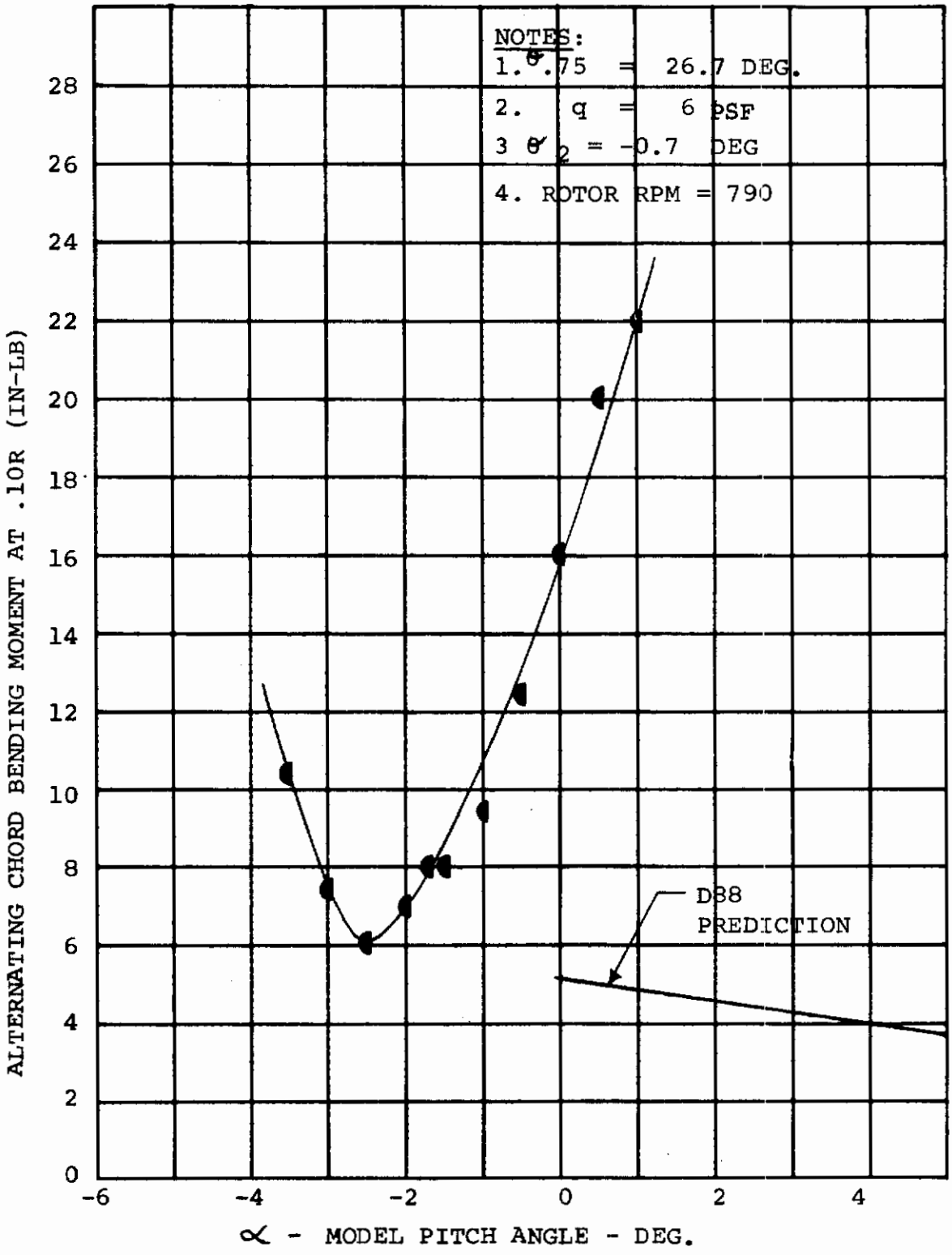

FIGURE 3.35 CORRELATION OF PREDICTED AND MEASURED BLADE ALTERNATING CHORD BENDING MOMENT WITH MODEL PITCH ANGLE FOR CRUISE FLIGHT, TILT ROTOR DYNAMIC MODEL

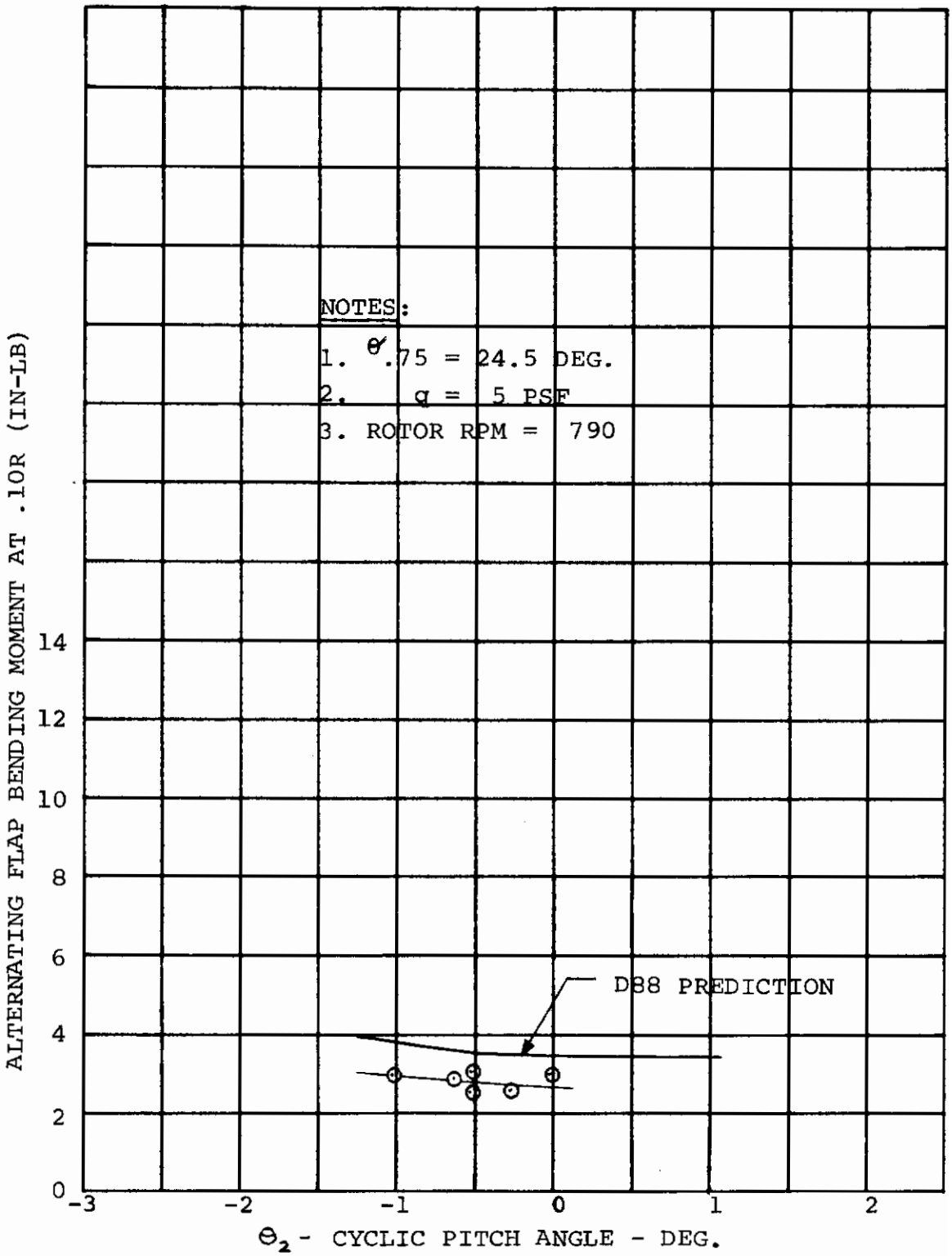

FIGURE 3.36 CORRELATION OF PREDICTED AND MEASURED BLADE ALTERNATING FLAP BENDING MOMENT WITH CYCLIC PITCH FOR CRUISE FLIGHT, TILT ROTOR DYNAMIC MODEL

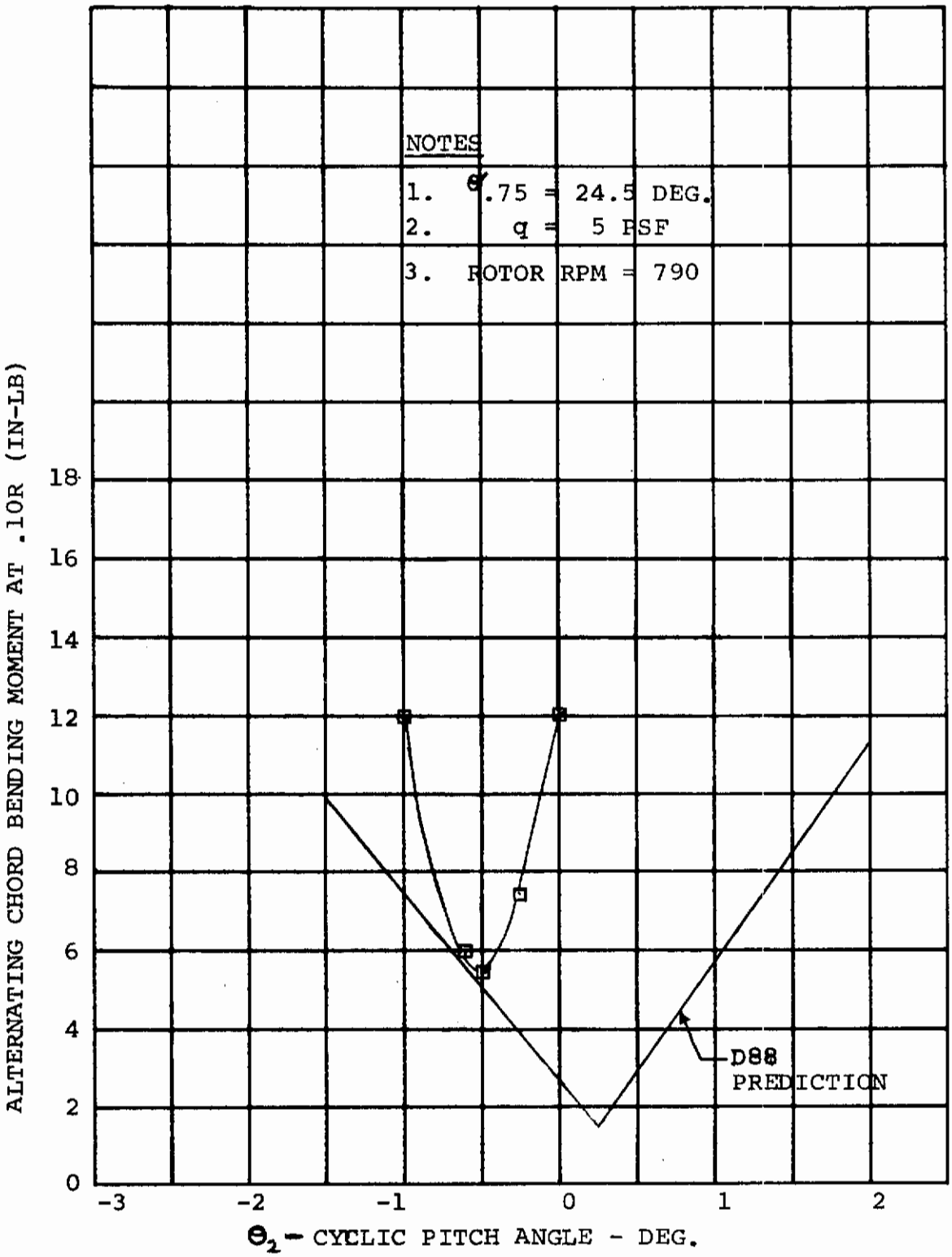

FIGURE 3.37 CORRELATION OF PREDICTED AND MEASURED BLADE ALTERNATING CHORD BENDING MOMENT WITH CYCLIC PITCH FOR CRUISE FLIGHT, TILT ROTOR DYNAMIC MODEL

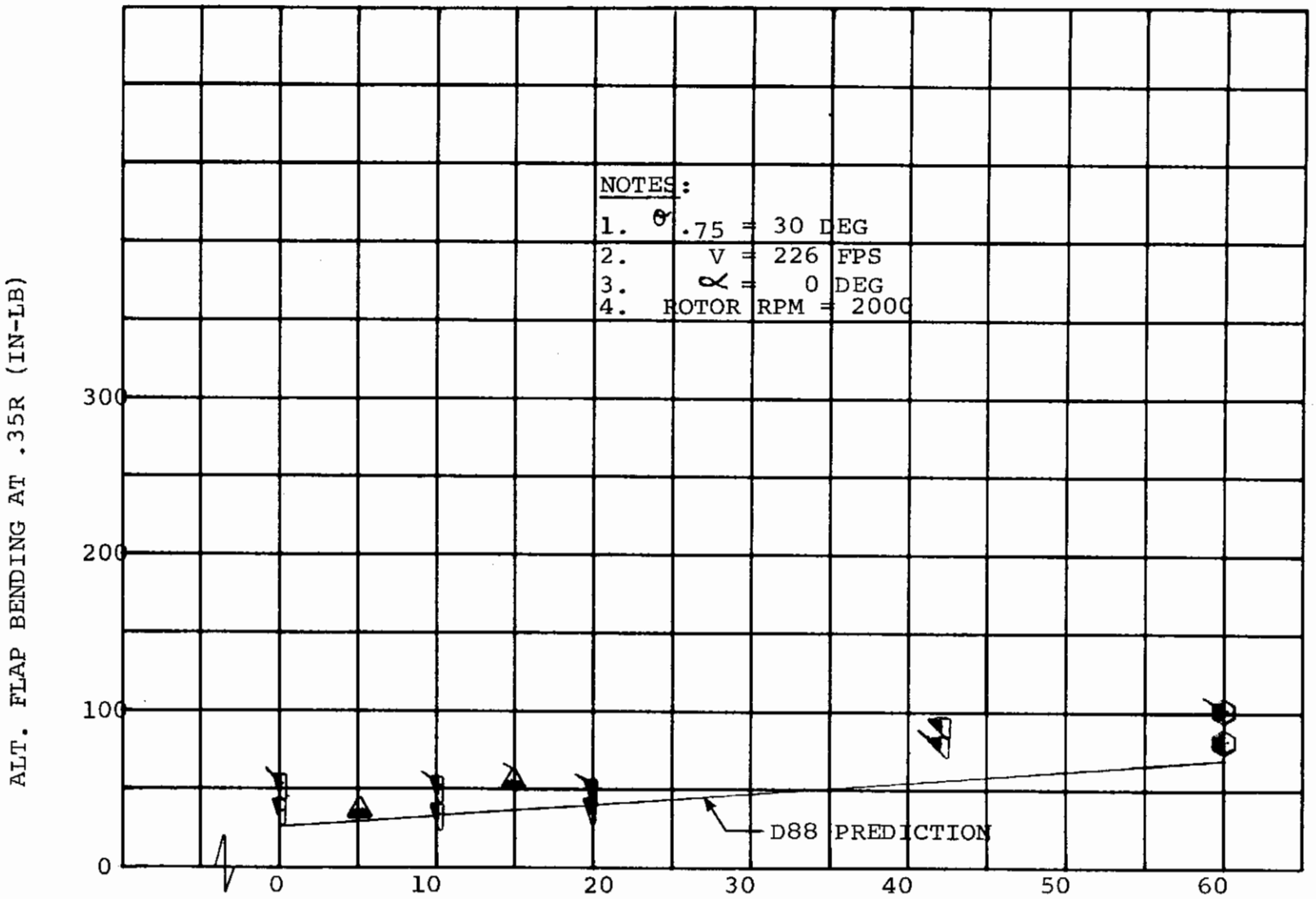

FIGURE 3.38 CORRELATION OF PREDICTED AND MEASURED BLADE ALTERNATING FLAP BENDING MOMENT WITH WING FLAP DEFLECTION FOR CRUISE FLIGHT, TILT ROTOR PERFORMANCE MODEL

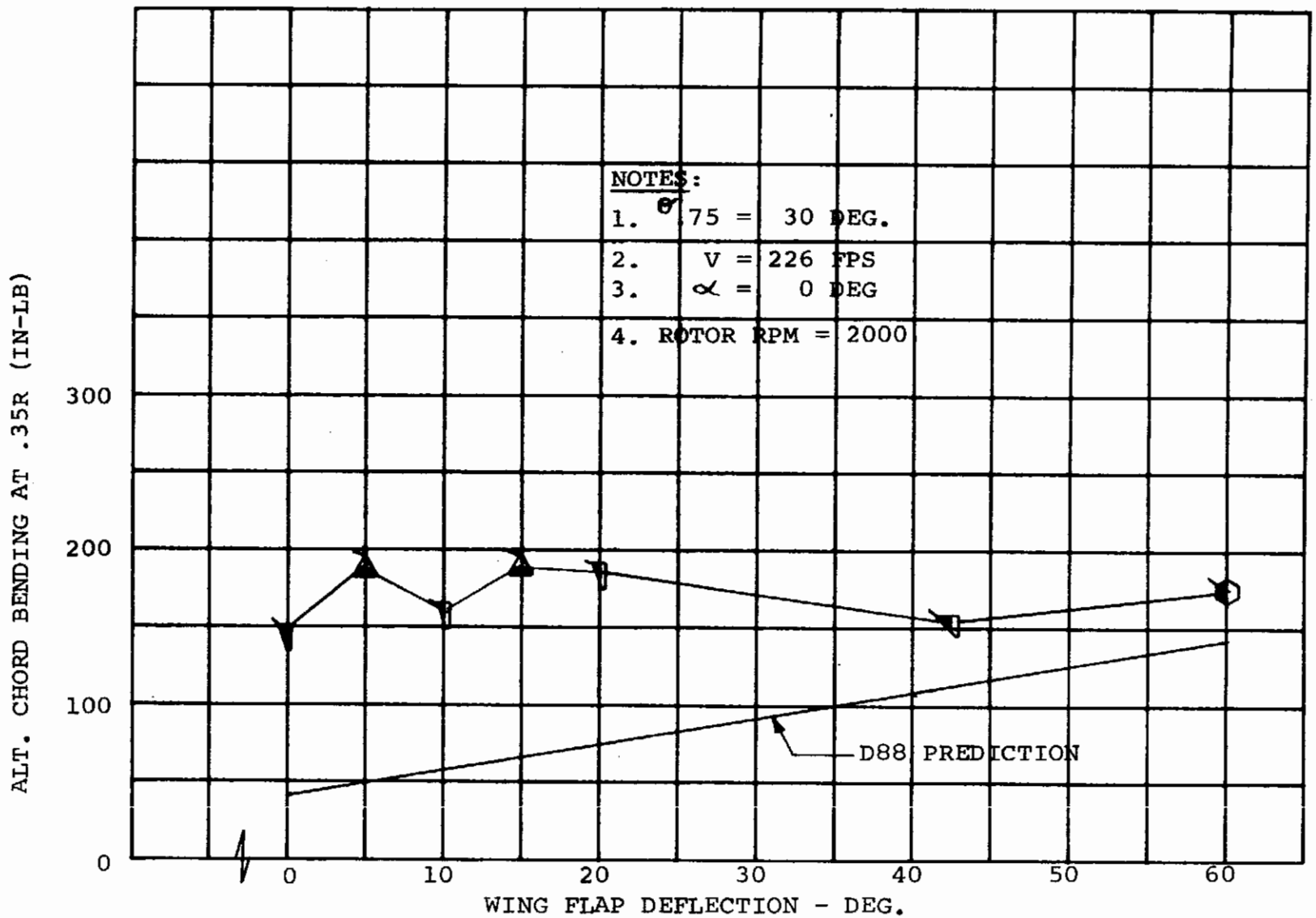

FIGURE 3.39 CORRELATION OF PREDICTED AND MEASURED BLADE ALTERNATING CHORD BENDING MOMENT WITH WING FLAP DEFLECTION FOR CRUISE FLIGHT, TILT ROTOR PERFORMANCE MODEL.

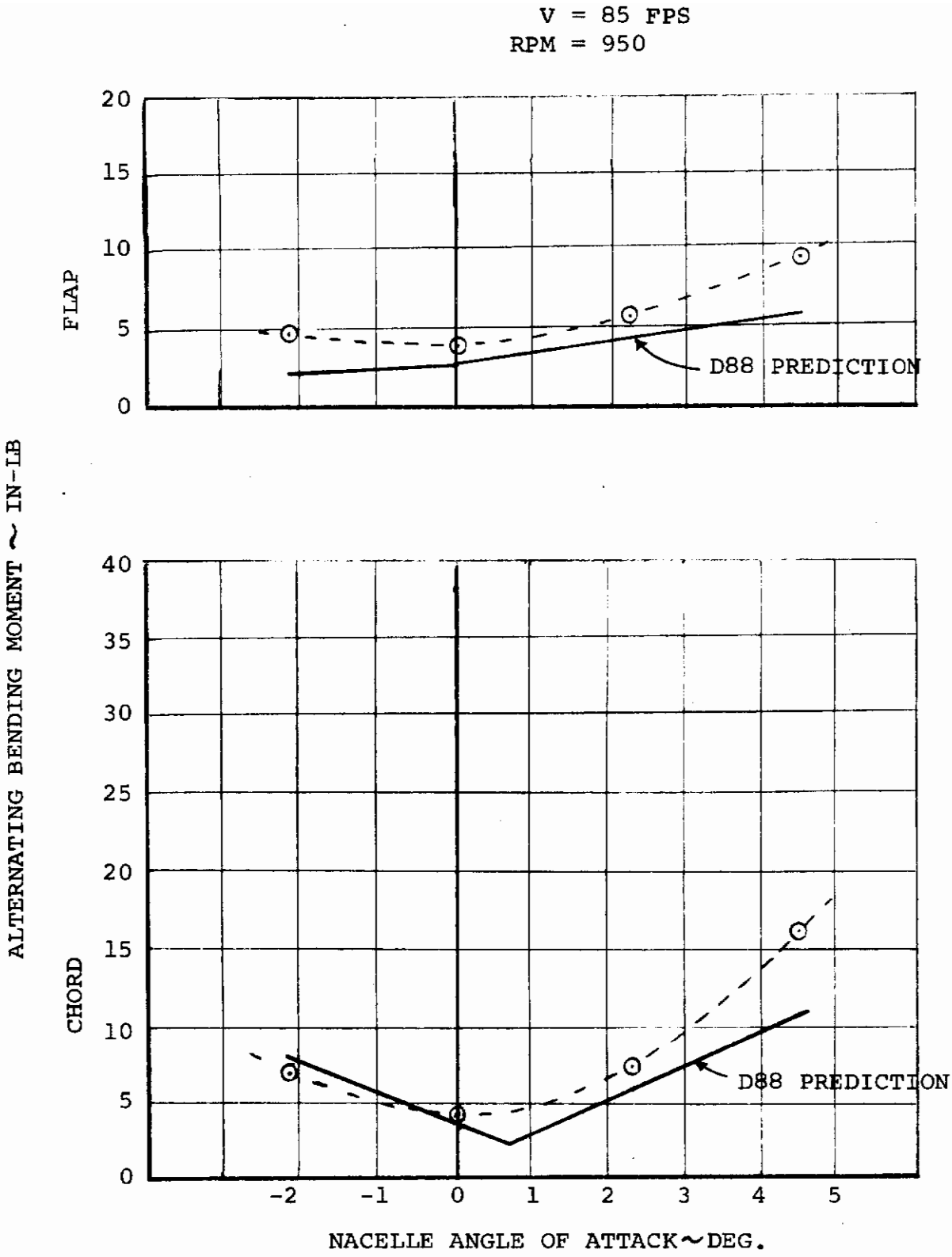

FIGURE 3.40 CORRELATION OF MEASURED AND PREDICTED BLADE BENDING MOMENT FOR STEADY WINDMILLING ROTOR 1/9 SCALE CONVERSION MODEL

3.7 CRITICAL FLIGHT CONDITIONS

Summaries of the measured blade bending moments for a spectrum of conditions tested are given in Tables 3.6 and 3.7 in Section 3.5. The critical design loads are blade alternating bending moments due to cyclic pitch and prop/rotor attitude.

The critical flight conditions will be hover maneuvers with cyclic pitch control and maneuvers with pitch motion in airplane or cruise flight. A slow acting cyclic pitch trim is required to alleviate the bending moments caused by rotor attitude in transition flight. In order to accomplish a maximum reduction in bending moment the cyclic pitch trim must have both longitudinal and lateral inputs. The conversion process does not produce limiting loads provided that the aircraft pitch attitude is low.

3.8 AIRFRAME/ROTOR DYNAMICS PREDICTION TECHNIQUES

This section consolidates and documents the airframe/rotor dynamic information learned from the four test programs.

A brief description of the most often used current analytical techniques for investigating dynamic aeroelastic phenomena will be presented. Aeroelastic responses discussed are:

1. Coupled Modal Frequencies
2. Modal Dampings
3. Whirl Flutter
4. Static Divergence
5. Air/Ground Resonance
6. Pitch-Lag-Flap Coupling

Aeroelastic response correlation between test and theory will be presented and criteria for design discussed as applicable. Vibration characteristics will also be discussed.

3.8.1 Analytical Methods

Two analytical programs (each restricted to axial rotor disc inflow) currently used to investigate aeroelastic stability are designated C-40 and C-41. Program C-40 determines modal frequencies and dampings of rotor-nacelle-wing systems and therefore can be used to predict classical wing flutter, air/ground resonance, and whirl flutter stability boundaries for these systems. Program C-41 determines the stability derivatives for an isolated rotor system and is used as a tool in the determination of static divergence of rotor-nacelle-wing systems.

Three new programs expanding the analytical capability are in various stages of development. Each of these programs will have the capability of treating all conditions of nacelle tilt and non-axial aerodynamic rotor disc inflow.

1. Program C-39 (an aeroelastic stability program) is now being used.

2. Program Y-71 will be available for use later in 1971. This program will be used to determine rotor blade coupled torsion, flap bending, and chord bending frequencies both with and without initial large blade deflections.

3. Program C-49 will be available for use later in 1971. This program determines the stability derivatives for an isolated rotor system.

Table 3.9 compares features of the programs discussed.

TABLE 3.9 COMPARISON OF PROGRAM FEATURES

DESIRABLE FEATURES/PROGRAM	ROTOR DERIVATIVE		AERO ELASTIC STABILITY		
	C-41	C-49	C-40	C-39	Y-71
Blade Flap Coning	Yes	Yes	Yes	Yes	Yes
Blade Flap Pitch and Yaw of Disc Plane	Yes	Yes	Yes	Yes	Yes
Blade Lag	Yes	Yes	Yes	Yes	Yes
Blade Torsion	No	Yes	No	Yes	Yes
Blade Flap Hinge Offset Representation	Yes	Yes	Yes	Yes	Yes
Blade Flexible Modes	Yes	Yes	Yes	Yes	Yes
Nacelle Tilt (Non-Axial Flow)	No	Yes	No	Yes	Yes
Large Deflections	No	Yes	No	Yes	Yes
Rotor Blade Cyclic	No	*	No	*	Yes
Nacelle Pitch and Yaw	Yes	Yes	Yes	Yes	Yes
Varying Blade Lift Curve Slope	No	Yes	No	Yes	Yes
Different Nacelle Pitch and Yaw Inertias	No	Yes	No	Yes	Yes
Feedback	No	*	No	*	Yes
Rigid Body Freedoms			Yes	Yes	
Wing Aero			Yes	Yes	
Wing Rotor Interference			No	Yes	
Feedback			No	*	

* = Scheduled for inclusion in 1971

3.8.2 Coupled Frequencies and Dampings

Program C-40 is currently used to establish coupled modal frequencies and modal damping characteristics over the operating range of tilt rotor aircraft. Typical frequency and damping spectrums are presented on Figures 3.41 and 3.42 generated for the 1/16 scale conversion model. The modes are highly coupled. Thus, they are labeled according to their dominant response, but because of the high degree of coupling, the modes will often show frequencies and other characteristics substantially different from the uncoupled modes with which such labels are usually associated.

3.8.2.1 Wing Response

The typical buildup in wing modal response at per/rev crossing is shown on Figure 3.43. This figure shows the alternating wing response for the semispan 1/16 scale conversion model during cruise testing. As can be seen, wing torsion response is prominent at 850 rpm. Figure 3.41 shows that this rotor speed is very close to the predicted speed for coincidence between the wing torsion mode and the three-per-rev rotor frequency. Thus, it appears that near 850 rpm the three-per-rev rotor excitation is forcing the wing torsional mode at its natural frequency. Measurements during test of the wing torsion response confirmed it to be composed of predominantly three-per-rev motion. Another significant response is the vertical bending response at 1460 rpm. This is near the predicted wing flap and 1/per rev intersection. Measurements of the response showed predominantly once per rev motion. The 3/rev, 2/rev and 1/rev crossings of wing chord frequency are clearly identifiable on Figure 3.43, as are 5/rev wing torsion and the 3/rev wing vertical bending, though none of these show loads approaching those of the multiple interaction previously discussed.

Similar response amplifications (to those for the cruise configuration discussed previously) occur at wing frequency and per rev intersections for hover and transition flight configurations.

Wing frequencies were found to vary only slightly with nacelle tilt. This is illustrated by Table 3.10 which gives frequency and dampings from tweak test measurements with nonrotating rotors. Modal damping varies substantially with nacelle tilt. This is primarily due to the large contribution of the rotors

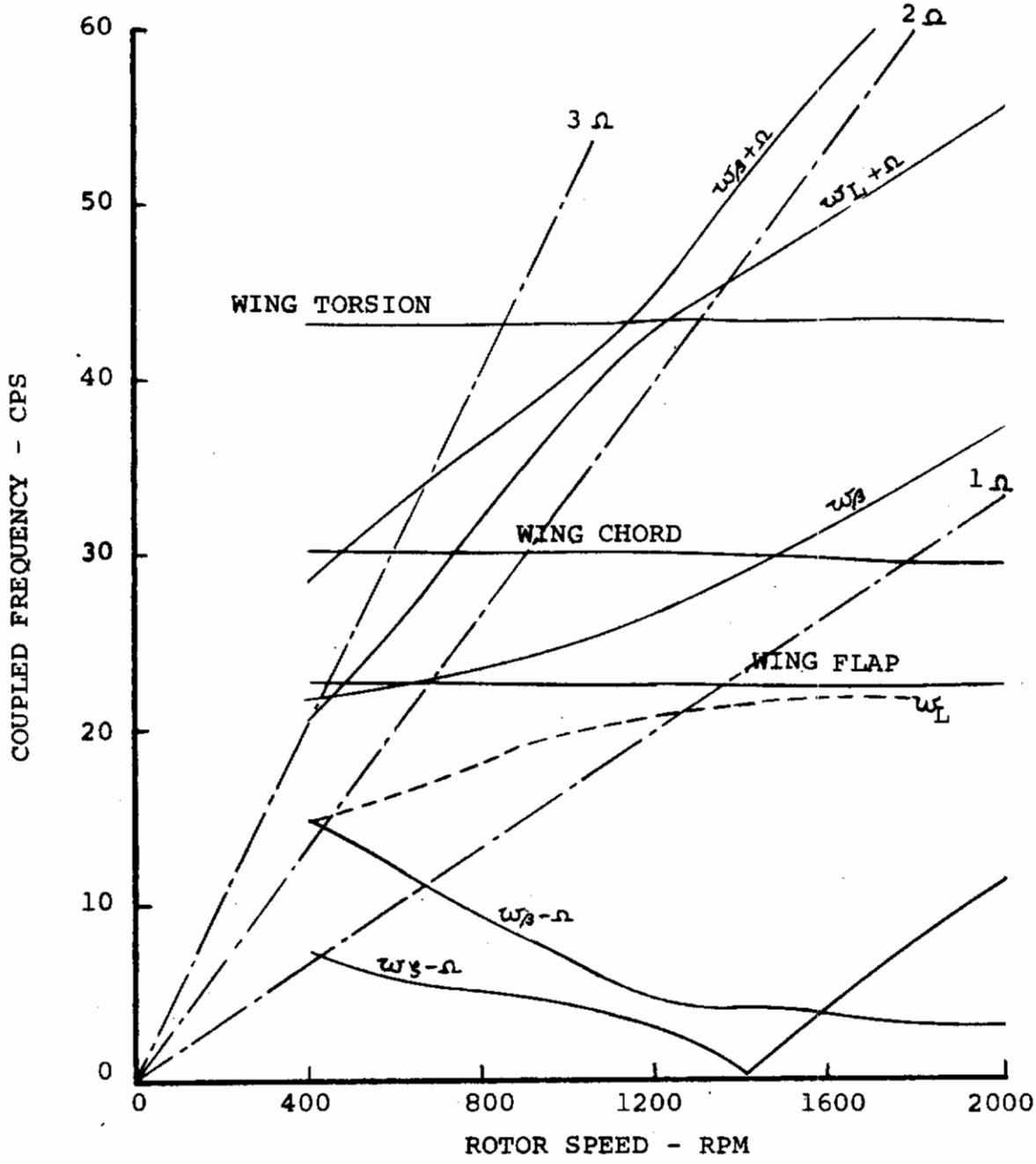

FIGURE 3.41 FREQUENCY SPECTRUM FOR 1/16 SCALE CONVERSION MODEL - CRUISE MODE V = 135 FPS

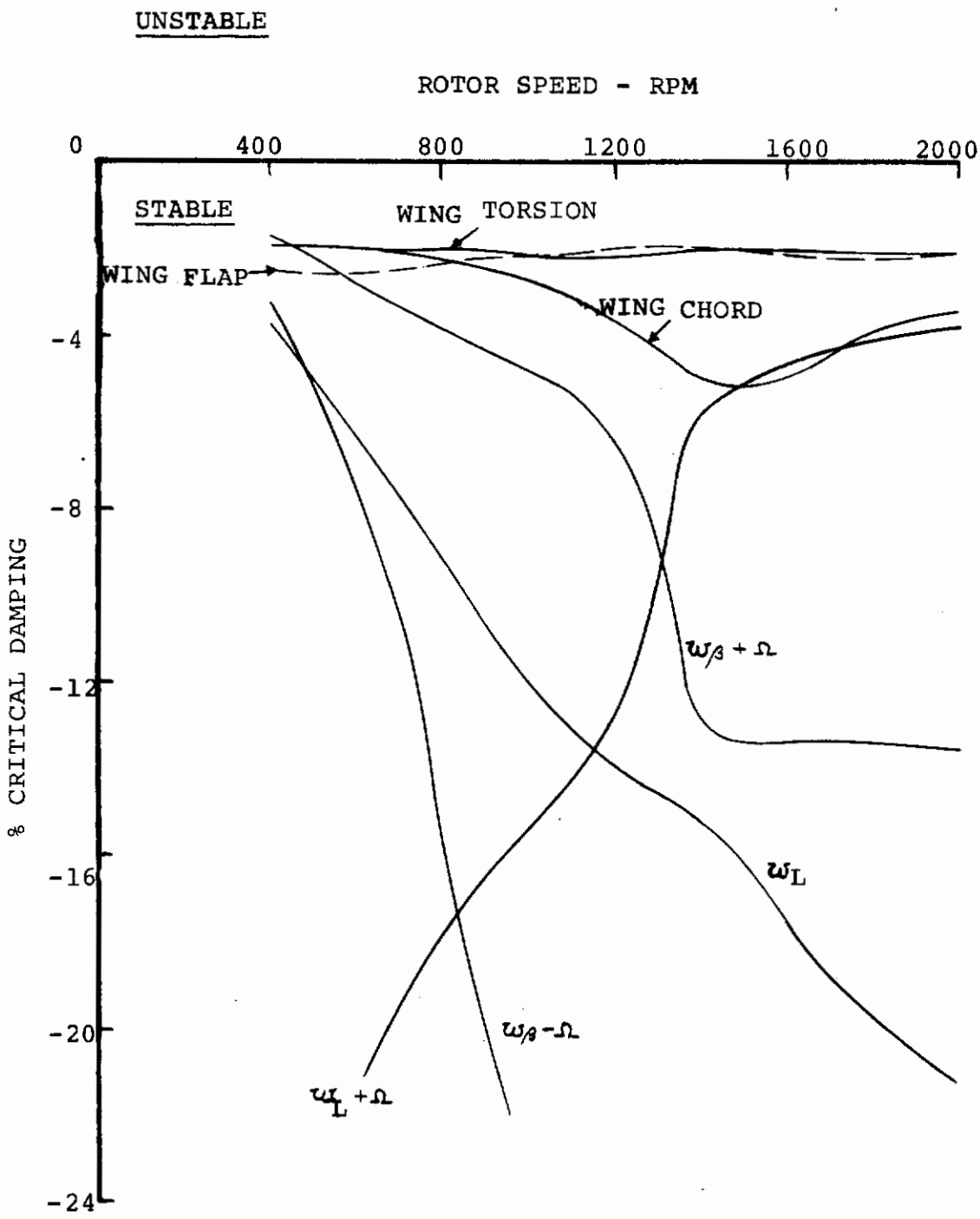

FIGURE 3.42 DAMPING SPECTRUM FOR 1/16 SCALE CONVERSION MODEL - CRUISE MODE - V = 135 FT/SEC

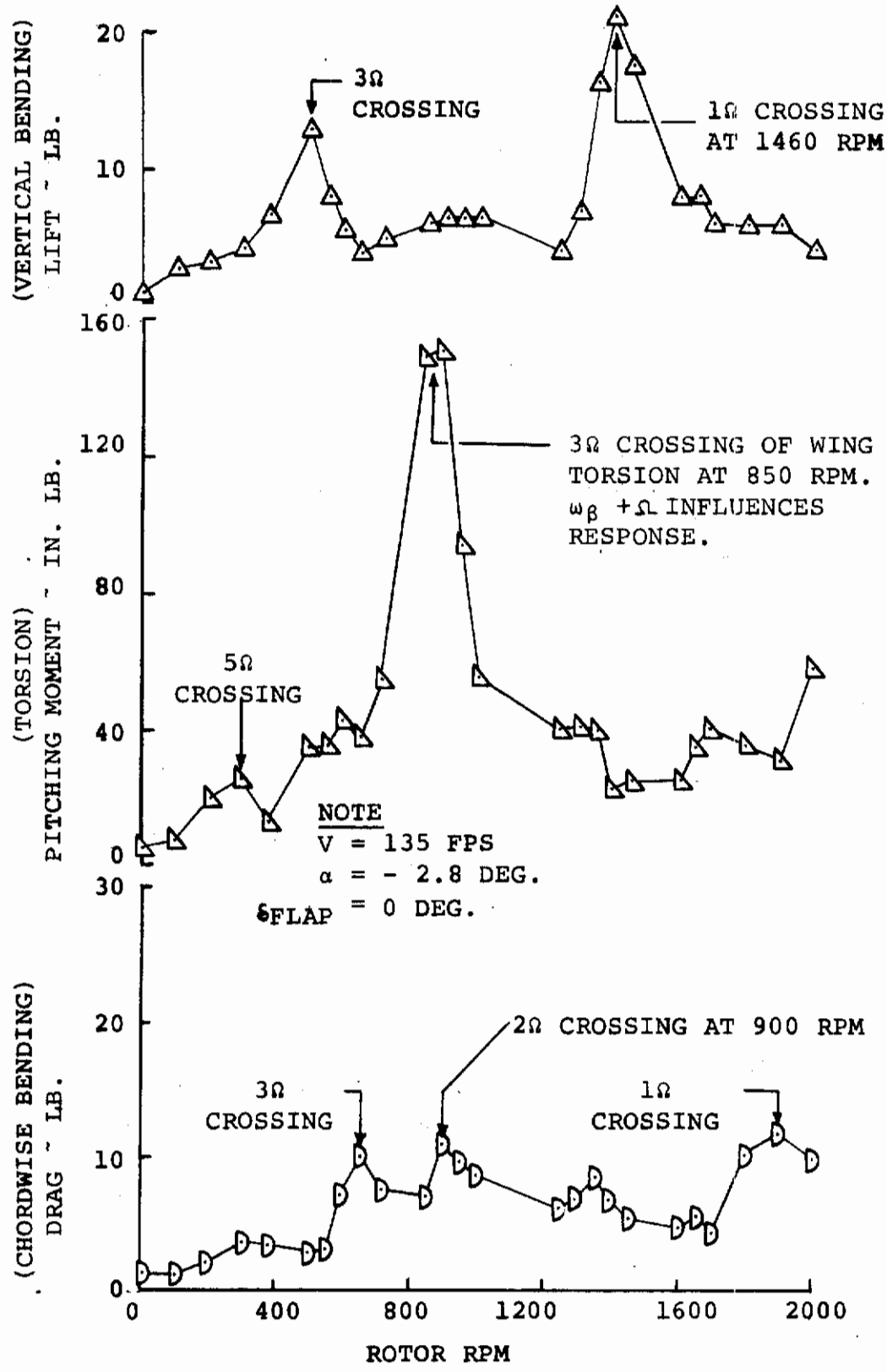

FIGURE 3.43 ALTERNATING WING LOADS DATA SHOW GOOD CORRELATION WITH DYNAMIC PREDICTIONS, 1/16 SCALE CONVERSION MODEL - CRUISE MODE

TABLE 3.10. WING FREQUENCIES AND DAMPINGS FROM TWEAK TEST (1/10 SCALE DYNAMIC MODEL--NON-ROTATING ROTORS)

NACELLE INCIDENCE	SYM. WING FLAP		SYM. WING CHORD		SYM. WING TORSION	
	FREQ. (CPS)	DAMPING	FREQ. (CPS)	DAMPING	FREQ. (CPS)	DAMPING
0° (Cruise)	5.2	.022	10.5	.012	16.8	.010
40°	5.1	.041	10.5	.015	17.0	*
60°	5.1	.032	10.3	.017	*	*
90° (Hover)	5.1	.033	10.5	.017	17.5	.012

* = NOT MEASURED

to total damping, and the fact that the rotor disc plane is tilting through 90° relative to the wing plane.

Wing Design Criteria

Frequency and damping spectrums of the type shown by Figures 3.41 and 3.42 are valuable as an aid to design. Each of the modal damping curves must at a minimum show stabilizing damping over all operating conditions. The higher the damping percentage the more stable the system. The system frequency spectrum can be used to design away from high blade and wing loadings by avoiding multiple intersections. Designs producing modal intersections or modal frequency crossover of forced response frequencies (per rev lines) at prolonged operating conditions should be avoided.

3.8.3 Aeroelastic Stability

In this section the capability of the currently used programs to predict aeroelastic instabilities (i.e., correlation between test and theory) is discussed in terms of each type of instability. The 1/9 scale conversion model was used to determine the capability of analytical computerized programs C-40 and C-41 of predicting ground/air resonance, whirl flutter, and static divergence stability boundaries.

An air/ground resonance instability region was predicted near enough to the normal test schedule of rotor speeds and tunnel velocities that additional testing to define this boundary could be conducted using the nominal model system. Whirl flutter and static divergence, however, were not predicted to occur anywhere near nominal test conditions using the basic 1/9 scale conversion model. A new wing spar was built (with a wing torsional stiffness of 0.31 nominal) to test for these stability boundaries.

Air Resonance

Stability program C-40 is currently used to predict air/ground stability boundaries. The calculated coupled wing-nacelle-rotor system modal frequencies and damping as a function of rotor speed for the 1/9 scale conversion model are presented in Figures 3.44 and 3.45. These spectra are for a cruise tunnel speed of 104 ft/sec. The analysis predicted an air/ground resonance instability lower boundary at 1070 RPM. This occurs when the modal damping of the wing flap bending mode

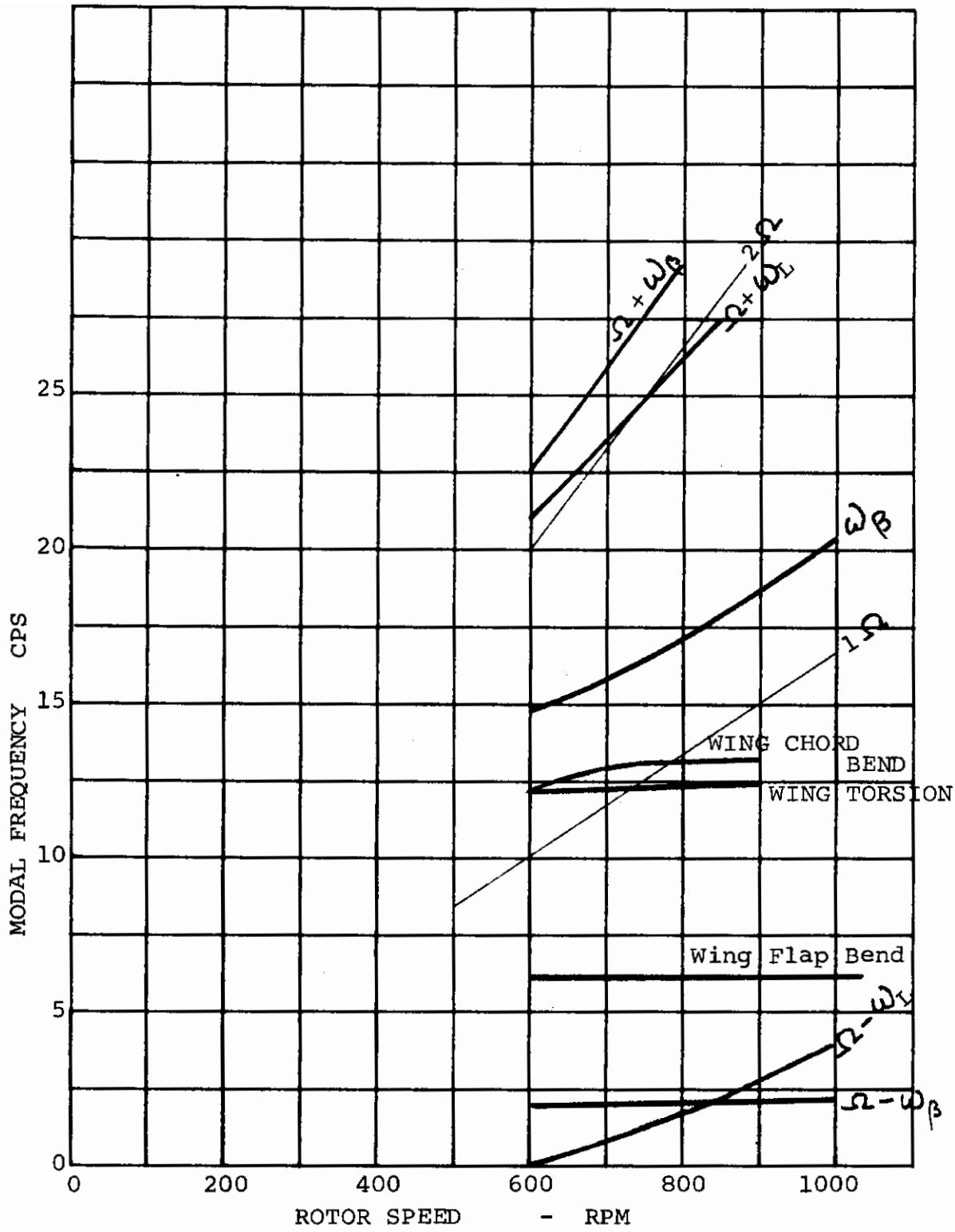

FIGURE 3.44. FREQUENCY SPECTRUM FOR NOMINAL STIFFNESS WING SPAR--WINDMILLING CONDITION--V=104 FPS 1/9 SCALE CONVERSION MODEL

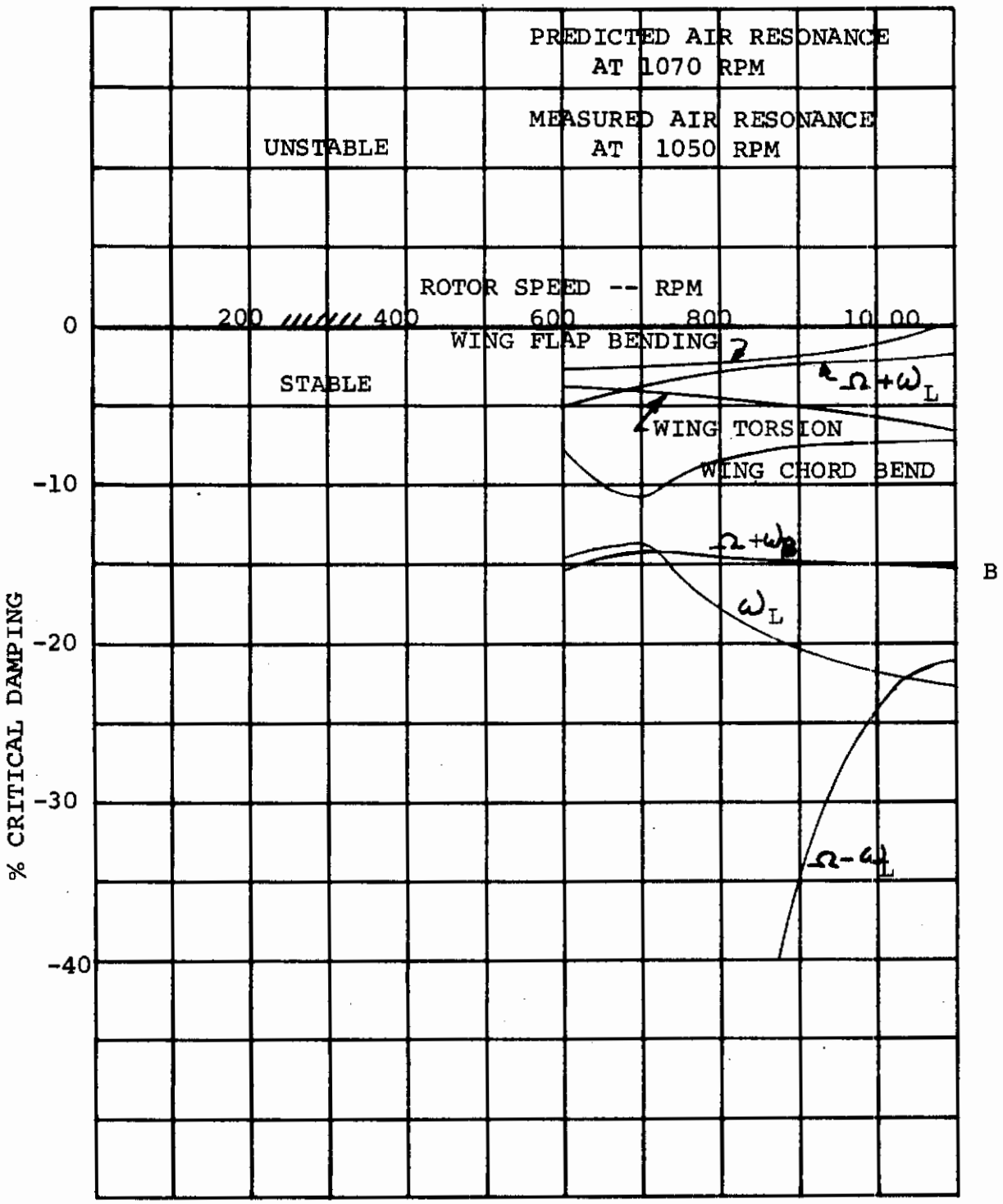

FIGURE 3.45. DAMPING SPECTRUM FOR NOMINAL STIFFNESS WING SPAR--WINDMILLING CONDITION--V=104 FT/SEC--1/9 SCALE CONVERSION MODEL

becomes zero (Figure 3.45) and is brought about by the approaching coalescence (Figure 3.44) of the wing flap bending mode and the lower in-plane blade mode (Ω-ω_L). Testing conducted in the cruise configuration at a tunnel speed of 104 ft/sec confirmed the prediction of air resonance at a rotor speed of 1050 RPM.

Static Divergence

The equivalent pitch resisting spring of the reduced torsional stiffness wing spar of the 1/9 scale conversion model was obtained by direct measurement. The moment producing wing torsion (as a function of airstream velocity and rotor speed) was obtained by summation of the torsion force on the wing from the rotor and the torsional force on the wing from wing aerodynamics. Derivatives from stability derivative program C-41 were used to obtain the pitching moment from the rotor about the wing pitch axis. Static divergence was predicted to occur when the total aerodynamically produced pitching moment on the wing equaled or exceeded the elastic restoring moment.

The predicted static divergence as a function of rotor speed and airstream velocity is shown on Figure 3.46. Static divergence boundaries obtained from test data on the reduced torsional stiffness spar at tunnel speeds of 130, 140 and 145 FPS all coalesce (within experimental accuracy) to give the experimental static divergence boundary shown. The static divergence predicted boundary based on measured reduced torsion spar stiffness showed good agreement with test.

Whirl Flutter

No whirl flutter instabilities were predicted for any of the model tests at or near any normal test conditions. No indication of whirl flutter was observed during any of the nominal stiffness wing model tests.

Limited measured damping of the whirl flutter mode ($\Omega - \omega_\beta$) was obtained during test of the 1/9 scale conversion model with reduced torsion stiffness wing spar at a tunnel velocity of 130 ft/sec. Frequency and damping values obtained from decay decrements of the whirl flutter mode are shown on Figure 3.47 for a series of rotor speeds. Correlation with predicted damping using aeroelastic stability Program C-40 is also shown. These limited data show good correlation between test and theory.

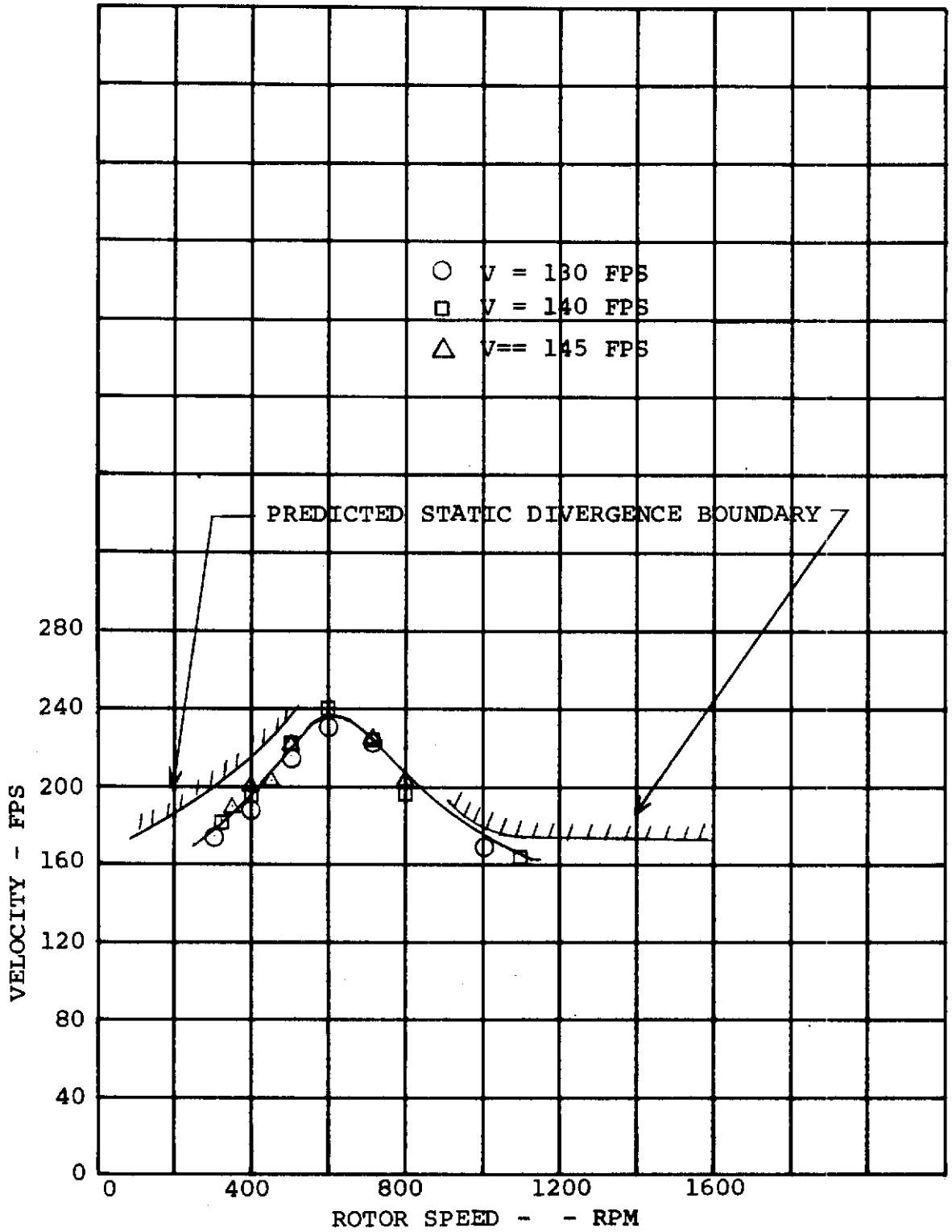

FIGURE 3.46 STATIC DIVERGENCY BOUNDARY EXTRACTED FROM TEST DATA - RUN 126 - REDUCED TORSION STIFFNESS SPAR - 1/9 SCALE CONVERSION MODEL

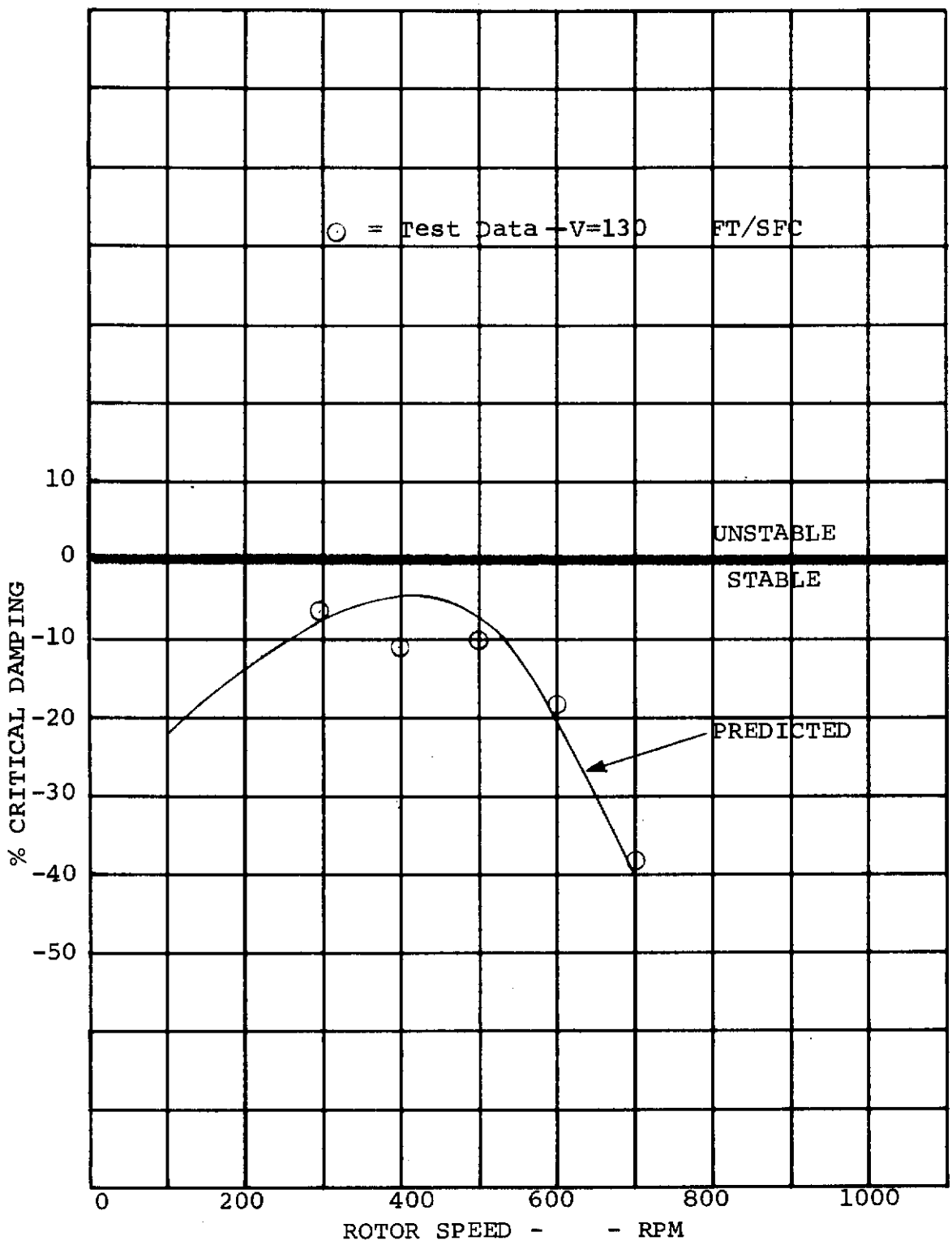

FIGURE. 3.47. DAMPING IN WHIRL MODE ($\Omega - \omega_\beta$)
REDUCED TORSION STIFFNESS SPAR, V=130 FT/SEC
1/9 SCALE CONVERSION MODEL

Pitch-Flap-Lag Coupling

During testing of the 1/10 scale dynamic model there were some conditions near zero thrust in hover and slow velocities in transition where a mode, associated primarily with blade chord bending, was lightly damped. In some cases, a limit cycle oscillation developed. This response did not occur at the higher tunnel speeds tested in the cruise mode.

The mode was always sufficiently stable that a substantial volume of test data could be taken at the conditions where it was encountered. A typical oscillograph tape showing the nature of the mode as a limit cycle oscillation is given in Figure 3.48.

The primary characteristic is shown on the blade chord bending trace where a substantial 0.72/rev (blade chord bending natural frequency) is superimposed on the normal 1/rev. This shows up as the 0.28/rev beat visible in the trace which appears to be directly related to the $(\Omega - \omega_L)$ frequency which was predicted to be 0.28/rev at this rotor speed. The blade flap bending and torsion traces show the same frequencies though with less amplitude, while wing torsion (fixed system) shows a corresponding 1-.72 = 0.28/rev superimposed on the 1/rev. Aircraft pitching motion also shows a small response at the same 0.28/rev frequency. There is little response at this frequency in wing chord bending or torsion.

Boeing computer program C-39 now coming into use provides an analytical capability to deal with blade pitch-lag-flap oscillations including finite blade deflections. Correlation studies with data from this test and previous test data has been initiated using Program C-39.

Design Criteria

Capability of the presently used methodology programs and other analytical tools now available for use have been discussed. In general, good correlation between test and theory has been obtained. These analytical programs can be used as tools in the design of stowed tilt-rotor vehicles to meet the specified design criteria.

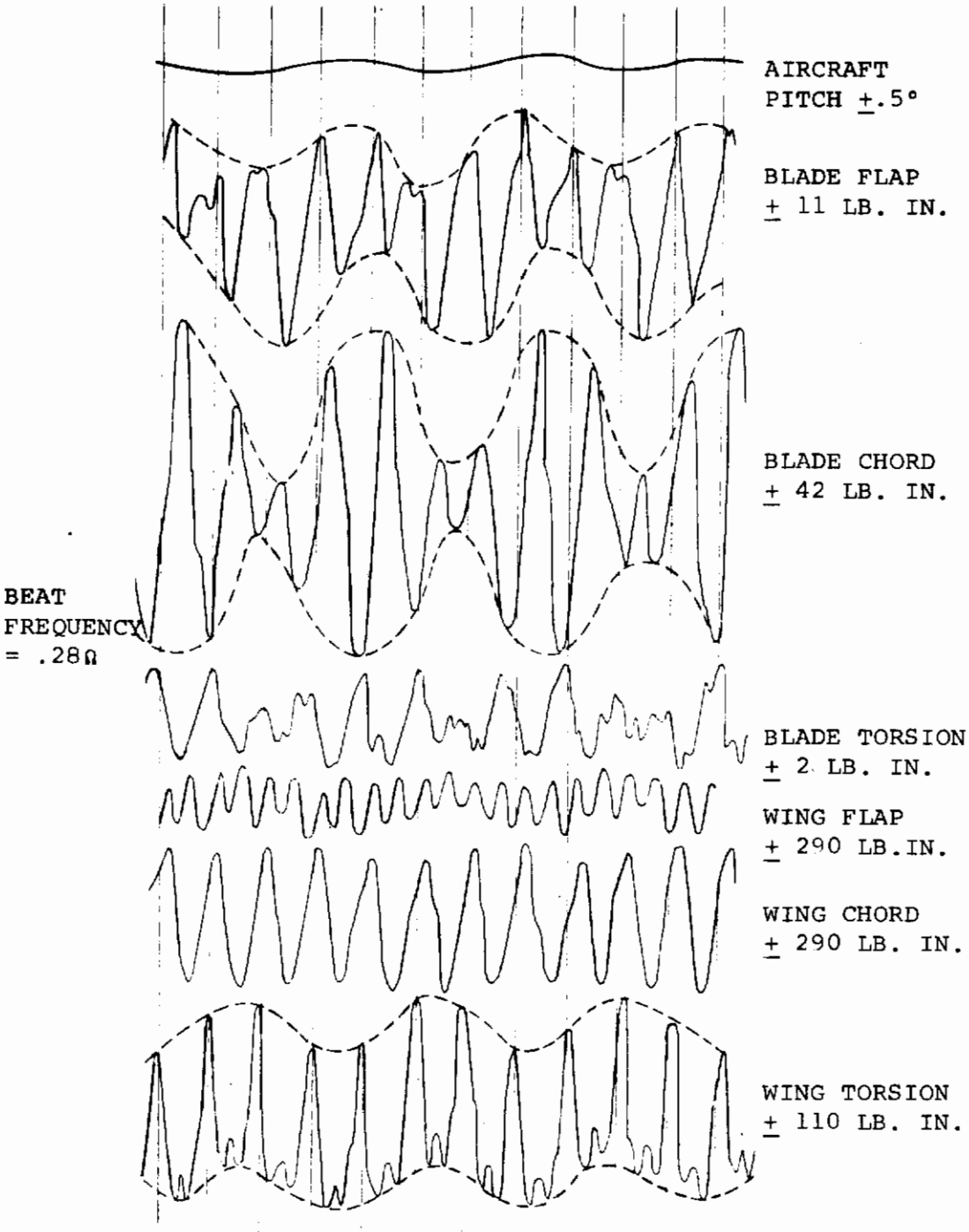

NOTE: Oscillation started at q = 25 psf

FIGURE 3.48. BEAT FREQUENCY RESPONSE OSCILLOGRAM
RIGHT BLADE AND WING, Ω = 790 RPM
$\theta_{.75}$ = 10.2 DEG., θ_2 = 3.5 DEG.
q = 2.75 PSF, i_N = 60 DEG.,
1/10 SCALE DYNAMIC MODEL

The flight vehicle shall be free from all instabilities such as whirl flutter, ground/air resonance, static divergence, and blade pitch-lag-flap instabilities at all normal operating conditions. In addition, margins of safety on stability as defined in the specifications shall be provided. Minimum modal dampings as prescribed in the specifications shall be equaled or exceeded.

3.8.4 Vibration

For folding tilt rotor aircraft, the initial rotor design (the number of blades, tip speed in hover and cruise, blade radius, chord, twist) is usually dictated by performance requirements. Subsequently, the rotor design must be optimized to provide minimum vibratory hub loads since the vibratory response of the aircraft comes principally from the rotor forcing functions.

In typical stowed tilt rotor aircraft the nacelle/rotor system is mounted at the wing tips. At prolonged operating conditions (for example, hover and cruise) any fundamental wing or body frequency coalescence or near coalescence with rotor frequencies (per rev lines) should be avoided. By separating the wing and body frequencies from the rotor forcing frequencies, the vibratory forces originating at the rotor hub will tend to be attenuated before reaching the fuselage.

Analyses that have been used to successfully predict vibration characteristics of helicopters can be used to predict the vibratory response of tilt rotor aircraft. These analyses have been proven to be accurate in predicting vibratory response of aircraft systems. Typical plots for forced response to vibratory loads are shown on Figure 3.49 where correlation between predicted and measured g levels and phase angles at the rotor hub is presented for the CH-46 aircraft.

The design of the aircraft shall be such that freedom from fatigue resulting from vibrations is maintained. A particularly critical area to be examined in this regard is the area at and near the engines. The vibration of crew seats and other items affecting crew comfort in the cockpit and at all crew stations shall meet the specifications.

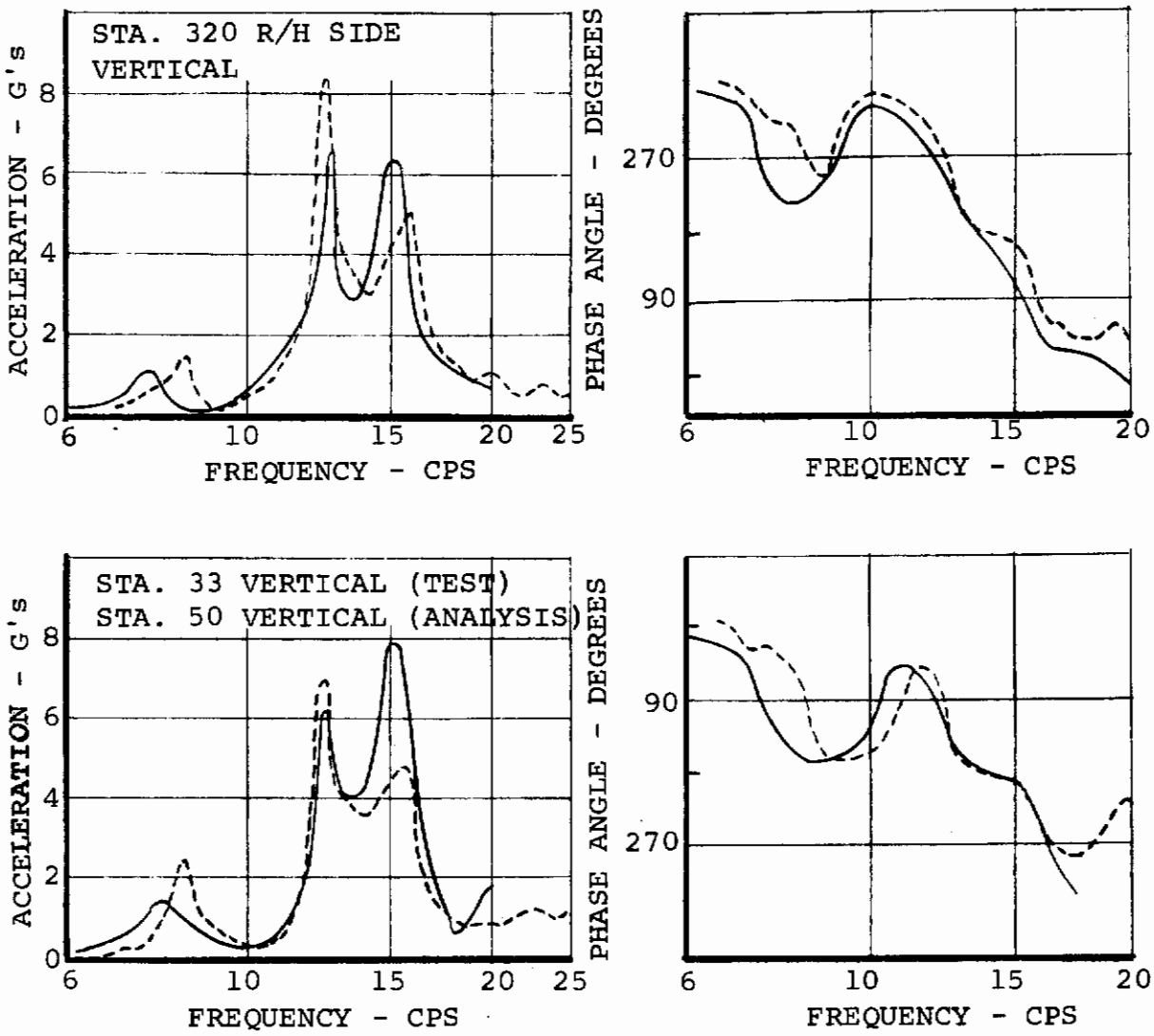

FWD HUB LONGITUDINAL EXCITATION
.03 DAMPING

------ SHAKE TEST
_____ ANALYSIS

RAMP FORCE
300 LB AT 10 CPS TO
650 LB AT 20 CPS

FIGURE 3.49. CH-46 AIRCRAFT FREQUENCY RESPONSE

3.9 CONCLUSIONS

Structures

1. The correlation for blade loads is fair and further improvement of the analytical methodology is being performed by Boeing under USAF contract.

2. Further testing for rotor blade loads is recommended with a dynamically scaled rotor rigidly mounted in the tunnel to separate out the effects of unbalance and hub motion from the basic blade loads.

3. Critical design conditions for loads in the rotor system are the use of cyclic pitch for control in hover and transition Blade loads during spinup, feather, fold and deploy are not critical.

Rotor/Airframe Dynamics

4. Good correlation between aeroelastic stability test and theory has been obtained using current methodology.

5. Blade and wing frequencies should be designed away from integer per rev frequencies under normal operating conditions.

6. Under certain conditions tilt rotor aircraft can develop a limit cycle oscillation apparently involving pitch-flap-lag coupling of the blade. Further investigation of this dynamic response is required.

3.10 RECOMMENDATIONS

Structures

1. Additional fold and deploy testing is desired to define the steady bending moments over the mid and outboard portion of the blade.

2. Use of advanced composites in the airframe should be investigated to improve the payload fraction of the aircraft further.

Rotor/Airframe Dynamics

3. Additional model testing is desired to provide more data for correlation of aeroelastic stability boundaries.

4. Further correlation studies on the blade pitch-lag-pitch limit cycle response observed during the 1/10 scale dynamic model test be conducted using aeroelastic stability program C-39.

4.0 AERODYNAMIC PREDICTION TECHNIQUES

In the development of the stowed/tilt rotor aircraft the technology program objectives as stated previously are:

- Identify and evaluate risks
- Put risk in perspective
- Define design criteria approaches that minimize risks
- Substantiate prediction techniques that show design meets criteria

This last objective is addressed in this section. The aerodynamic prediction techniques that are currently available to define the characteristics of the stowed/tilt rotor aircraft are summarized in this section. These techniques are employed to predict the characteristics of the wind tunnel models utilized in Test Programs II and IV and are compared with the test data to indicate the degree of correlation. In the major flight modes there will be a discussion of the impact on the total aircraft capability resulting from any significant difference between theory and test data.

4.1 HOVER PERFORMANCE

In the development of the stowed/tilt rotor aircraft many analytical methods have been developed. These analyses are an adaptation of existing analytical methods or in certain instances a development of a prediction technique specifically oriented to the stowed/tilt rotor. Hover performance is predicted by an adaptation of techniques developed for application to helicopter rotors and V/STOL propellers. These are shown to be equally accurate in predicting the performance of a stowed/tilt rotor aircraft with highly twisted rotors. Hover performance for the aircraft is obtained by predicting the performance of the isolated rotor; defining the download on the airframe, and integrating both of these to obtain total aircraft performance.

4.1.1 Hover-Rotor Performance

Performance of the isolated rotor is calculated by the procedure described in detail in Reference 4.1. A brief synopsis is presented here. This analysis of propeller and rotor performance in axial flow uses an explicit vortex influence technique to define the thrust, power and radial distribution of aerodynamic loading on a rotor or propeller of arbitrary planform, twist,

and radial variation of airfoil characteristics. It is applicable to static operation (hover) or in axial flight (airplane cruise mode), for rotor blades with square tips.

Each rotor blade is treated as a rotating, lifting line, trailing a vortex wake which is mathematically approximated by a finite number of concentrated vortex filaments. The radial distribution of aerodynamic load on the blades determines their strength and geometry. When these parameters are established, the radial variation of induced velocity can be computed. An iterative procedure is followed to make the induced flow and the aerodynamic loading mutually consistent.

For adequate prediction of hover performance, slipstream acceleration and contraction must be accounted for in the establishing of the geometry of the vortex system trailed by the blades. This analysis includes the effects of thrust coefficient on the slipstream acceleration as determined by analytical studies of finite-core vortex ring flows and empirically by correlation of calculated and measured propeller static performance.

Airfoil sections for the blade may be specified at ten radial stations. The associated aerodynamic characteristics utilized in this analysis are described in Reference 4.2.

Substantial correlations have been performed to date with propellers of different size and shape. The results from these correlations are reported in Reference 3.2 and 5.8 for both cruise and hover flight.

Presented in Figure 4.1 is a comparison of rotor performance from tests of the 1/10 scale Model 160 Tilt Rotor aircraft tested in Test Program II with analysis. The model rotor is operating out of ground effect at a Reynolds number of 0.6 to 0.9 x 10^6 at the three-quarter radius. The variation of rotor thrust coefficient with power coefficient at a rotor speed of 2000 rpm and variable collective is shown. The agreement is very good. Figures 4.2 and 4.3 present the variation of the rotor thrust and power coefficient with blade collective at the three-quarter radius $\theta_{.75}$). The agreement with the trend with collective is good but there appears to be a difference of one degree between the right rotor test data and the theory. This difference is about the setting accuracy of the blade collective on the model. Data obtained at 14 degrees blade collective shows some deviation from the trend established by the theory while there is excellent agreement at 7, 10 and 18 degrees blade collective.

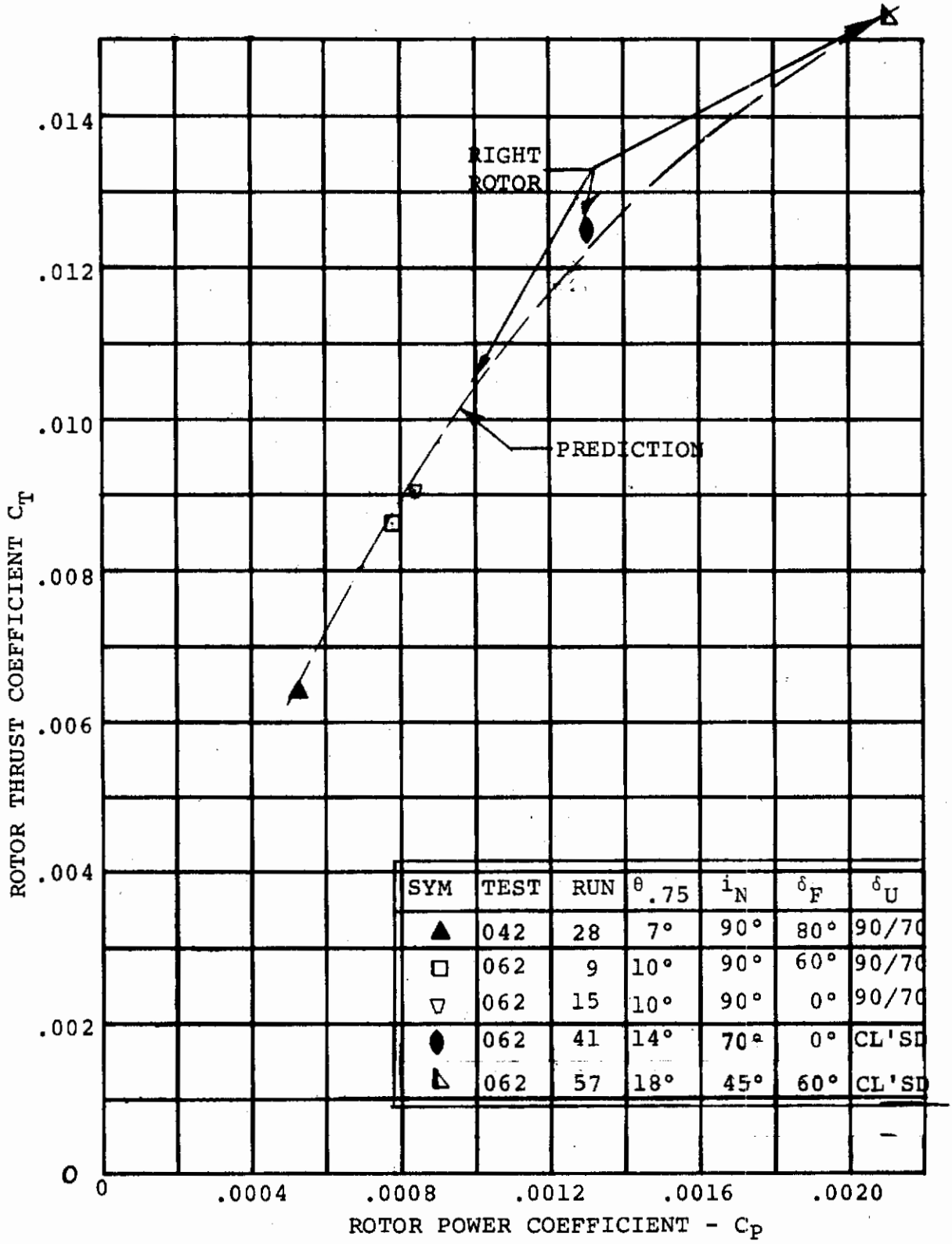

FIGURE 4.1: COMPARISON OF TEST DATA AND PREDICTION OF ROTOR THRUST/POWER COEFFICIENT VARIATION IN HOVER OUT-OF-GROUND EFFECT, 2000 RPM (ISOLATED ROTOR)

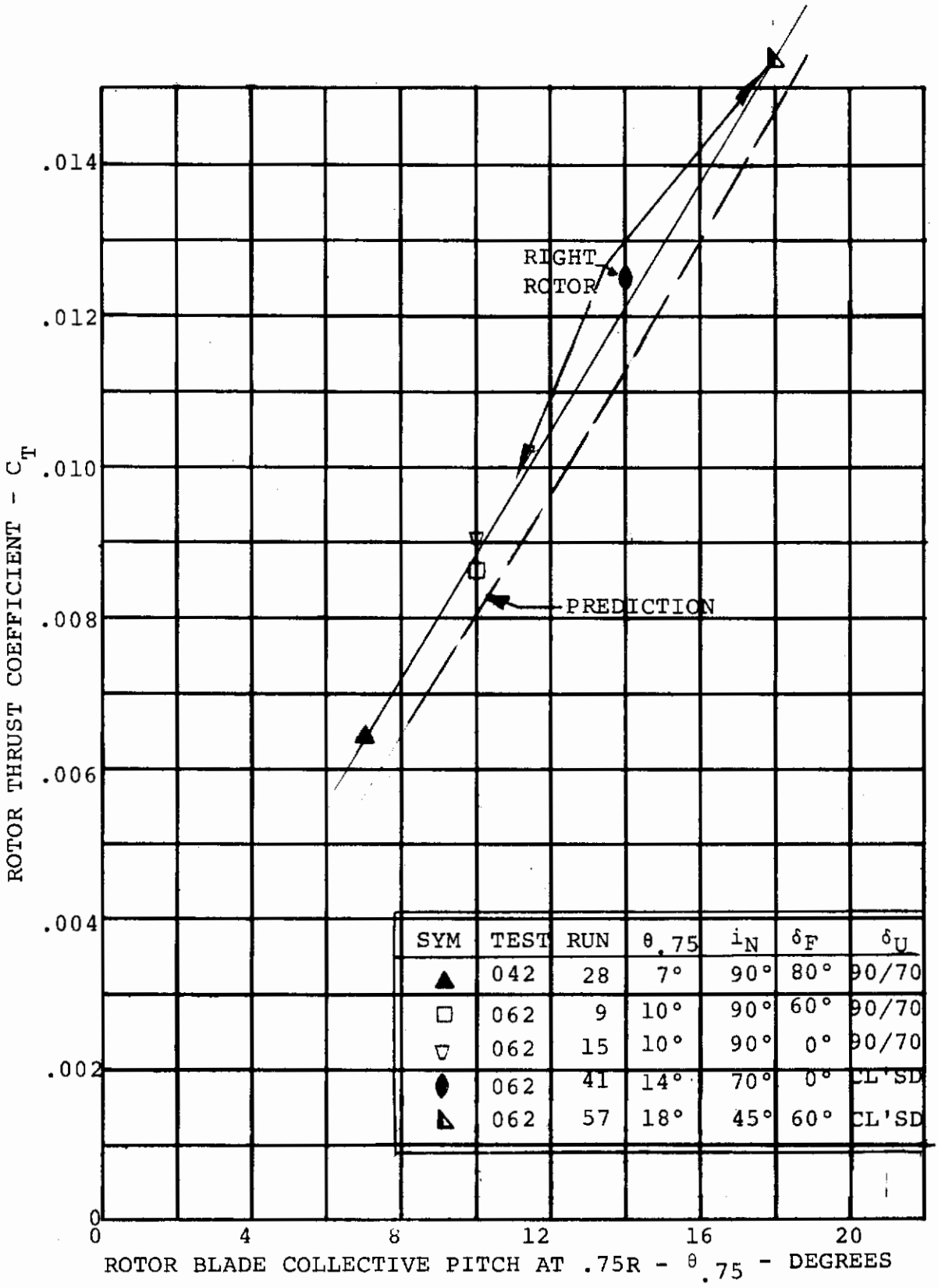

FIGURE 4.2: COMPARISON OF TEST DATA AND PREDICTION OF ROTOR THRUST COEFFICIENT/COLLECTIVE VARIATION IN HOVER OUT-OF-GROUND EFFECT, 2000 RPM (ISOLATED ROTOR)

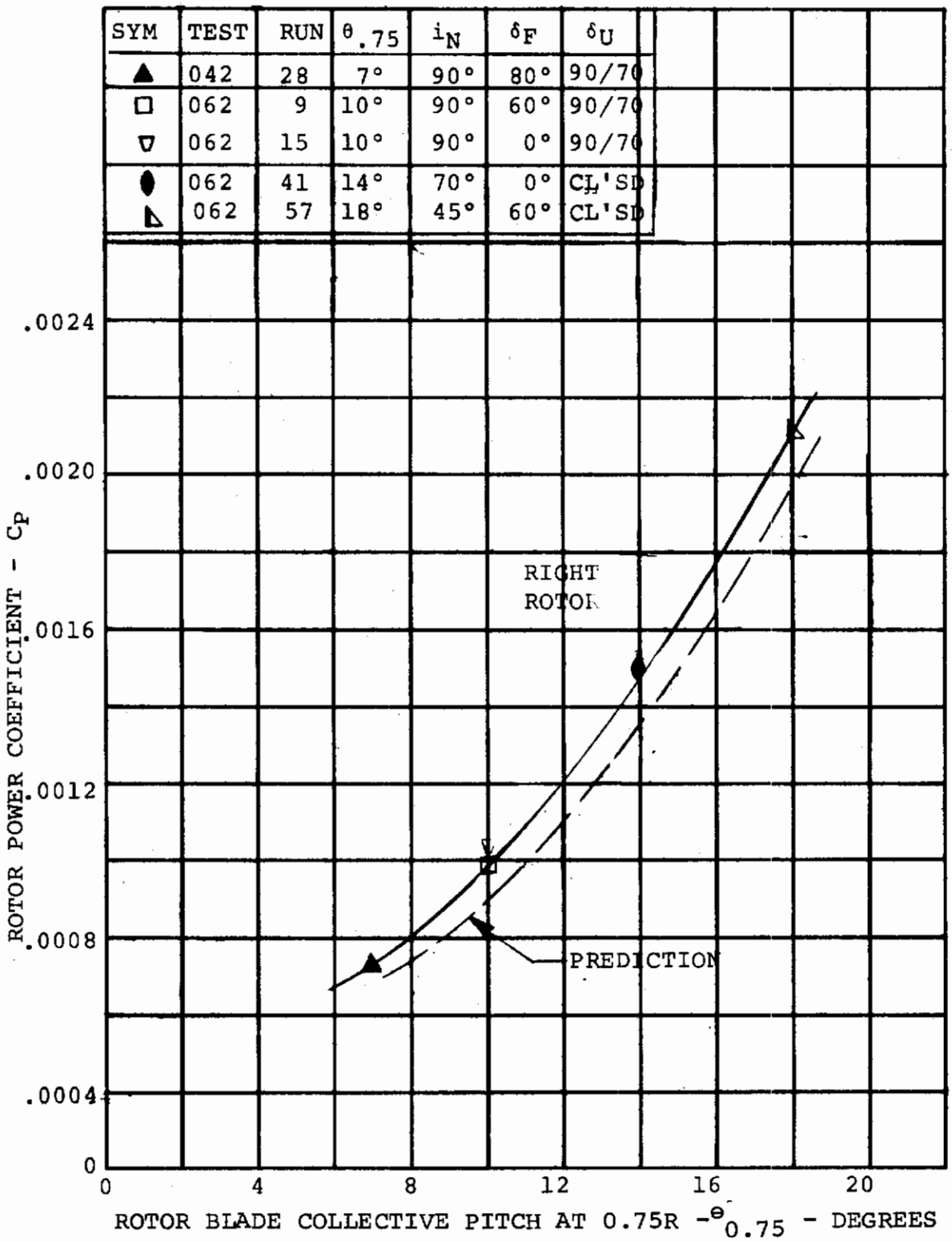

FIGURE 4.3: COMPARISON OF TEST DATA AND PREDICTION OF ROTOR POWER COEFFICIENT/COLLECTIVE VARIATION IN HOVER OUT-OF-GROUND EFFECT, 2000 RPM (ISOLATED ROTOR)

Since these data were presented at a rotor speed of 2000 rpm, it is necessary to establish the capability of the prediction method to adequately account for the variation in Mach number resulting from rpm changes. Figure 4.4 shows the degree of correlation with the variation of rotor rpm. Rotor thrust and power coefficient data are presented for blade collective angles of 10 and 14 degrees at rotor speeds of 1800 to 2600 rpm. The variation of predicted thrust and power agree with the test data, and as indicated in Figures 4.2 and 4.3, there is a shift of one degree in blade collective.

Test data shown in Figure 4.4 is for single and twin rotor operation. The solid line is a fairing through the single rotor data and the dotted line is for the same rotor for twin rotor operation. At 10 degrees collective there is no difference between the single and twin rotor operation, indicating no rotor to rotor interference, while there is a difference in the thrust and power shown for the 14 degrees collective. This implies that there is rotor to rotor interference. The rotor data presented in Figures 4.2 and 4.3, however, indicate that the isolated rotor data at 14 degrees collective is questionable. There is data available at 18 degrees collective but only at one rotor speed (1000 rpm) that show that the thrust coefficient of 0.014 for twin rotor operation is the same as single rotor operation and the associated power coefficient is 0.00176 for both modes of operation. This indicates that there is no rotor to rotor interference for this configuration which has a rotor overlap of -23.5 percent. [overlap = (1-distance between rotor/rotor diameter) 100] . Reference 4.3 indicates rotor to rotor interference decreases to zero as rotor overlap approaches zero and this trend indicates that there should be at least zero rotor to rotor interference and possibly a beneficial effect for negative overlaps.

The test data shown in Reference 1.5, Test Program II Analysis Report, Figure 4-14, for the single rotor operation at 14 degrees and the twin rotor operation at 10 degrees blade collective are not consistent with the majority of the test data. The probable cause is model oscillations producing data system errors.

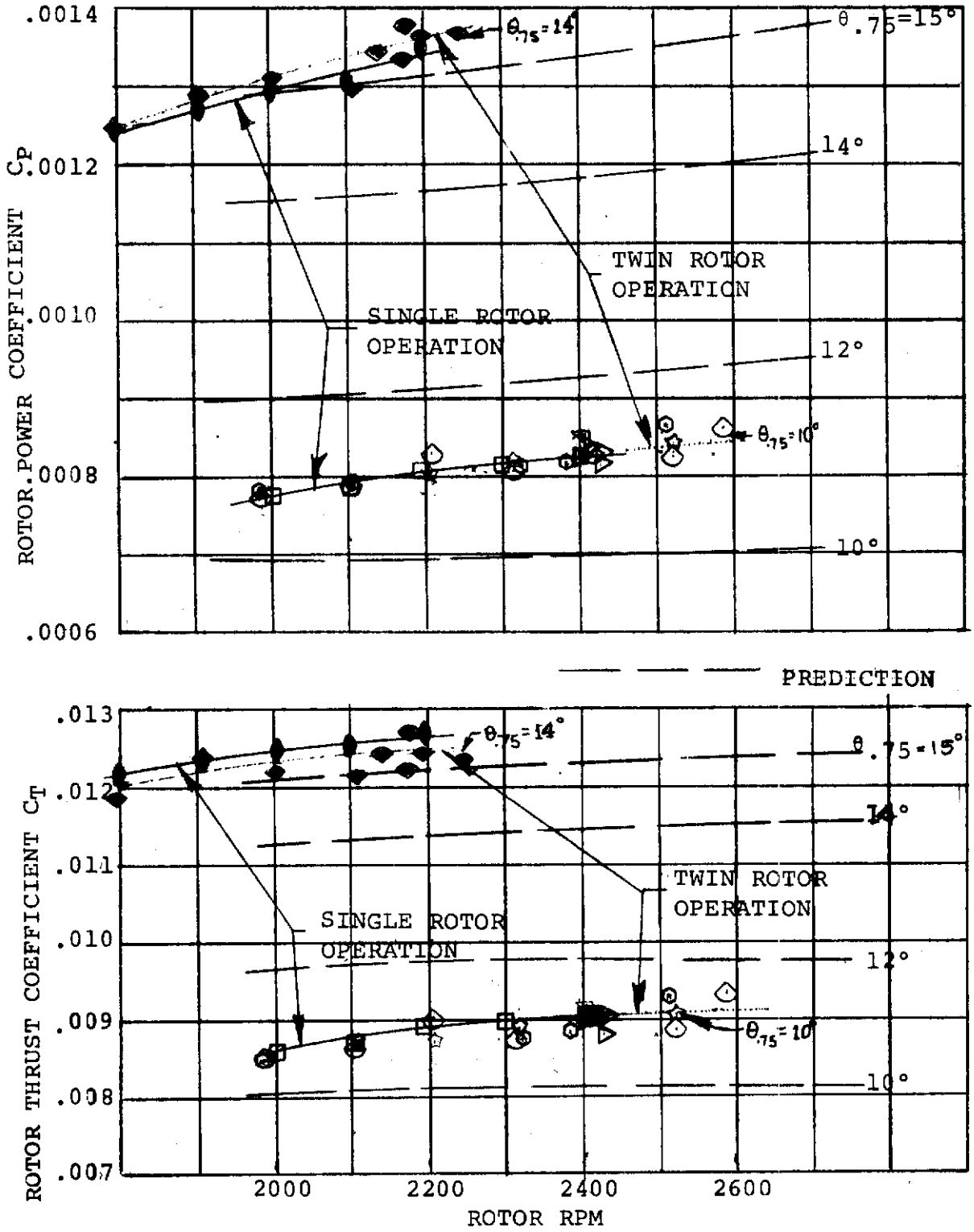

FIGURE 4.4: COMPARISON OF TEST DATA AND PREDICTION OF ROTOR THRUST AND POWER COEFFICIENT/ROTOR SPEED VARIATION IN HOVER O.G.E.

Rotor Performance data obtained in Test Program II are presented in Figure 4.5, for the following three configurations:

- Wing with umbrellas closed and zero flap deflection
- Wing with umbrellas closed and 60 degree flap deflection
- Wing with umbrellas open and 70 degree flap deflection

This indicates that wing configuration has no influence on rotor performance.

The effect of ground height on rotor performance is presented in Figure 4.6 as a ratio of power in ground effect to power out of ground effect variation with rotor height/diameter ratio. A limited amount of testing was performed in Test Program II at various ground heights but the random nature of the test data indicates that model motions have influenced the performance trends and rendered it useless. Additional testing should be performed to obtain more data for a highly twisted rotor and substantiate the trend indicated in Figure 4.6 for rotors with a small amount of blade twist.

4.1.2 Hover Download

The second major factor affecting aircraft hover performance is download. A tilt rotor aircraft develops its lift in cruise from a wing and its propulsive force from the rotors mounted on the wing tips. To hover, the rotors are tilted up 90 degrees to provide vertical thrust, but the rotors are directly over the wing resulting in a download or thrust penalty. Download is a vertical drag that is a function of the drag coefficient of the configuration, exposed area, and the slipstream dynamic pressure, which is directly dependent on thrust. Dividing the vertical drag, or download, by thrust results in a ratio that is dependent only on the product of the drag coefficient, the exposed area and a constant which is developed as follows:

$$\text{Download} = \text{Vertical Drag} = C_{D_D} q_s S,$$

where q_s is the slipstream dynamic pressure and varies radially and is a function of rotor thrust. Therefore,

$$\frac{\text{Download}}{\text{Thrust}} = \int_0^R \frac{C_{D_D} 1/2 \rho V^2 dS}{T}$$

Thrust for two rotors is equal to $4\rho\pi R^2 v_o^2$ where
v_o is the ideal induced velocity and dS = exposed wing chord XdR

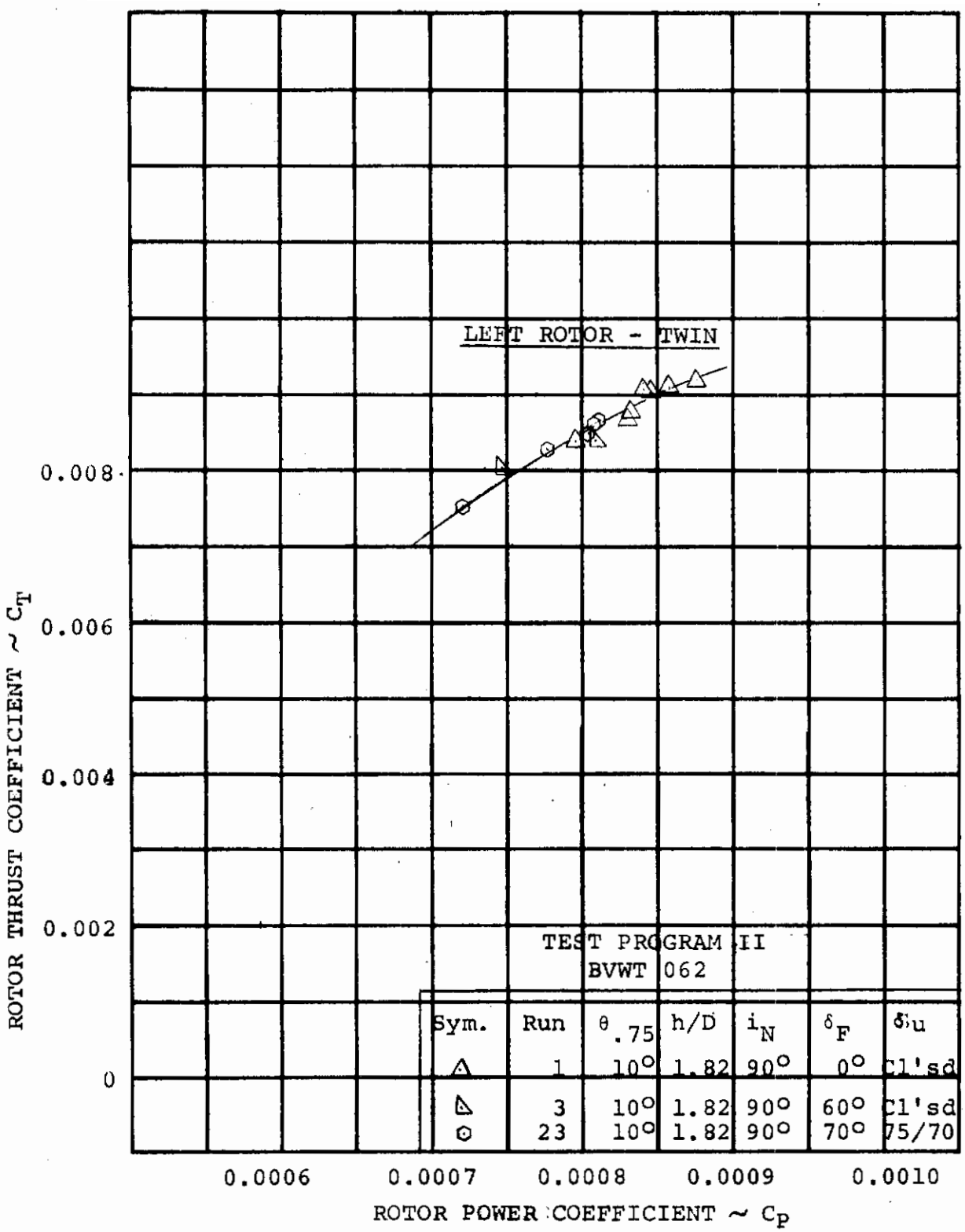

FIGURE 4.5: EFFECT OF UMBRELLA & FLAP ANGLE ON ROTOR HOVER PERFORMANCE

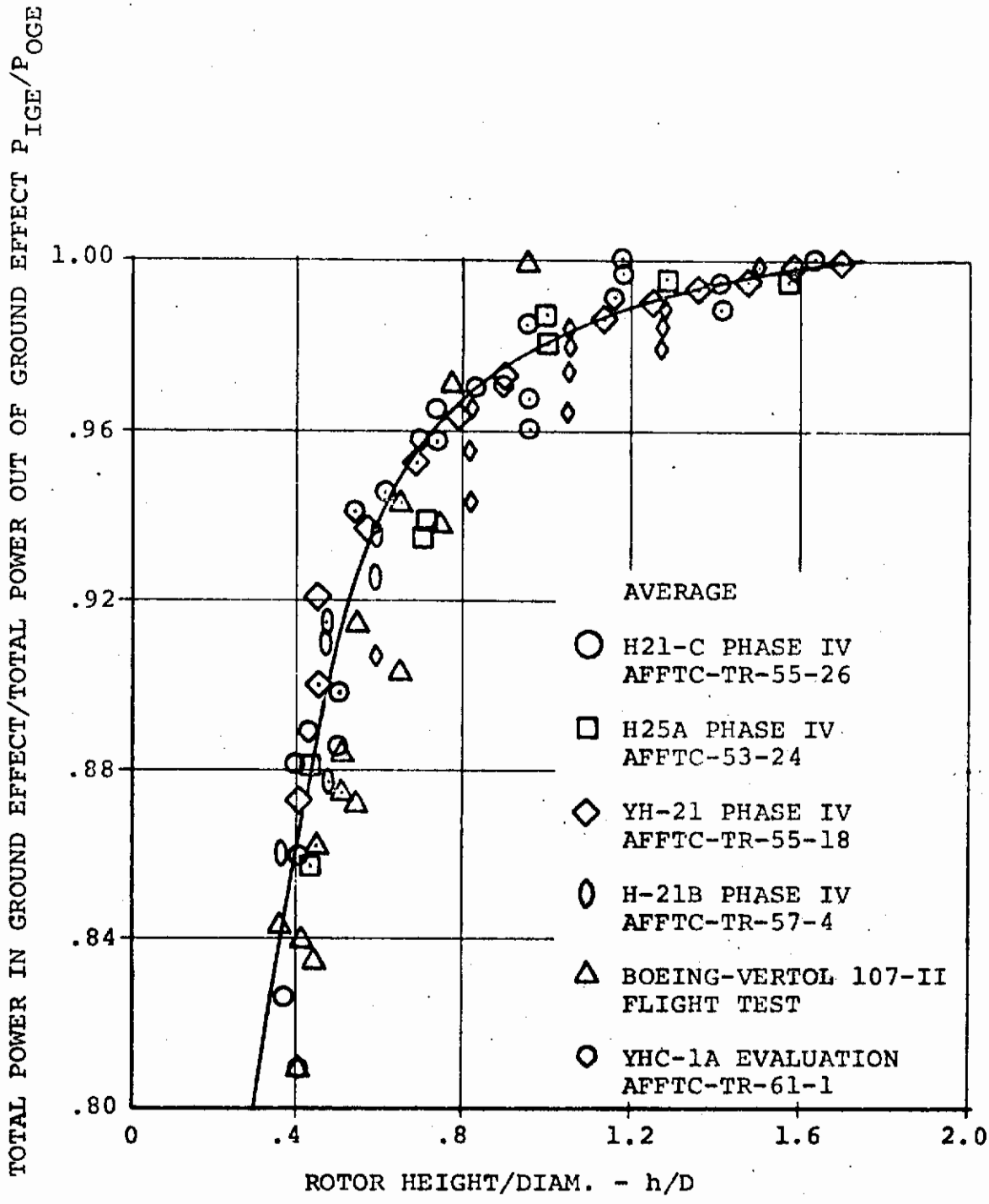

Figure 4.6: Effect of Ground Proximity on Rotor Power

which results in the following:

$$\text{Download} = \frac{C_{D_D}\, C\, R}{8\pi R^2} \int_0^R \frac{V}{V_O}^2 dX$$

The integral in the above equation is the area under the curve of the downwash velocity ratio profile versus percent radius as shown in Figure 4.7.

$$\text{Therefore } \frac{D}{T} = \frac{C_{D_D}\, C(2.75)}{8\pi(2.75)^2} \quad (8.52) = .123\, C_D\, C$$

Using the drag coefficient, C_D = 1.2 with zero flap deflection from Reference 4.3 and the model chord of .857 ft, the resulting download to thrust ratio is 0.127 as compared to a measured value of 0.128. Prediction of the download to thrust variation with various flap deflection and umbrella angles requires definition of the drag coefficient for the specific configuration under consideration. For the Model 160 the empirical download drag coefficients are presented in Figure 4.8. Utilizing these data, the download to thrust ratio for flap deflections of zero to 80 degrees with umbrellas closed and open were calculated by the method just described and is presented in Figure 4.9. The agreement with the test data is good. It is recommended that this method and empirical drag data be used for first cut preliminary design studies prior to obtaining the data from wind tunnel testing for the specific configuration under consideration.

To predict the download to thrust variation that results from varying the upper umbrella flap angle, the variation in chord and C_D are used. Examining the geometry of the Model 160 umbrellas indicates that there is no influence on the slot between the wing and lower umbrella until an angle of 70° is obtained on the upper flap. Therefore, the exposed chord and the download drag coefficient will not change for the range tested in Test Program II. Therefore, the download/thrust ratio prediction is constant as shown in Figure 4.10. The download/thrust value of 0.06 at 90° upper umbrella angle is from a run which is questionable as indicated in the discussion on rotor performance.

The effect of ground height on hover download is presented in Figure 4.11. This shows that as the aircraft height is decreased the download/thrust ratio is reduced until it is zero at a rotor height to diameter of 0.66. As the aircraft is brought to a height equivalent to zero wheel height, there is

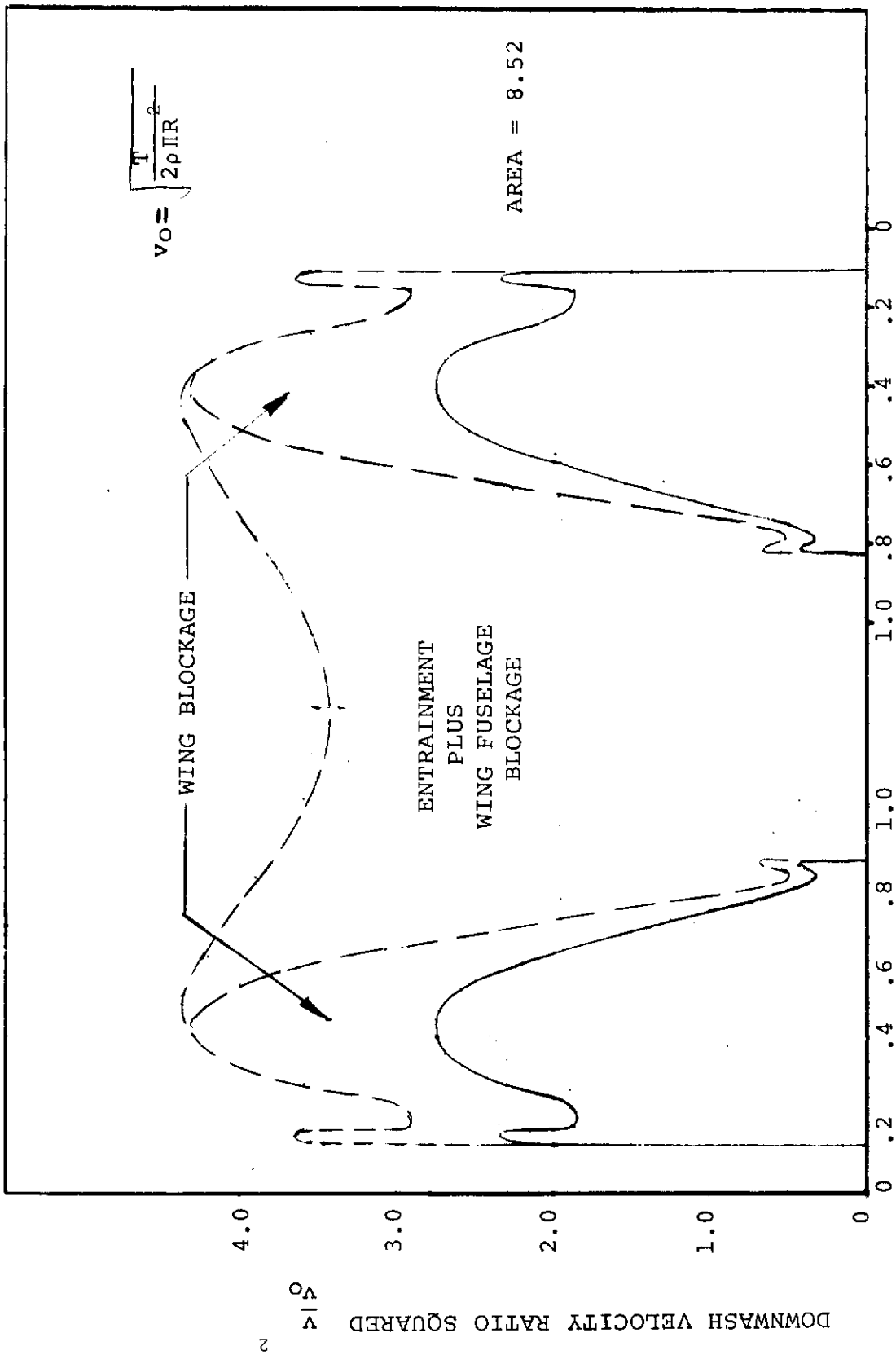

FIGURE 4.7: DOWNWASH VELOCITY PROFILE

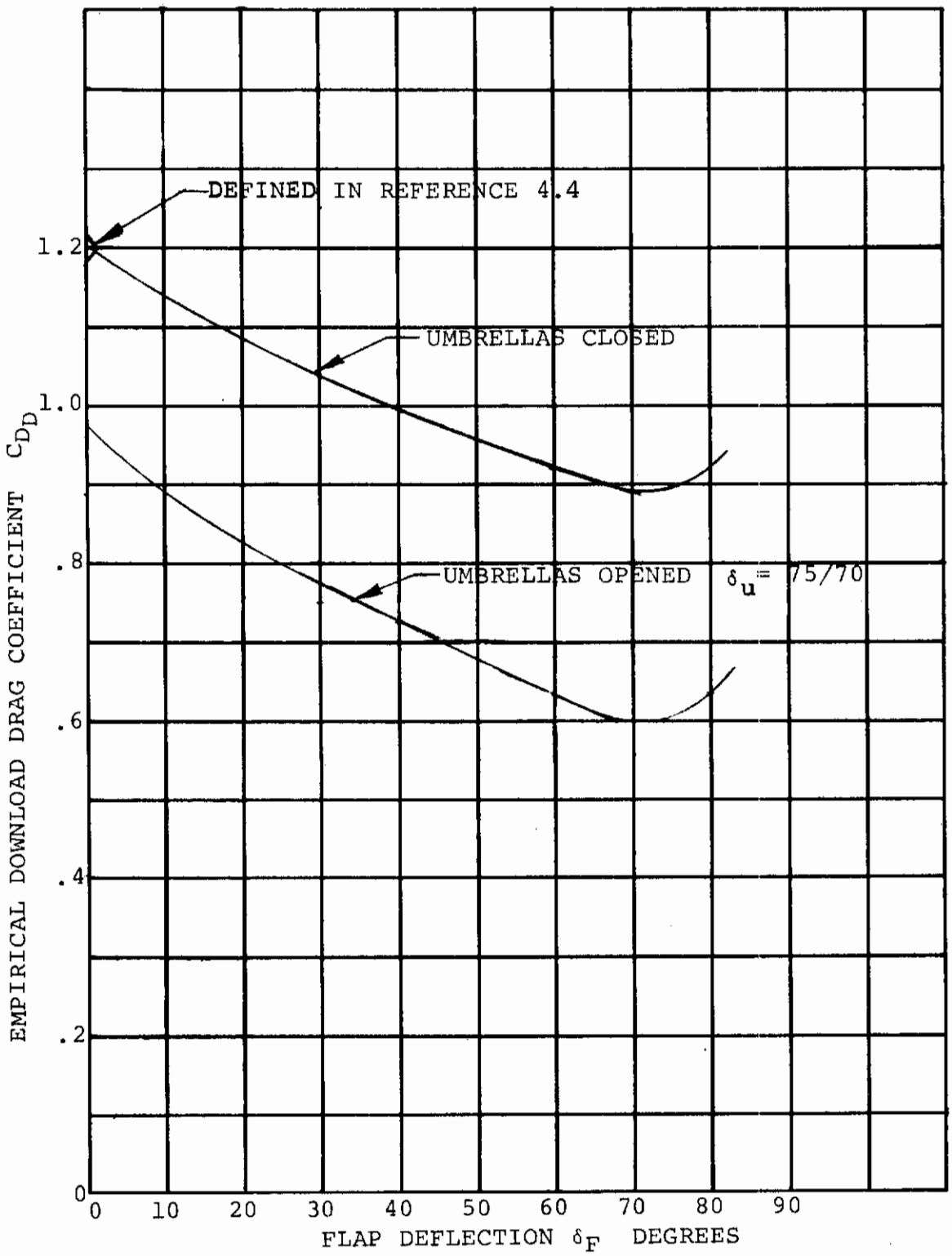

FIGURE 4.8: EMPIRICAL DOWNLOAD DRAG COEFFICIENT AS INFLUENCED BY FLAP DEFLECTION AND LEADING EDGE UMBRELLAS

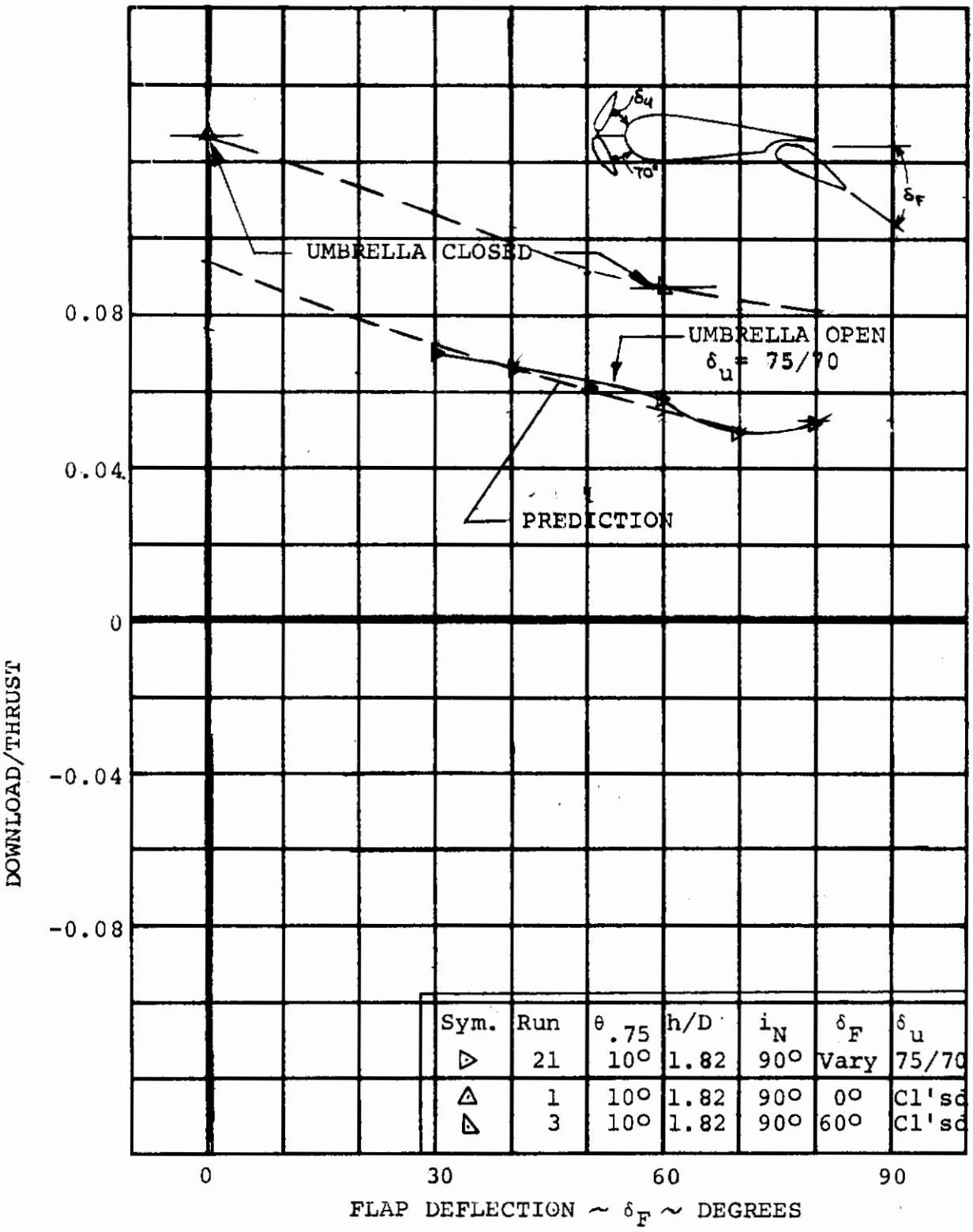

FIGURE 4.9: EFFECT OF FLAP DEFLECTION ON AIRCRAFT HOVER DOWNLOAD/THRUST RATIO

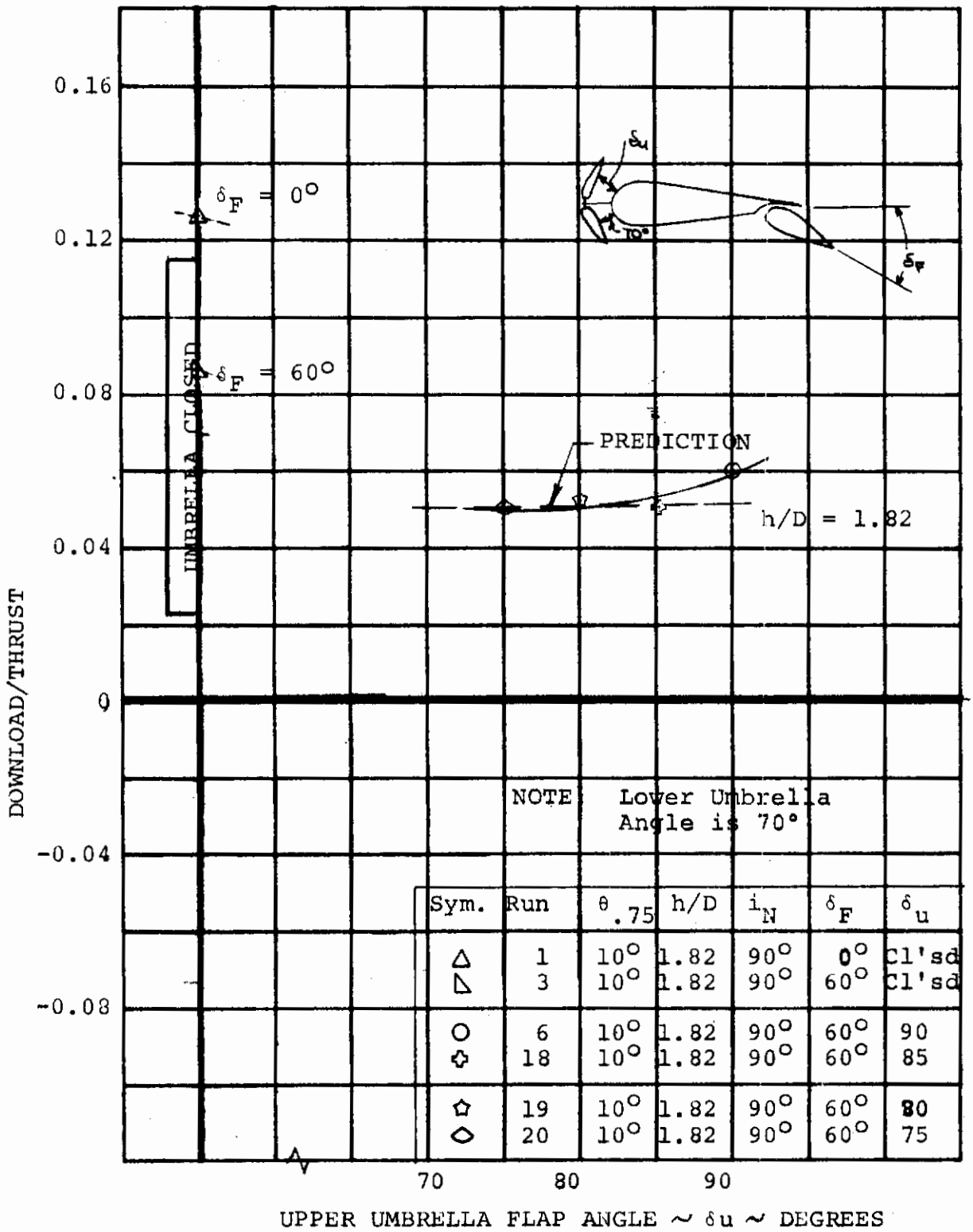

FIGURE 4.10: EFFECT OF UMBRELLA FLAP ANGLE ON AIRCRAFT HOVER DOWNLOAD/THRUST RATIO

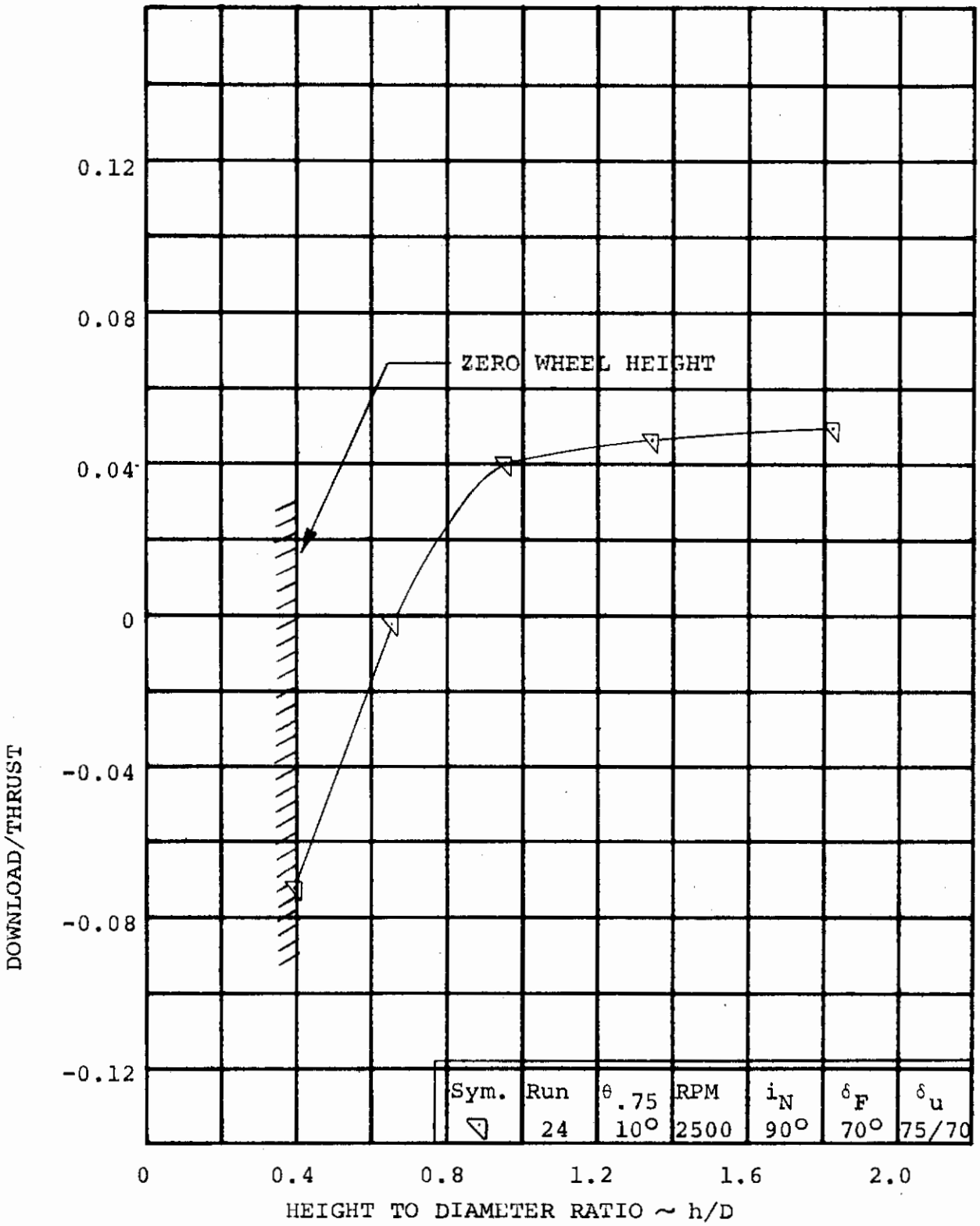

FIGURE 4.11: EFFECT OF GROUND HEIGHT ON AIRCRAFT HOVER DOWNLOAD/THRUST RATIO

an upload on the fuselage and wing which appears to be the result of the rotor downwash creating a pressure pad under the fuselage. No methodology exists presently for predicting this effect and this is an area requiring further testing to obtain pressure data on the fuselage and wing.

4.1.3 Hover-Aircraft Performance

These prediction techniques were combined to estimate the total aircraft hover capability shown in Figure 4.12 for the aircraft with the flaps and umbrellas deflected. Accounting for the difference in performance characteristics between the right and the left rotor the agreement is very good. There is a slight deviation at the lower gross weight coefficient which is in the lower RPM range and well below the normal hover RPM operation for the full scale aircraft.

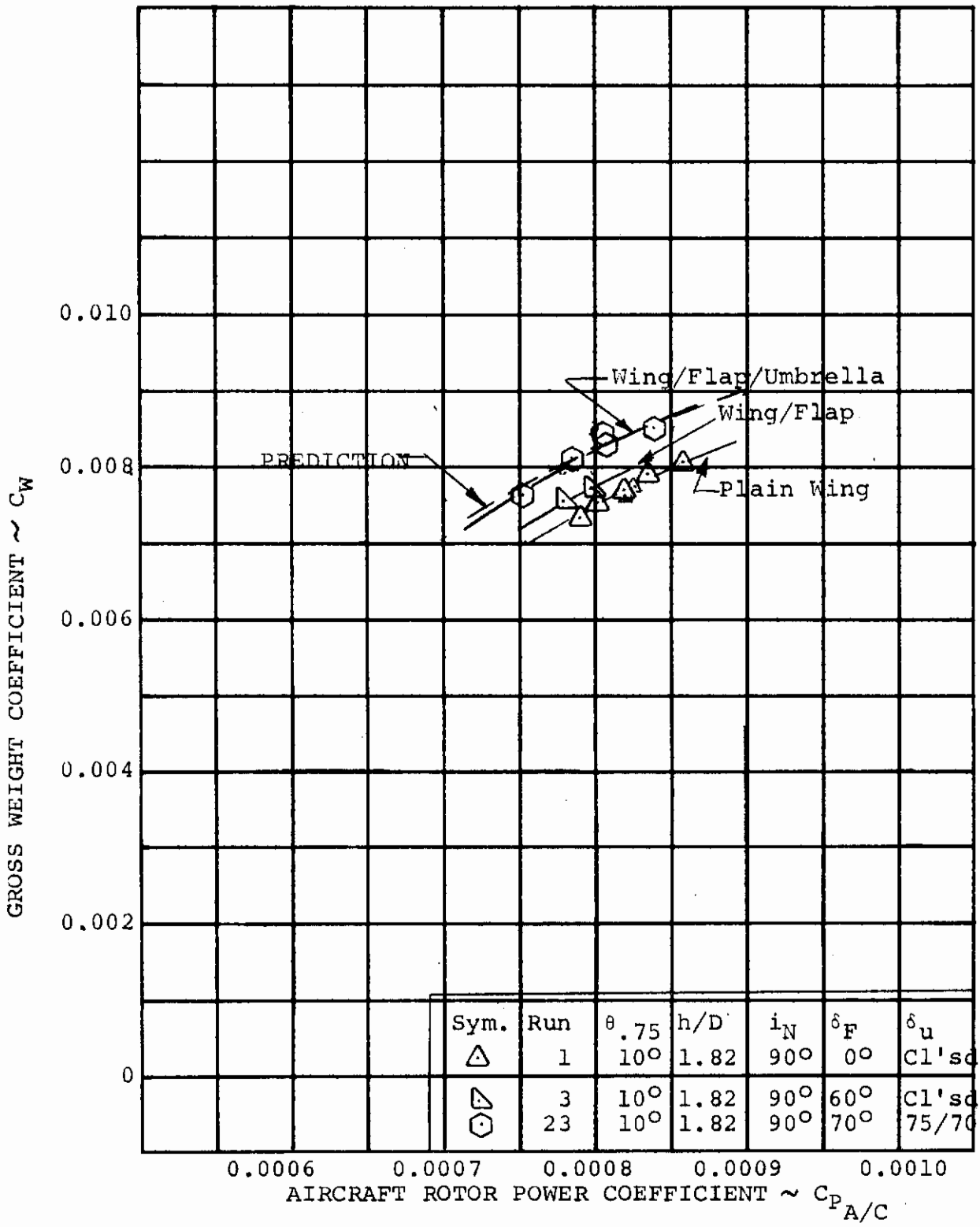

FIGURE 4.12: EFFECT OF UMBRELLA & FLAP ANGLE ON TOTAL AIRCRAFT HOVER PERFORMANCE

4.2 TRANSITION PERFORMANCE

The transition mode refers to operation out-of-ground effect from hover to the cruise regime. The nacelles rotate from 90 degrees incidence (i_N) to zero degrees incidence. During this flight regime, the rotor has a significant influence on the aircraft performance since it provides part of the lift as well as all the propulsive force.

4.2.1 Rotor Performance in Transition

Rotor performance prediction techniques used for transition have been developed for the helicopter rotor flight regimes and are applicable to tilt rotor operation in transition. Reference 4.5, the Rotor Airloads and Performance Analysis with Non-Uniform Inflow, describes this prediction method in detail. A brief description will be included here. This analysis computes the airloads, performance and flapping equilibrium of props and rotors in steady forward flight. The rotor geometry may be of arbitrary planform, twist and radial variation of airfoil characteristics. This analysis determines a simplified solution utilizing a uniform downwash approach based on momentum theory. The blade circulations and flapping angles are then defined and are used to generate the geometry and to calculate the induced velocities from the trailed vortex system. The trailed vortex system is nondistorted by vortex-to-vortex interactions and does not contract. After this, the equations of motion are once again solved using the influence of non-uniform induced inflows. An option available with this program is the capability of imposing circulations on the rotor resulting from the proximity of another rotor or a wing.

Using this analysis, the rotor performance was calculated for the 1/10 scale Model 160 Wind Tunnel Model that was tested in Test Program II. Figure 4.13 presents the rotor thrust coefficient variation with fuselage angle of attack for nacelle incidence values of 70 and 45° that was used as input into the program. Including the circulation developed by the wing as additional input, the rotor characteristics were then determined. Rotor power coefficient/angle of attack variation is presented in Figure 4.14. The agreement between the prediction and test data is very good. Total rotor hub moments were also predicted and the comparison with test data shown in Figure 4.15 indicates fair agreement. The slope is lower than the test data but is exactly the same at zero fuselage angle of attack. Further correlation must be done

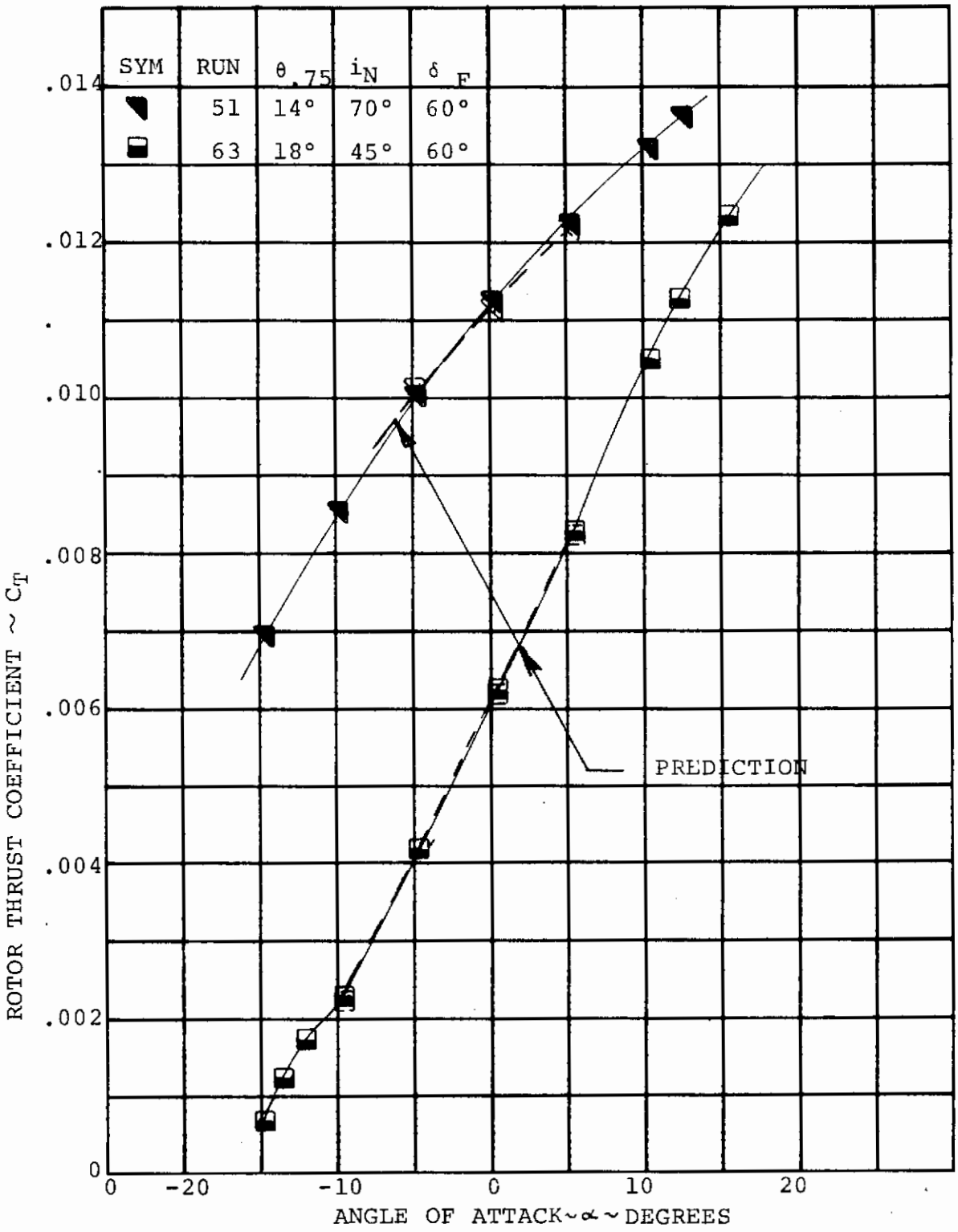

FIGURE 4.13: COMPARISON OF TEST AND PREDICTION FOR ROTOR THRUST COEFFICIENT/ANGLE OF ATTACK VARIATION IN TRANSITION

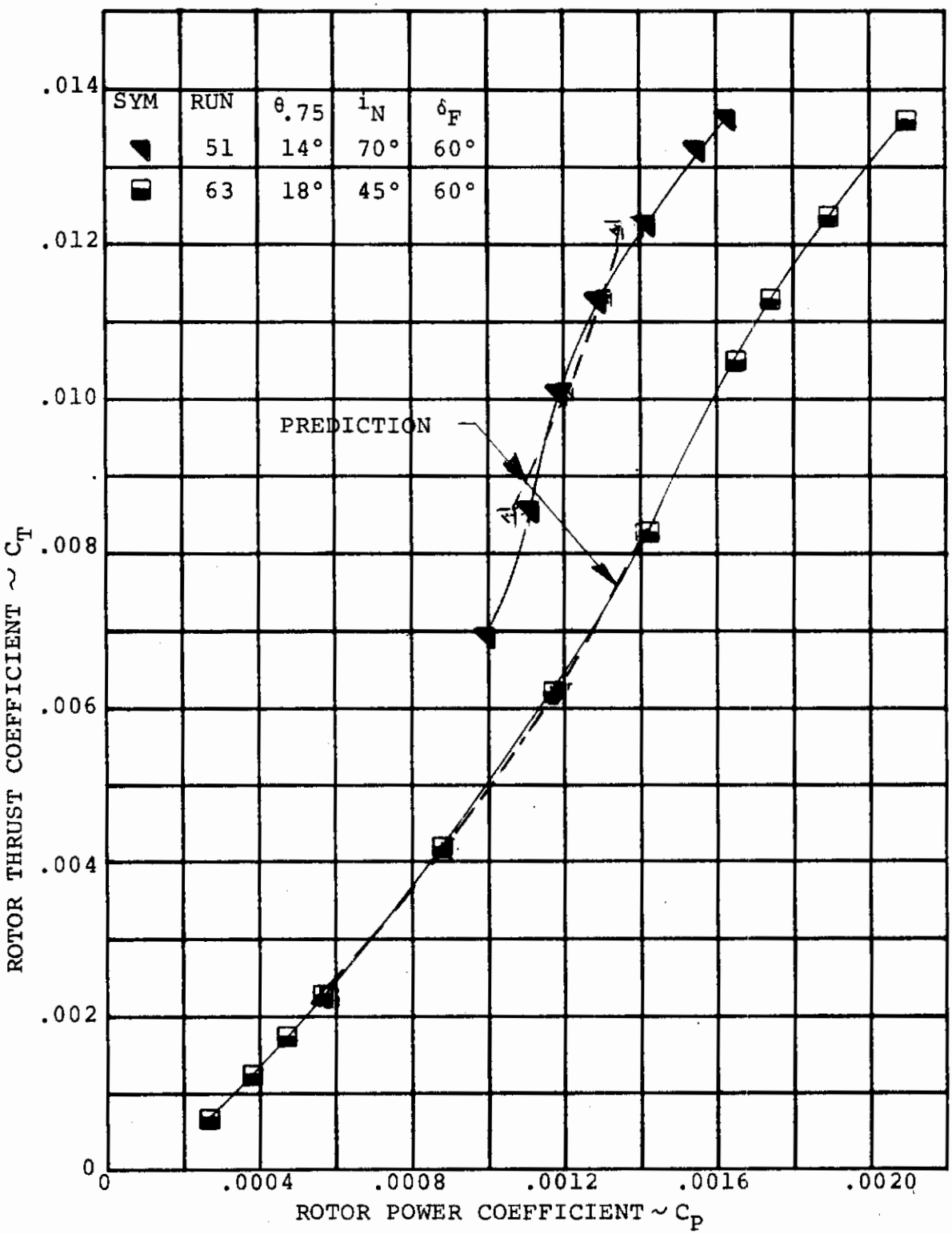

FIGURE 4.14: COMPARISON OF TEST AND PREDICTION FOR ROTOR THRUST/POWER COEFFICIENT VARIATION IN TRANSITION

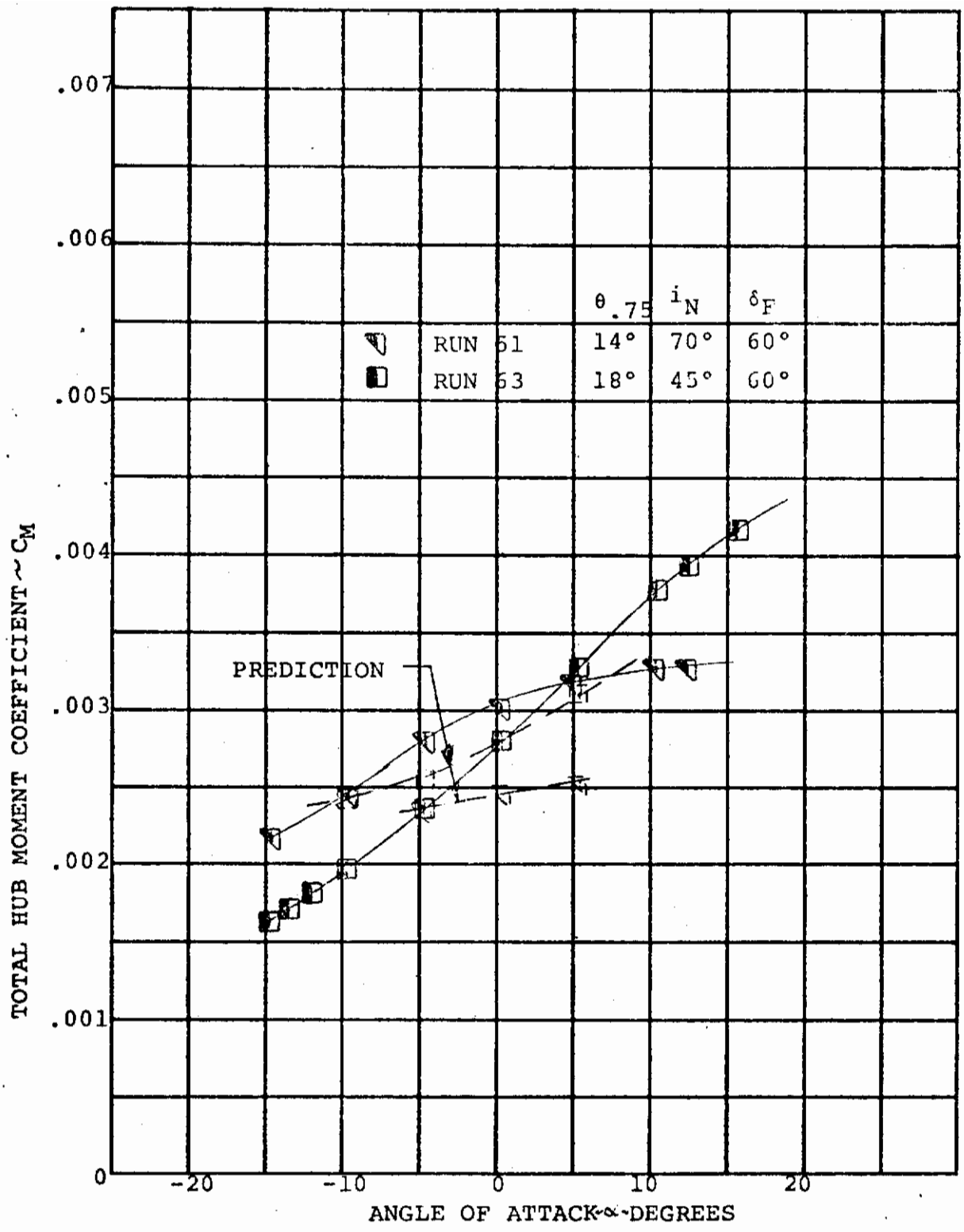

FIGURE 4.15: COMPARISON OF TEST AND PREDICTION FOR TOTAL HUB MOMENT IN TRANSITION

to determine the cause for this difference but since transition will be flown with a fuselage angle of attack of approximately zero, the performance and trim defined by this analysis will be accurate.

4.2.2 Rotor/Airframe Interactions in Transition

In the transition regime, the high rotor induced velocity and rotor shaft angles have a significant impact on the local angle of attack of the wing and possibly have some impact on the tail and fuselage contribution to the airframe characteristics. This effect results in a shifting of the airframe lift by an incremental angle of attack equal to the average downwash over the wing.

The aircraft lift data are presented in Figures 4.16 and 4.17 for the 70 and 45 degree nacelle incidence. At 70 degrees, the rotor downwash effect indicated by the shaded area has displaced the airframe lift curve by approximately 6 degrees as a result of the downwash. At 45 degrees nacelle incidence, the airframe lift curve is displaced by approximately 3 degrees at zero lift but decreases as the angle of attack is increased. This increase in lift curve slope appears to be the result of the increase in local dynamic pressure over the wing produced by the rotor. This also accounts for the increase in maximum lift coefficient to 2.0.

The displacement of the lift curve at 70 degrees and 45 degrees nacelle incidence is approximately the same as the downwash angle defined by the induced velocity through the rotor disc and the free-stream velocity.

4.2.3 Aircraft Performance in Transition

Testing was performed in transition at nacelle incidence values of 70, 45 and 0 degrees with 60 degrees flap deflection. This total aircraft performance obtained in Test Program II is presented in Figures 4.18 through 4.20. No correlation has been performed but since the rotor performance and the rotor-airframe interactions are known, it is reasonable to infer that these data would be predicted with good agreement.

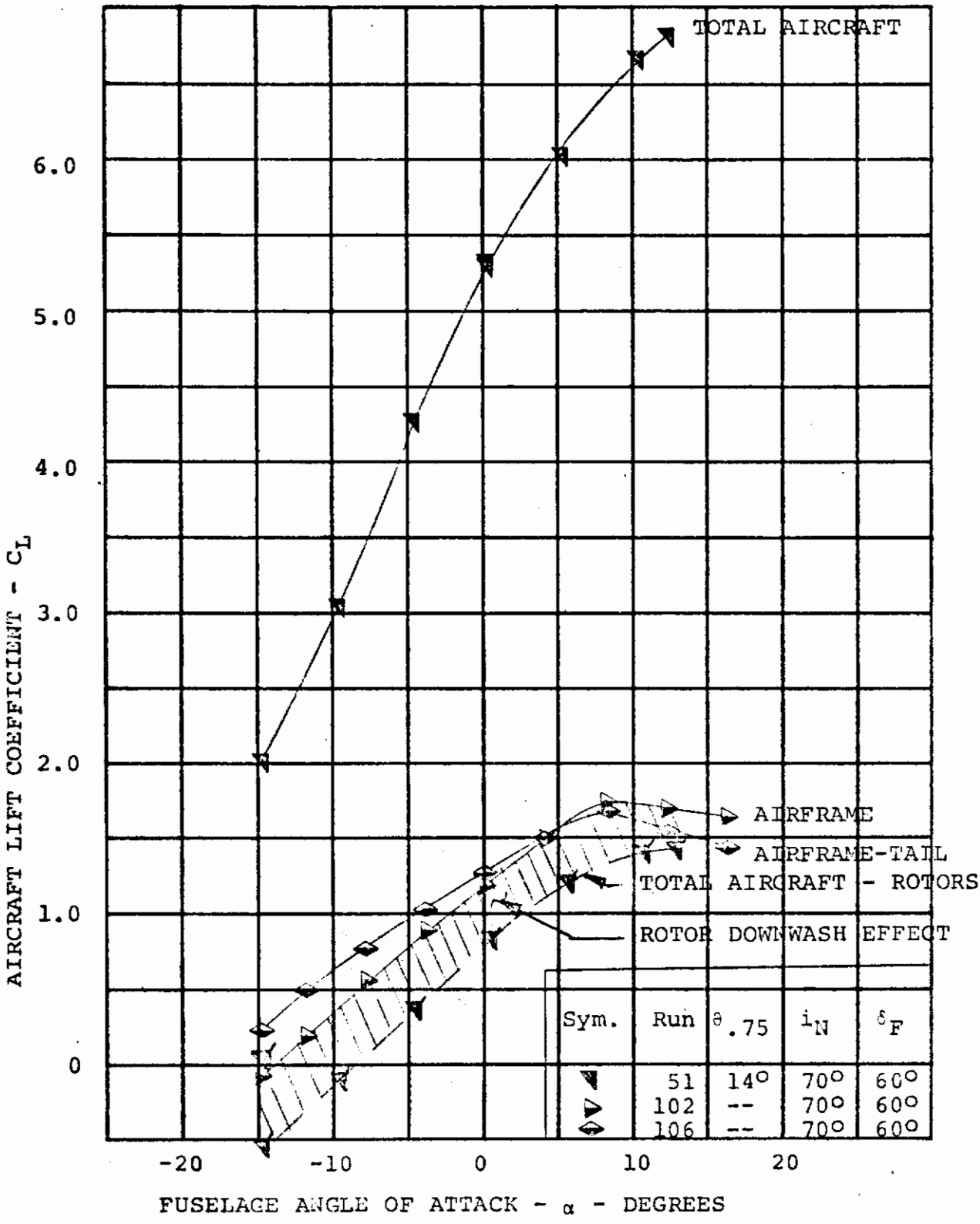

FIGURE 4.16 CONTRIBUTION OF PROP/ROTOR AND HORIZONTAL TAIL TO AIRCRAFT LIFT AT $V/V_T = 0.206$ WITH $i_N = 70^\circ$

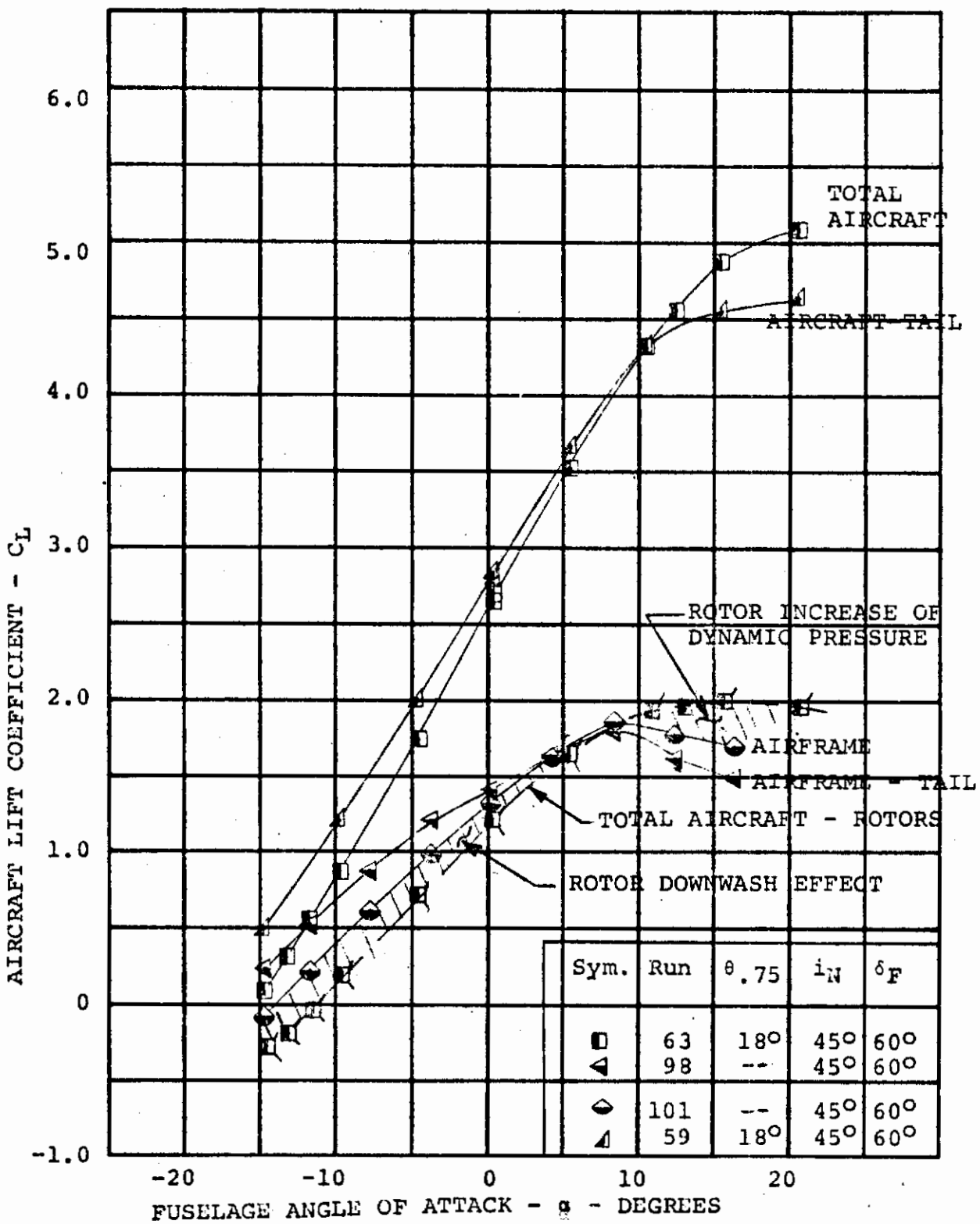

FIGURE 4.17 CONTRIBUTION OF PROP/ROTOR AND HORIZONTAL TAIL TO AIRCRAFT LIFT AT $V/V_T = 0.260$ WITH $i_N = 45°$

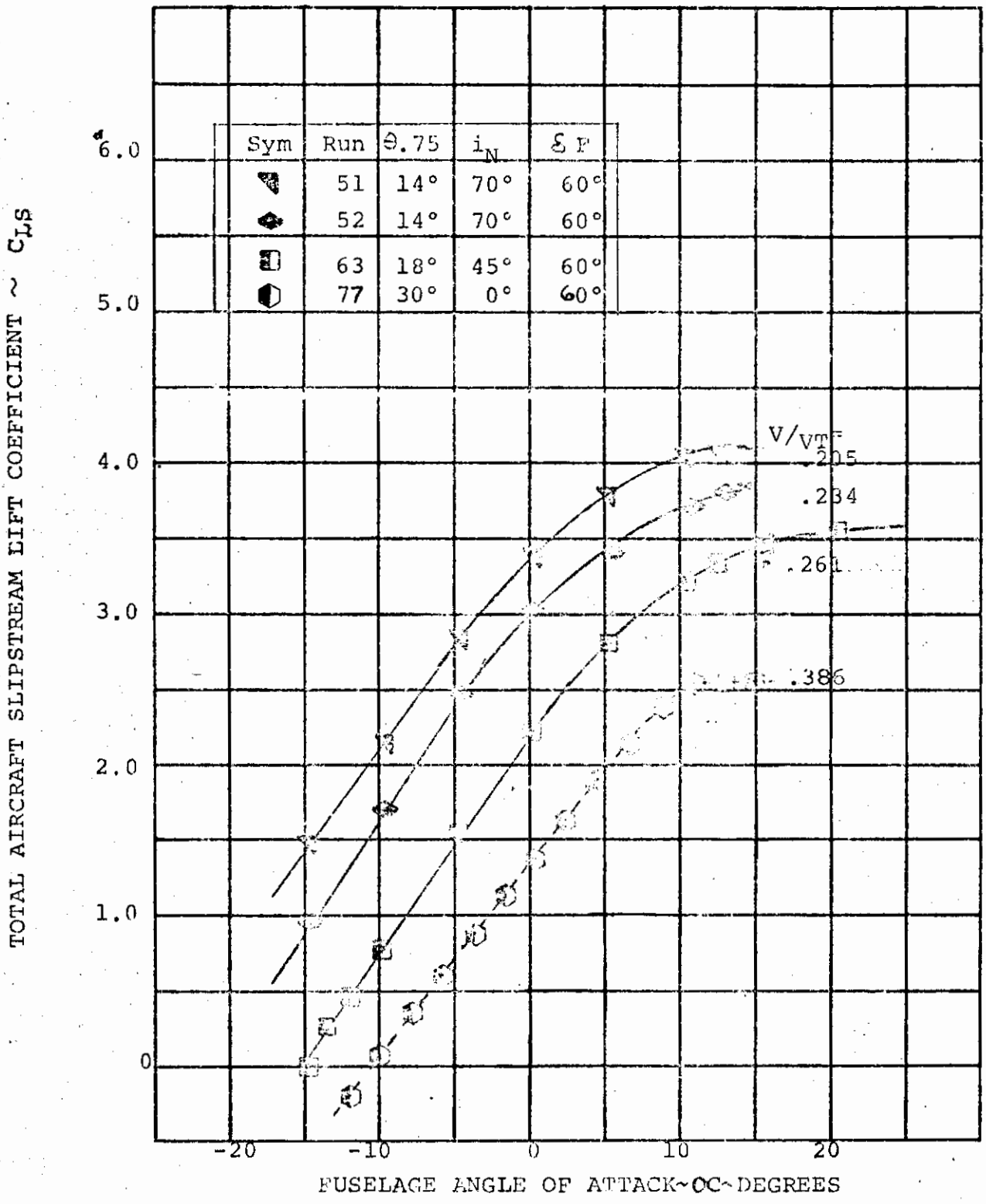

FIGURE 4.18 AIRCRAFT LIFT/ANGLE OF ATTACK VARIATION DURING TRANSITION

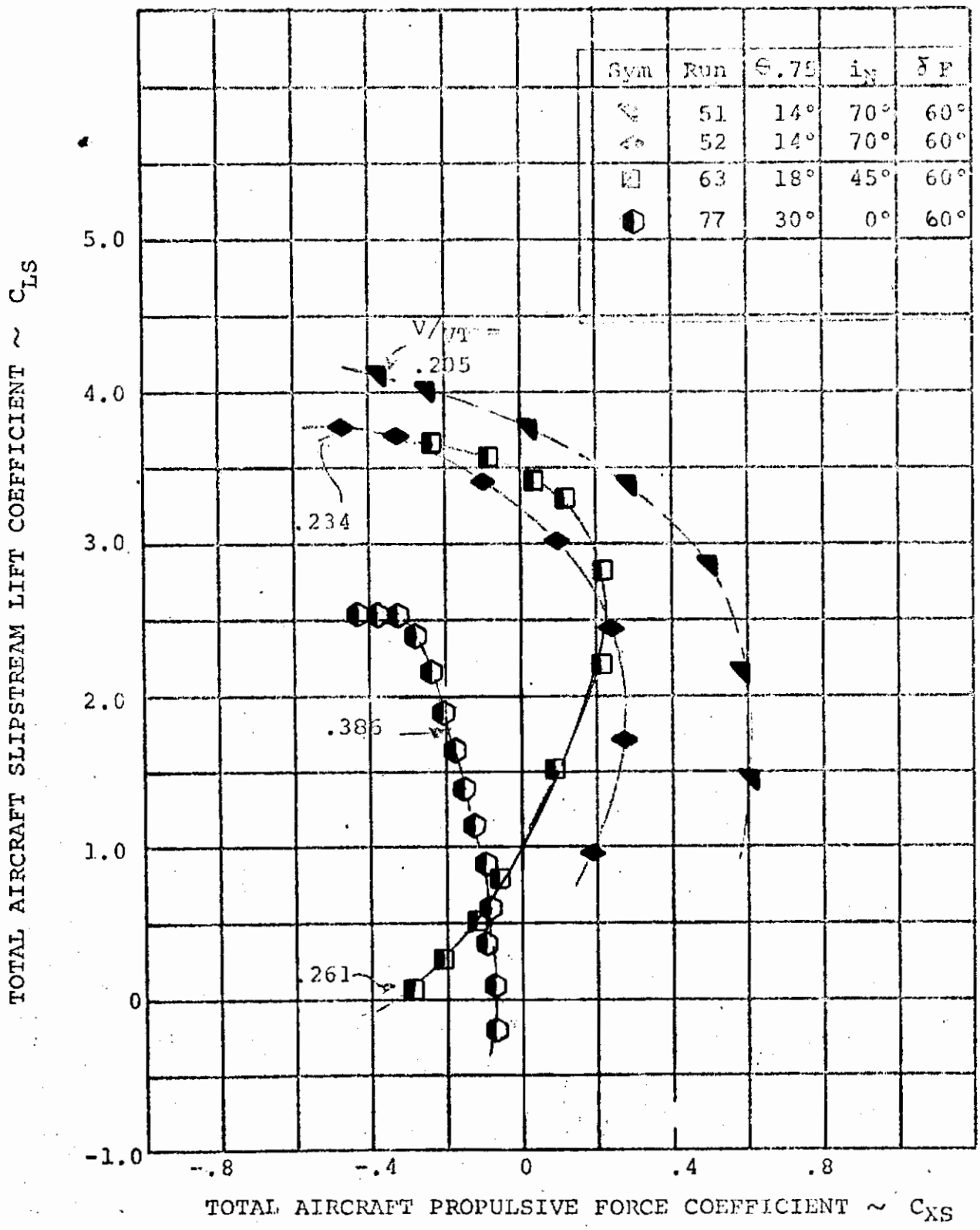

FIGURE 4.19 AIRCRAFT LIFT/PROPULSIVE FORCE VARIATION DURING TRANSITION

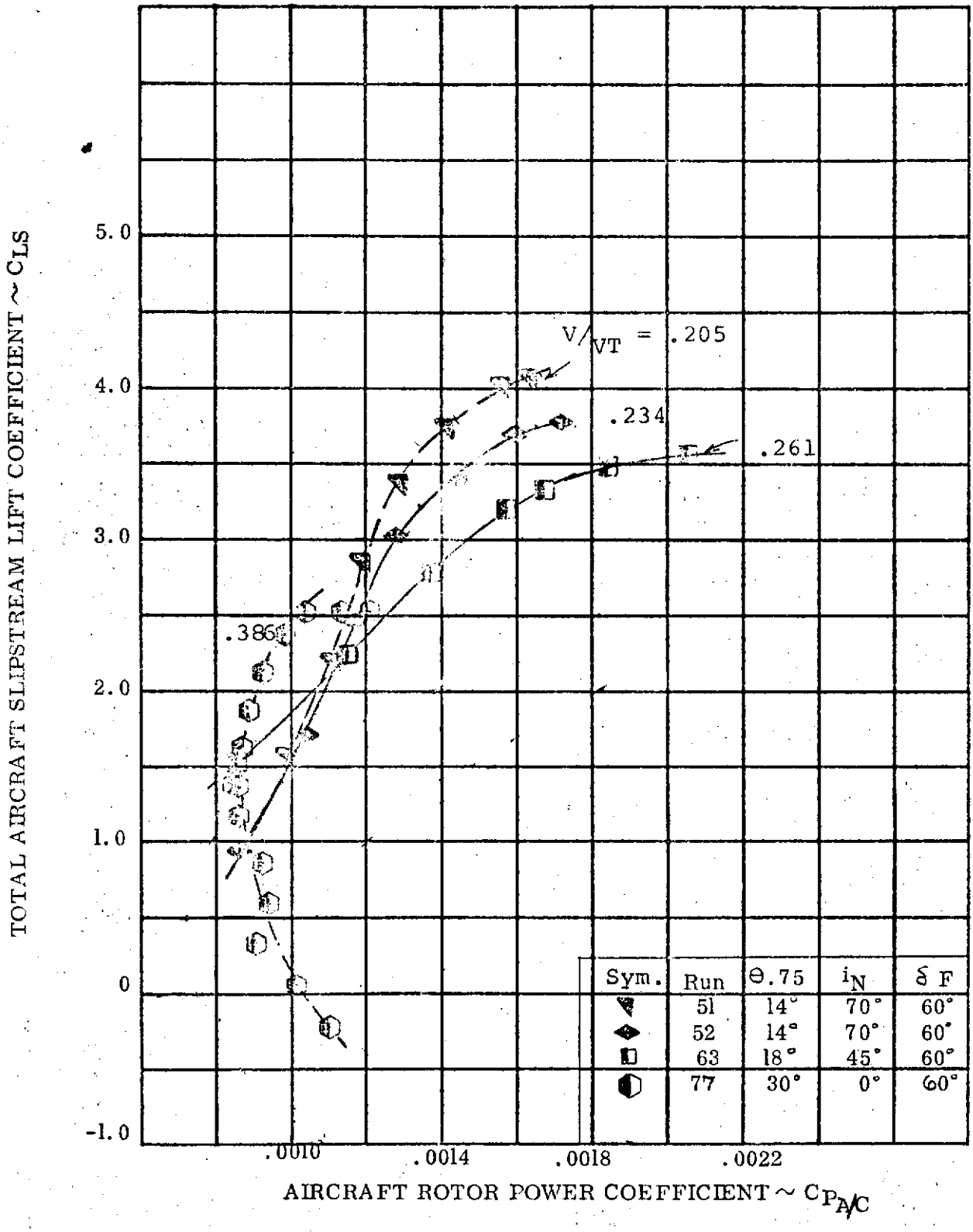

FIGURE 4.20 AIRCRAFT LIFT/POWER REQUIRED VARIATION DURING TRANSITION

4.3 CRUISE PERFORMANCE IN TILT ROTOR MODE

The cruise mode, as discussed here, will refer to operation with the nacelle incidence of zero and the rotors in axial flight. In this flight regime, the rotors have a major impact on the aircraft stability and performance in that they are larger and more flexible than conventional propellers. Both these factors can greatly affect the rotor performance and gust sensitivity.

4.3.1 Rotor Performance in Cruise

The prediction method used for cruise is the same as described in Section 4.2.1. A comparison of the predicted rotor performance with test data is shown in Figures 4.21 and 4.22. For the rotor thrust variation with angle of attack defined in Figure 4.21, the resulting rotor power predicted is shown in Figure 4.22. As with transition, the agreement is very good and indicates that the prediction technique is satisfactory for both regimes of flight.

4.3.2 Rotor/Airframe Interactions in Cruise

The rotor influence on the airframe is very small since the thrust is very low in comparison to hover and transition. The increment in dynamic pressure over the wing is very low and results in no increase in airframe lift. Also, the rotor wake does not influence the horizontal tail and its contribution to stability over the range tested. Figure 4.23 presents the incremental aircraft pitching moment coefficient obtained with the rotors on and also the rotors off. There is no difference in the two sets of data; therefore, the rotor does not influence the airframe or the horizontal tail over the range tested because of the very low induced velocity compared with free-stream velocity in cruise.

4.3.3 Aircraft Performance in Cruise

When determining the aircraft performance and stability in cruise, it is important to correctly predict the airframe characteristics. These characteristics are not different from those for a conventional fixed wing airplane. Airframe lift and drag characteristics were obtained with the rotors removed in Test Program II and are presented in Figure 4.24. Prediction of the airframe lift variation with angle of attack was made using the methods presented in DATCOM, Reference 4.6. The prediction agrees reasonably well with the test data. Predictions of the airframe, the prop/rotor and tail contributions to total aircraft pitching moment characteristic were

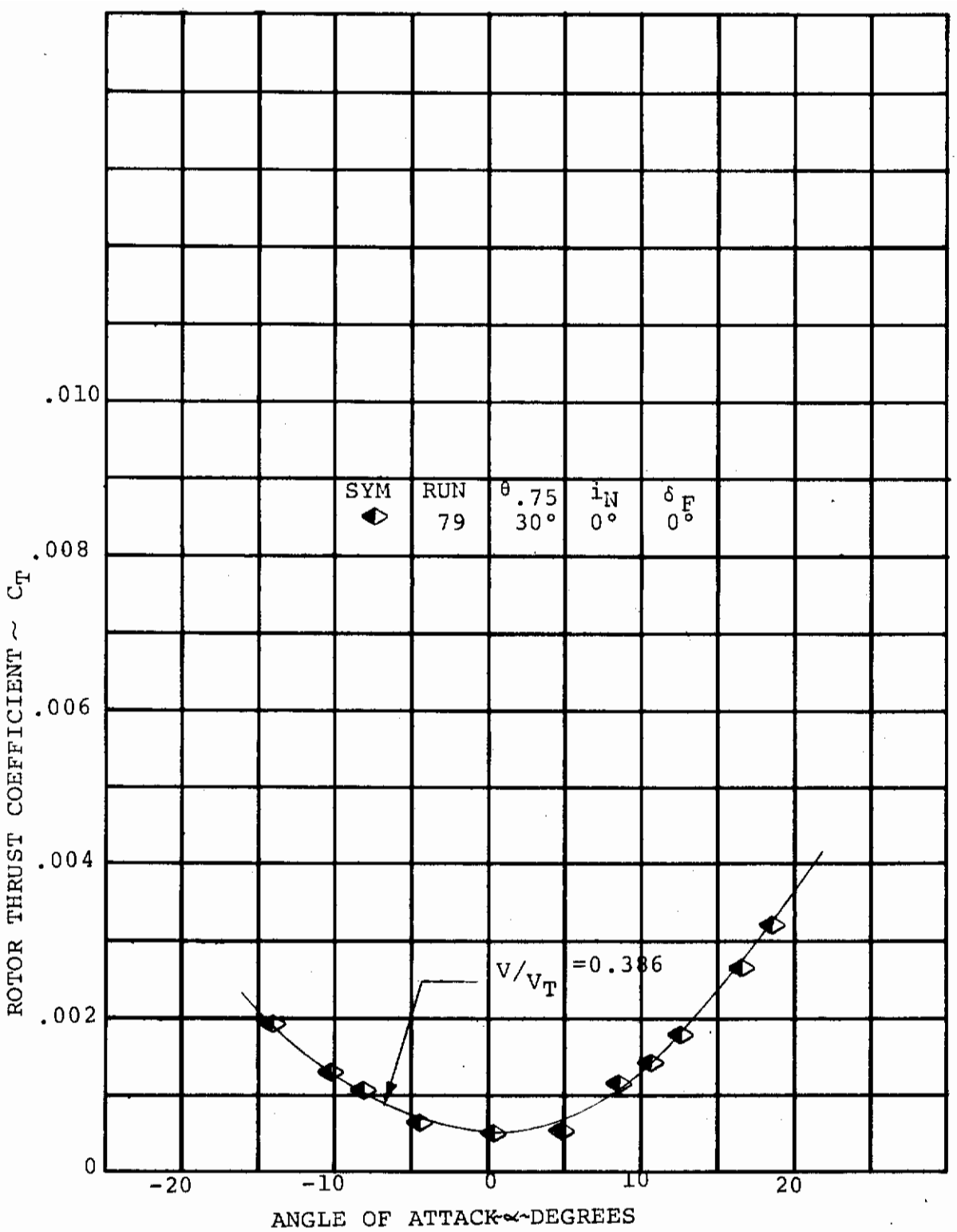

FIGURE 4.21: ROTOR THRUST/ANGLE OF ATTACK VARIATION IN CRUISE

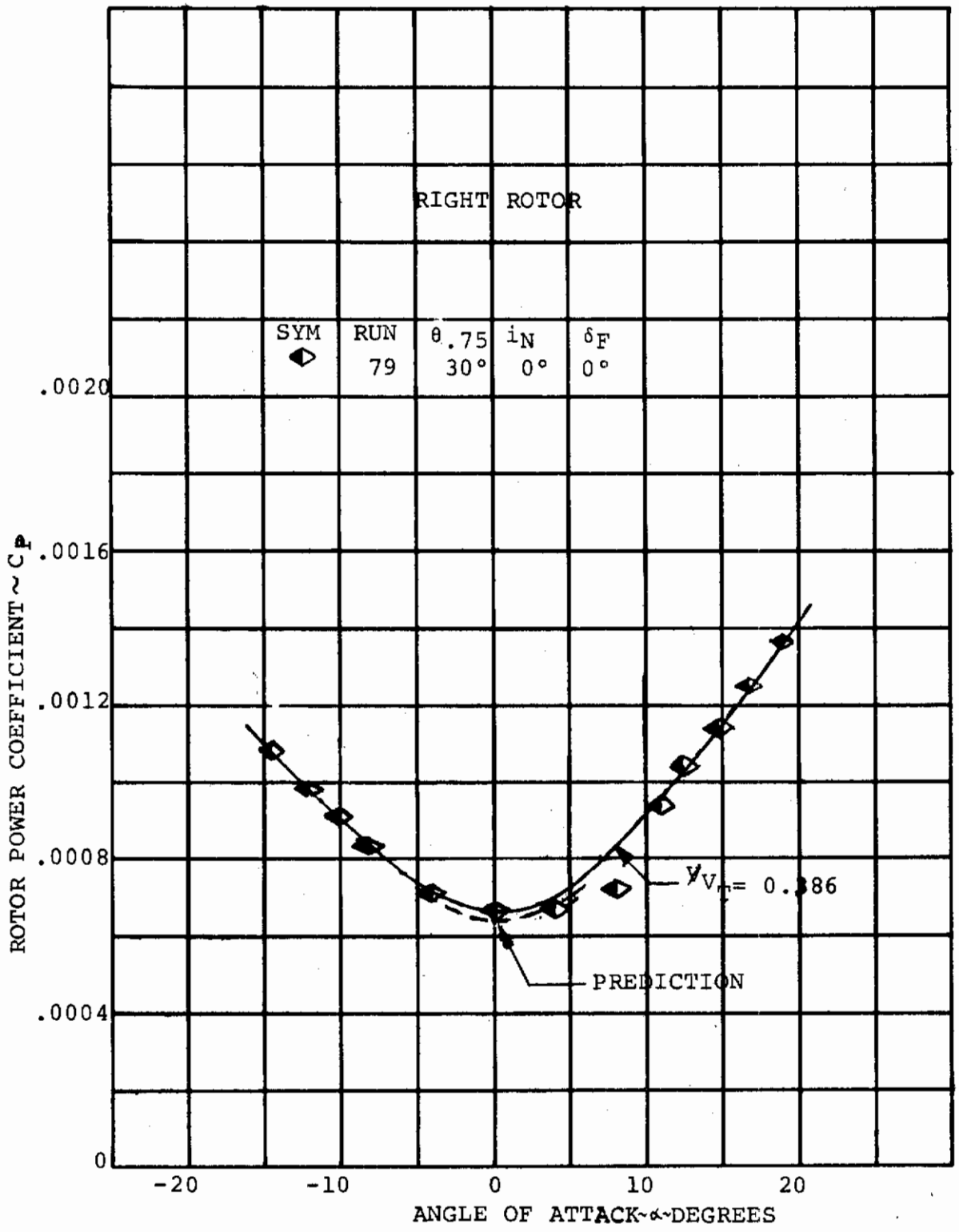

FIGURE 4.22: ROTOR POWER/ANGLE OF ATTACK VARIATION IN CRUISE

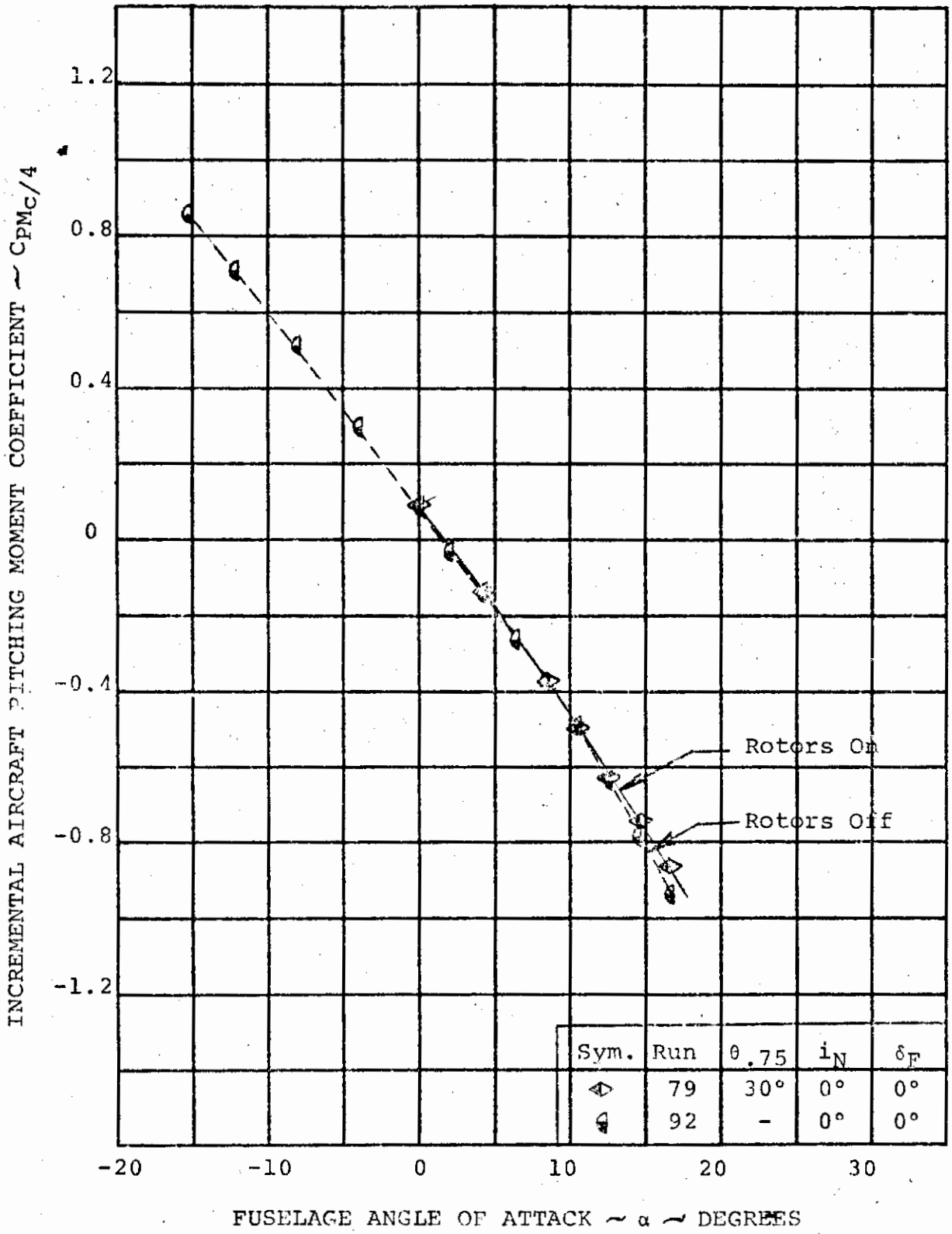

FIGURE 4.23 EFFECT OF ROTORS ON HORIZONTAL TAIL CONTRIBUTION TO AIRCRAFT PITCHING MOMENT

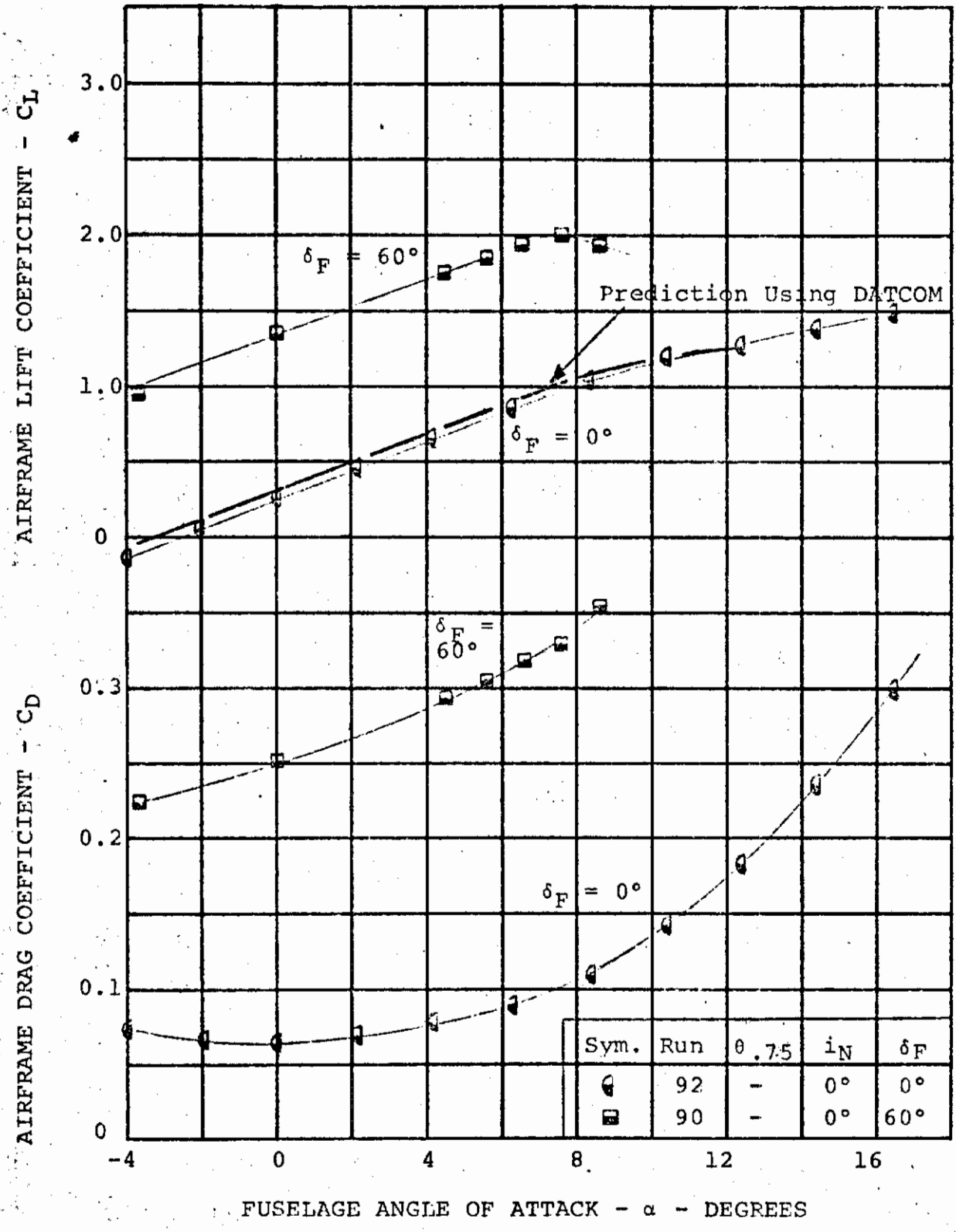

FIGURE 4.24 AIRFRAME LIFT AND DRAG CHARACTERISTICS IN CRUISE WITH ROTORS REMOVED AND i_t = 0°

made and are compared to test data in Figure 4.25. The airframe components were predicted by the methods defined in DATCOM, Reference 4.6. Airframe-minus-tail pitching moment prediction of $\partial C_{PM}/\partial\alpha = 0.011$ is lower than that obtained from test, $\partial C_{PM}/\partial\alpha = 0.018$. Further analysis must be made to determine the cause of this difference. The contribution of the horizontal tail to total aircraft stability ($\partial C_{PM}/\partial\alpha$) is 0.052 per degree as predicted by the methods defined in DATCOM. Adding this increment to the airframe-minus-tail test data results in excellent agreement with the airframe test data. This indicates that the tail characteristics as well as the wing downwash are correctly accounted for. The rotor contribution was defined by the isolated rotor characteristics as discussed in Reference 4.7 increased by the empirical circulation effects defined in Reference 1.5. This results in good agreement with the total model data.

Aircraft performance test data were obtained in Test Program II and are presented in Figures 4.26 through 4.28 showing the aircraft lift versus angle of attack, propulsive force and rotor power. No correlation work has been performed but with the agreement in the airplane and rotor performance characteristics described earlier, the correlation will be good.

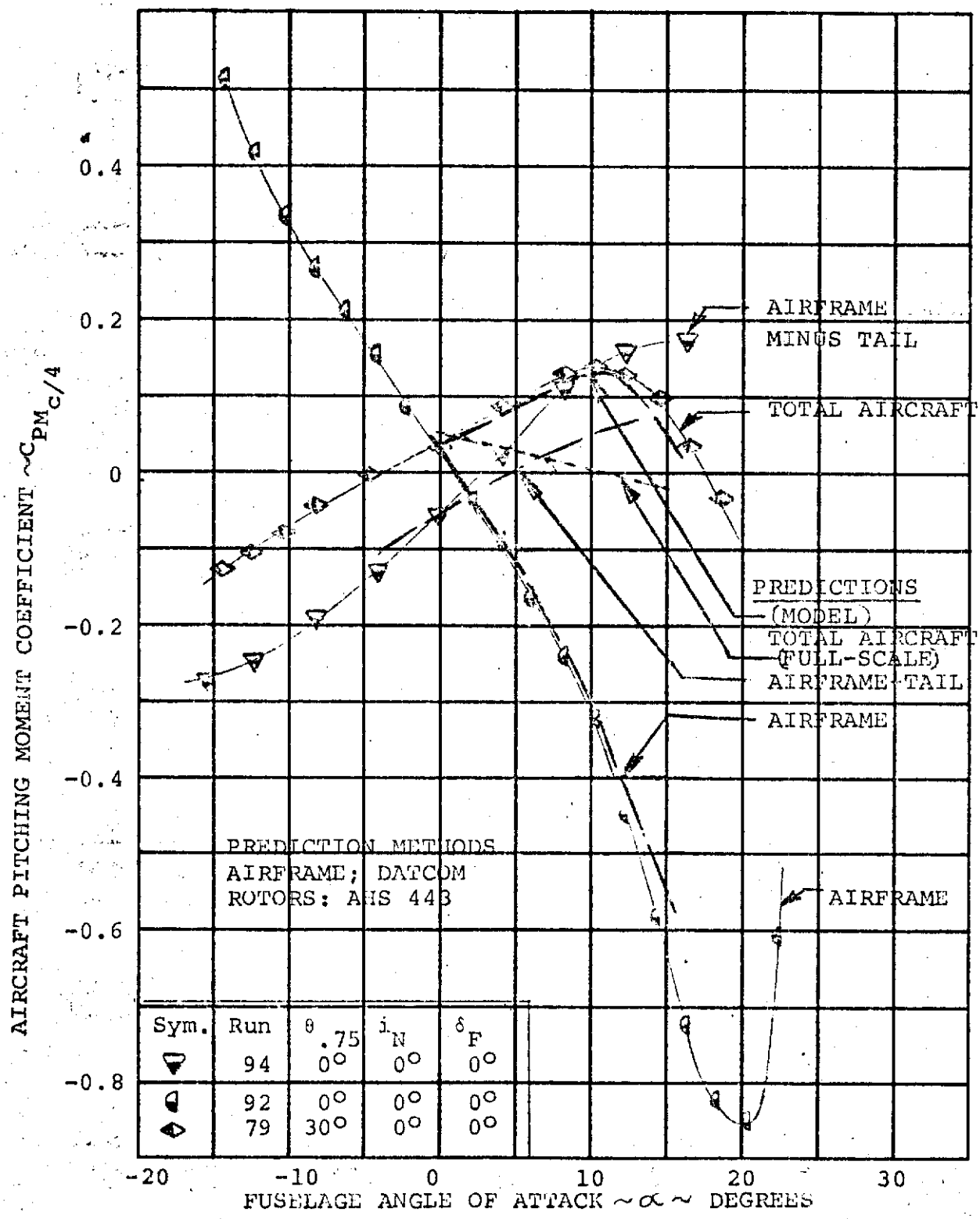

FIGURE 4.25 CONTRIBUTION OF PROP/ROTORS AND HORIZONTAL TAIL TO AIRCRAFT PITCHING MOMENT AT V/V_T = 0.386

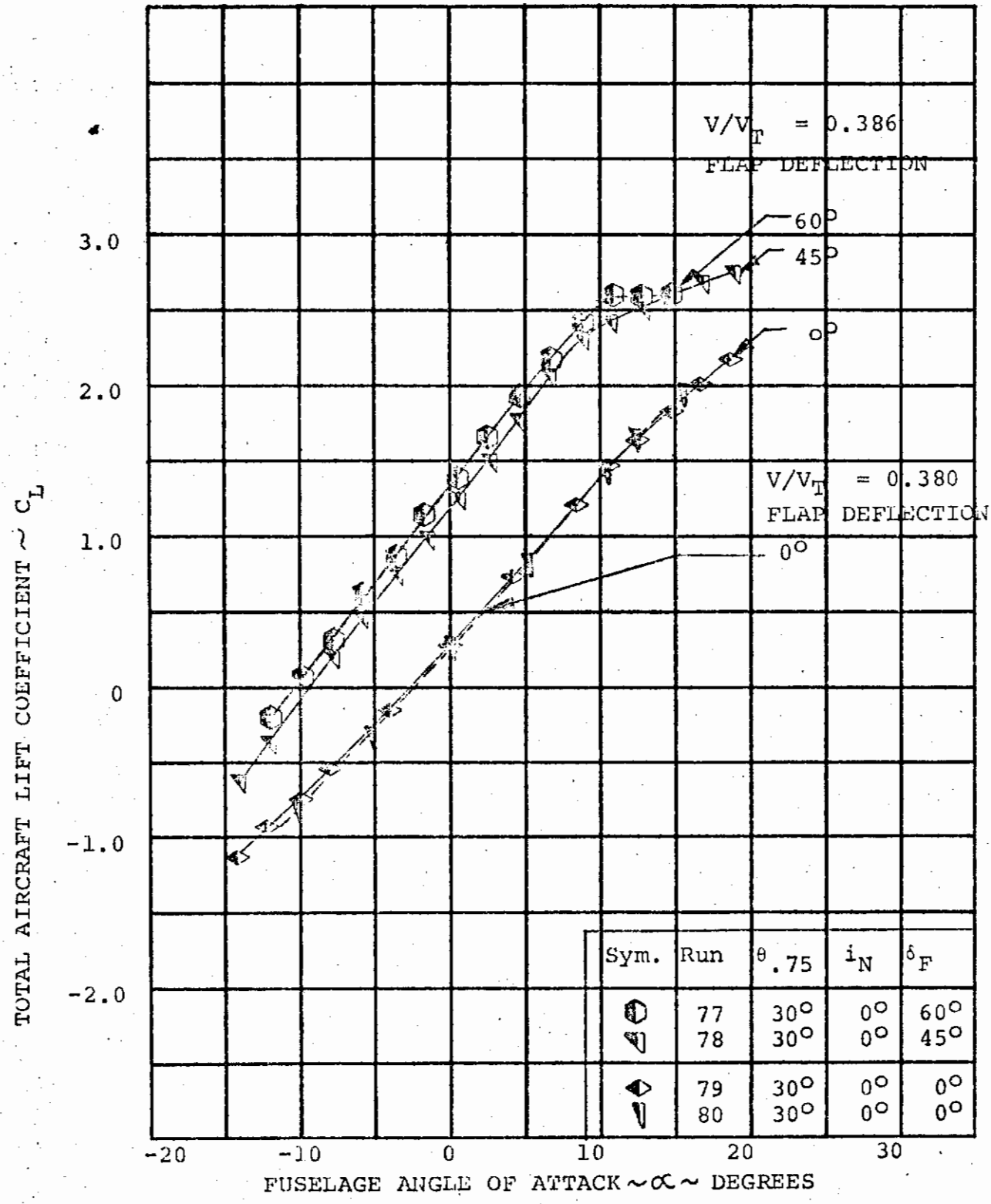

FIGURE 4.26 TOTAL AIRCRAFT LIFT/ANGLE OF ATTACK VARIATION IN CRUISE $i_N = 0$

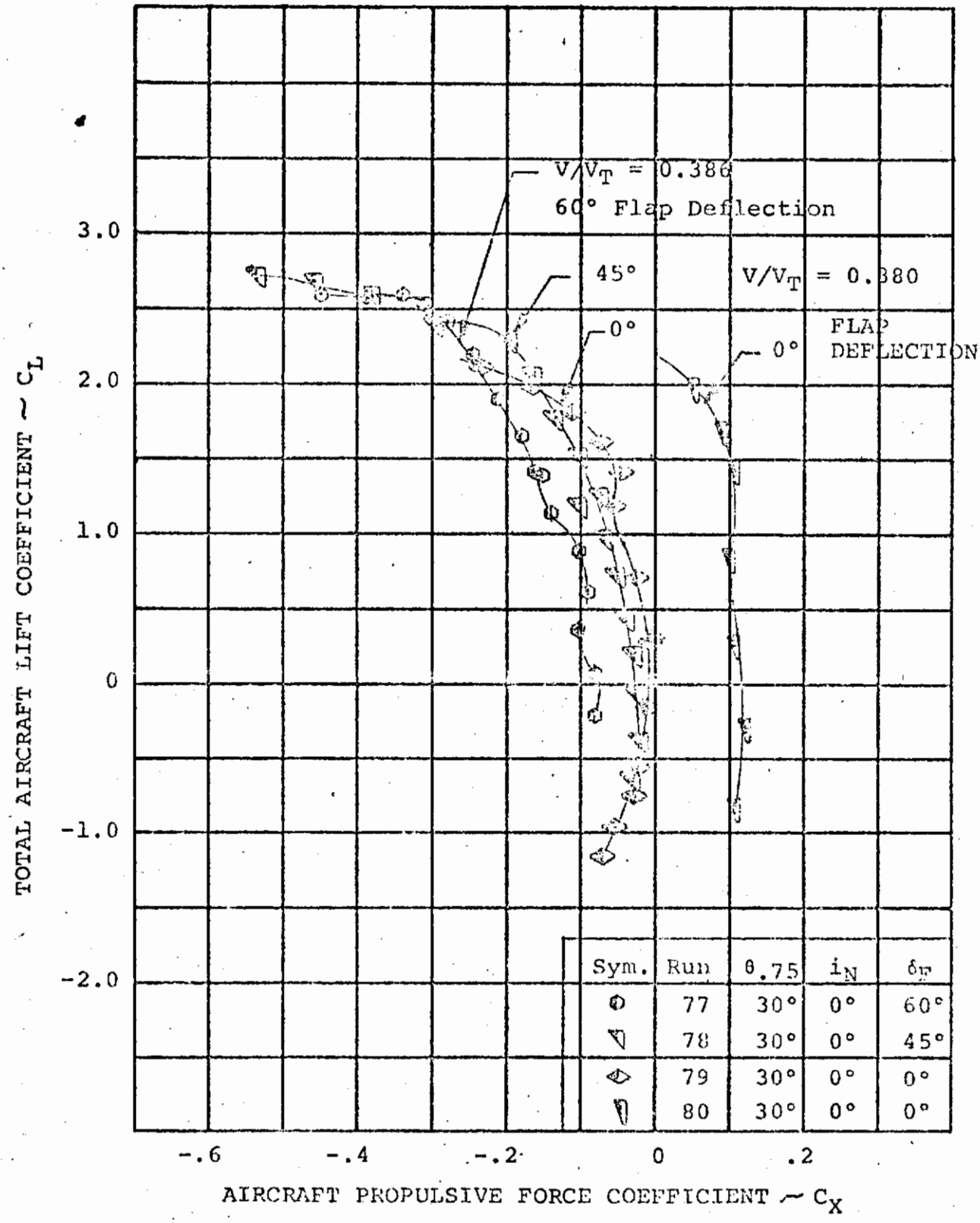

FIGURE 4.27 TOTAL AIRCRAFT LIFT/PROPULSIVE FORCE VARIATION IN CRUISE $i_N = 0$

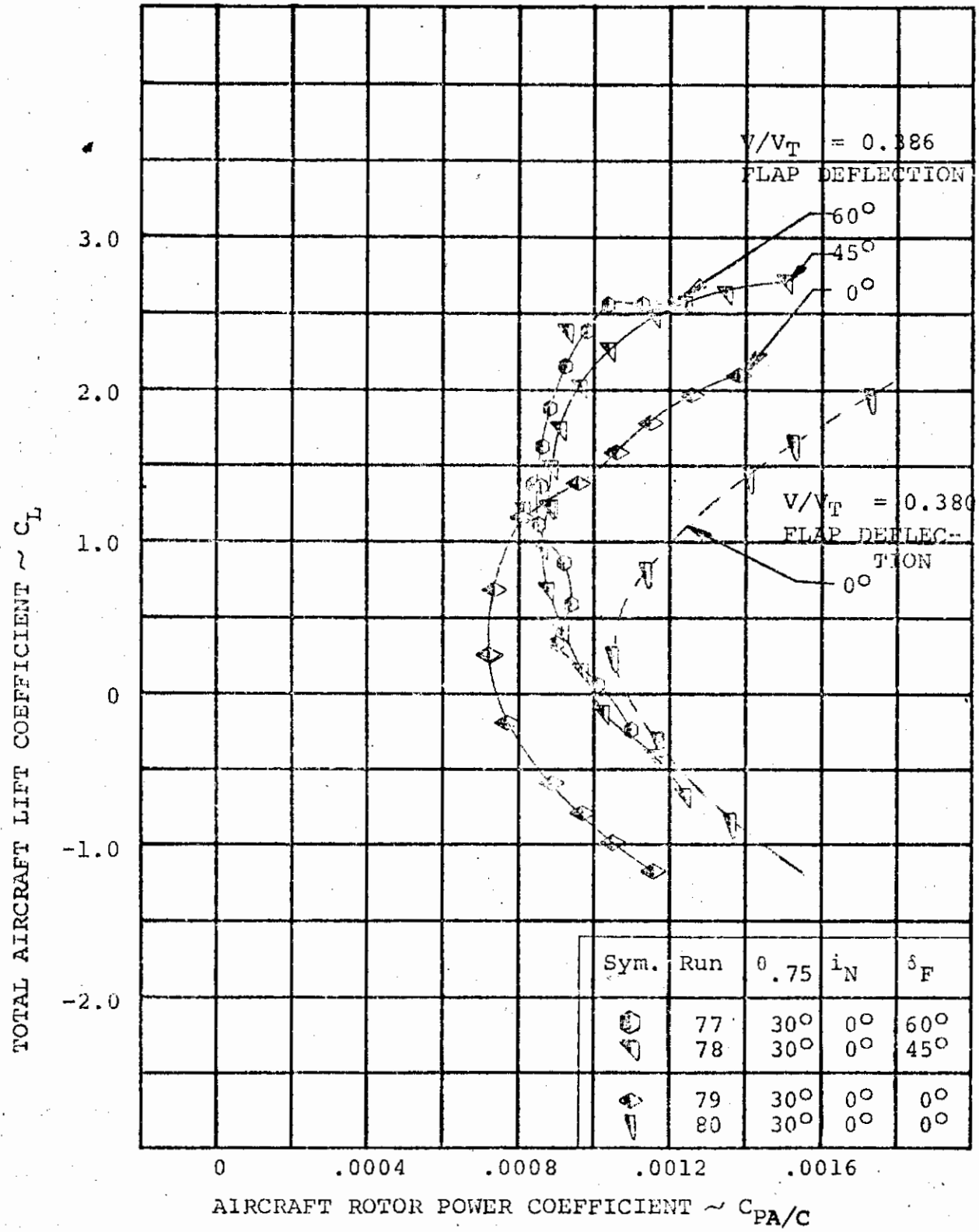

FIGURE 4.28 TOTAL AIRCRAFT LIFT/ROTOR POWER VARIATION IN CRUISE $i_N = 0^\circ$

4.4 CONVERSION PERFORMANCE

When the transition is completed, nacelle incidence is zero and conversion can be made from the tilt rotor cruise mode to the stowed rotor cruise configuration. Conversion is initiated by reducing collective and power to the rotor, thus operating in the steady windmilling state. The second regime of operation in conversion is the feathering of the rotor by rapidly increasing the collective and slowing down the rotor speed to zero. Blade folding is the final step in the conversion to the cruise configuration where the blades are retracted back onto the nacelle. The reverse procedure is employed in the conversion to the tilt rotor configuration. This section will present the comparison of the test data from Test Program III with the prediction techniques for these three regimes of operation.

4.4.1 Steady Windmilling Performance

Steady windmilling is the mode of rotor operation at the end of transition before conversion is made to the cruise configuration. Steady windmilling is defined as the specific combination of forward speed and blade collective that produces a steady rotor speed for zero rotor torque. A rapid prediction technique has been developed during this contract that calculates rotor forces and RPM under feathered, windmilling and transient operation. It has been programmed for computer operation and is designated "Windmill". It is described in detail in Reference 4.4 and a brief summary of it is presented here. The basic inputs define the flight condition, rotor geometry, airfoil aerodynamic characteristics, blade collective, and RPM. For the specified RPM and collective the angle of attack distribution along the blade is calculated to define the lift and drag radially. These forces are integrated to define the torque and the rotor drag. For steady windmilling operation, a range of collectives must be used to establish drag and torque variation with collective, and thus, to obtain the correct collective and rotor drag for zero torque at the specified RPM. If the RPM is input as zero, as for a feathered blade, the program will automatically check the calculated torque, if it is not zero the collective is changed until zero torque is achieved. The collective and the rotor drag are then defined.

Utilizing this prediction technique, the blade collective variation with RPM in steady windmilling was defined at forward speeds of 85 and 113 FPS and compared with test data in Figure 4.29. The prediction shows good agreement with the test data. Rotor drag variation with RPM obtained from theory and test data for forward speeds of 85, 113 and 141 FPS in steady windmilling is presented in Figure 4.30. The prediction agrees well with test data at zero RPM (feathered blades) and above 700 RPM. At lower RPM, for 113 and 141 FPS forward speed the prediction is low but this is in the region where the aircraft will not be operating in steady windmilling.

Since the aerodynamic characteristics of the blade define the relationship between the rotational speed and the forward speed that produces zero torque, this relationship should produce a unique trend of blade collective with advance ratio (μ), the ratio of forward speed to rotor tip speed. Figure 4.31 shows that the variation of blade collective with advance ratio does form a single trend.

Included on Figure 4.31 is a prediction of the blade collective with advance ratio that had been developed as part of the pretest predictions. The predictions are indicated by the X symbols and show good agreement with the test data.

Since there is a single trend of blade collective with advance ratio there must be an associated trend in rotor thrust coefficient for steady windmilling operation. Figure 4.32 presents the rotor thrust coefficient variation with advance ratio for forward speeds of 85, 113 and 141 FPS for flap deflections of 0, 15 and 30 degrees. The test data reduces to a unique trend and also indicates that the change in circulation from $\delta_F = 30°$ to $\delta_F = 0°$ flap deflection does not have a significant effect on rotor axial force.

The variation in wing circulation does not appear to have a significant effect on rotor thrust in steady windmilling but the rotor influence on the airframe characteristics can be seen in Figures 4.33 and 4.34. Rotor interference produces an increment in aircraft lift coefficient of 0.03 for both 0° and 30° flap deflection as shown in Figure 4.33. Pitching moment is also influenced by the rotor as indicated in Figure 4.34. There is a -0.06 change in aircraft pitching moment coefficient for 0° flap deflection and a -0.014 change for 30° flap deflection. This decrease in pitching moment indicates that there must be a change in the zero lift pitching moment and lift coefficient resulting from

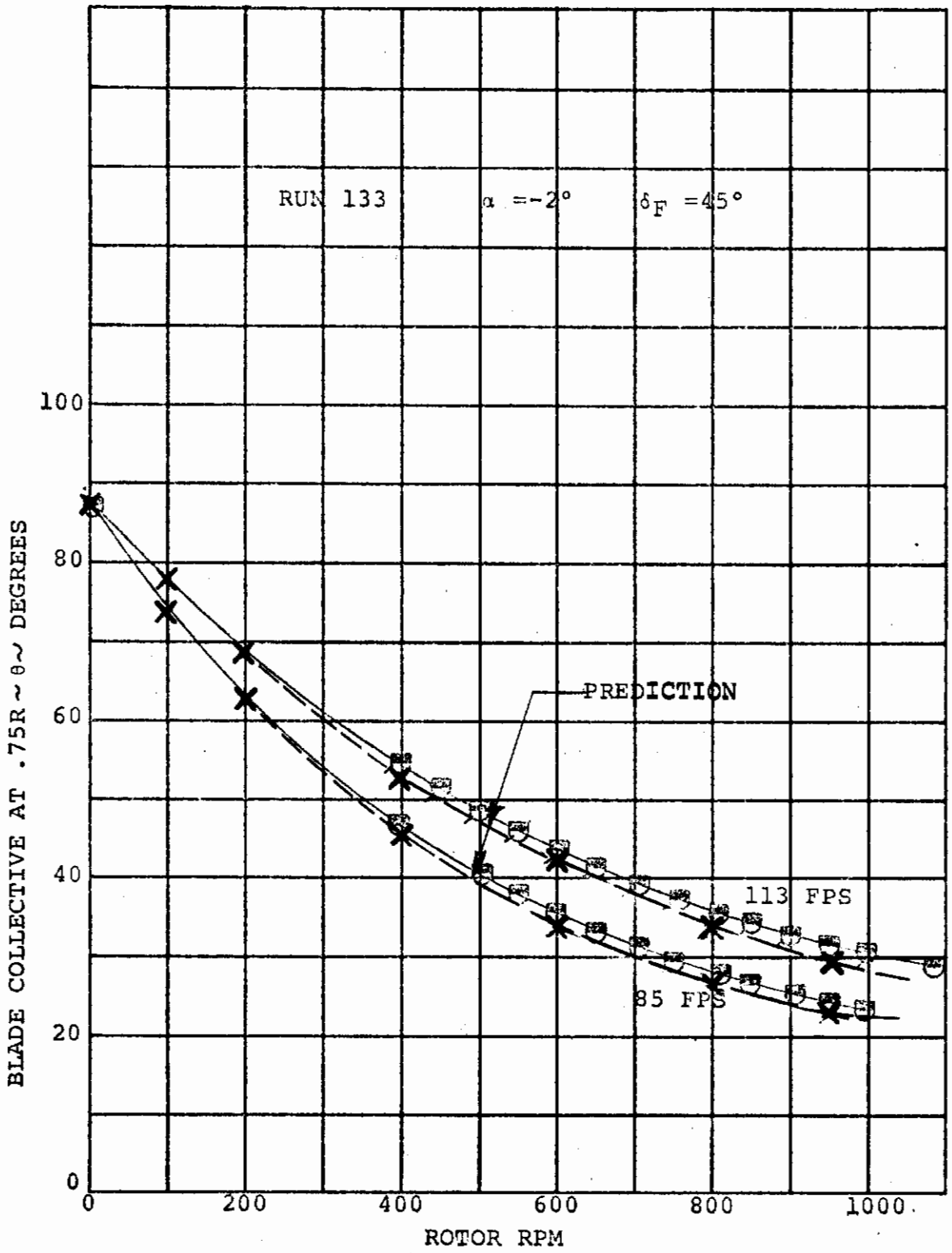

FIGURE 4.29 COMPARISON OF TEST AND PREDICTION FOR BLADE COLLECTIVE/ROTOR RPM VARIATION FOR STEADY WINDMILLING

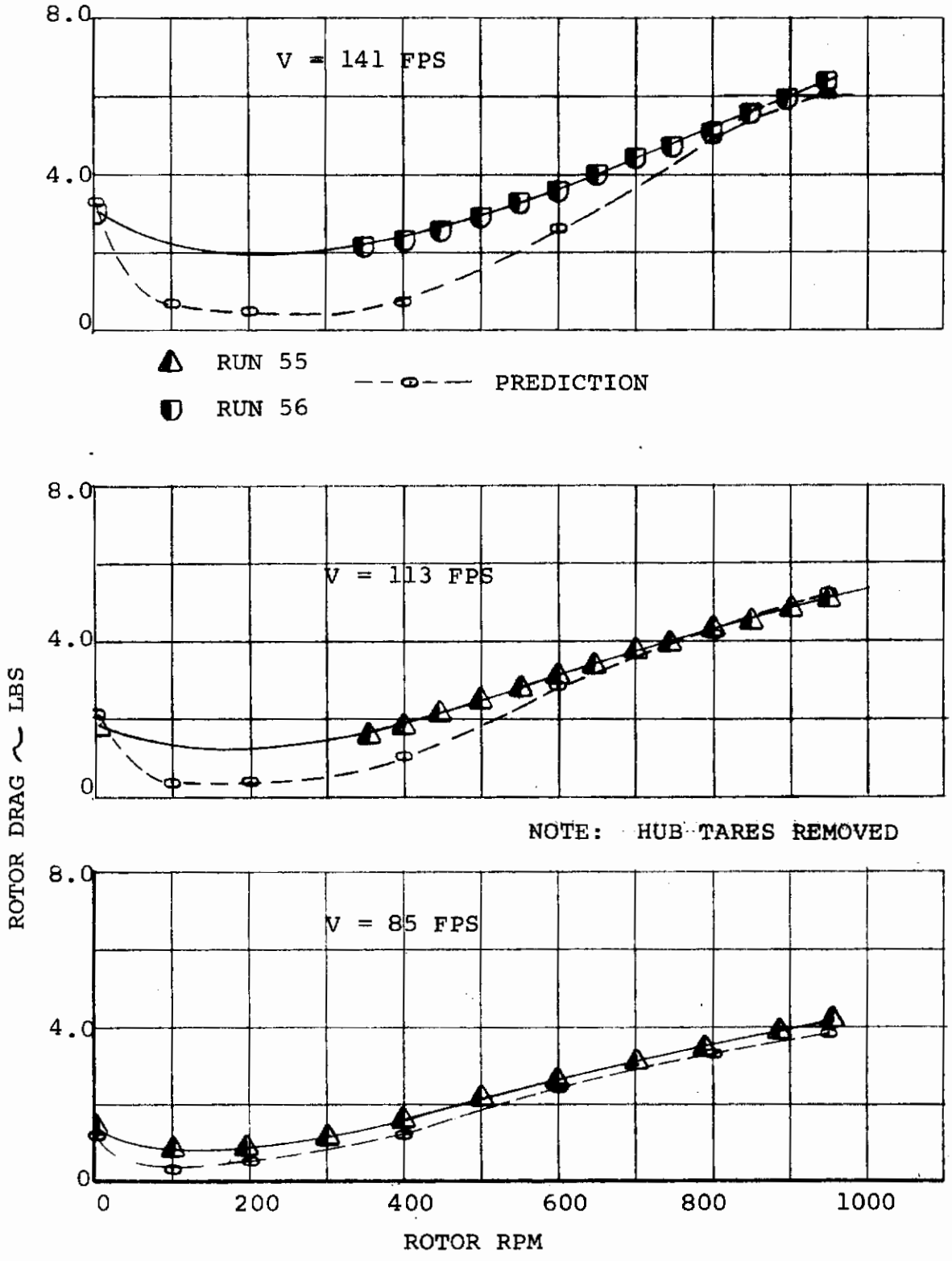

FIGURE 4.30: COMPARISON OF TEST AND THEORY FOR STEADY WINDMILLING DRAG VS RPM

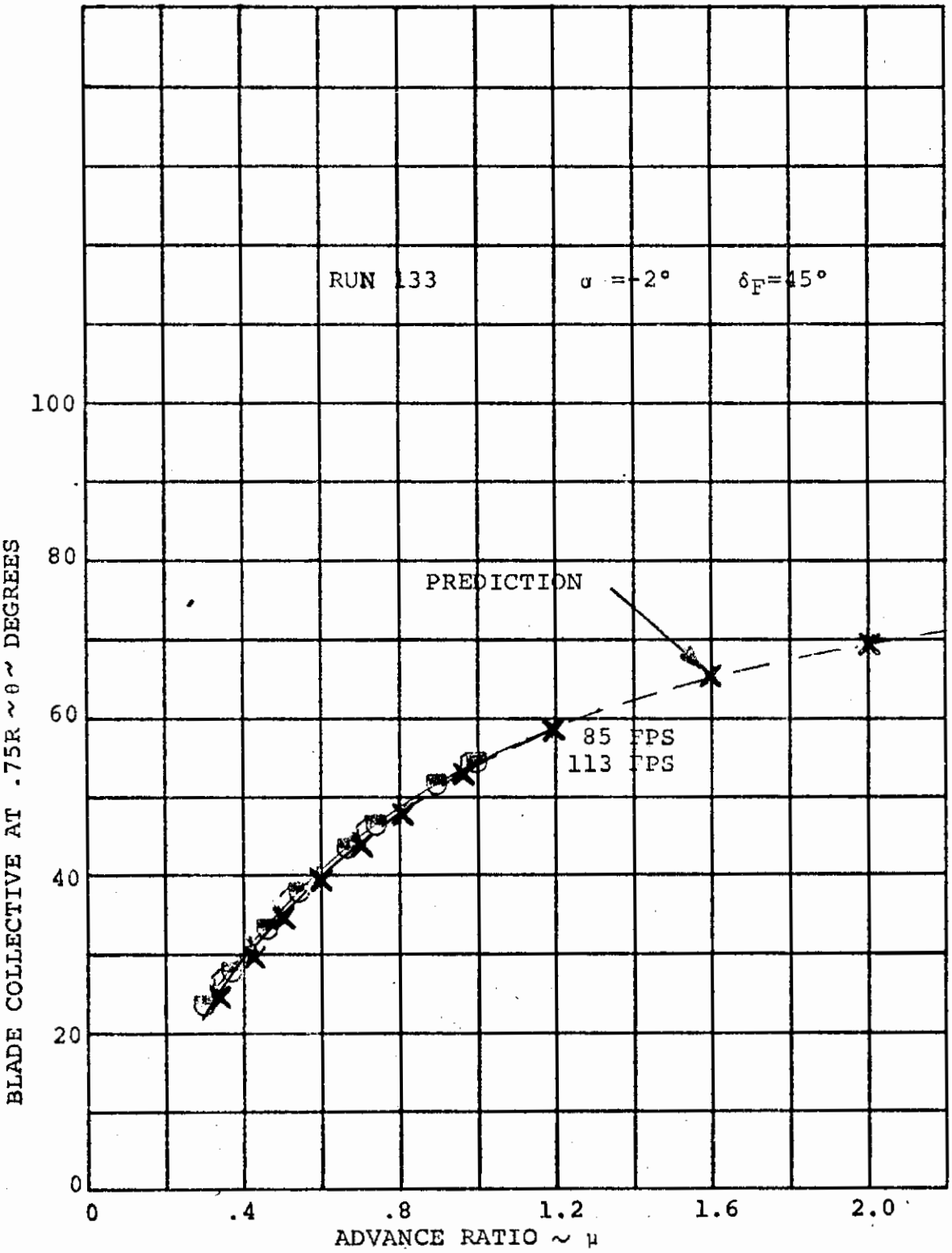

FIGURE 4.31 COMPARISON OF TEST DATA AND PREDICTION FOR BLADE COLLECTIVE/ADVANCE RATIO VARIATION FOR STEADY WINDMILLING

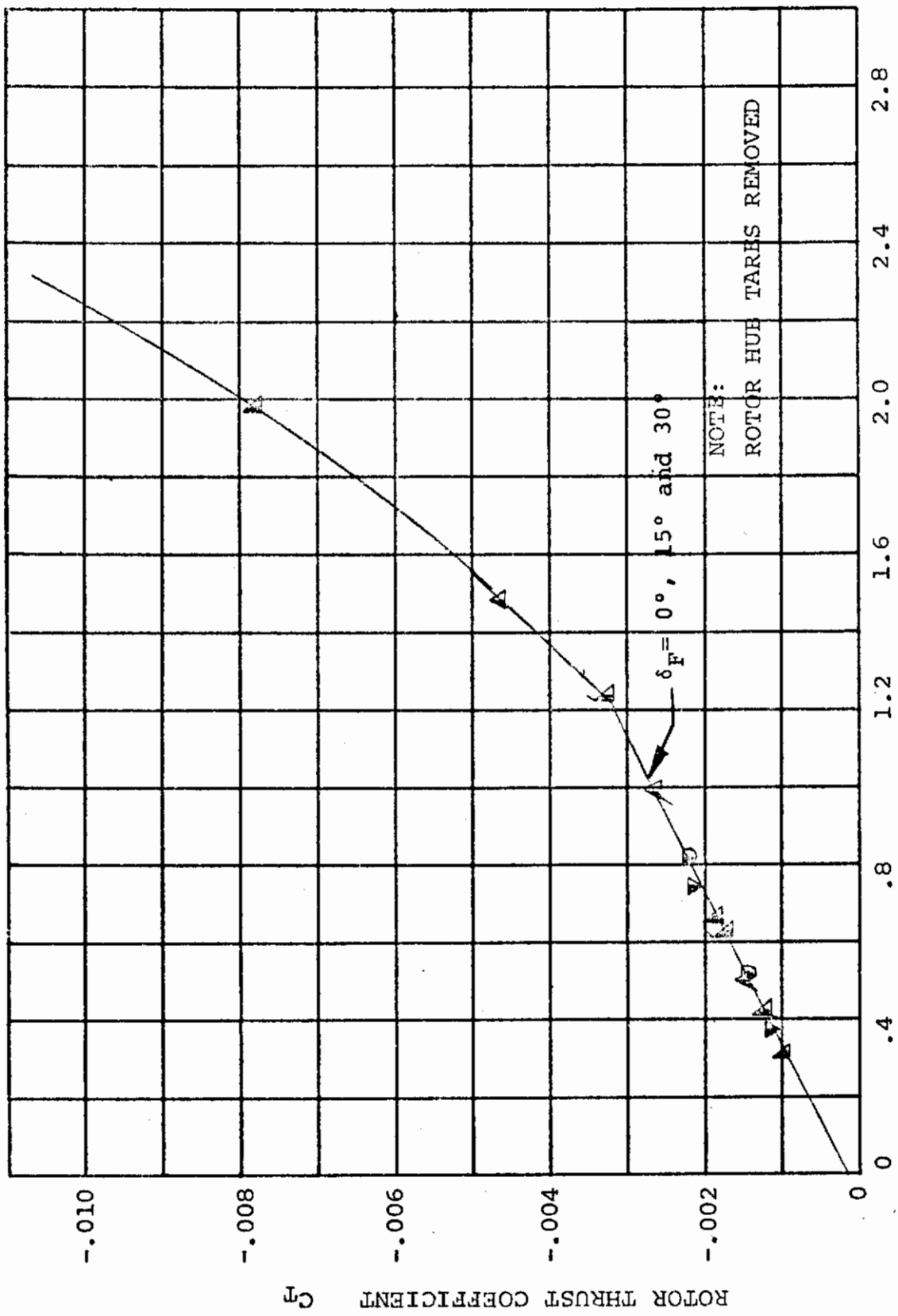

FIGURE 4.32: ROTOR PERFORMANCE DURING WINDMILLING OPERATION

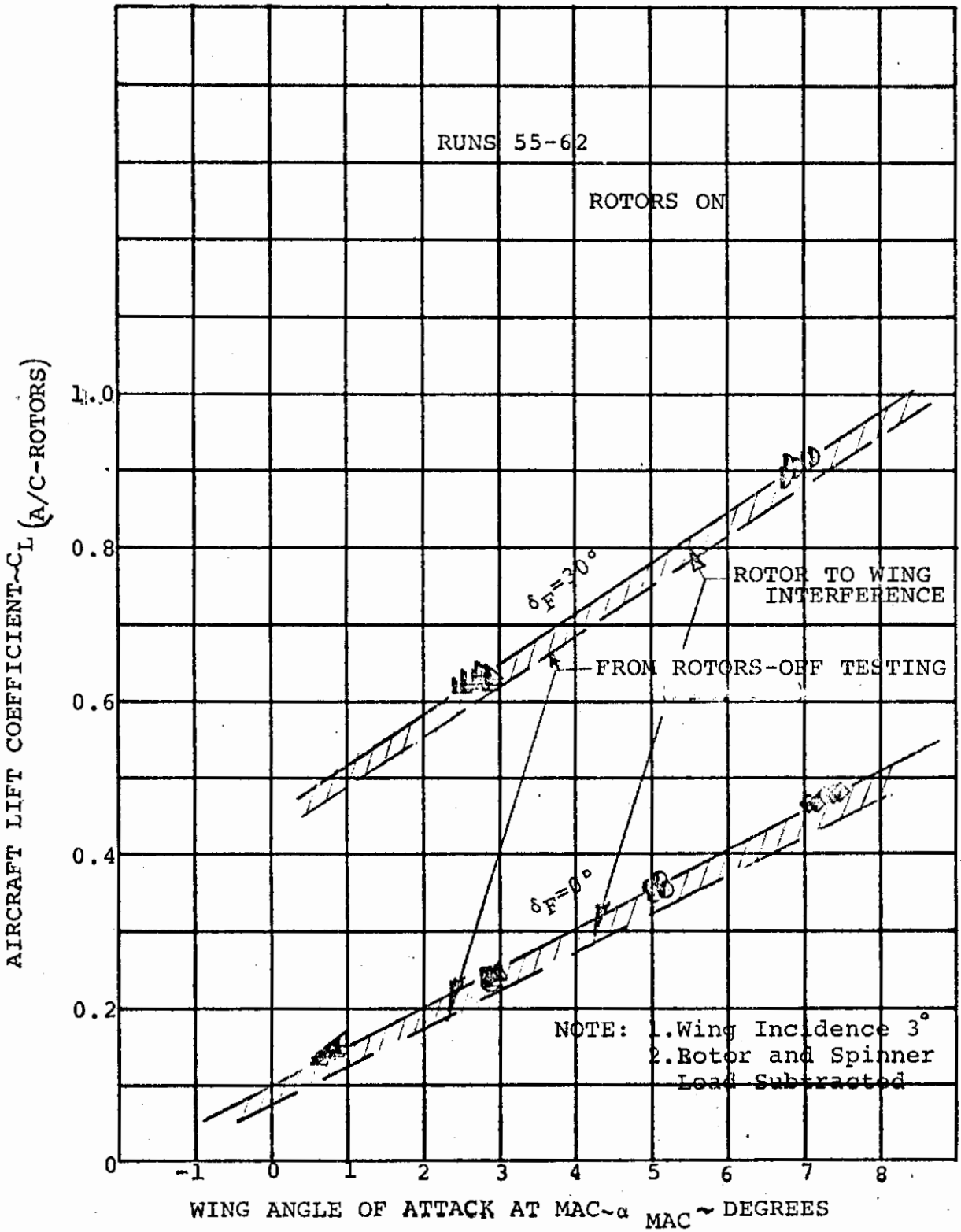

FIGURE 4.33 AIRFRAME LIFT/ANGLE OF ATTACK VARIATION FOR FLAP DEFLECTIONS OF 0° AND 30°

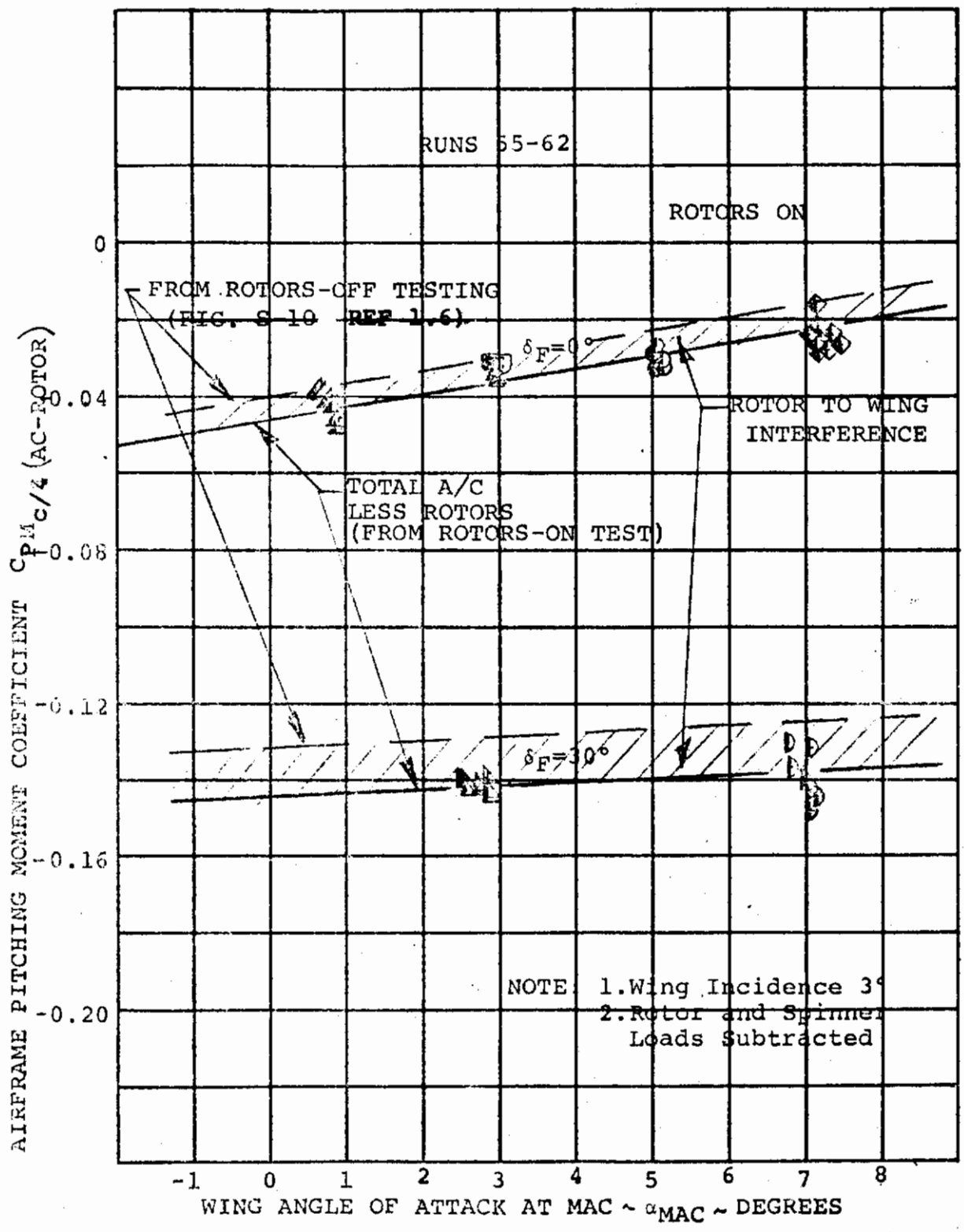

FIGURE 4.34 AIRFRAME PITCHING MOMENT/ANGLE OF ATTACK VARIATION FOR FLAP DEFLECTIONS OF 0° AND 30°

the rotor influence on the flow about the wing. The total aircraft performance in steady windmilling is presented here for a level fuselage attitude and a flap deflection of 30°. This configuration is representative of one "g" cruise at 200 knots where conversion would be initiated. The rotor contribution to total aircraft drag in steady windmilling is large and increases the airframe drag by approximately 0.07 as indicated in Figure 4.35. The prediction of the aircraft drag is excellent from 715 RPM, which is the RPM recommended to initiate the feather procedure, to 950 RPM which was the maximum tested.

4.4.2 Spinup and Feather Performance

The second regime of operation in conversion is the spinup and feather of the rotor. This is the process of bringing the rotor up to speed from the feathered condition or slowing down the rotor from the windmilling condition. It is achieved by an exchange of energy between the airstream and the rotor. The rotor takes energy from the airstream to accelerate in the spinup and therefore there is a transient drag force produced. Energy is given up to the airstream during the feather operation resulting in a transient propulsive force. The schedule of the blade collective pitch variation with time defines the magnitude of the transient drag or propulsive force. A 0.1 "g" peak transient force was adopted as a goal to maximize the ride qualities of the vehicle and as shown in Reference [1.6] can be met without undue sophistication.

Prediction of the rotor characteristics during the transient spinup and feather is accomplished with the "Windmill" analysis. This analysis described in the previous section will also calculate the rotor force, torque and RPM for any desired collective variation with time. This schedule with time defines the acceleration of the rotor with its specified polar moment of inertia. The force required to achieve this acceleration is then solved by a 4th order Runge Kutta numerical method. The resulting force, torque and RPM schedule with time is then obtained for the prescribed collective schedule.

Figure 4.36 presents the RPM and rotor drag variation predicted by this analysis for the prescribed 6.0 second parabolic collective schedule in comparison with test data from Test Program III. There is a slight difference in the rotor RPM. The rotor drag shows a trend very similar to the test data with some difference between 0.5 and 3.0 seconds but in good agreement during the

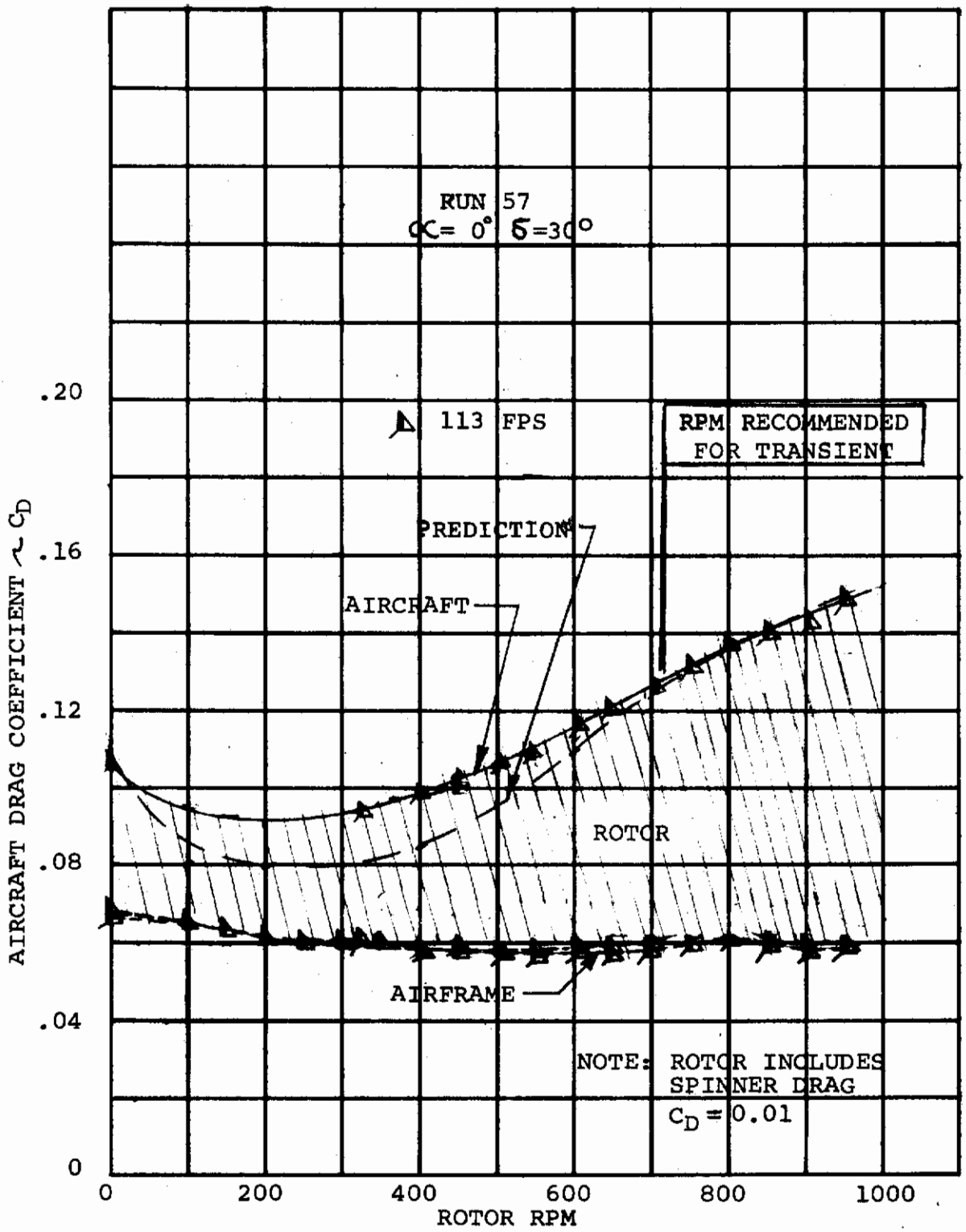

Figure 4.35: EFFECT OF ROTOR RPM AND FORWARD SPEED ON AIRCRAFT DRAG, $\alpha = 0°$ $\delta = 30°$ (STEADY WINDMILLING)

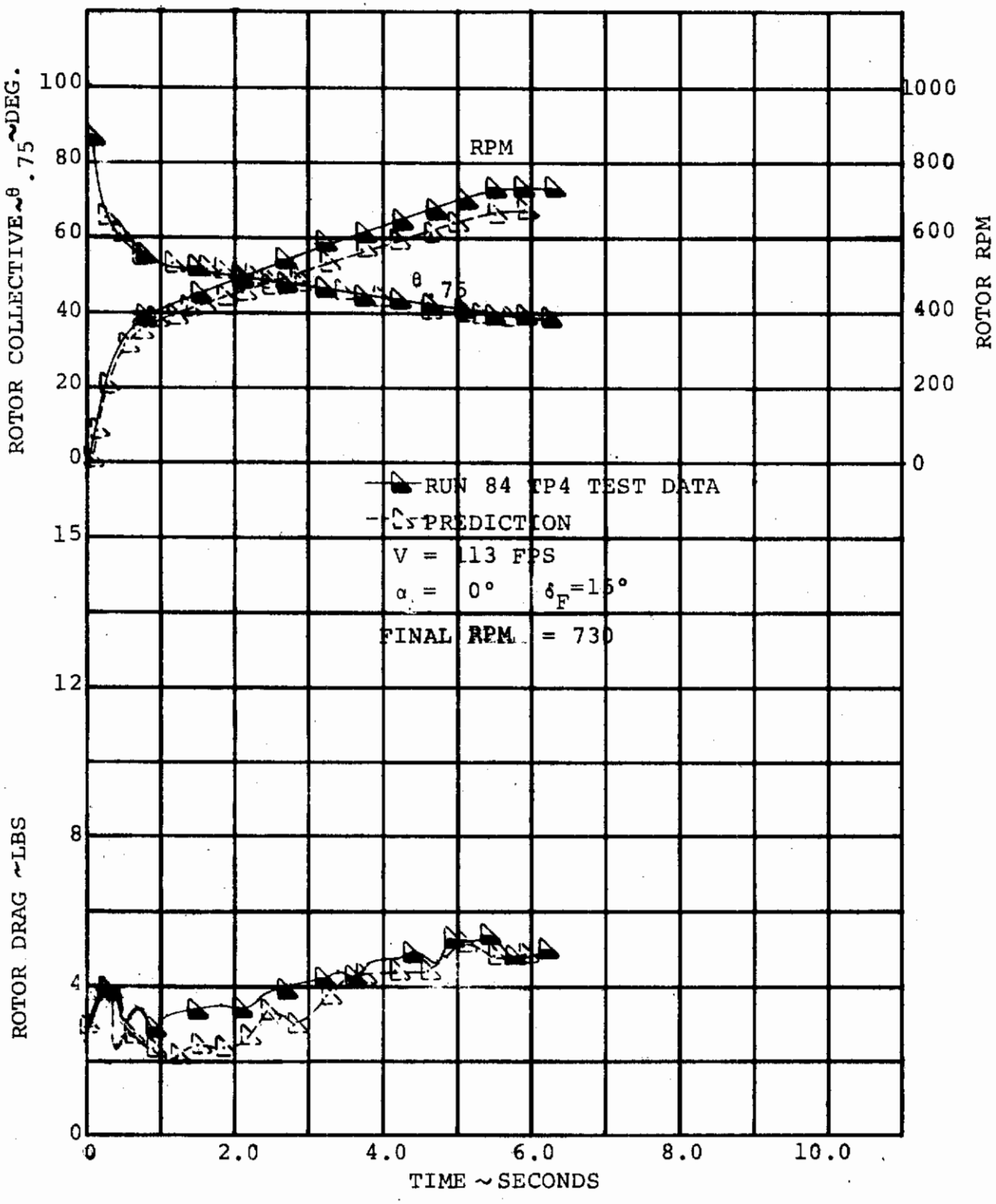

FIGURE 4.36: COMPARISON OF TEST DATA AND PREDICTION OF A SPIN-UP 6.0 SECOND PARABOLIC COLLECTIVE SCHEDULE

rest of the transient. The region of non-agreement is in the low RPM range and could possibly be the influence of Reynolds number on the test data.

A comparison of test data and theory for feather is presented in Figure 4.37. This again indicates that the prediction agrees with the test data over the major portion of the transient. For both feather and spinup, the peak drag variation is slightly overpredicted.

4.4.3 Folding and Deployment Performance

The third regime of the conversion is the blade fold and deployment which is the process of folding the blades from the feathered position into the wing tip nacelle. As the blades are folded, the total aircraft drag is reduced. The flatwise blade folding method was recommended in Reference 1.6 and the associated variation of total aircraft drag with blade fold angle is presented in Figure 4.38. The rotor drag increment is shown as the shaded area which decreases almost linearly to the rotors off drag level at 30 degrees blade fold angle. There is no change in drag until 15 degrees, where the blade is then rotated to the flatwise position and the aircraft drag coefficient is reduced an additional 0.01. This additional increment is a result of the blades improving the aerodynamic contour of the nacelle. The model nacelles have flat areas for the blades to fit on and a small step aft of where the folded blades would be to achieve a relatively smooth contour in the folded configuration. The folded blade improved the contour of the nacelle and thereby reduced the drag. The recommended methodology is to linearly decrease the rotor blade drag to zero at 30° blade fold angle and account for an aircraft drag coefficient increment of 0.01 resulting from flatwise folding improving the nacelle contour.

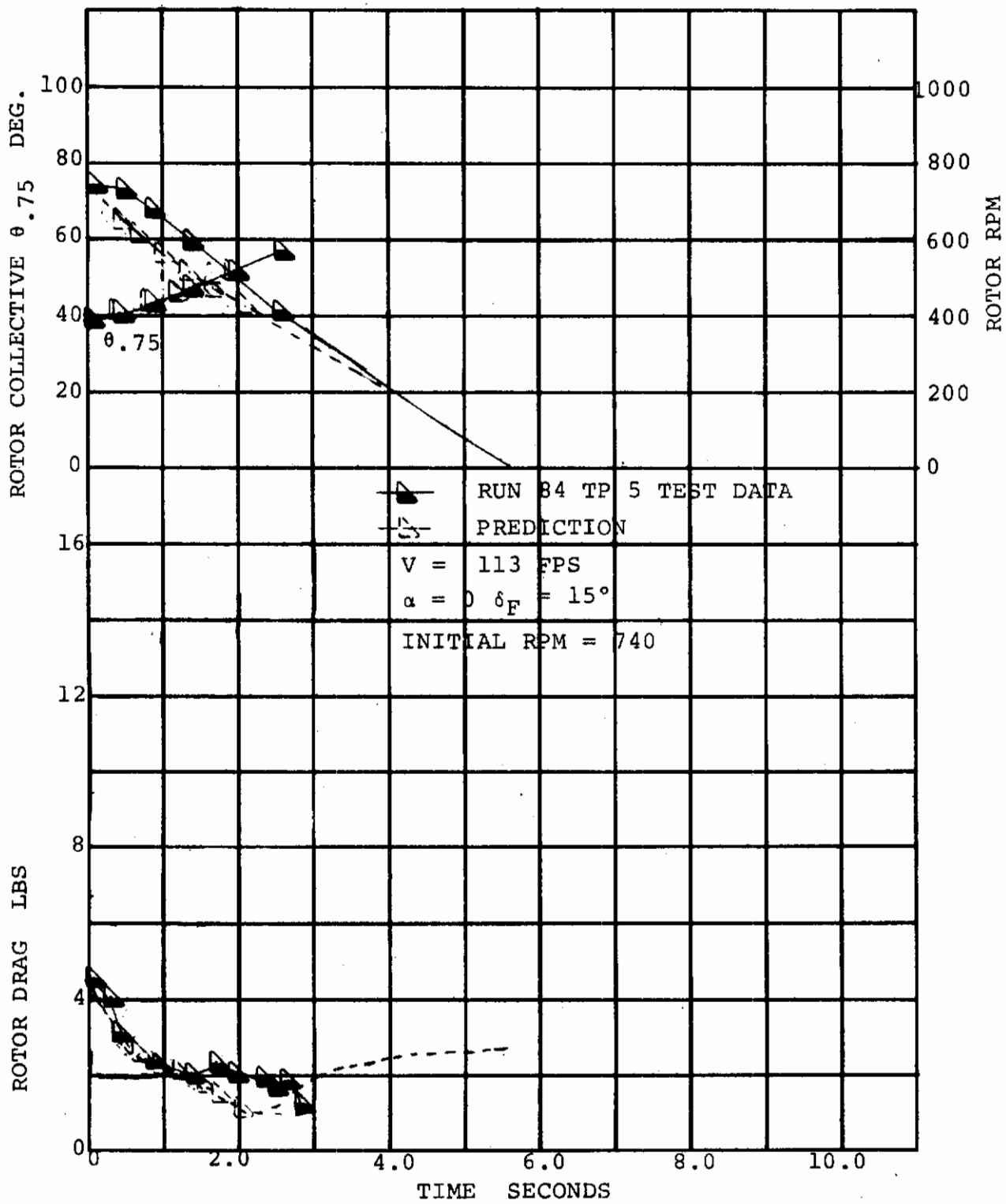

FIGURE 4.37: COMPARISON OF TEST DATA AND PREDICTION OF A FEATHER 6.0 SECOND COLLECTIVE SCHEDULE

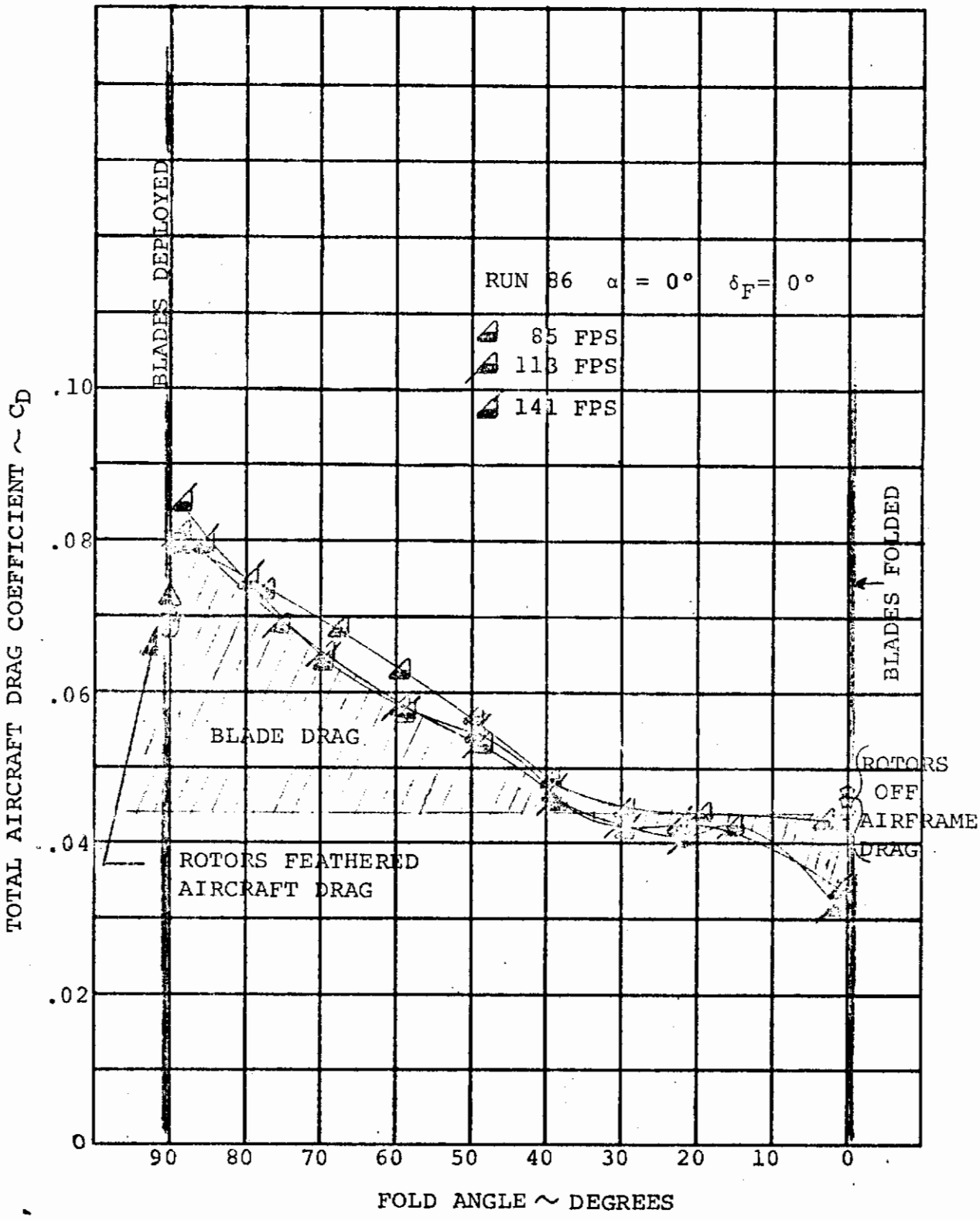

FIGURE 4.38 AIRCRAFT DRAG VARIATION WITH BLADE FOLDING AT $\alpha = 0°$ $\delta_F = 0°$ (FLATWISE FOLD)

4.5 CONCLUSIONS

1. Rotor/aircraft performance is well predicted by current methodology.

2. Provision of leading edge umbrella flaps and high angle trailing edge flaps can reduce hover download by 60%.

3. Rotor spinup and feather can be performed in 10 sec. with less than 0.1g acceleration or decelration of the aircraft.

4. Airplane drag for high speed cruise is minimized by folding the blades flatwise rather than edgewise.

4.6 RECOMMENDATIONS

1. Use of improved airfoils to improve hover Figure of Merit and rotor lift capability is recommended. An airfoil such as the Boeing VR-5 can improve the lift capability by more than 25% together with an increase in the Figure of Merit.

2. Descent boundaries including autorotation should be investigated by analysis and additional model testing.

5.0 STABILITY AND CONTROL

5.1 EFFECTS OF ROTOR FLEXIBILITY ON AIRCRAFT STABILITY

In hover, transition, and tilt rotor mode cruise flight the large flexible rotors have a dominating influence on aircraft stability. The effect of rotor blade flexibility on the rotor contribution is large and stems from two effects, out-of-plane flexibility and in-plane flexibility. A brief discussion of these effects is included here to introduce the experimental data obtained from the four tests.

5.1.1 Out-of-Plane Flexibility

The dominant terms in the rotor moment derivatives are functions of centrifugal force and blade flap bending stiffness which result from out-of-plane flapping, Reference 4.7. Theoretical examples of the rotor stability derivative variations with blade flap frequency and Locke number are shown in Figure 5.1. These parameters have strong effects on blade flap response and the rotor derivatives. In hover the in-plane force used for yaw control results mainly from tip path plane tilt (flapping). In cruise the in-plane force is mainly due to the first harmonic components of blade induced drag which, being dependent on the one per rev blade angles of attack, is strongly influenced by blade flapping.

The test rotor of Reference 1.5 is relatively stiff both in-plane ($\omega_L/\Omega > 2.0$) and out-of-plane ($\omega_F/\Omega \approx 1.6$) with a rotor blade Locke number about the equivalent flap hinge of 17.28. The data obtained from this model cannot be scaled directly to full scale without the use of analyses which account for the effects of frequency and Locke number. The rotor designed for the Model 213 is of the soft in-plane type and therefore the influence of lag frequency must also be considered in all rotor derivative calculations.

5.1.2 Inplane Flexibility

The inplane motion of the rotor blade contributes to the blade out-of-plane response through the mechanism of elastic, inertial and aerodynamic coupling. These effects are extremely large at operating rpm close to the lag frequency of the blades and have a favorable effect on the rotor stability derivatives. The change in blade out-of-plane response with lag frequency is shown in Figure 5.2 together with theoretical stability deriva-

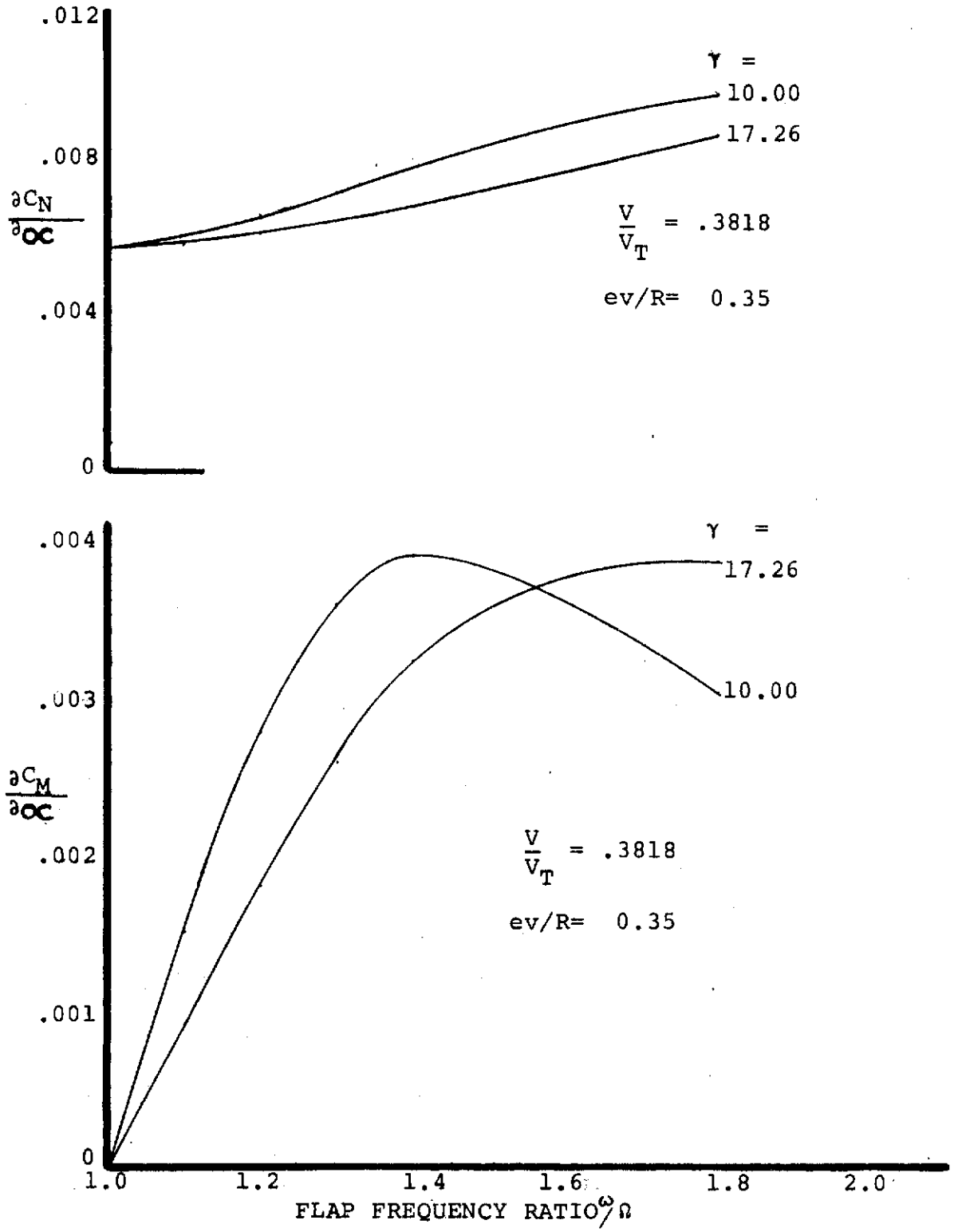

FIGURE 5.1: FLAP FREQUENCY EFFECT

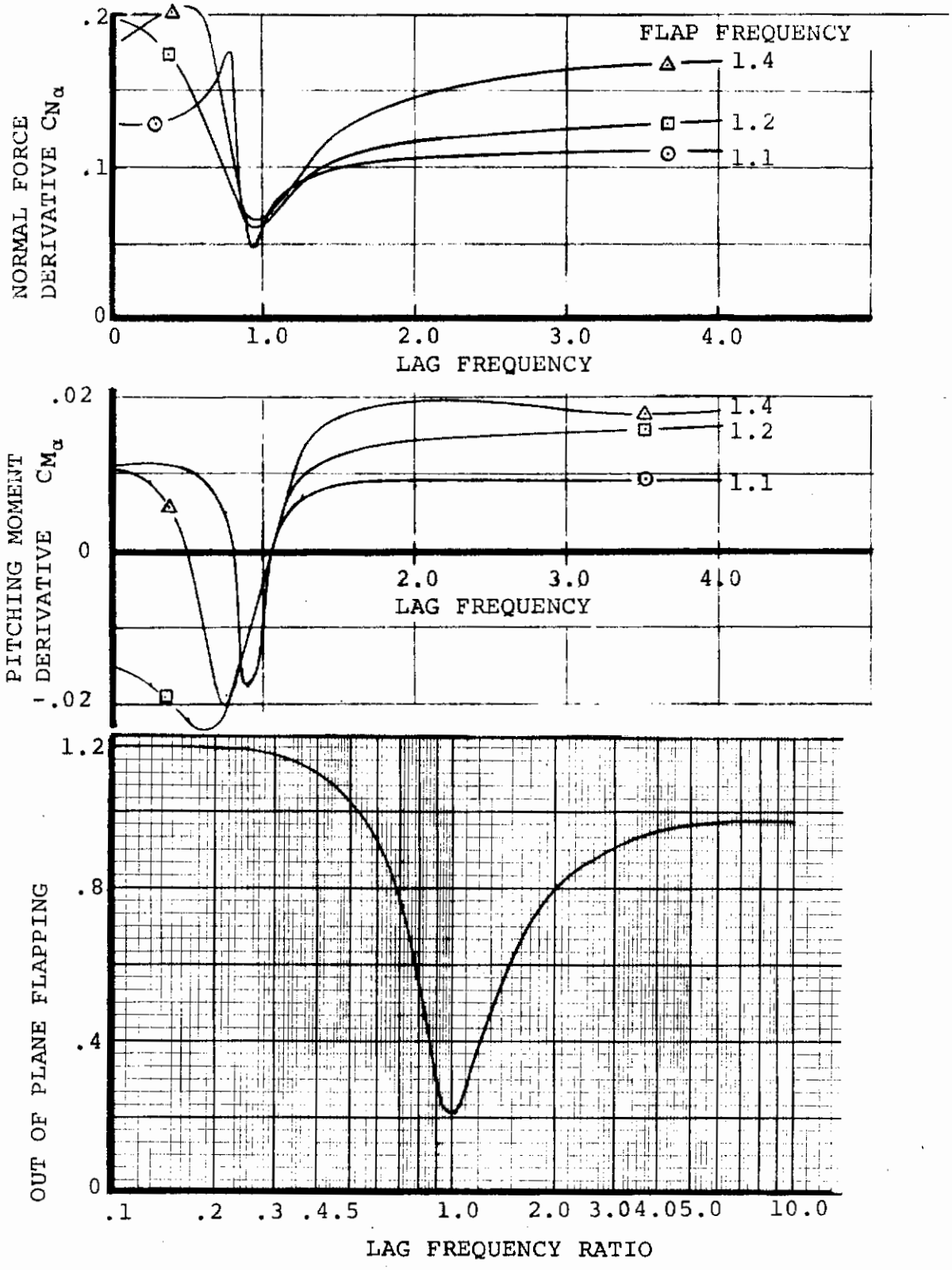

FIGURE 5.2: LAG FREQUENCY EFFECTS

tives to illustrate this effect.

The windmilling model of Reference 1.6 has a soft inplane rotor having a lag frequency less than 1.0 per rev at normal operating RPM. This test rotor is scaled from the Model 213 design blade.

The impact of the rotor properties which influence the out-of-plane blade response must be included in any attempt to use the data obtained in the test reports, References 1.4, 1.5, 1.6 and 1.7, for full scale calculations.

5.2 HOVER REGIME

Military specification MIL-F-8300 (Reference 5.1) is used as the primary basis for discussion of tilt stowed rotor flying qualities in the hover regime. Other specifications and studies by both Government agencies and Boeing, as noted in the references, are also used.

The Reference 5.1 specification defines minimum levels of control sensitivity (response per inch of control motion) and then defines minimum control power (response to maximum control motion) by requiring essentially that one inch of control travel be available from trim in the most critical wind condition. It also requires that response be substantially linear with control deflections. Using conventional cockpit control travels and the specification response per inch, this results in a much greater total control power (especially in the yaw axis) than is required by the adverse wind trim plus one inch of control travel. During design studies of the LIT aircraft, Boeing had many discussions with USAF, NASA and other Government agencies on total hover control power requirements for aircraft in the 50 - 100,000 lb. gross weight category. Fairly general agreement was reached on requirements about the axes of:

Pitch	- 0.6 rad/sec^2
Roll	- 1.0 rad/sec^2
Yaw	- 0.5 rad/sec^2

These values are still recommended as control power criteria and in the subsequent section existing aircraft are evaluated against these criteria as well as the stowed tilt rotor aircraft.

5.2.1 Cyclic Control

Cyclic control effectiveness data were obtained in the wind tunnel test of Reference 1.5. The test data were obtained with the rotor swashplate set to give 3 degrees nose-up cyclic and with the control phase angle set at 65 degrees. That is, the swashplate was set so that the zero longitudinal cyclic pitch position was at 65 degrees azimuth, Figure 5.3, rather than 0 degrees as for articulated helicopter rotor phasing. This cyclic phase angle required for pure longitudinal or lateral control reflects the effects of blade stiffness. For a rigid rotor the inplane force and hub moment are separated by 90 degrees phase angle, i.e., the hub moment is directly in phase with the cyclic input and leads the inplane force by 90 degrees. For a hinged rotor the hub moment and inplane force are in phase and both lag the cyclic input by 90 degrees. The rotor blades tested in Reference 1.5 were not hinged but were flexible but stiff inplane. Thus, the phase angle between hub moment and inplane force lay in between that for the rigid and for the hinged rotor. Data from the test indicated a phase difference of approximately 45 degrees as illustrated by Figure 5.4.

The blades tested on this model were stiffer in and out of plane and had a higher Locke number than those proposed for the full scale stowed tilt rotor aircraft. Data obtained cannot be extrapolated directly to full scale, but they serve to verify the prediction methods and lend credence to the predictions for full scale rotor cyclic effectiveness and orientation of the force and moment vectors. Figures 5.5 and 5.6 illustrate comparisons of test and predicted hub moment and inplane force as a function of rotor RPM for the model tested. The predictions are based upon the 65 degree phase angle pitch input used in the test and indicate good prediction for the moment data. The inplane force data is approximately 10 percent high.

5.2.2 Yaw Control

Yaw control is the most difficult control requirement for the tilt rotor aircraft to meet in hover. Yaw control is obtained by using differential longitudinal cyclic pitch. This control input will be phased to provide a maximum inplane force along the rotor x-axis because yawing moment results only from the inplane force times the distance from the force vector to the center of gravity of the aircraft. Pitching moment is obtained from the addition of hub moment and the moment resulting from

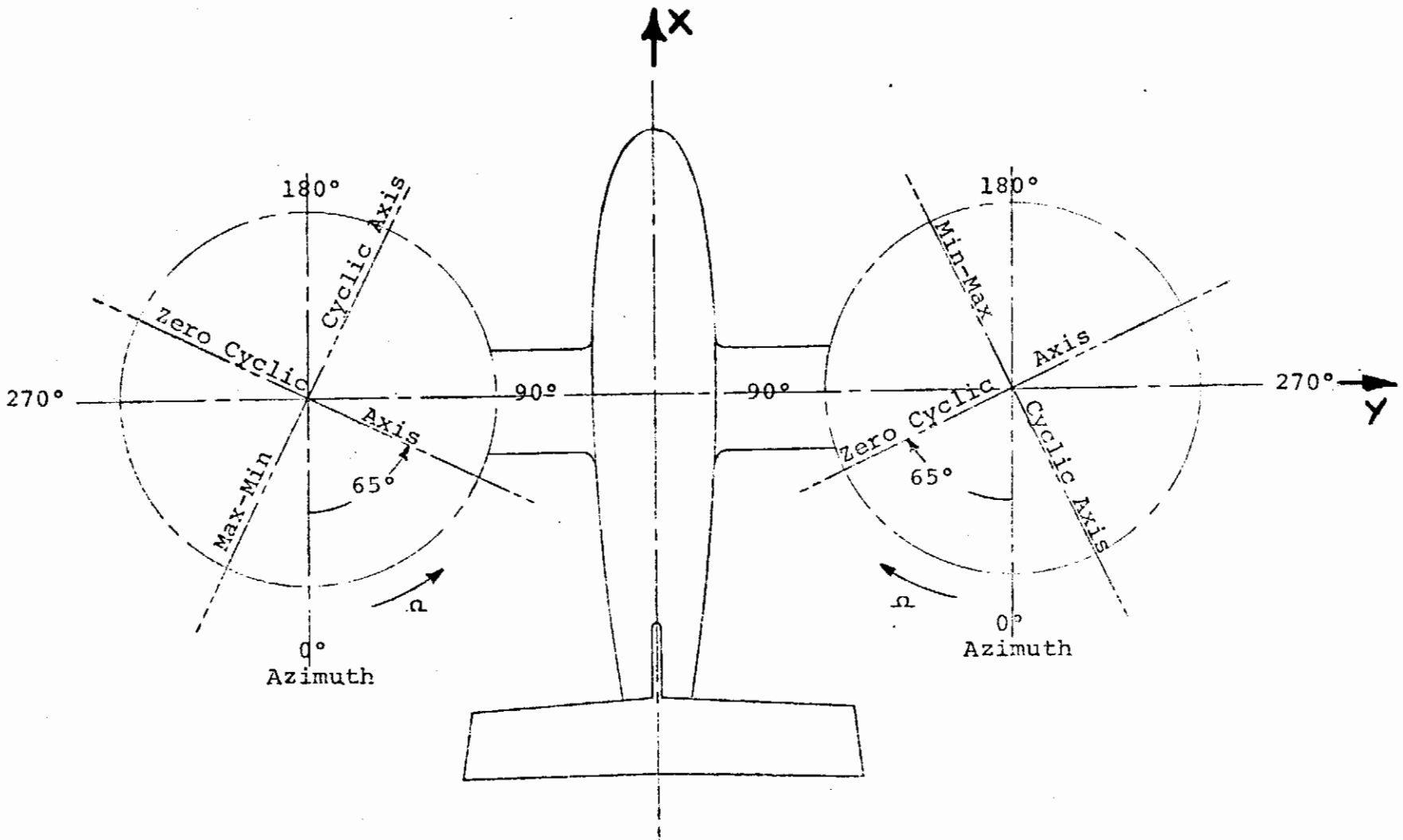

FIGURE 5.3. INPUT CYCLIC PITCH PHASE ANGLE GEOMETRY

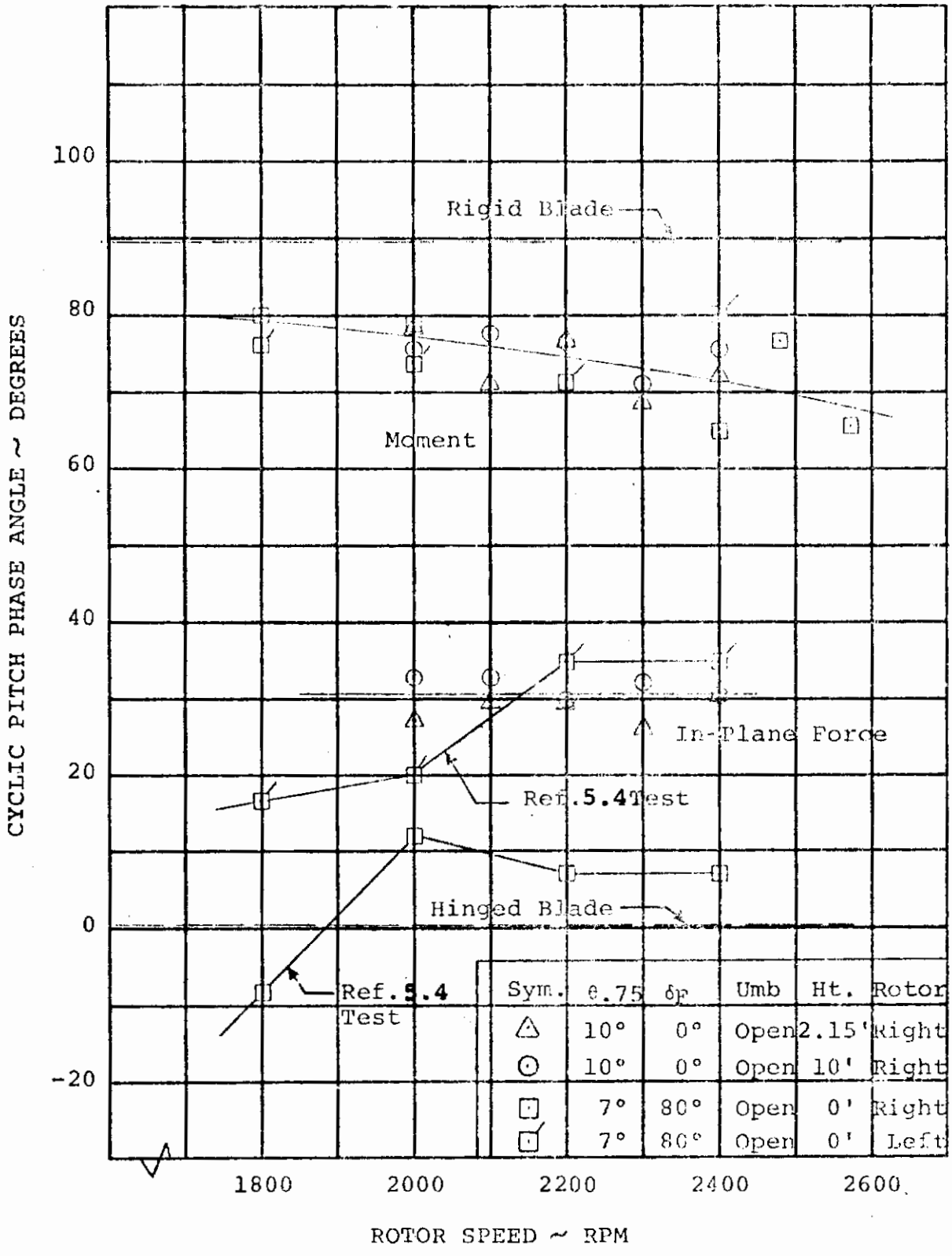

FIGURE 5.4. HOVER CYCLIC PITCH PHASE ANGLE

1/10 SCALE MODEL 160 PERFORMANCE MODEL

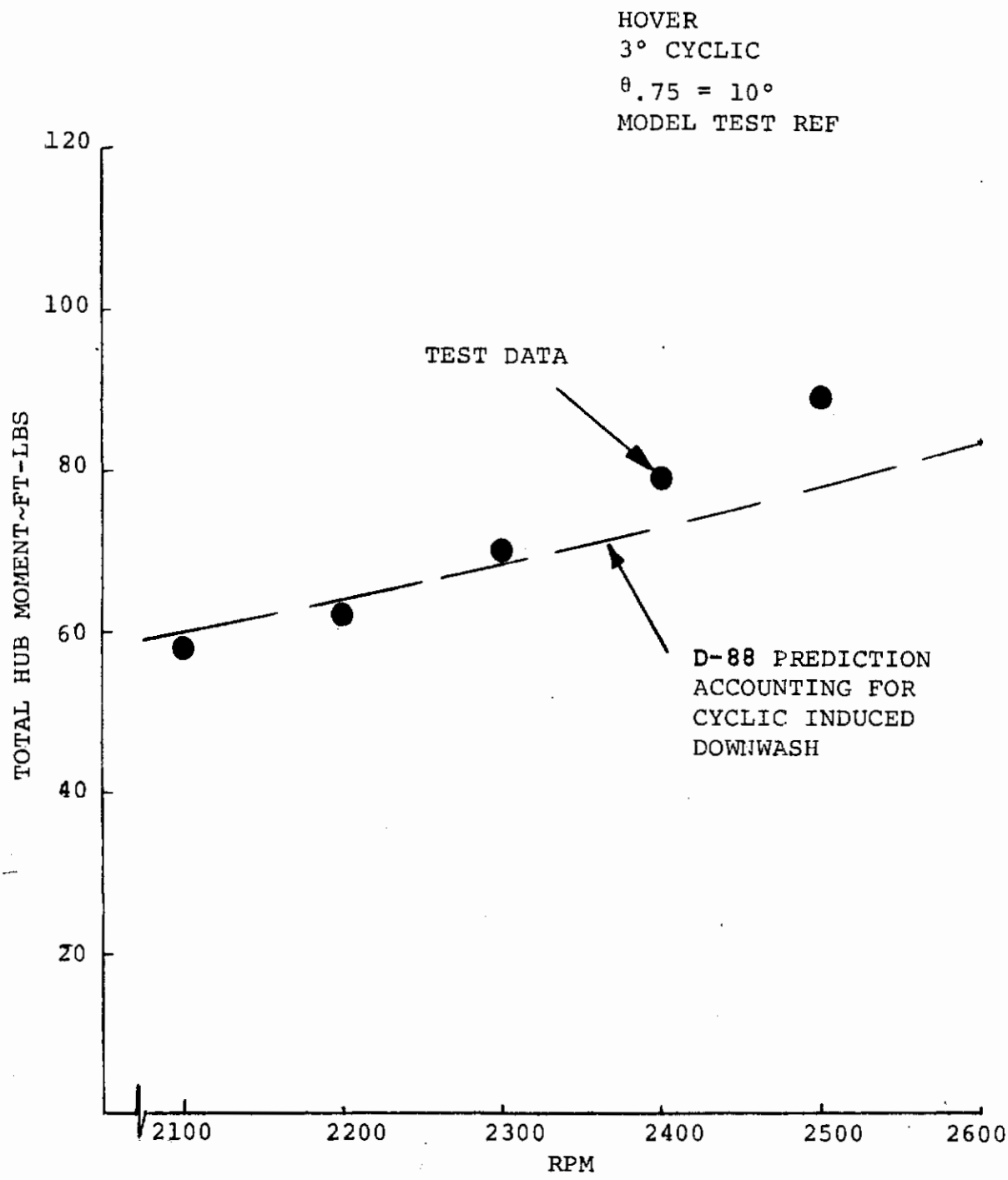

FIGURE 5.5: CORRELATION OF ROTOR HUB MOMENT DUE TO 3° CYCLIC IN HOVER WITH PREDICTION

1/10 SCALE MODEL 160 PERFORMANCE MODEL

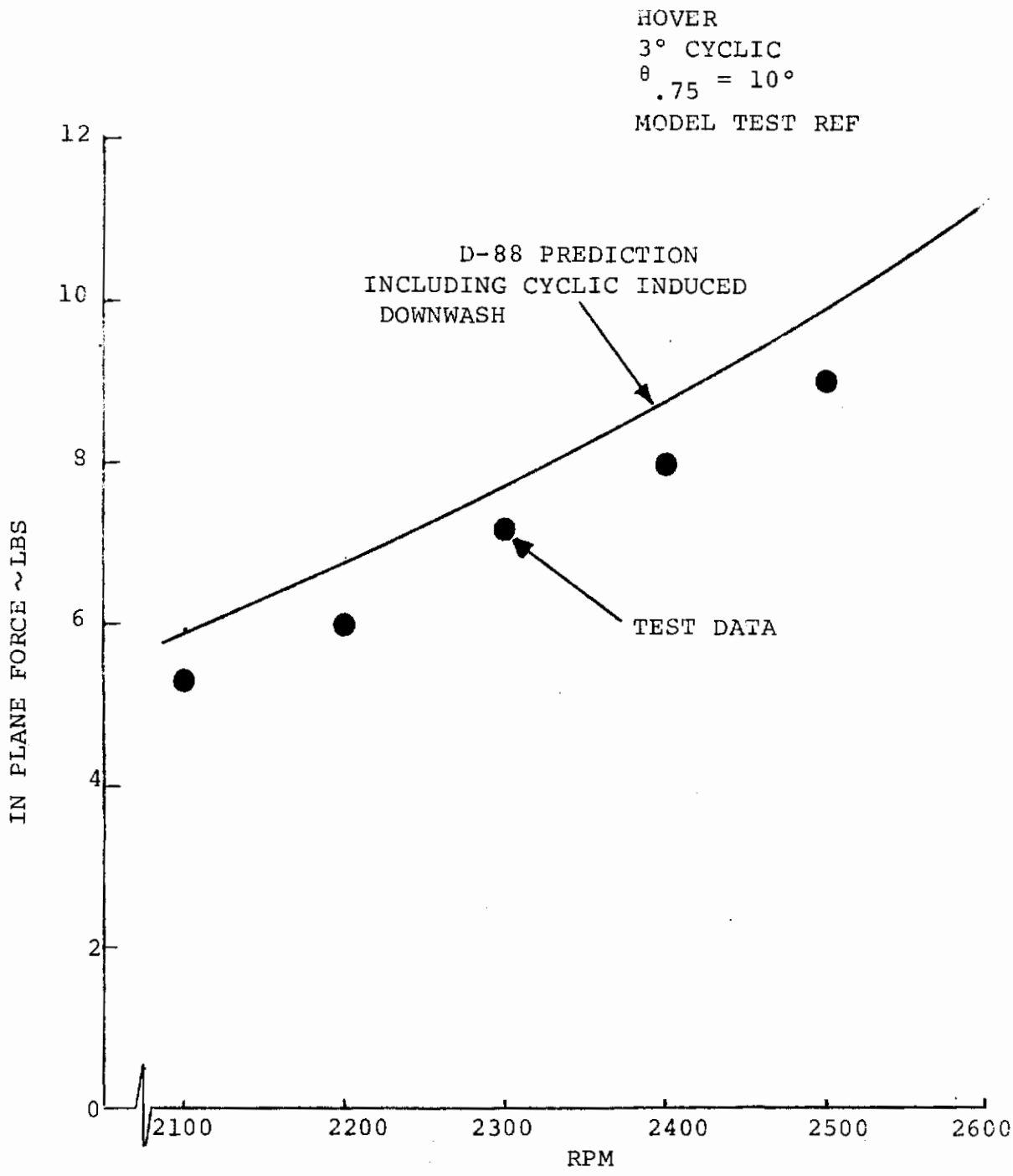

FIGURE 5.6: CORRELATION OF IN PLANE FORCE DUE TO 3° CYCLIC IN HOVER

the inplane force. Figure 5-7 illustrates the effect of cyclic pitch on yaw control for cyclic phase angles of 30 degrees and 75 degrees. The 30 degree phase angle is oriented for maximum inplane force along the x-axis and 75 degrees is the angle for maximum hub moment about the y-axis for the model tested (Reference 1.5). Note that there is approximately 35 percent increase in yawing moment when the 30 degree phase angle is used. Figure 5.8 illustrates the effect of cyclic control phasing on pitch control moment. The reduced level of pitch control moment resulting when phase angle is optimized for yaw control does not constitute a problem because of the much higher control moment capability from hub moment and inplane force. Also, while the pitch angular acceleration required is 20 percent higher, the pitch inertia of the aircraft is only one-third of the yaw inertia.

The required level of yaw control power as a function of damping as interpreted from the military specification of Reference 5.1 is compared in Figure 5.9 with the control sensitivity and control power results of a Vertol study, and the predicated capability of the Model 213 aircraft is indicated. Some of the data examined during the Boeing study are illustrated in Figure 5.10. If the minimum attitude response requirement of Reference 5.1 is satisfied with a reasonable range of pedal motion ($\pm$2.50 inches, minimum), the total installed angular acceleration capability required will be 0.65 rad/sec^2. Boeing experience with tandem rotor helicopters and tilt wing aircraft indicates that an angular acceleration capability in excess of 0.5 rad/sec^2 is not required. With this level of control power and a pedal control range of $\pm$3.0 inches, the attitude response in 1.0 second,per inch of control input,will be approximately 4.0 degrees. The control characteristics represented by the shaded area of Figure 5.9 are recommended as a reasonable and useful yaw control objective.

5.2.3 Pitch Control

Pitch control is achieved by using longitudinal cyclic pitch. As discussed in Section 5.2.2, the cyclic control inputs are phased to result in maximum inplane force to optimize cyclic for yaw control. Data obtained from Reference 1.5 wind tunnel test are presented in Figures 5.11 and 5.12 to illustrate, as anticipated, that angle of attack has no effect on rotor pitching moment and inplane force in hover and essentially zero effect in near-hover conditions. Figures 5.13 and 5.14 present total aircraft lift and pitching moment coefficients based on slipstream dynamic pressure in the near-hover condition.

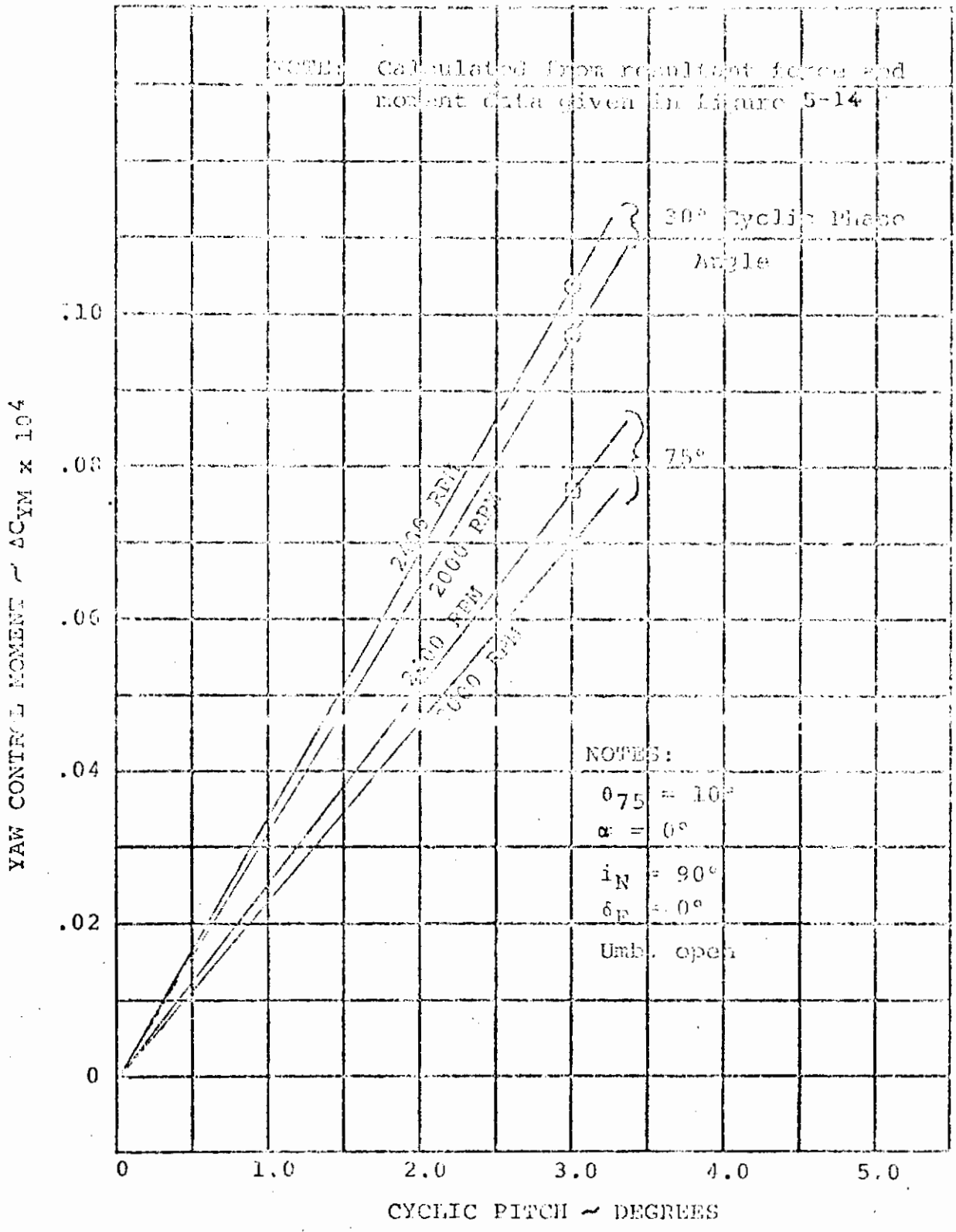

FIGURE 5.7. YAW CONTROL HOVER, OGE

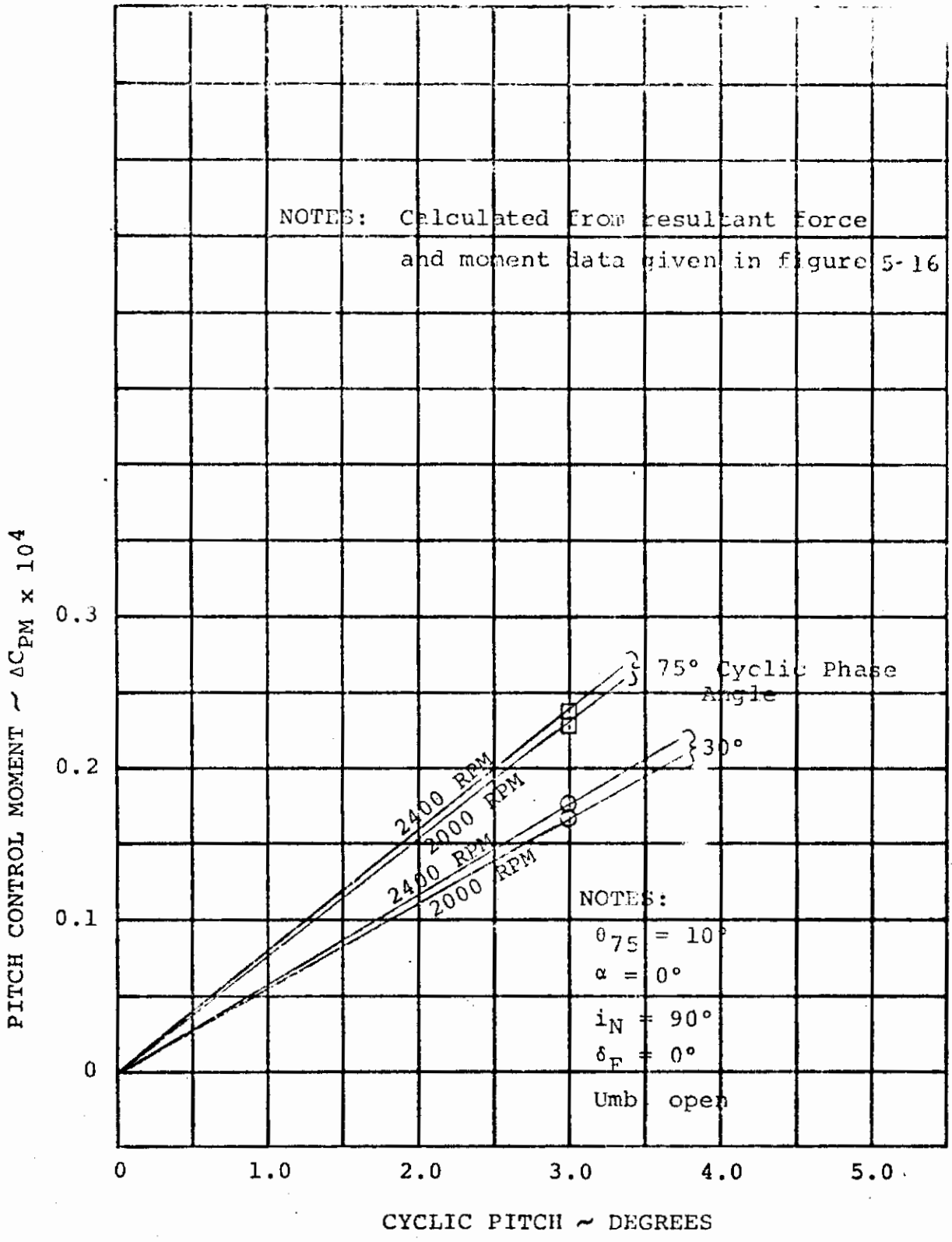

FIGURE 5.8. PITCH CONTROL HOVER, OGE

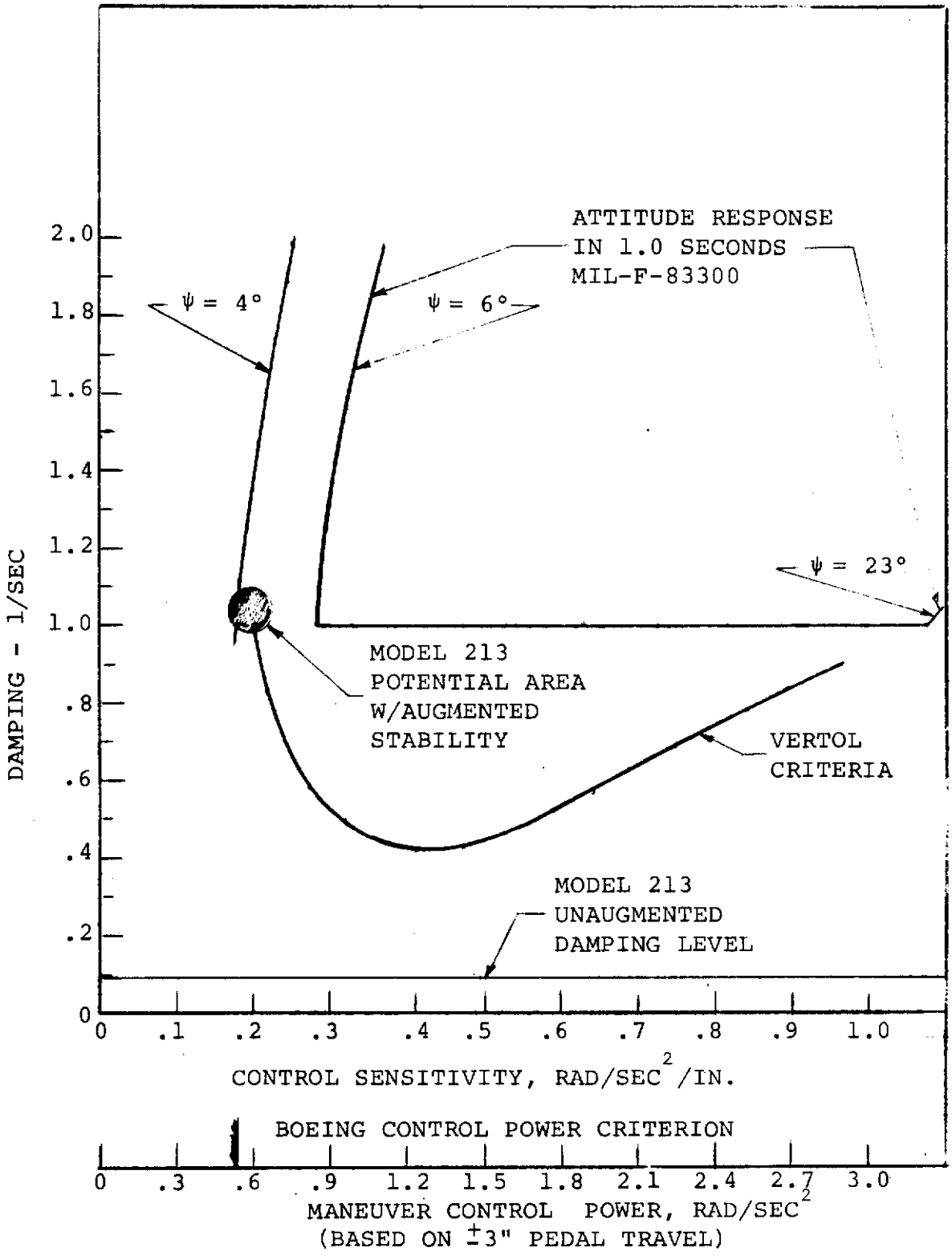

FIGURE 5.9. YAW CONTROLLABILITY IN HOVER

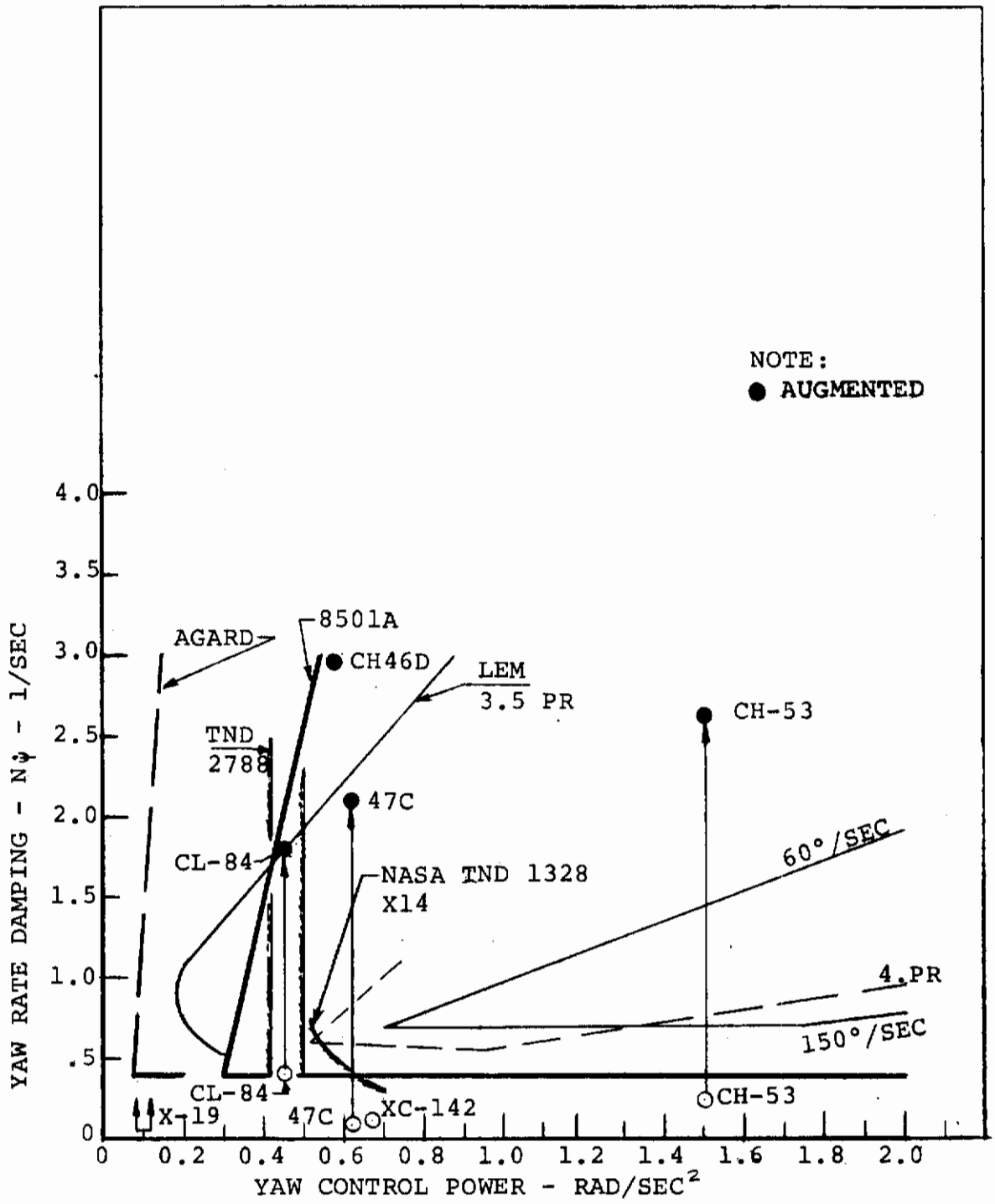

FIGURE 5.10. YAW CONTROL POWER

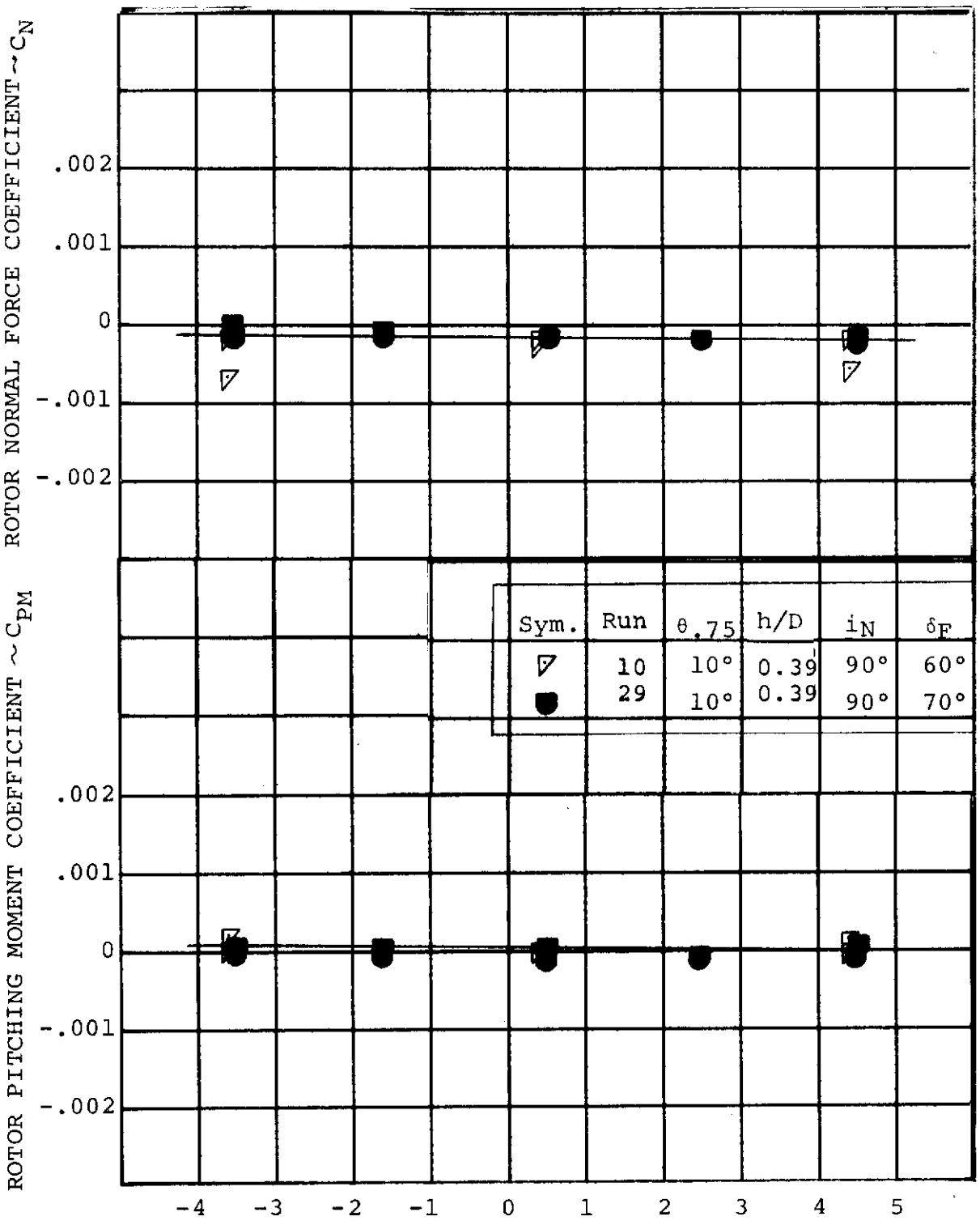

FIGURE 5.11 EFFECT OF ANGLE OF ATTACK ON ROTOR NORMAL FORCE IN HOVER

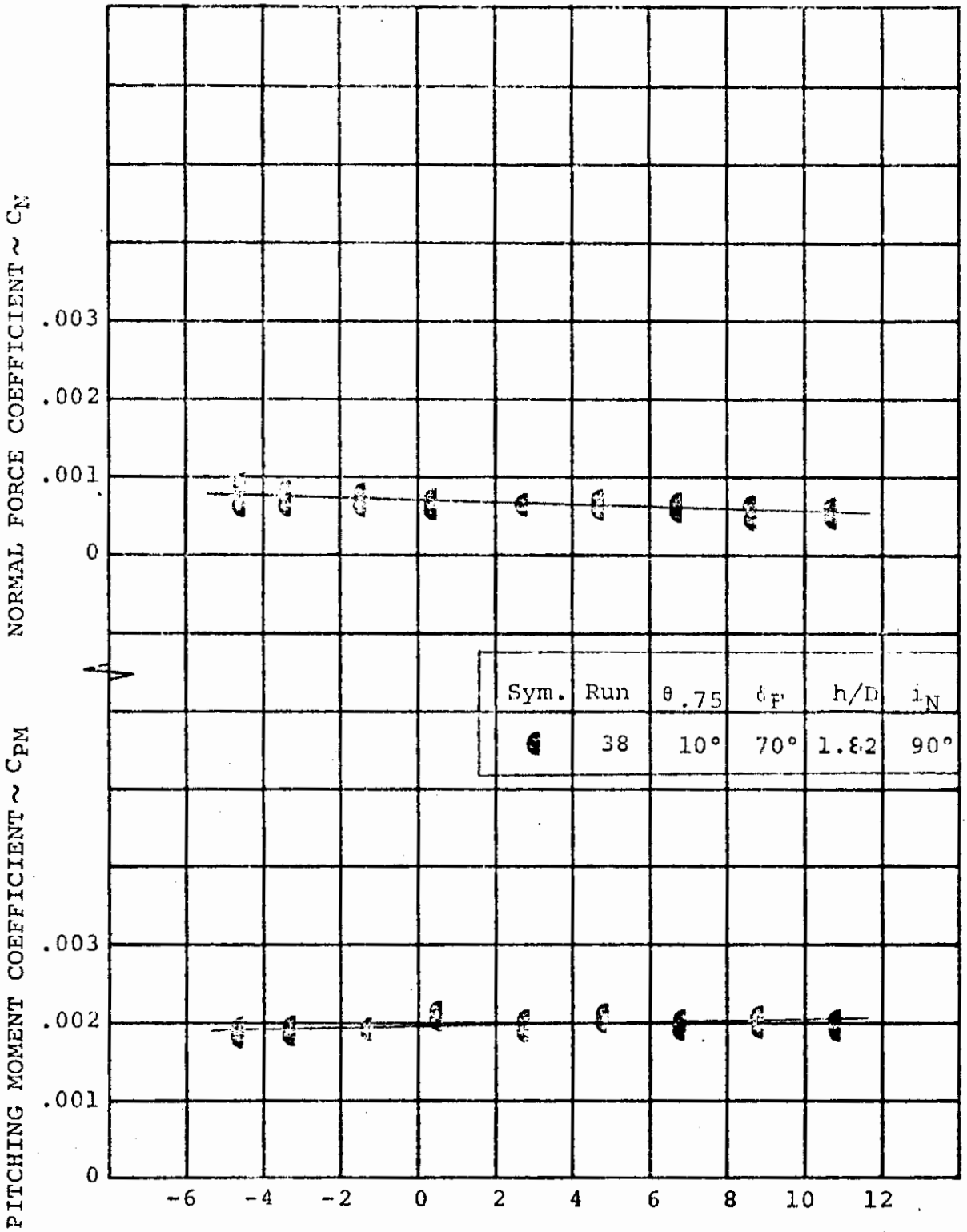

FUSELAGE ANGLE OF ATTACK ~ DEGREES

FIGURE 5.12 EFFECT OF ANGLE OF ATTACK ON ROTOR NORMAL FORCE AND PITCHING MOMENT IN THE NEAR HOVER MODE AT q=4 psf.

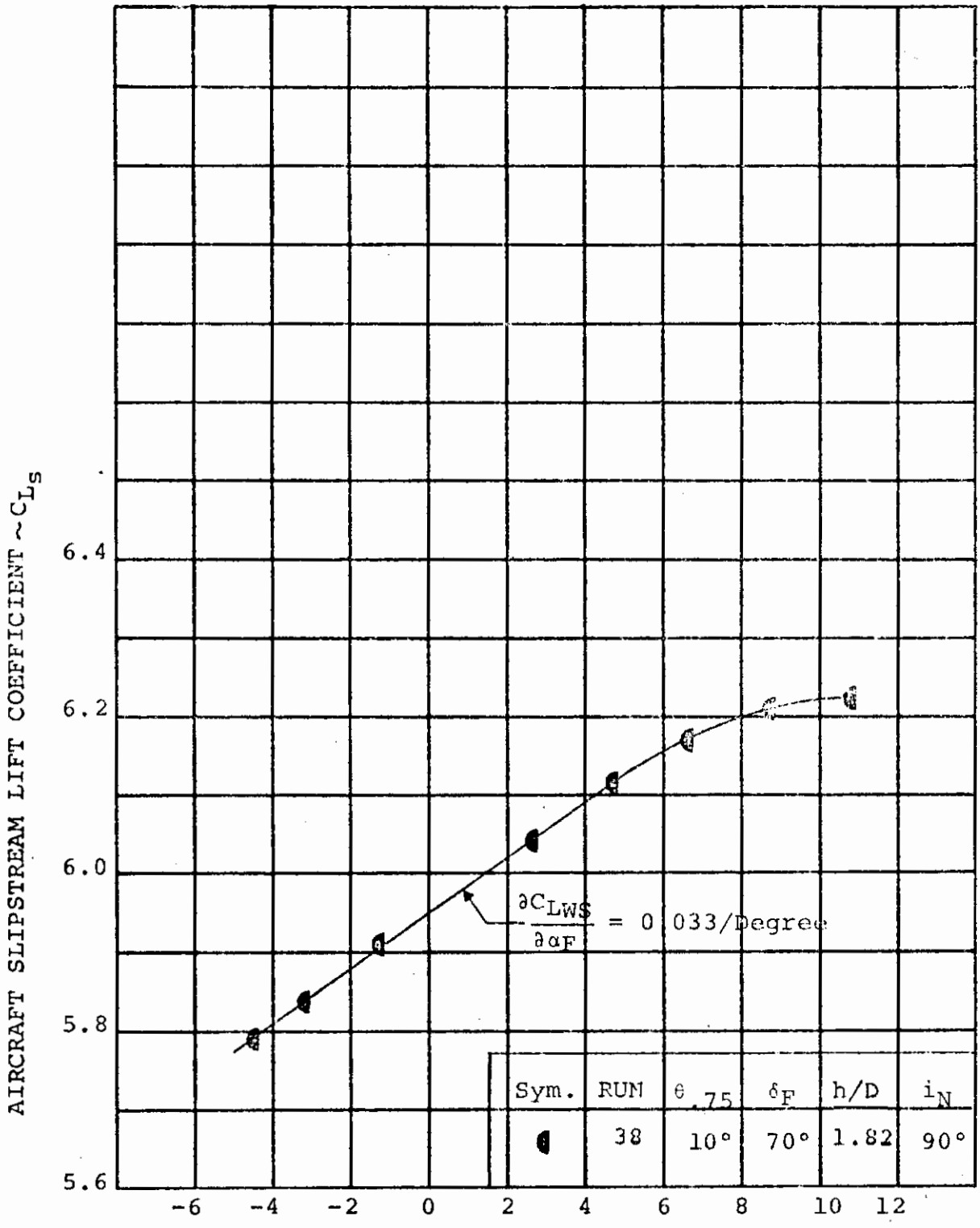

FIGURE 5.13 EFFECT OF ANGLE OF ATTACK ON AIRCRAFT LIFT IN THE NEAR HOVER MODE AT q=4 psf.

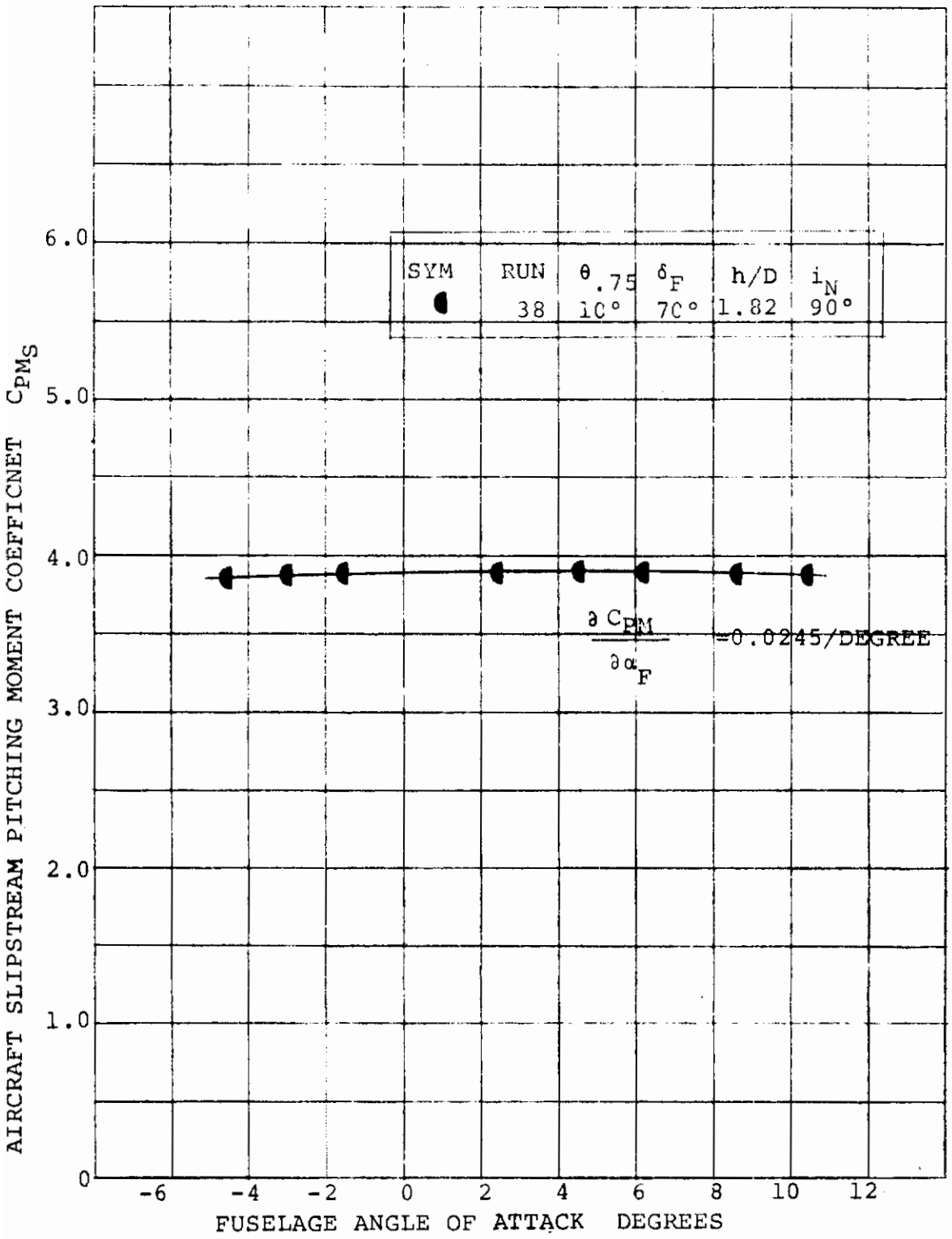

FIGURE 5.14: EFFECT OF ANGLE OF ATTACK ON AIRCRAFT PITCHING MOMENT IN THE NEAR HOVER MODE AT q = 4 PSF

The Level 1 control sensitivity requirements interpreted from Reference 5.1 are shown in Figure 5.15 along with the sensitivity and control power criterion from a Vertol study. Data examined during the Vertol study are illustrated in Figure 5.16. The agreement between the military specification and the Boeing study indicates that a control sensitivity of 0.15 rad/sec^2/inch is a reasonable objective. Assuming a nominal range of control motion available for maneuver of $\pm$4.0 inches yields a total control power requirement of $\pm$0.6 rad/sec^2. Predictions of the capability of the pitch control for the Model 213 indicate that the above requirements can be met easily.

5.2.4 Roll Control

Roll control is obtained from differential collective pitch changes between the two laterally displaced rotors. The resulting attitude response also produces a laterally directed thrust force for sideward velocity control. Satisfactory pilot ratings of lateral controllability are dependent upon qenerating a linear thrust response from the rotors of sufficient magnitude to achieve the attitude response requirements of the Reference 5.1 military specification. This is the identical means used to provide pitch control on all tandem rotor helicopters.

The Level 1 requirements of Reference 5.1 are that the ratio of maximum attitude response within one second to abrupt control displacement shall range between 4.0 and 20.0 degrees per inch. The system damping required at each level of control sensitivity to satisfy the attitude requirement is shown in Figure 5.17. The aerodynamic, or unaugmented,damping of the Model 213 was determined by the stability program of Reference 5.2 and is noted in Figure 5.17 to be -0.34/sec. Damping can be augmented by a conventional SAS to achieve a roll damping of -2.0 to -3.0/second resulting in the illustrated Model 213 potential capability. The flying qualities criteria will be satisfied with a control sensitivity of 0.25 to 0.30 rad/sec^2/in. With a nominal control motion range of $\pm$4.0 inches and a hover roll inertia of 688,000 slug-ft^2 at the design gross weight of 67,000 pounds for the Model 213 aircraft, a differential thrust of $\pm$11,250 pounds is required to achieve an angular acceleration of 1.0 rad/sec^2. Prop/rotor thrust effectiveness data of Reference 1.5 is shown in Figure 5.18 and indicates that the required thrust can be achieved with a collective pitch change of $\pm$3.5 degrees.

The minimum spec-recommended attitude response is noted to be consistent with the Vertol control power criteria. Data

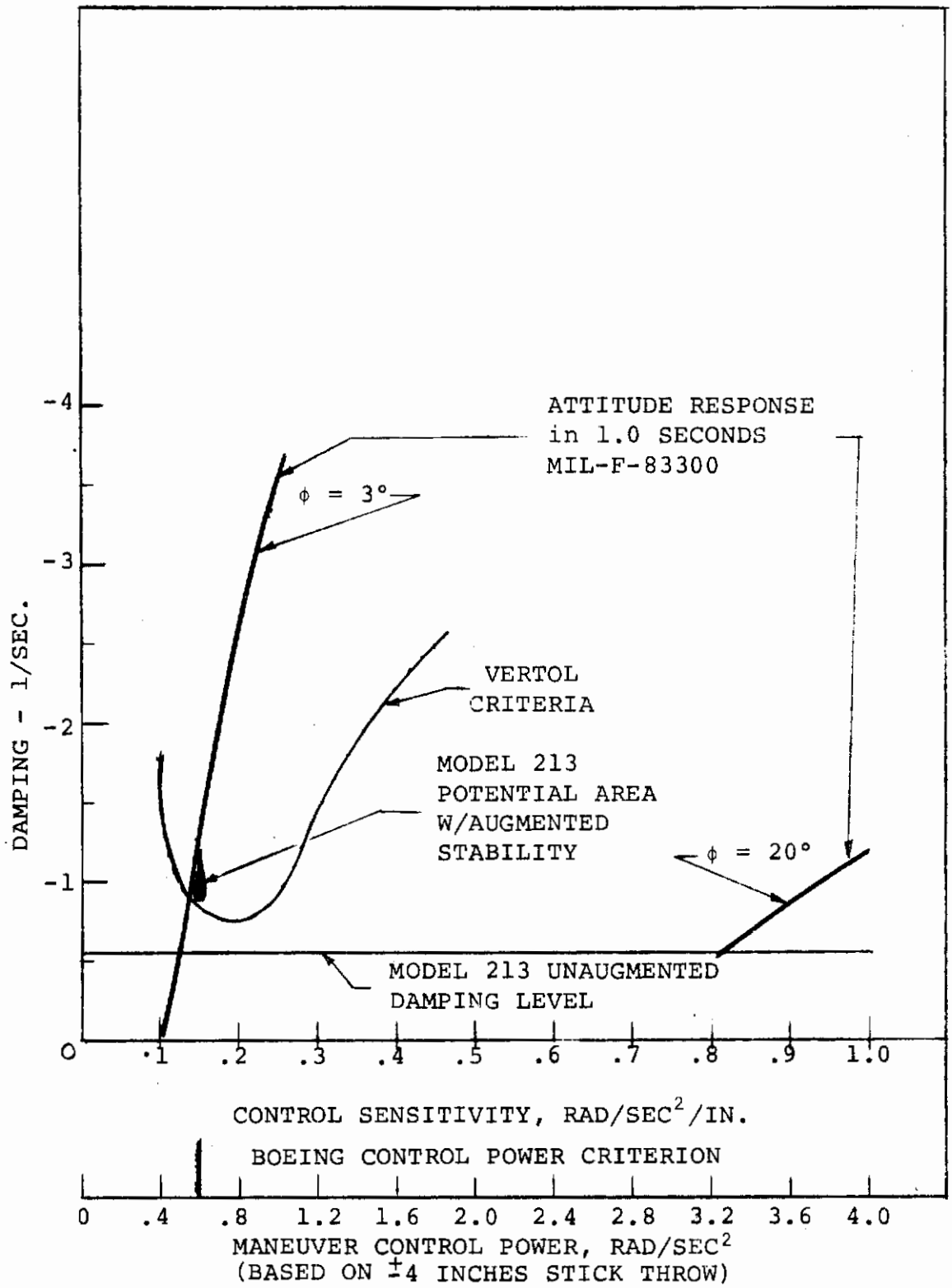

FIGURE 5.15. PITCH CONTROLLABILITY IN HOVER

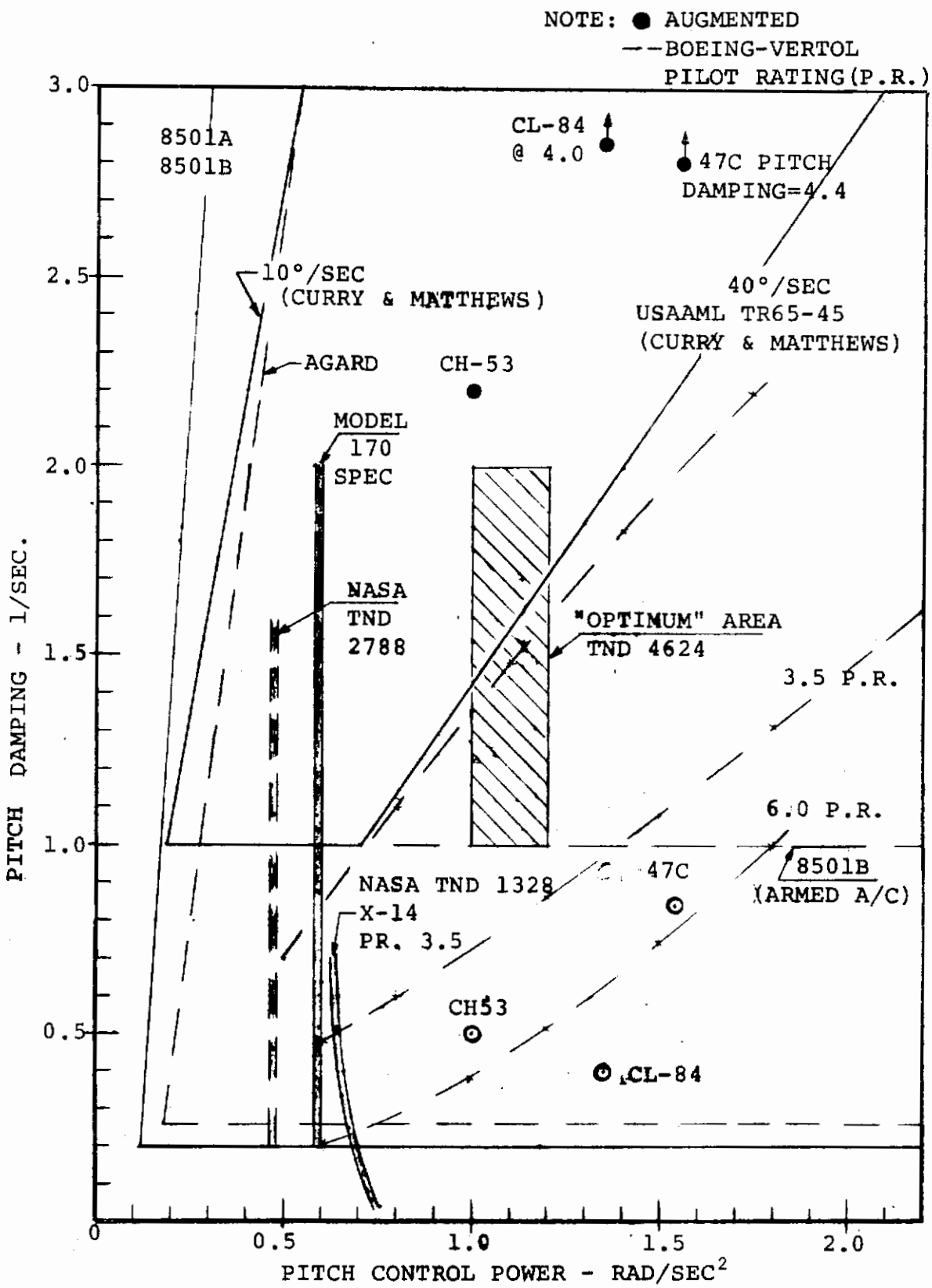

FIGURE 5.16. PITCH CONTROL POWER

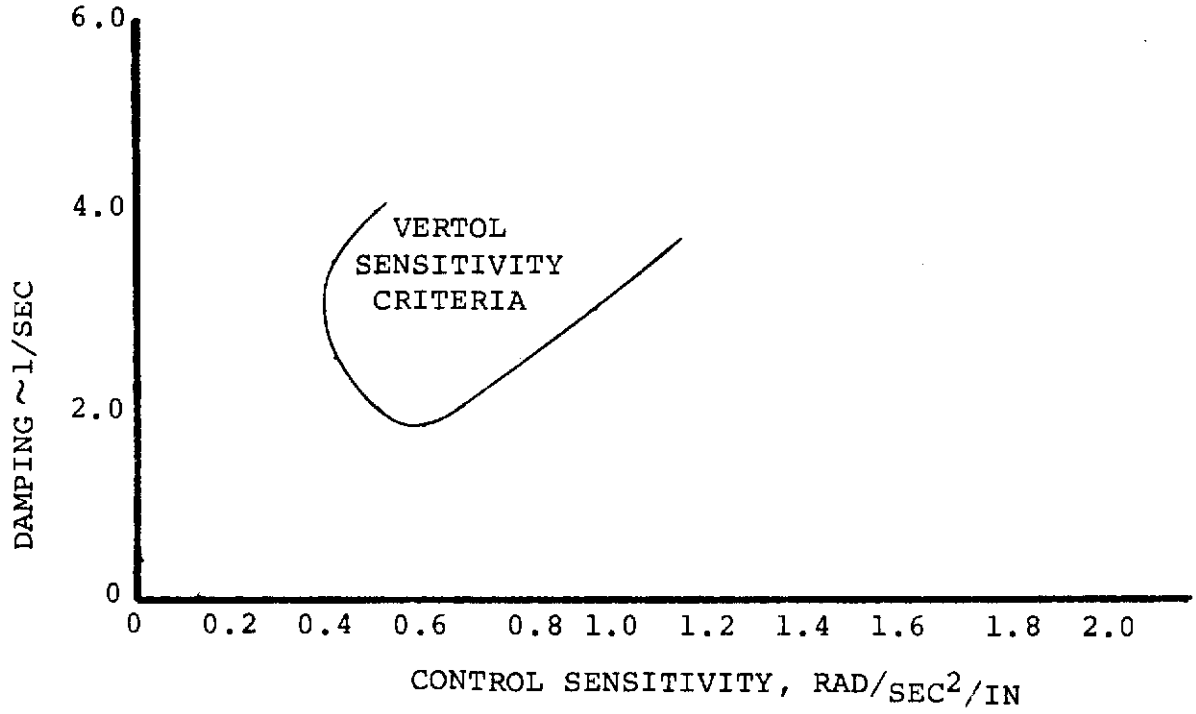

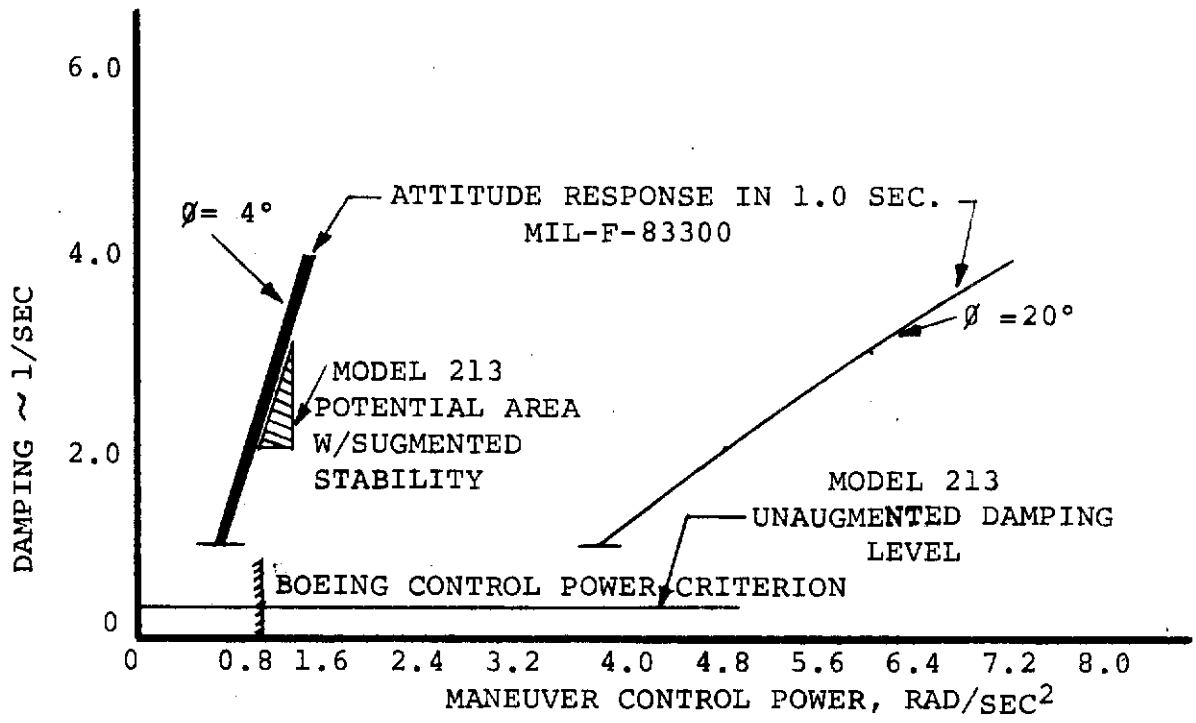

FIGURE 5.17: ROLL CONTROLLABILITY

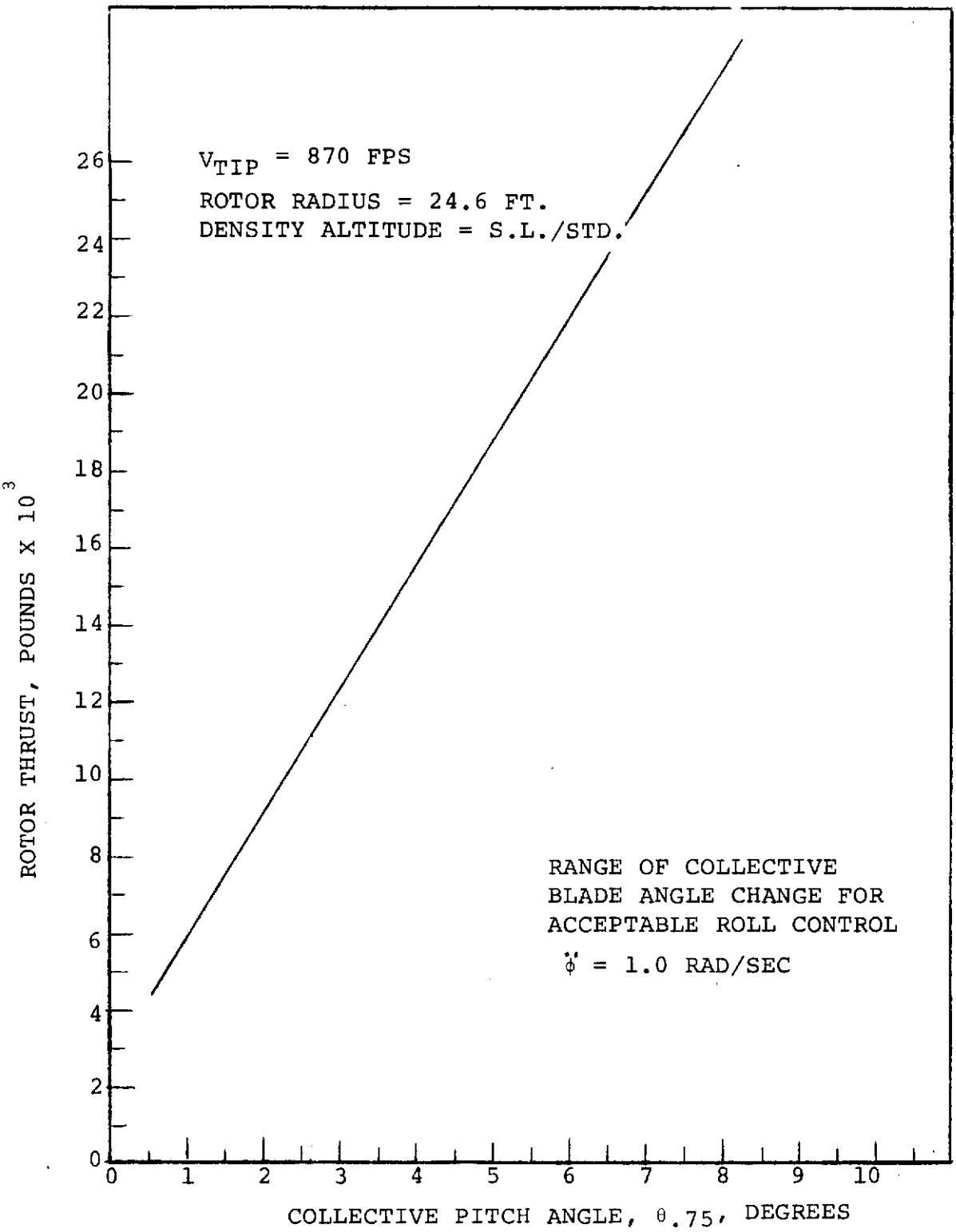

FIGURE 5.18 COLLECTIVE PITCH EFFECTIVENESS

examined in conjunction with establishment of the Vertol criteria are illustrated in Figure 5.19. Therefore, the shaded area of Figure 5.17 is considered to be a reasonable roll control objective.

5.2.5 Control Coupling

Application of differential longitudinal cyclic for low speed yaw moment control also results in a coupled response about the roll axis. Cyclic flapping of the prop/rotor blades results in the inplane force used for yaw control and a corresponding hub moment. Because of the relative stiffness of the blade attachment to the hub, the azimuthal position of maximum moment lags the position of maximum force. Since the inplane forces between the rotors are designed to be 180° out-of-phase for yaw controllability, the hub moments are out-of-phase by only 45°. Thus, differential cyclic pitch will produce pitching moments from the two rotors which cancel and rolling moments from the two rotors which add. The phasing is such that nose right yaw control results in a small right wing down rolling moment.

Cyclic pitch effectiveness was investigated in the wind tunnel test report of Reference 1.5. The resulting data is summarized in Figure 5.20 for a 3.0 degree longitudinal cyclic setting. Control phasing for the tests was 65°, i.e., the swashplate was set so that the zero longitudinal cyclic input position was at the 65° azimuth location. The inplane forces arising from the 3.0° cyclic setting are approximately 4% of the thrust forces. This corresponds to 0.8 degrees of tip-path-plane tilt per degree of cyclic and is predictable from the stiffness characteristics of the model blades. Although the model blades were not dynamically scaled to the blades of the full scale vehicle, the results do substantiate the method of estimating the maneuverability cyclic ranges of Sections 5.2.2 and 5.2.3.

5.2.6 Skittishness in Ground Effect

Random aircraft response, or skittishness, to external disturbances when close to the ground has been experienced with various configurations of V/STOL aircraft. Since it is not possible at this time to analytically predict the aircraft's sensitivity to skittishness, a powered wind tunnel dynamic model was used to investigate the problem. Two tests were conducted with the

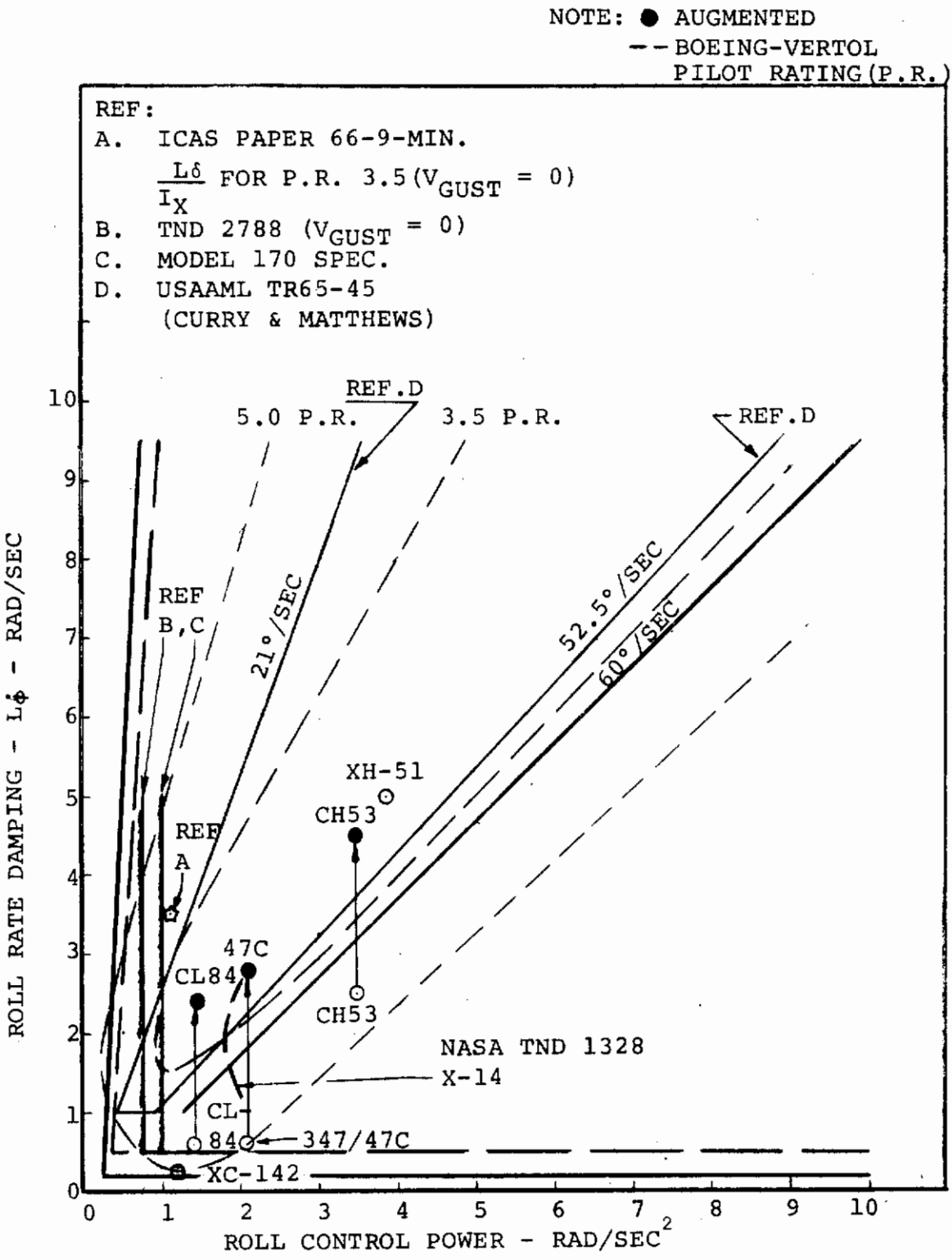

FIGURE 5.19. ROLL CONTROL POWER

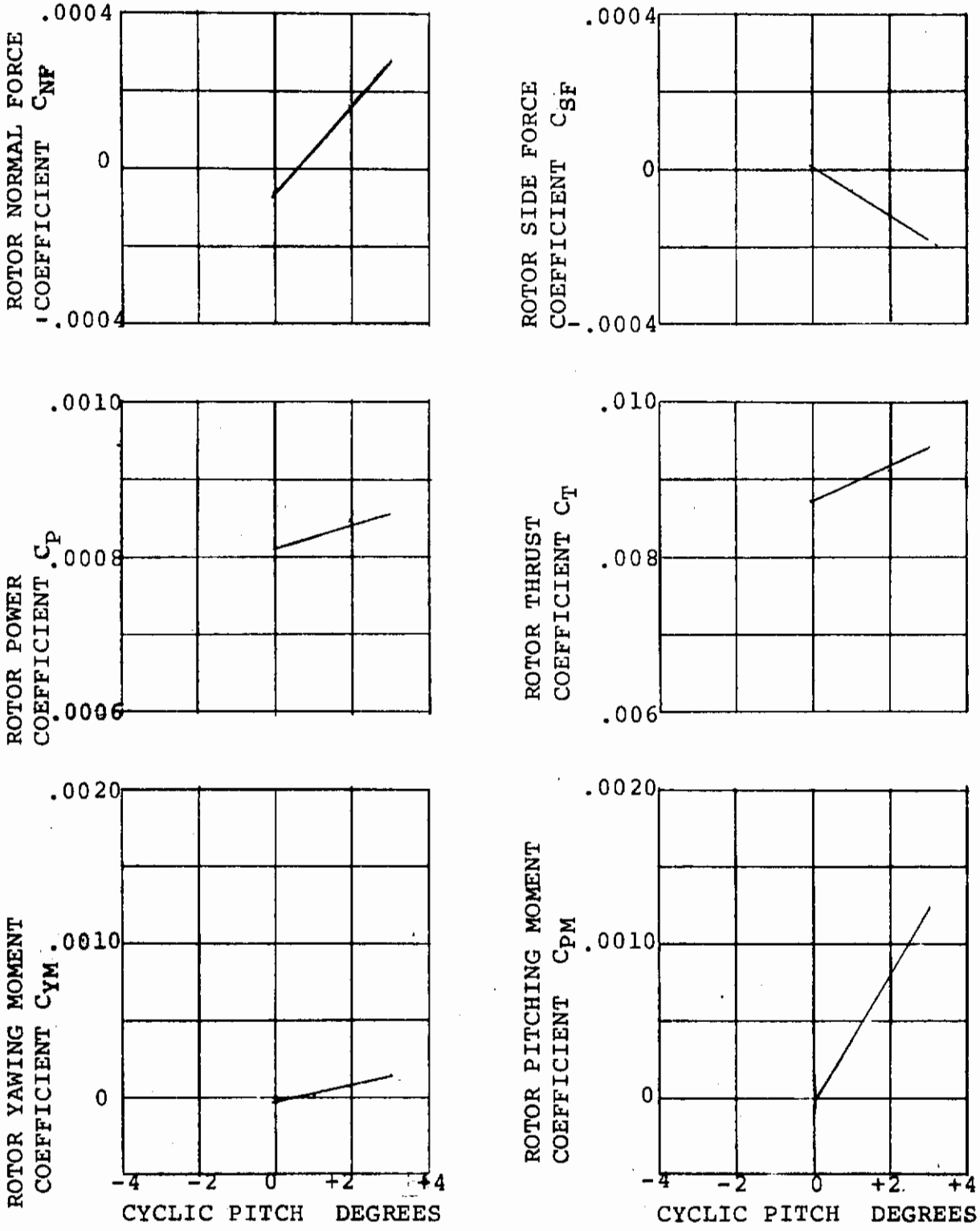

FIGURE 5.20: CYCLIC PITCH EFFECTIVENESS FOR HOVER YAW CONTROL

1/10 scale dynamic model in Test Program IV. The results of these test programs are reported in Reference 1.7 and 5.3 and the salient points are discussed below.

The model was "softly" supported to simulate free-flight operating conditions. Data were obtained in and out-of-ground effect and with and without simulated attitude stabilization. In-ground-effect roll attitude motions of the model are shown in Figure 5.21 in response to discrete gust-like pulse disturbances. The h/D ratio for this data was .41 and attitude stabilization was not included. The resulting motion is shown to be stable and the .331 cps oscillations are at least neutrally damped. Long-term self-induced motions which indicate the skittishness of the vehicle are also shown in Figure 5.21. The skittish motions are stable and are at least neutrally damped with an average frequency of 0.35 cps. Maximum unperturbed roll displacements are on the order of $\pm 2°$.

Out-of-ground effect gust response is shown in Figure 5.22 along with the comparable in-ground effect time history. The OGE response is highly damped and there is no tendency for the model to be excited by any disturbance other than the initial, intentionally imposed upset.

The effect of a simple roll attitude feedback control system was evaluated by adding mounting springs in the pitch and roll axes. These springs added a stiffness of 15.0 in-lb/deg in pitch and 5.0 in-lb/deg in roll, or in terms of control sensitivity in the hover mode, 1.01 rad/sec^2 and 0.061 rad/sec^2, respectively, per degree of fuselage attitude. Figure 5.23 shows that the IGE response of the aircraft to a discrete gust is a 0.45 cps oscillation with a damping coefficient of 0.165. Since there is no tendency for the model to respond to any unintentional disturbances, it is expected that IGE skittishness can be eliminated by a simple feedback system.

5.3 TRANSITION REGIME

The transition mode refers to operation out-of-ground effect from hover to the tilt rotor cruise regime. In this mode the nacelles rotate from 90 degrees incidence to zero degree incidence. During operation in this regime, the rotors have a significant influence on the aircraft stability and control since they provide the majority of the lift as well as all of the propulsive force.

NOTE:
1. MODEL 160 CONFIGURATION
2. HOVER MODE - IGE, i_N = 90°, Ω = 825 RPM
3. 1/10 SCALE MODEL DATA

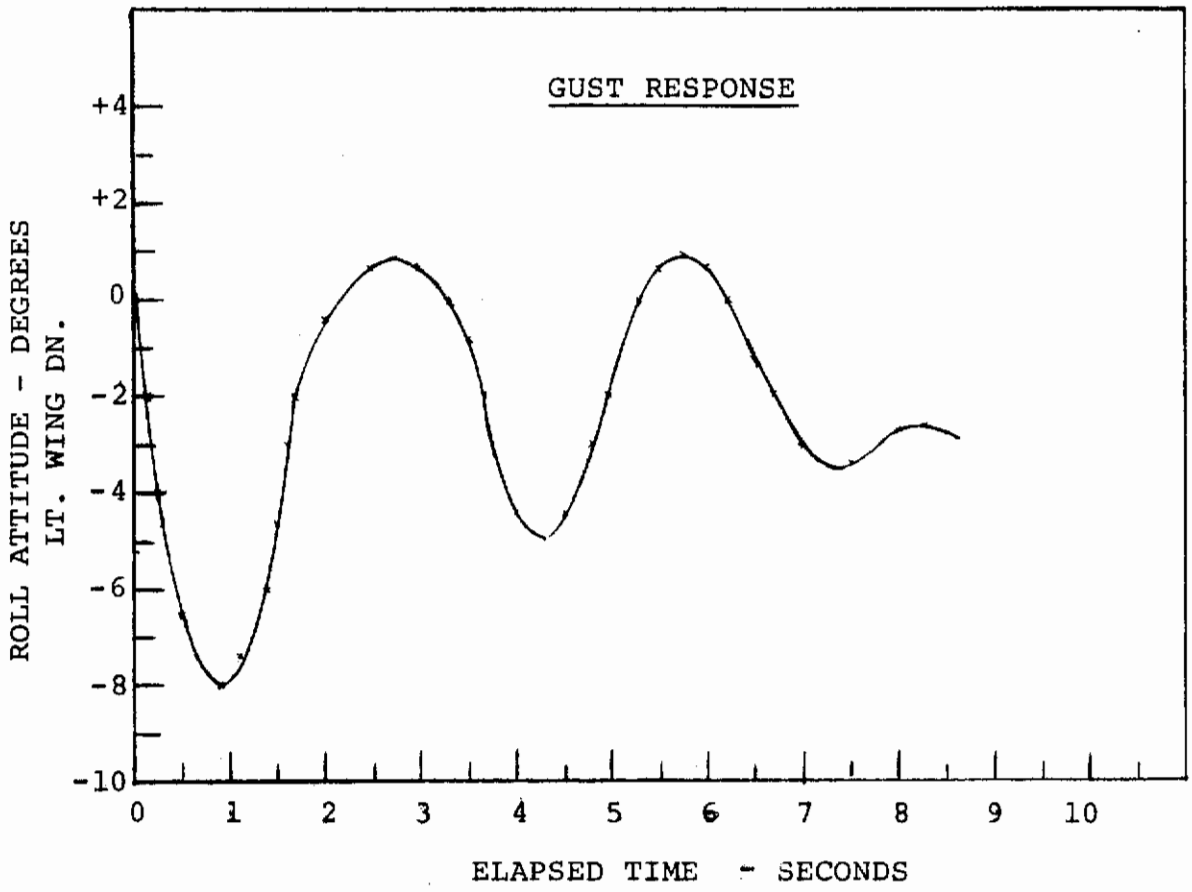

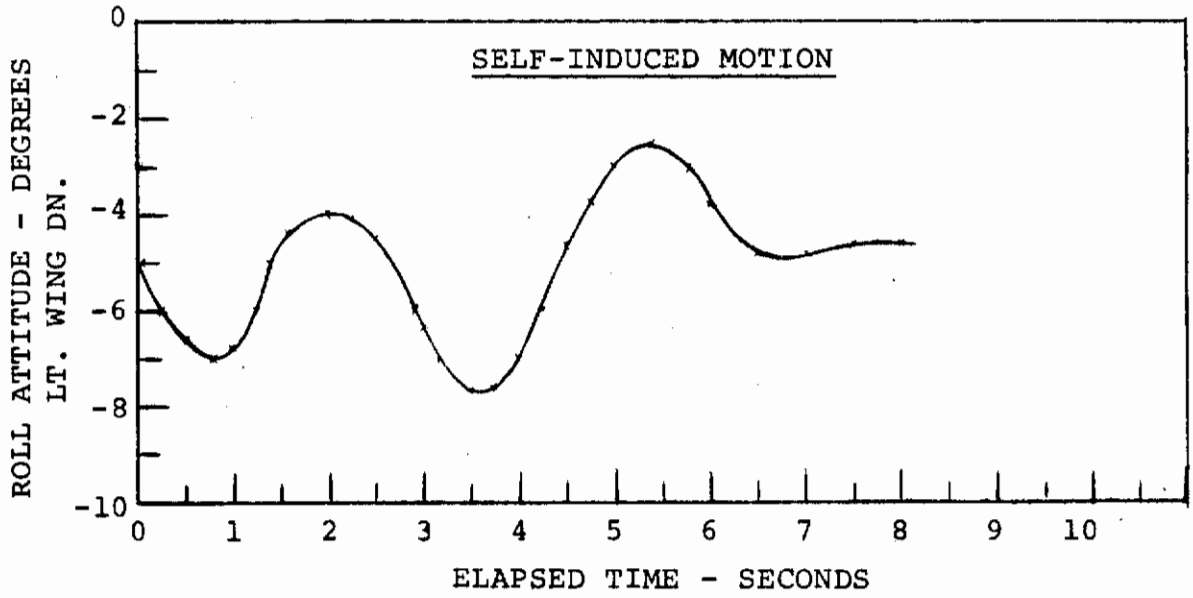

FIGURE 5.21. IGE ROLL STABILITY W/O ATTITUDE STIFFNESS

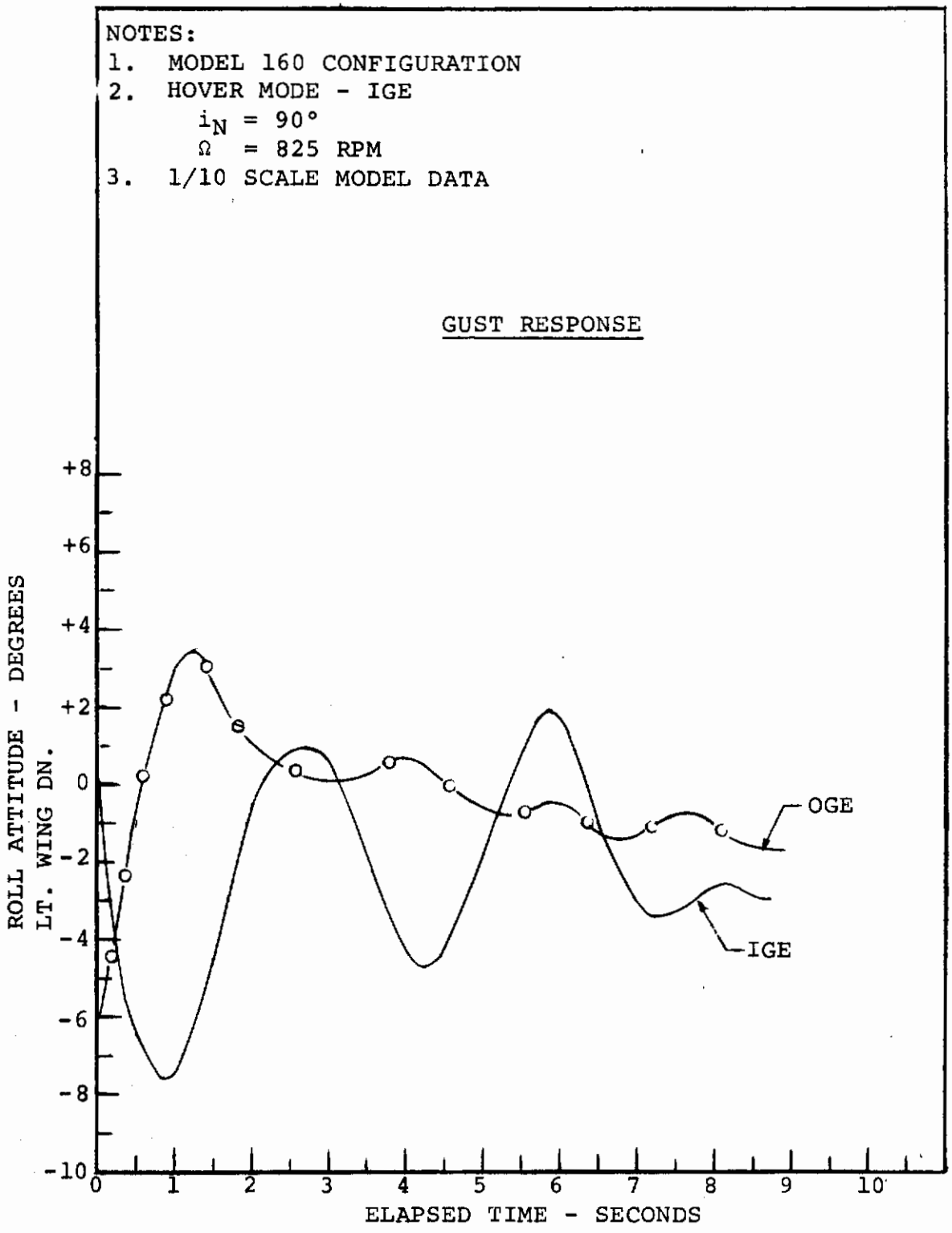

FIGURE 5.22. IGE/OGE ROLL STABILITY W/O ATTITUDE STIFFNESS

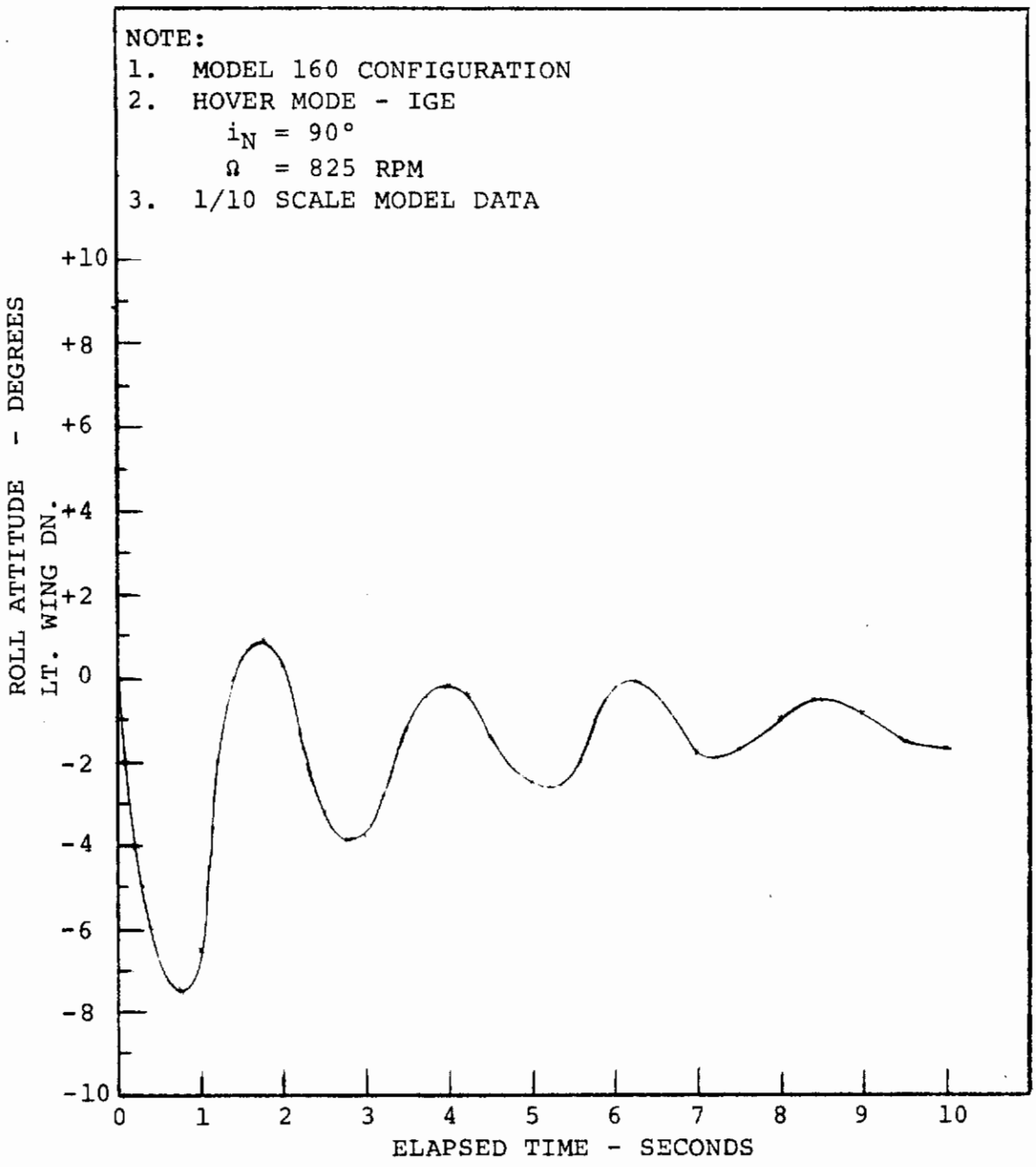

FIGURE 5.23. IGE ROLL STABILITY W/ ATTITUDE STIFFNESS

5.3.1 Rotor Derivatives

Data obtained from the wind tunnel tests of Reference 1.5 have been correlated with predictions and the results are illustrated here. Test results have also been presented in Reference 1.6.

Figure 5.24 illustrates typical correlation between prediction and test data for the rotor normal force coefficient versus fuselage angle of attack for a representative transition condition. The rate of change of normal force with angle of attack from test is in good agreement with predictions but the magnitude is slightly in error indicating a difference in trim. Similarly Figure 5.25 indicates good agreement between test and prediction for the rate of change of rotor pitching moment coefficient but a difference in absolute magnitude which would result in a small trim error. Figures 5.26 and 5.27 illustrate the variation of tested rotor side force and yawing moment coefficients with fuselage yaw angle. Again, it must be remembered that the model used in the test program had dynamic characteristics substantially different from a full scale rotor. The data must therefore be taken as a substantiation of analytical predictions rather than a directly scaleable indication of full scale values.

5.3.2 Aircraft Stability

Total aircraft stability characteristics in transition are strongly affected by the rotor contribution. Figure 5.28 illustrates aircraft longitudinal stability at a mid-transition condition. These data were obtained from the wind tunnel test of Reference 1.5 and because of the rotor not being dynamically similar to the full scale Model 213 serve only to show the correlation of predictions with test data. Note that there is good agreement between the predicted stability for the complete aircraft with rotors on and the test data up to the stall angle of attack as indicated by the similarity of the slopes. The absolute level of pitching moment is overestimated, however, which would result in a difference between test and predicted trim. Figure 5.29 indicates the contribution of the prop/rotor and the vertical tail to yawing moment versus fuselage yaw angle, i.e., directional stability.

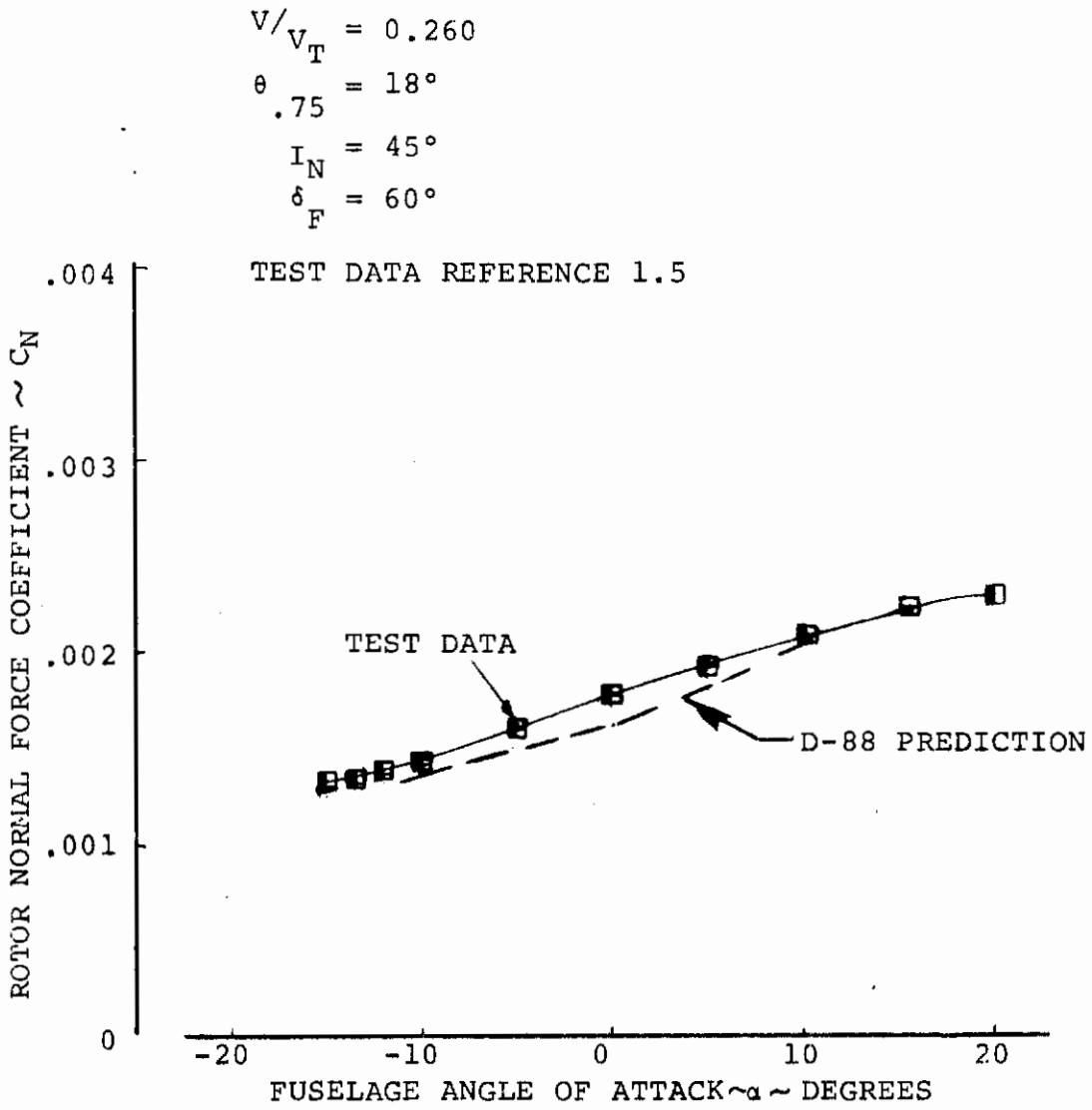

FIGURE 5.24: COMPARISON OF TEST DATA AND PREDICTION OF ROTOR NORMAL FORCE IN MID-TRANSITION

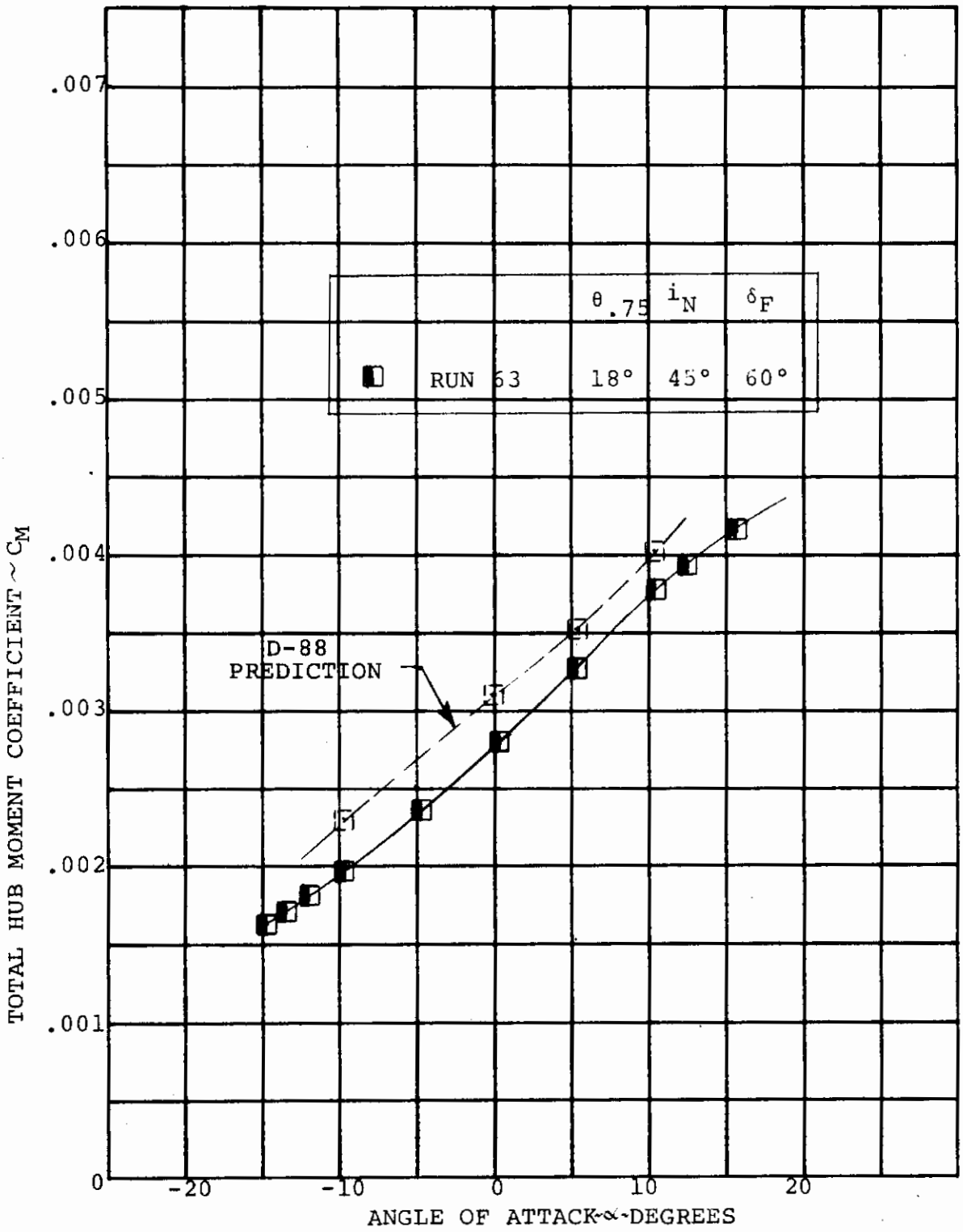

FIGURE 5.25: COMPARISON OF TEST AND PREDICTION FOR TOTAL HUB MOMENT IN TRANSITION

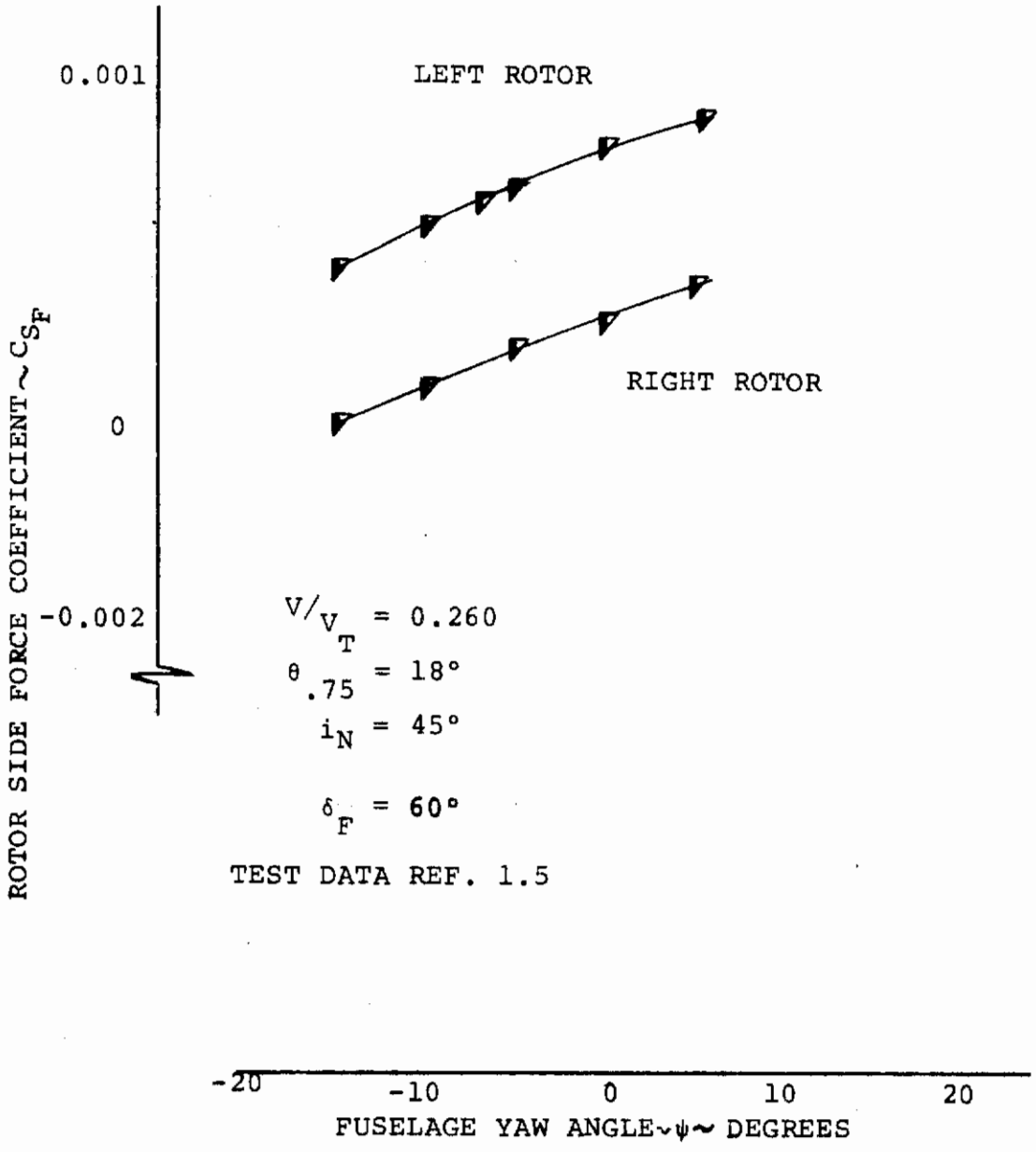

FIGURE 5.26: ROTOR SIDE FORCE IN MID-TRANSITION

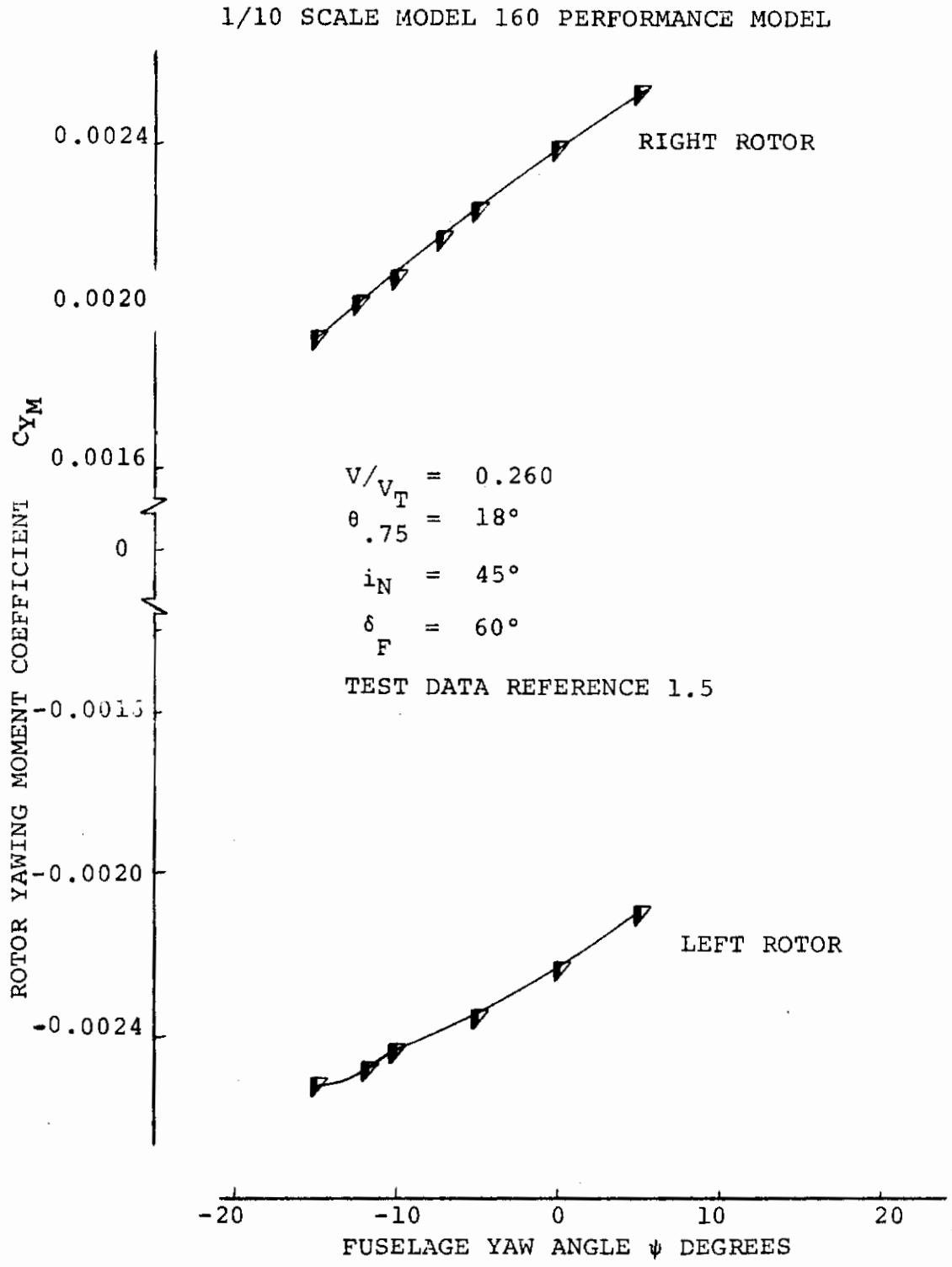

FIGURE 5.27: ROTOR YAW MOMENT IN MID-TRANSITION

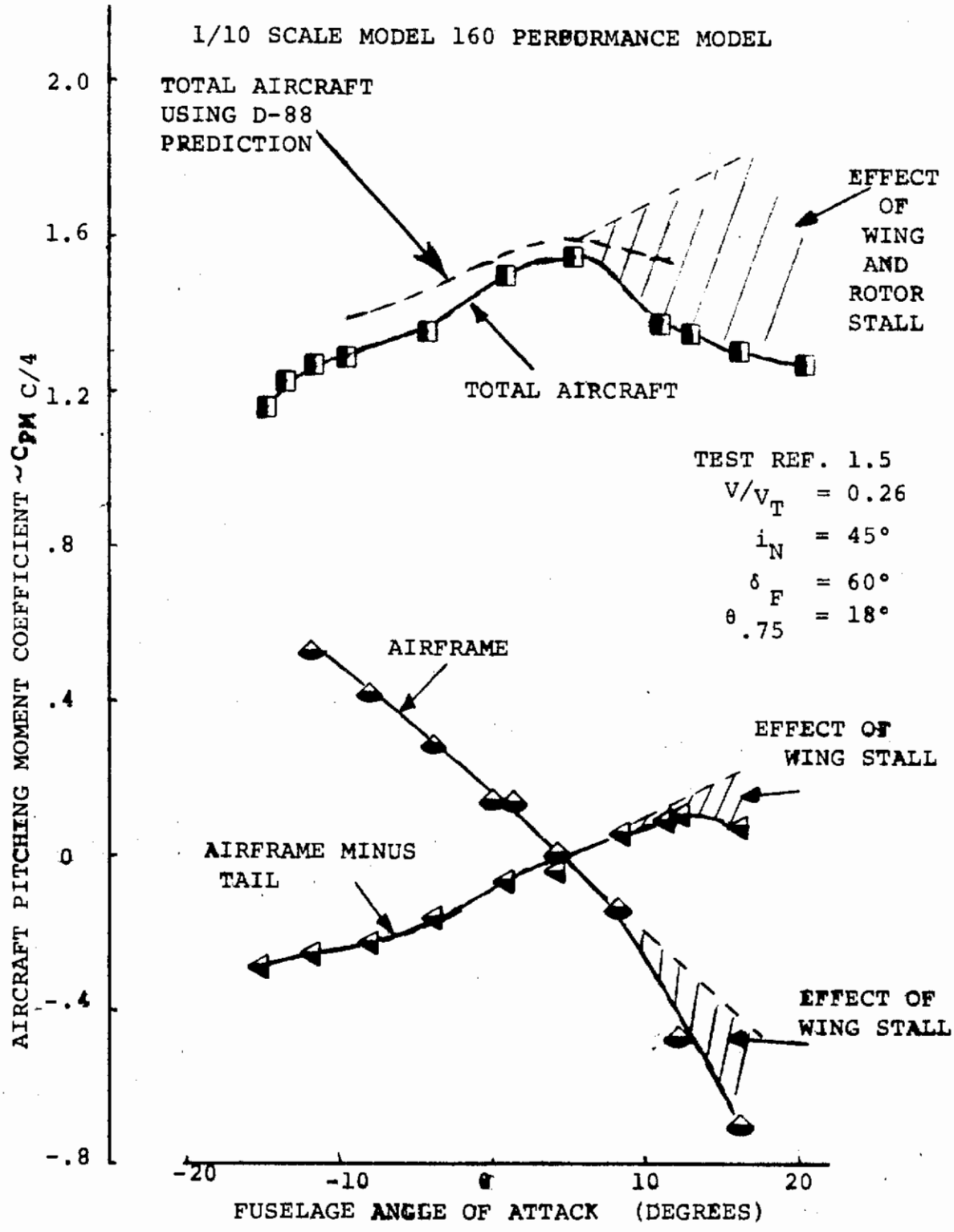

FIGURE 5.28: TOTAL AIRCRAFT LONGITUDINAL STABILITY CORRELATION - MID-TRANSITION

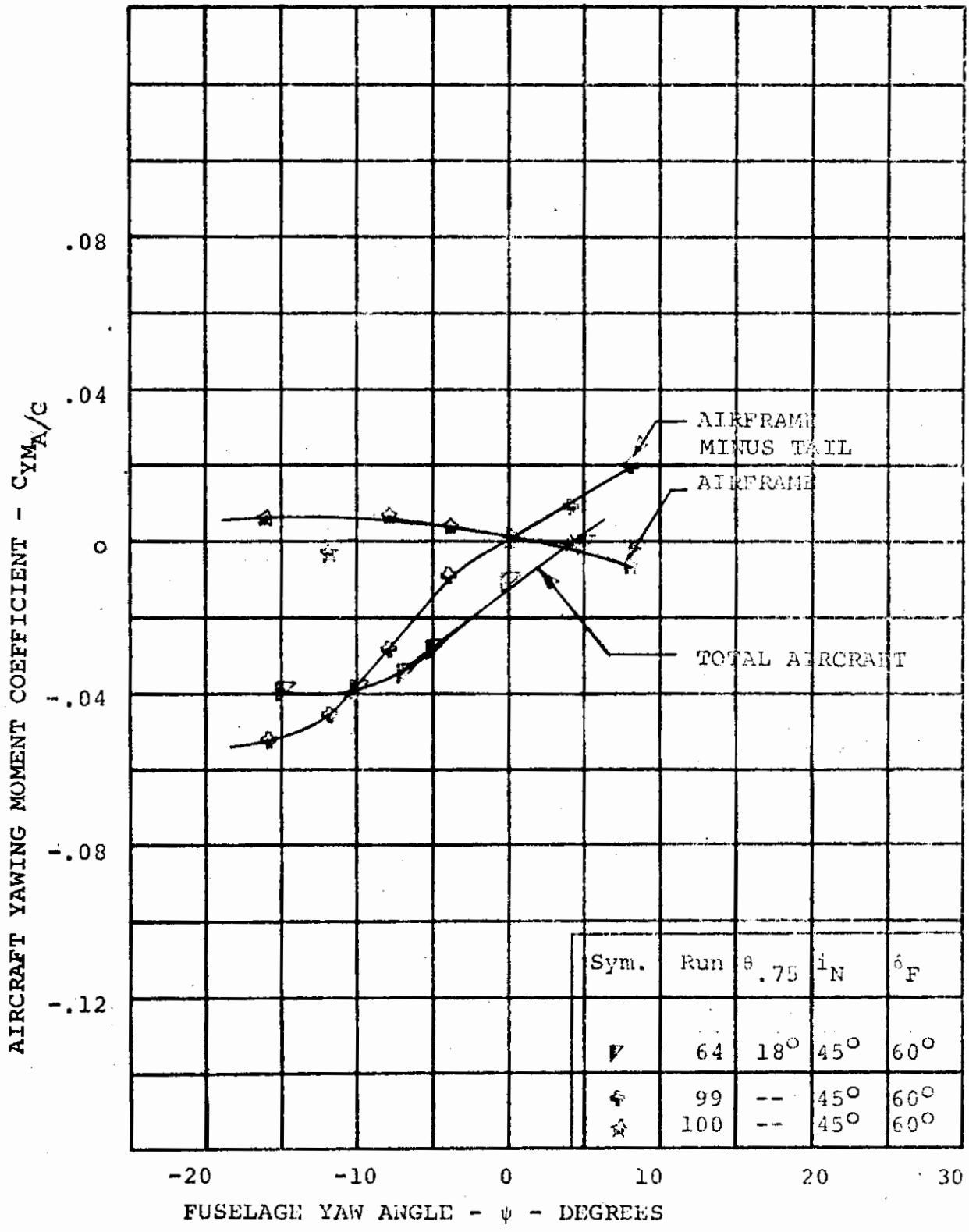

FIGURE 5.29. CONTRIBUTION OF PROP/ROTORS AND VERTICAL TAIL TO AIRCRAFT YAWING MOMENT AT V/V_T = 0.26 WITH i_N = 45°

It is anticipated that the full scale aircraft with its flexible rotors will be mildly unstable or neutrally stable statically at the low transition speeds at which the tail surfaces are relatively ineffective and stable at the higher transition speeds. Stability augmentation will be provided as required to meet or exceed the military specification requirements for frequency and damping of the longitudinal and lateral-directional modes.

5.3.3 Control Phasing

During transition it is important that the collective and cyclic controls be mixed properly to prevent "coupled" motions or accelerations of the aircraft in response to control commands particularly about the roll and yaw axes. For example, differential thrust is used for roll control during transition and when the nacelle is at less than 90° incidence, this also results in a yawing moment being applied to the aircraft. Differential cyclic is applied to counter the yawing moment by utilizing the differential inplane forces generated by the cyclic control. The differential inplane forces generated are in the direction to increase the rolling moment, thereby augmenting the roll control moment while cancelling the yawing moment. The yaw condition is handled in a similar manner.

It is anticipated that the normal aerodynamic controls, ailerons, elevators, or unit horizontal tail, and rudder will be operated throughout transition through their full ranges to reduce complexity of the control system and to take advantage of the resulting control effectiveness.

5.3.3.1 Roll Control

The roll control available in transition from differential collective pitch and aileron were analytically investigated during Boeing in-house studies for the Boeing Model 222 tilt rotor configuration. The results are presented in Figure 5.30 and are considered to be generally representative of the tilt/stowed rotor configuration. The minimum angular acceleration capability meets the requirement of 1.0 rad/sec^2 in hover, exceeds the requirements of Reference 5.1 in transition and provides a reasonable rate of decrease in the available response through transition. The angular acceleration control predicted for the aileron assumes that the outboard half of the flap is used for roll control. The maximum deflection of the aileron is assumed to be $\pm$20 degrees from the initial flap deflection.

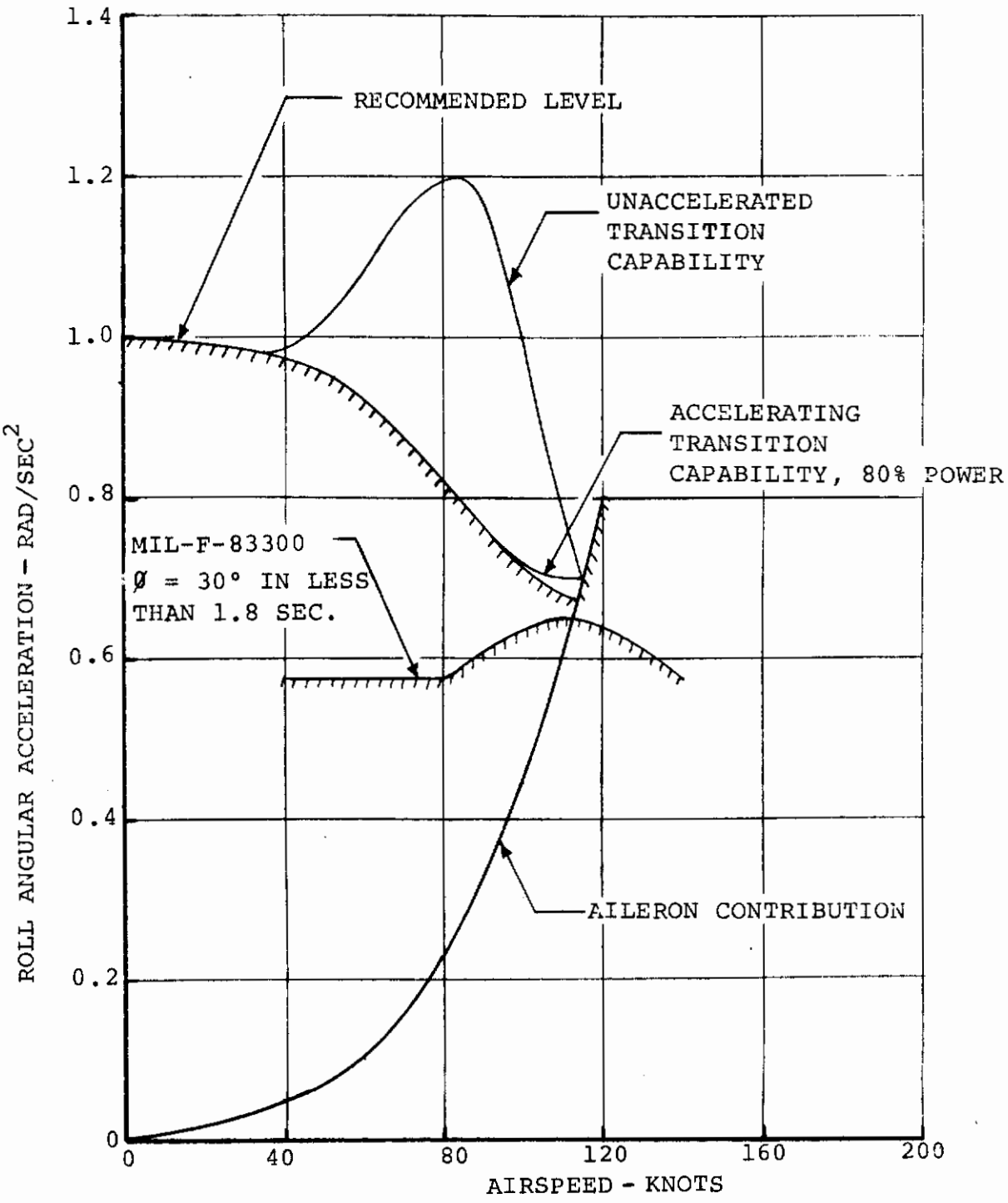

FIGURE 5.30: ROLL CONTROL POWER THROUGH TRANSITION

The differential collective pitch control required to provide the recommended roll response is shown in Figure 5.31 along with the differential cyclic scheduling required to achieve an uncoupled roll-yaw response during accelerating transitions. During unaccelerated transitions there will be some yaw coupling. The magnitude of the yaw response would be approximately 0.03 to 0.04 rad/sec^2 angular acceleration for a full roll control input. The angular acceleration capability resulting from the recommended control scheduling is compared with the recommended levels in Figure 5.30.

5.3.3.2 Yaw Control

The requirements of References 5.1 and 5.6, the recommended requirements of Reference 5.7, and the results of the Boeing control criteria study were reviewed in order to define an acceptable control capability through transition. The resulting criterion established is shown in Figure 5.32. The criterion satisfies the requirements of References 5.6 and 5.7 and meets the requirements of Reference 5.1 above 35 knots. At nacelle tilt angles other than 90°, the inplane forces associated with the yaw input will also produce a roll moment. The forces will be in a direction to produce a left roll response to a nose right yaw control input and will predominate over the right roll moment arising from the hub moment. Differential collective can be scheduled along with yaw inputs to cancel the roll moment. Careful attention to control phasing between differential cyclic and differential collective will ensure uncoupled roll and yaw control.

The differential cyclic pitch schedule is shown in Figure 5.33 along with the differential collective pitch schedule required for an uncoupled roll-yaw response during accelerating transitions. It is also assumed that the rudder is functioning at all times and the cyclic control is phased to maximize the yawing moment obtained from the inplane rotor forces. The resulting acceleration capability is compared in Figure 5.32 with the recommended criteria. It is apparent that the criterion is satisfied during a maximum accelerating transition and is exceeded during an unaccelerated transition.

5.3.3.3 Pitch Control

Utilization of the pitch controls will not result in coupling with the roll and yaw axes during transition. Therefore, "coupling" provisions are not required. Cyclic control will provide the major portion of the pitch control moment at the lower transition speeds. As speed is increased and the elevator

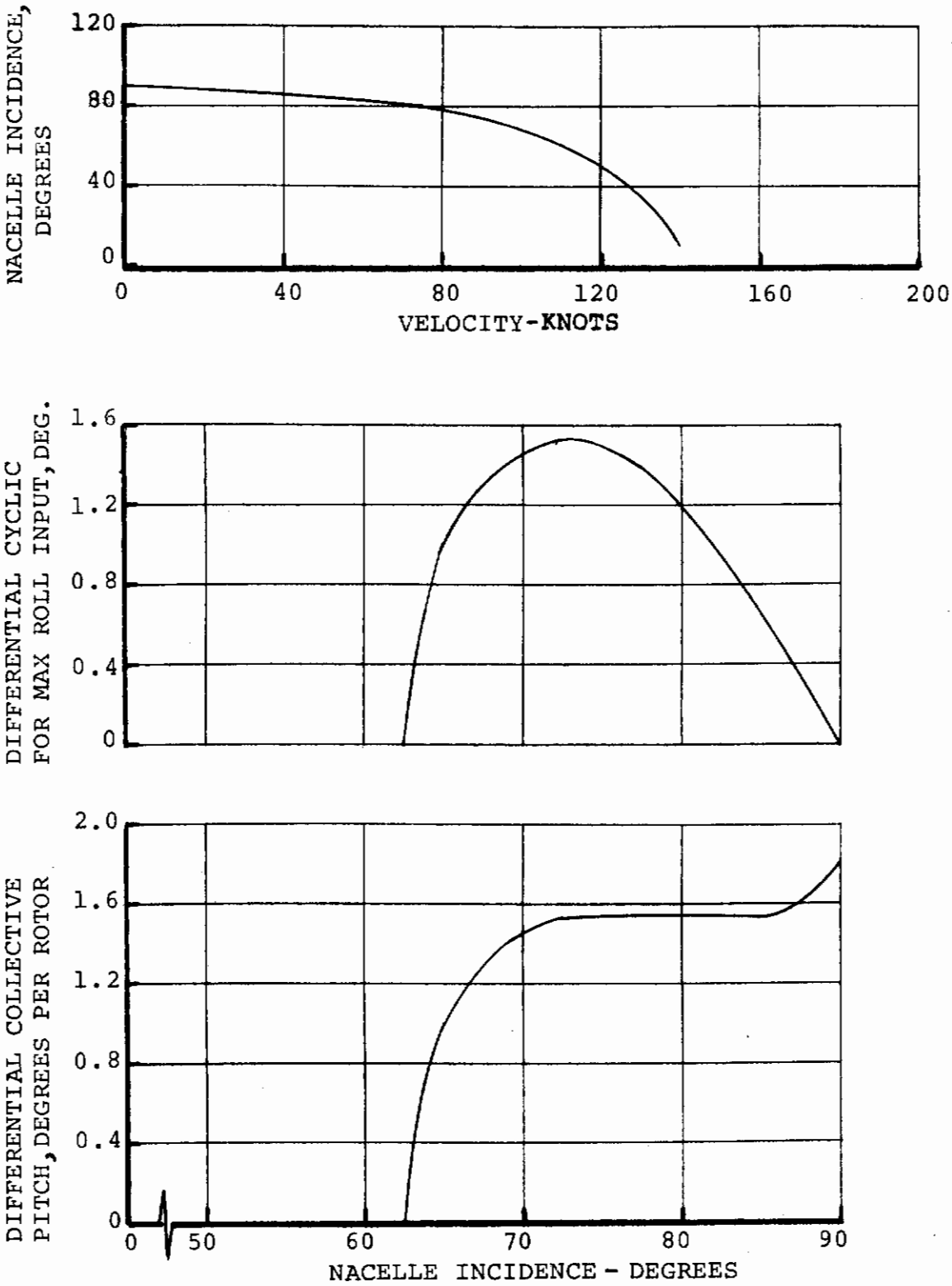

FIGURE 5.31: ROLL CONTROL PHASING THROUGH TRANSITION

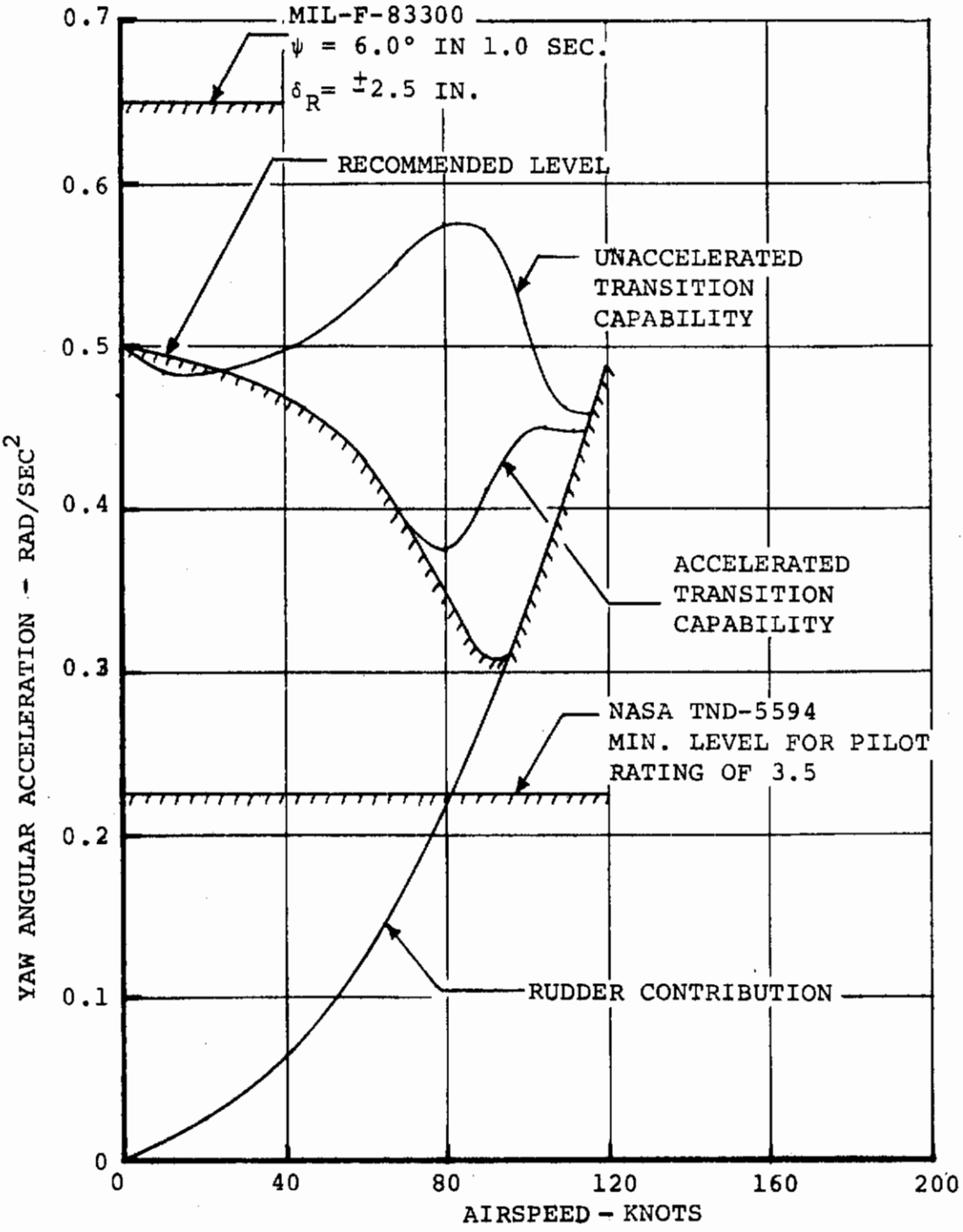

FIGURE 5.32: YAW CONTROL POWER THROUGH TRANSITION

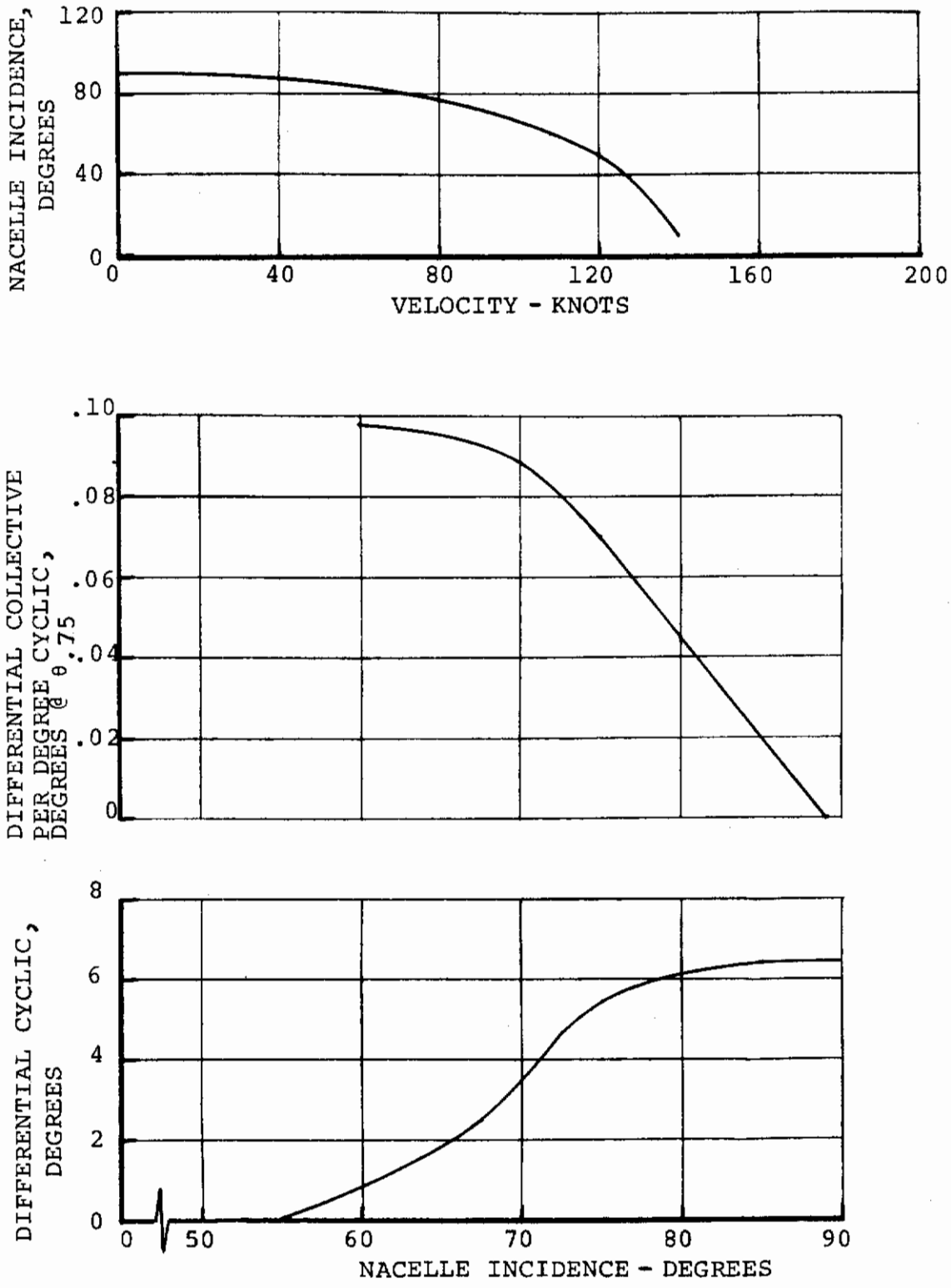

FIGURE 5.33: YAW CONTROL PHASING THROUGH TRANSITION

or unit horizontal tail becomes effective, the cyclic control will be phased out. Pitch control requirements are easily met as discussed in Section 5.2.3 for hover. The rotor controls are very powerful in hover and at low forward speeds and produce the required 0.6 rad/sec^2 acceleration. At the higher speeds the unit horizontal tail/elevator becomes effective and will provide pitch maneuver control to attain $C_{L_{MAX}}$ or limit load factor. The cyclic pitch control is phased out as the tail becomes effective (Figure 5.34).

5.3.4 Interactions

The interactions of the rotor on the airframe are shown in Figure 5.35 for a typical point in mid-transition. This effect represents an elimination of flow separation on the wing tip nacelles which were oversized for this model in order to accommodate the electric drive motors.

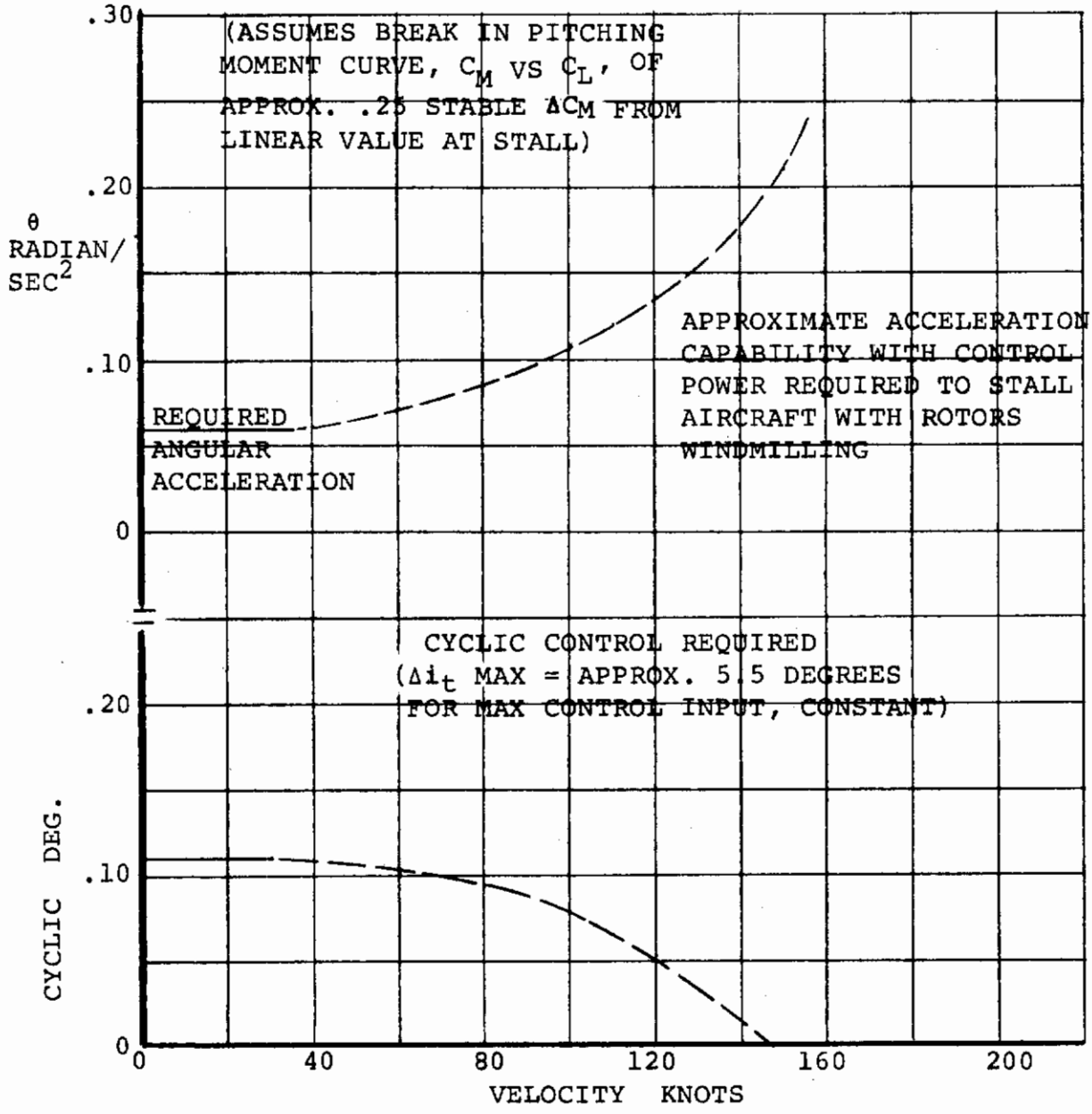

FIGURE 5.34: MODEL 222 LONGITUDINAL CONTROL CAPABILITY AND REQUIREMENT

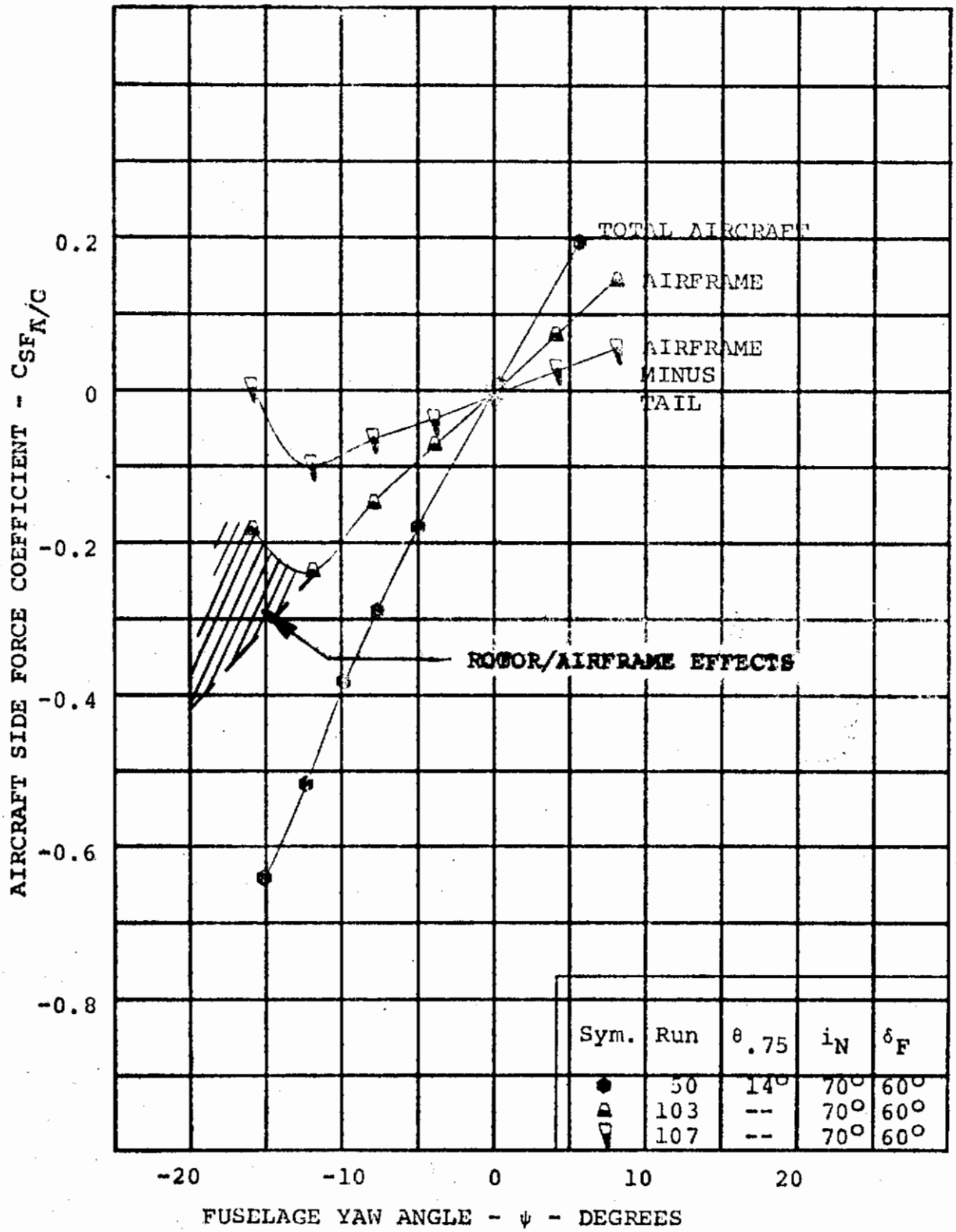

FIGURE 5.35: CONTRIBUTION OF PROP/ROTOR AND VERTICAL TAIL TO AIRCRAFT SIDE FORCE AT $V/V_T = 0.206$ WITH $i_N = 70^\circ$

5.4 CRUISE STABILITY - TILT ROTOR MODE

The cruise regime in the tilt rotor mode consists of the range of operation prior to start of the conversion process during which the nacelle incidence is zero and thrust for forward flight is derived from the rotors. In this flight regime the rotors have a major impact on the aircraft stability.

5.4.1 Rotor Derivatives - Stiff Inplane Rotor

Testing was performed, Reference 1.5, to obtain data in the cruise tilt rotor mode for correlation with predictions to verify the prediction techniques. The model rotors were not dynamically scaled and had a Lock Number of 17.28 and flapwise frequency of 1.66 in the cruise condition. Both of these parameters are significantly higher than the corresponding properties of the full scale rotor. In addition, the model rotors were much stiffer in-plane, $\omega_L/\Omega > 2.0$, than the full scale rotors. Therefore, the destabilizing influence of the rotors on the model are much greater than for the full scale rotors.

A summary of the rotor stability derivatives for the model is presented in Table 5.1 for the longitudinal and directional modes. It indicates the magnitude of the derivatives obtained directly from test. Also the longitudinal mode derivatives are shown with the wing lift equal to zero which is equivalent to an isolated rotor. As can be seen, the wing lift significantly affects the rotor pitching moment and sideforce derivatives. There is also a somewhat smaller effect on the normal force and yawing moment derivatives.

As substantiation for the derivatives in pitch with the wing lift removed, the comparable derivatives in yaw are shown directly below the pitch derivatives. The variation of lift with yaw angle is negligible and therefore, will not affect the derivative. The agreement in magnitude is very good and indicates that the wing lift effects are correct. The reversal in signs on the directional pitching moment and sideforce derivatives is a result of sign convention.

Figure 5.36 indicates the influence of wing lift on the rotor pitching moment coefficient. The prediction of pitching moment coefficient for the isolated rotor is shown and the derivative (slope) is in good agreement with the test data.

TABLE 5.1

CRUISE ROTOR STABILITY DERIVATIVES

LEFT ROTOR

LONGITUDINAL MODE

WING LIFT	$\partial C_{PM}/\partial\alpha$	$\partial C_N/\partial\alpha$	$\partial C_{YM}/\partial\alpha$	$\partial C_{SF}/\partial\alpha$
VARIABLE	0.00009	0.000168	-0.000118	0.000058
ZERO	0.00006	0.000143	-0.000106	0.000030

DIRECTIONAL MODE

WING LIFT	$\partial C_{YM}/\partial\psi$	$\partial C_{SF}/\partial\psi$	$\partial C_{PM}/\partial\psi$	$\partial C_N/\partial\psi$
CONSTANT	0.00006	0.000137	0.000107	-0.000031

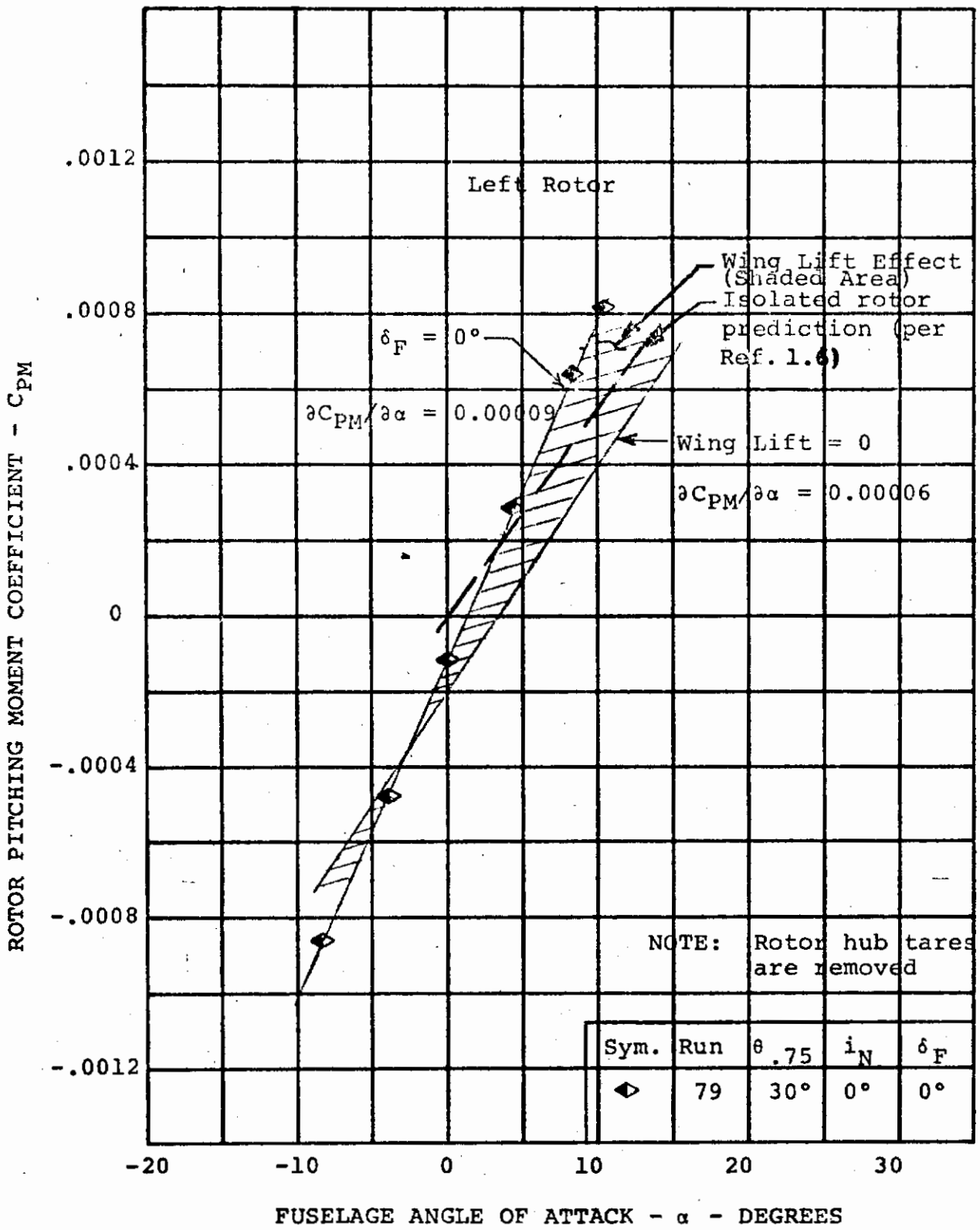

FIGURE 5.36. INFLUENCE OF WING LIFT ON ROTOR PITCHING MOMENT AT V/V_T = 0.386

Figure 5.37 shows the influence of wing lift on the rotor normal force coefficient. There is a substantially smaller effect on normal force than there is on pitching moment. The predicted normal force coefficient for the isolated rotor shows good agreement with test.

5.4.2 Rotor Derivatives - Soft In-Plane Rotor

The effects of in-plane and out-of-plane rotor stiffnesses on the rotor contributions to aircraft stability were discussed in Section 5.1.2 of this report. Wind tunnel test data were obtained in the tests on the 1/9 scale Model 213 and the results of these tests are reported in Reference 1.6. Although the tests in Reference 1.6 were in the windmill configuration the stability derivatives are directly applicable because the difference in collective pitch, the primary variable, is no more than 2-3 degrees.

Figures 5.38 and 5.39 illustrate the effect of variation of in-plane frequencies, $\frac{\omega_{LAG}}{\Omega}$, on the rotor normal force and pitching moment coefficients at constant angle of attack. The in-plane frequency of the model rotors is 1.0 at 600 rpm and is lower at the higher rpm. The full-scale rotor in-plane frequency will be approximately 0.75.

Figure 5.39 presents the rotor pitching moment coefficient variation with rpm. There is a peak in the coefficient at 200 rpm; it rapidly decreases to a minimum at approximately 600 rpm then increases sharply to approximately 850 rpm and then it levels off. Nondimensionalizing by rotor tip speed causes the apparent peak in the coefficient at 200 rpm when there is an actual peak between 300 and 400 rpm in the pitching moment. This peak occurs in the same rpm region as the wing vertical bending natural frequency. The minimum shown at approximately 600 rpm appears to be the result of passing through the 1/rev first mode crossover which is the lag mode for this rotor. This produces a change in rotor flapping resulting from lag/flap coupling.

Normal force coefficient variation with rpm, presented in Figure 5.38, shows a rapid decrease with increasing rpm up to approximately 600. The slope becomes almost zero and then drops off rapidly as the rpm is increased to 950. The plateau illustrates the effect of passing through the 1/rev lag frequency crossover.

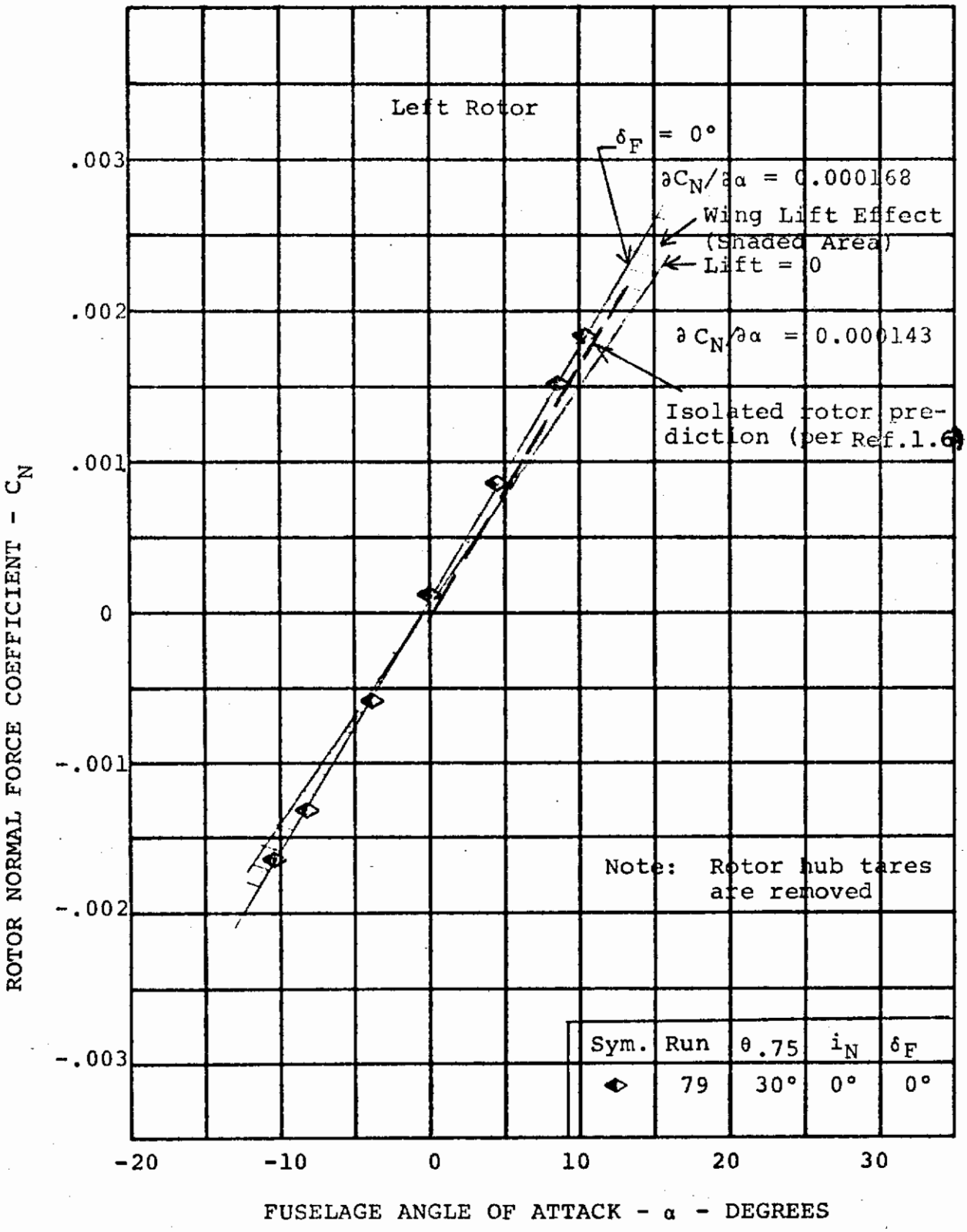

FIGURE 5.37. INFLUENCE OF WING LIFT ON ROTOR NORMAL FORCE AT V/V_T = 0.386

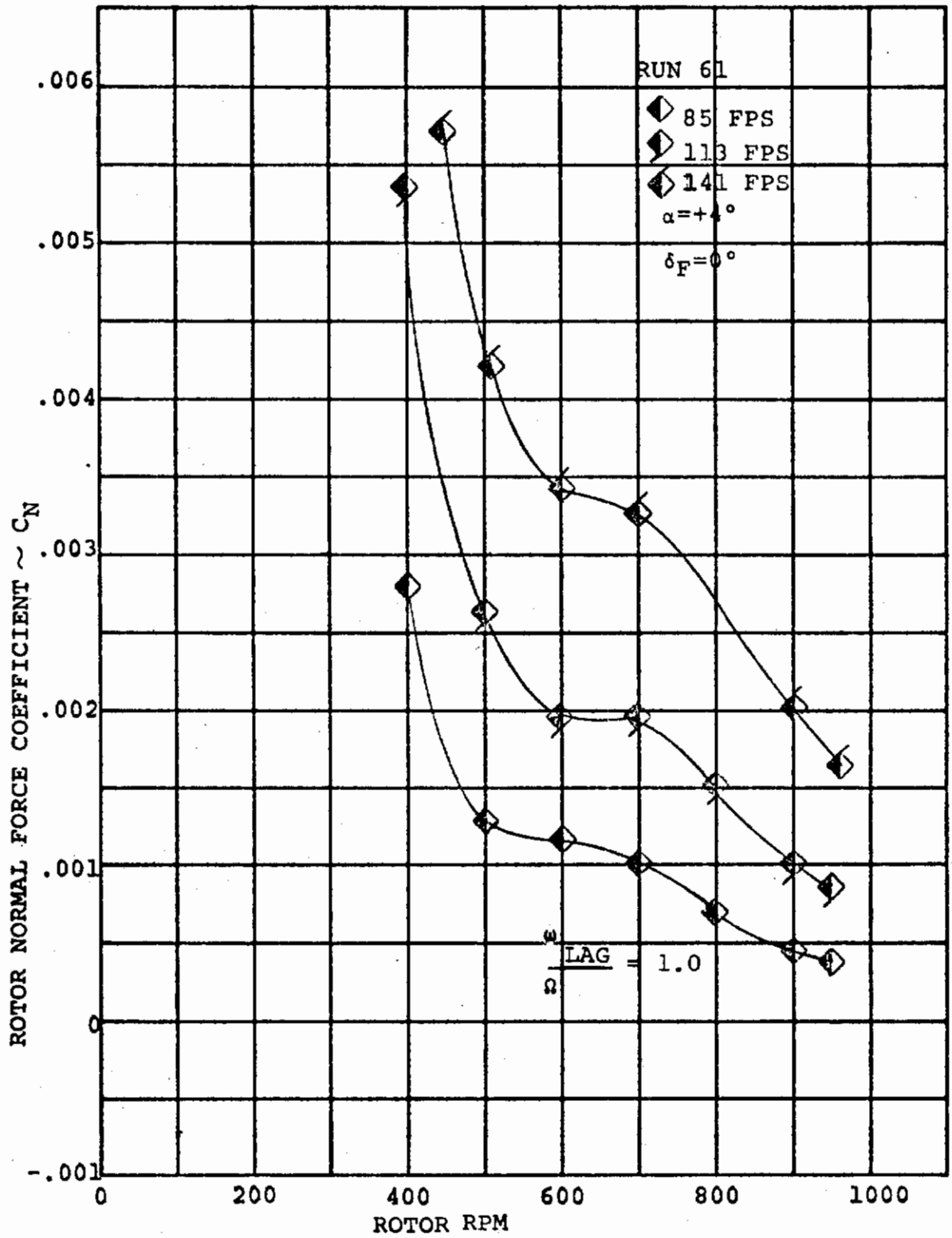

FIGURE 5.38. ROTOR NORMAL FORCE/RPM VARIATION
FUSELAGE ATTITUDE = +4° δ_F=0°
(STEADY WINDMILLING)

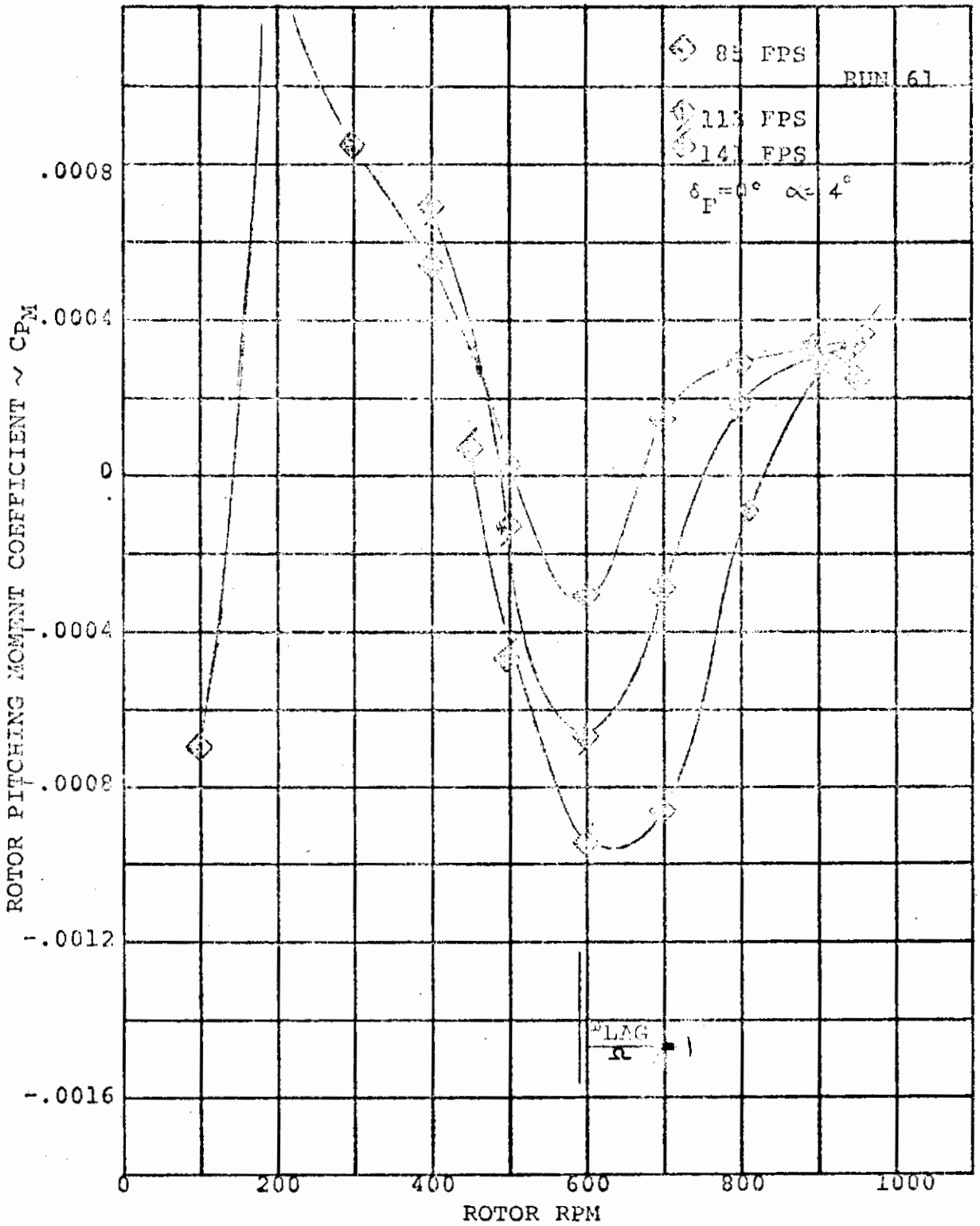

FIGURE 5.39 ROTOR PITCHING MOMENT/RPM VARIATION
FUSELAGE ATTITUDE = 4° δ_F =0°
(STEADY WINDMILLING)

Figures 5.40 and 5.41 show the variation in rotor pitching moment coefficient as a function of nacelle angle-of-attack at constant rpm. Note that at 600 rpm the pitching moment coefficient is highly stable while at 950 rpm the coefficient is unstable. It is significant to note that the coefficient is stable at 600 rpm when previous discussions of the stiff-in-plane rotor characteristics have indicated a highly destabilizing rotor pitching moment contribution.

Figure 5.42 illustrates the variation of the rotor pitching moment derivative with rpm. Again, it shows that the derivative is most stabilizing at a lag frequency of approximately 1.0 corresponding to 600 rpm. The rotor normal force derivative variation with rpm is presented in Figure 5.43. The variation with rpm illustrates a sharp drop to approximately 500 rpm, a plateau to 700 rpm and further decrease at the higher rpm's.

Figure 5.44 shows that the rotor yawing moment derivative with angle-of-attack reaches a maximum negative value at approximately 700 rpm with a relatively rapid change at lower or higher rpm.

The rotor side force variation reaches a maximum negative value at approximately 600 rpm and is near zero at 800-900 rpm (Figure 5.45).

Figures 5.46 and 5.47 show the effect of wing lift on rotor pitching moment coefficients at 600 and 950 rpm respectively. These figures indicate that increasing lift produces a slight negative increment in pitching moment coefficient at 600 rpm (stable variation) but produces a positive increment in pitching moment coefficient at 950 rpm (unstable variation).

Comparisons of the rotor pitching moment derivatives, rotor normal force derivatives, yawing moment derivatives and side force derivatives are presented in Figures 5.48, 5.49, 5.50 and 5.51, respectively. There is one unique trend for all of the derivatives for all rpm and forward speeds tested. This trend indicates a ratio of test derivative to derivative with circulation effects removed of 0.93.

A summary of the rotor derivatives without circulation effects is presented in Figures 5.52 through 5.55 for pitching moment, normal force, yawing moment, and side force as influenced by rotor rpm. Imposed on these summary curves

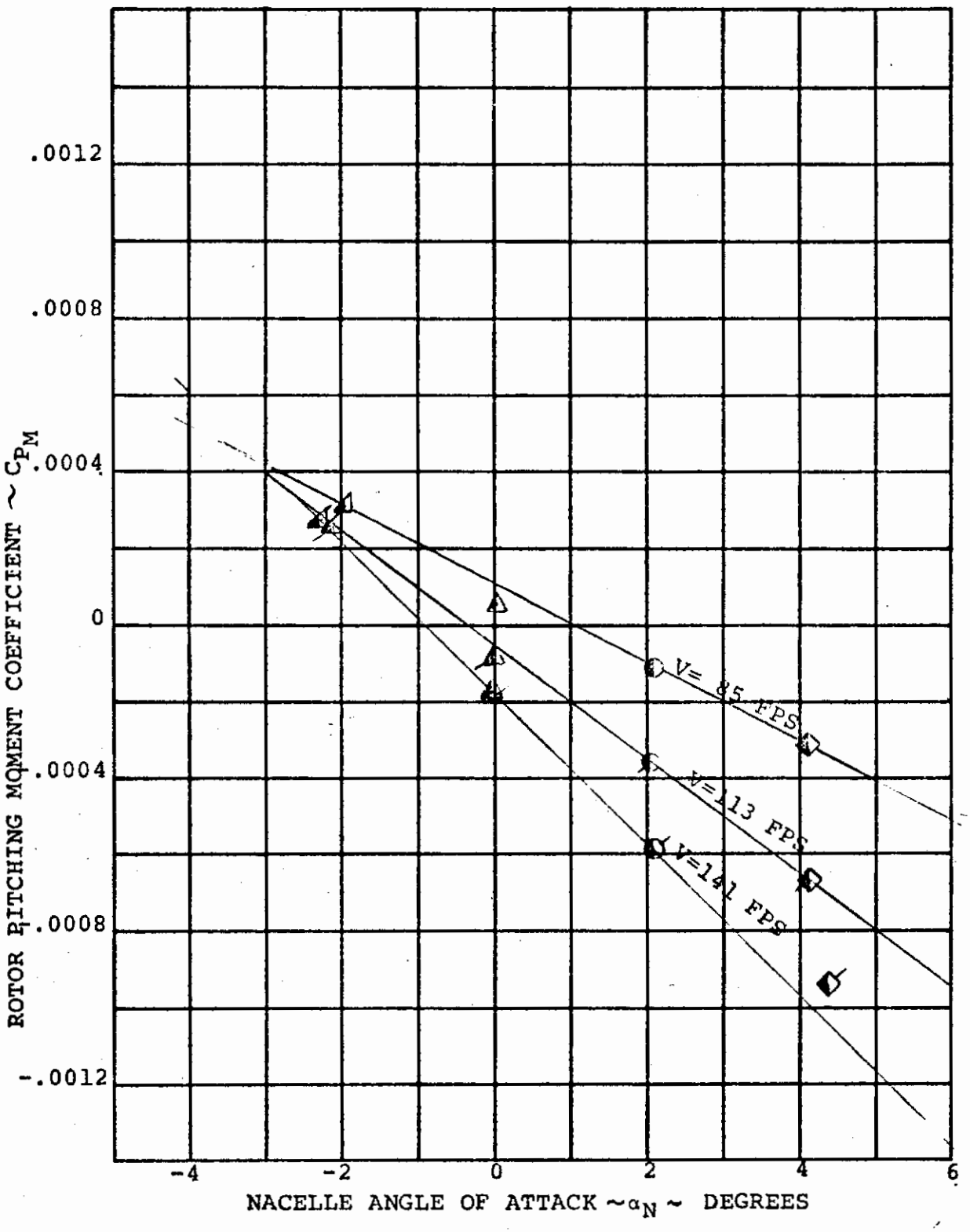

FIGURE 5.40. ROTOR PITCHING MOMENT/NACELLE ANGLE OF ATTACK FOR ROTOR RPM = 600 $\delta_F = 0°$

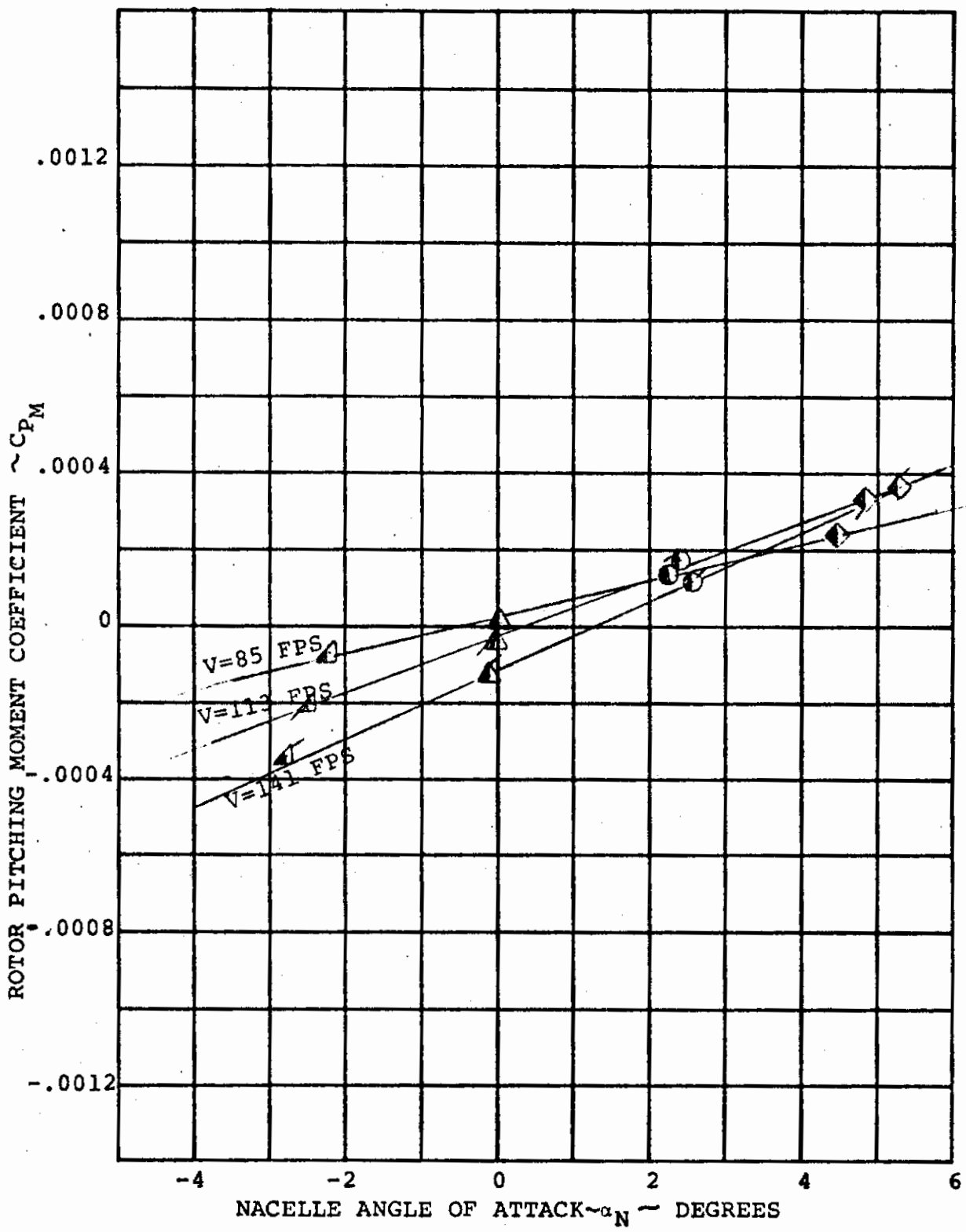

FIGURE 5.41. ROTOR PITCHING MOMENT/NACELLE ANGLE OF ATTACK FOR ROTOR RPM = 950 $\delta_F = 0°$

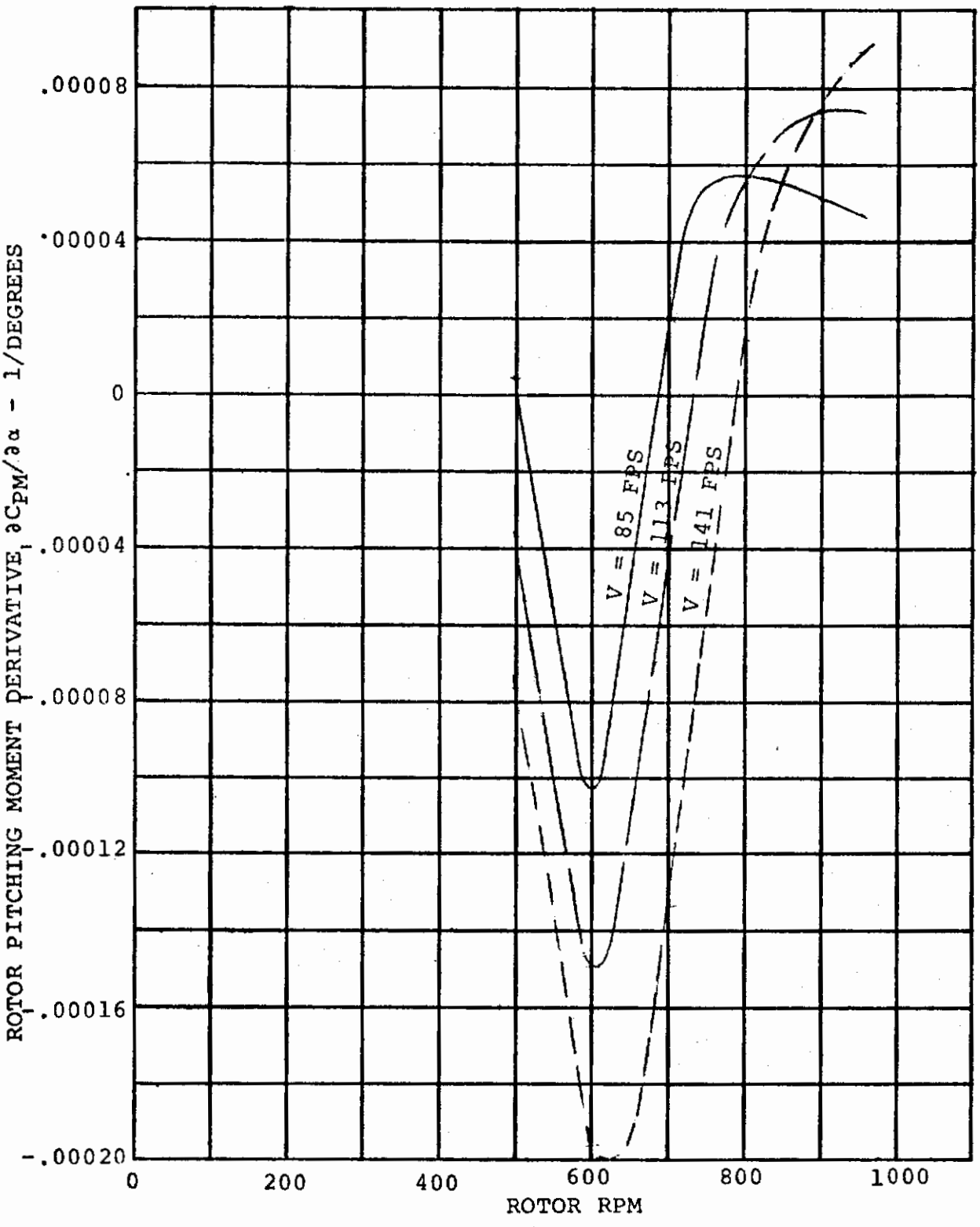

FIGURE 5.42 ROTOR PITCHING MOMENT DERIVATIVE VARIATION WITH ROTOR RPM, $\delta F = 0°$

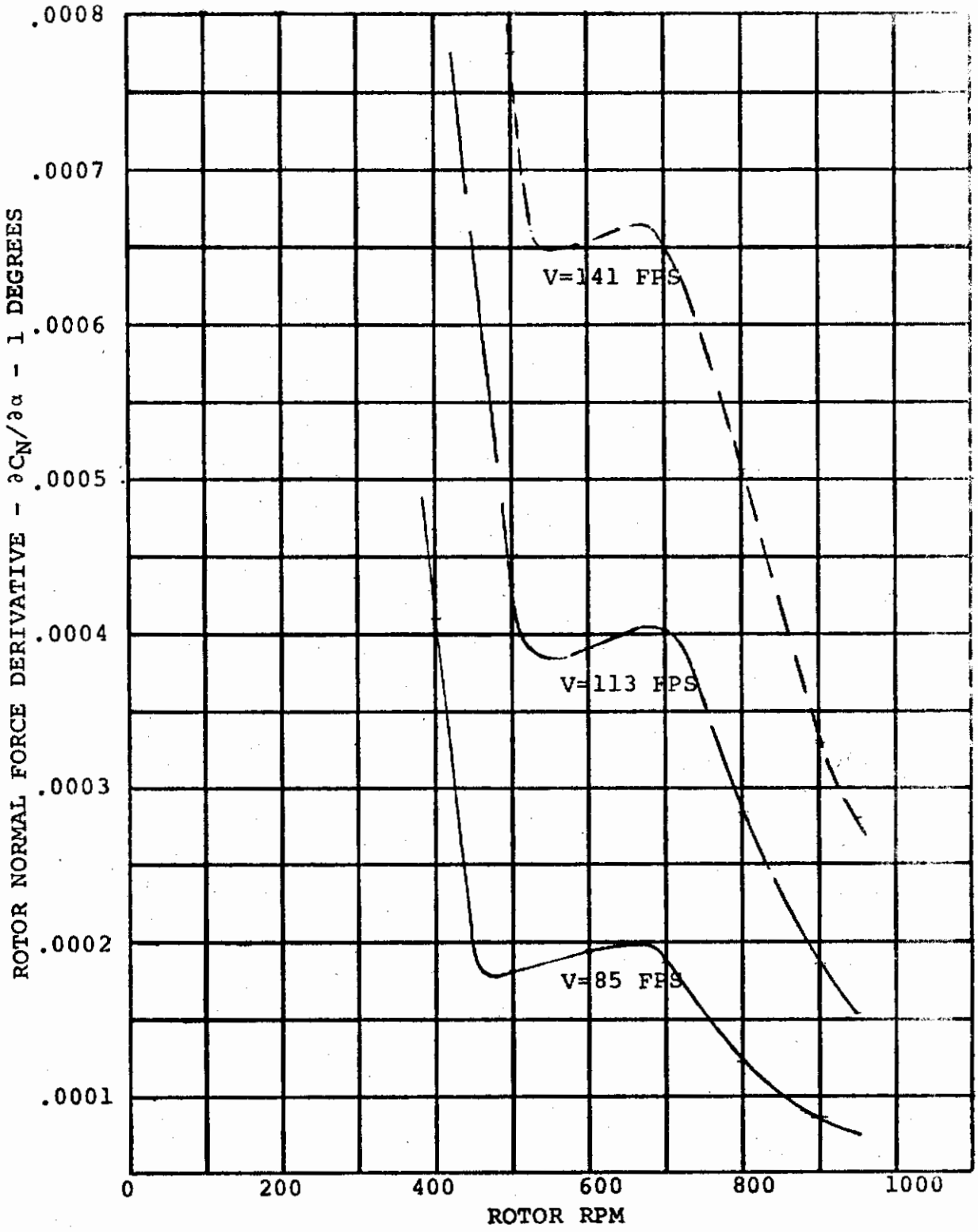

FIGURE 5.43. ROTOR NORMAL FORCE DERIVATIVE VARIATION WITH ROTOR RPM $\delta_F = 0°$

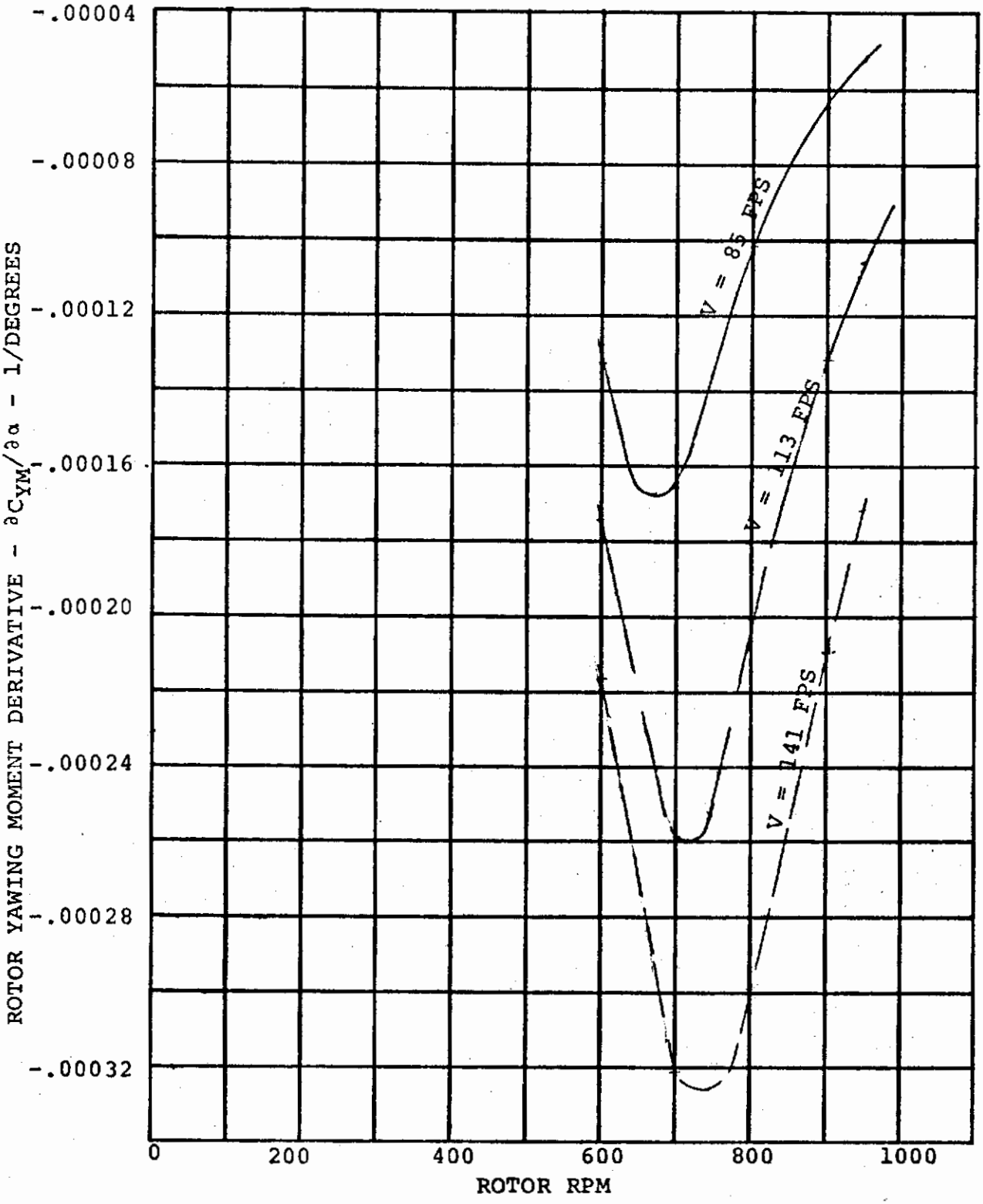

FIGURE 5.44. ROTOR YAWING MOMENT DERIVATIVE VARIATION WITH ROTOR RPM, δ_F = 0.°

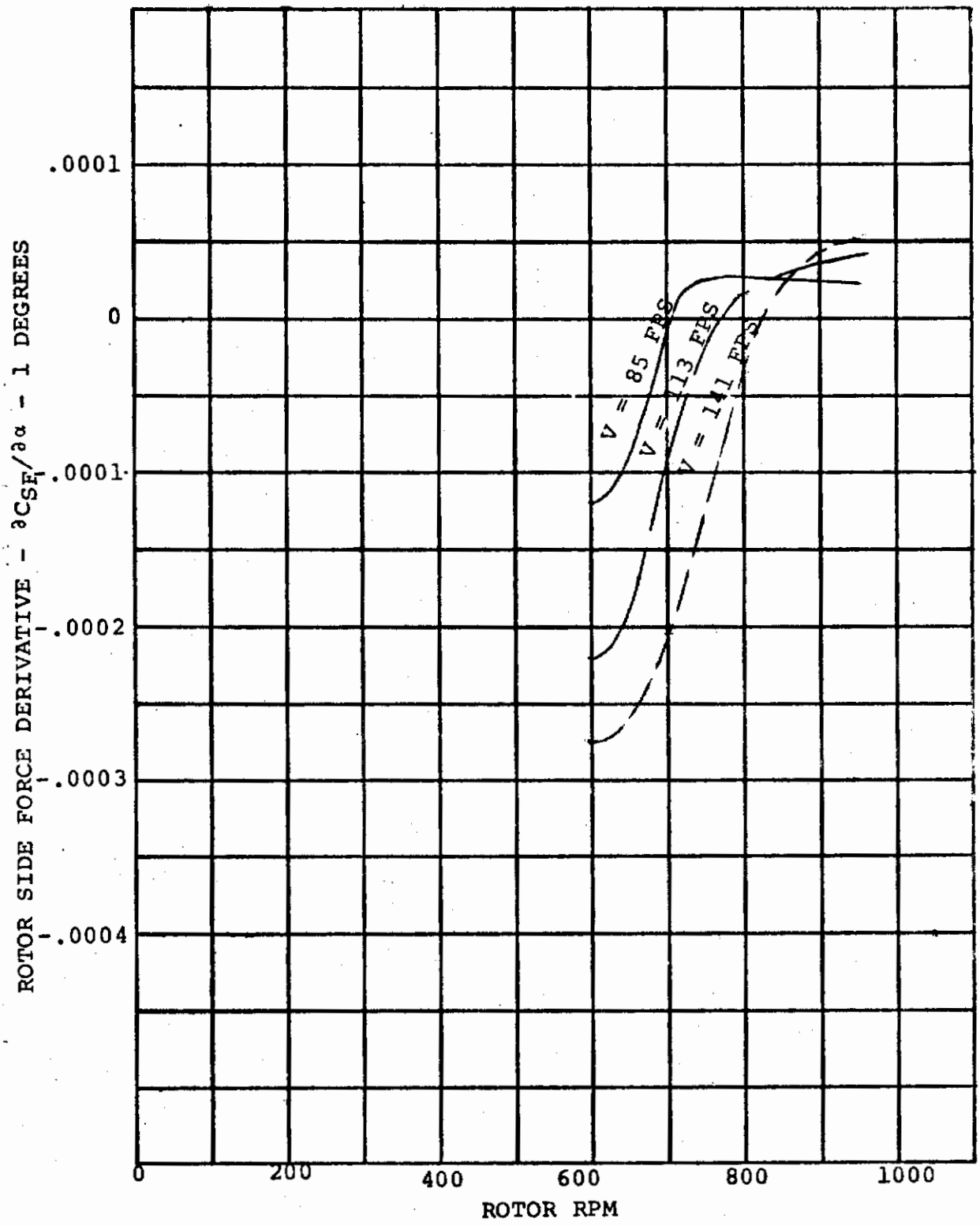

FIGURE 5.45 ROTOR SIDE FORCE DERIVATIVE VARIATION WITH ROTOR RPM, $\delta_F = 0°$

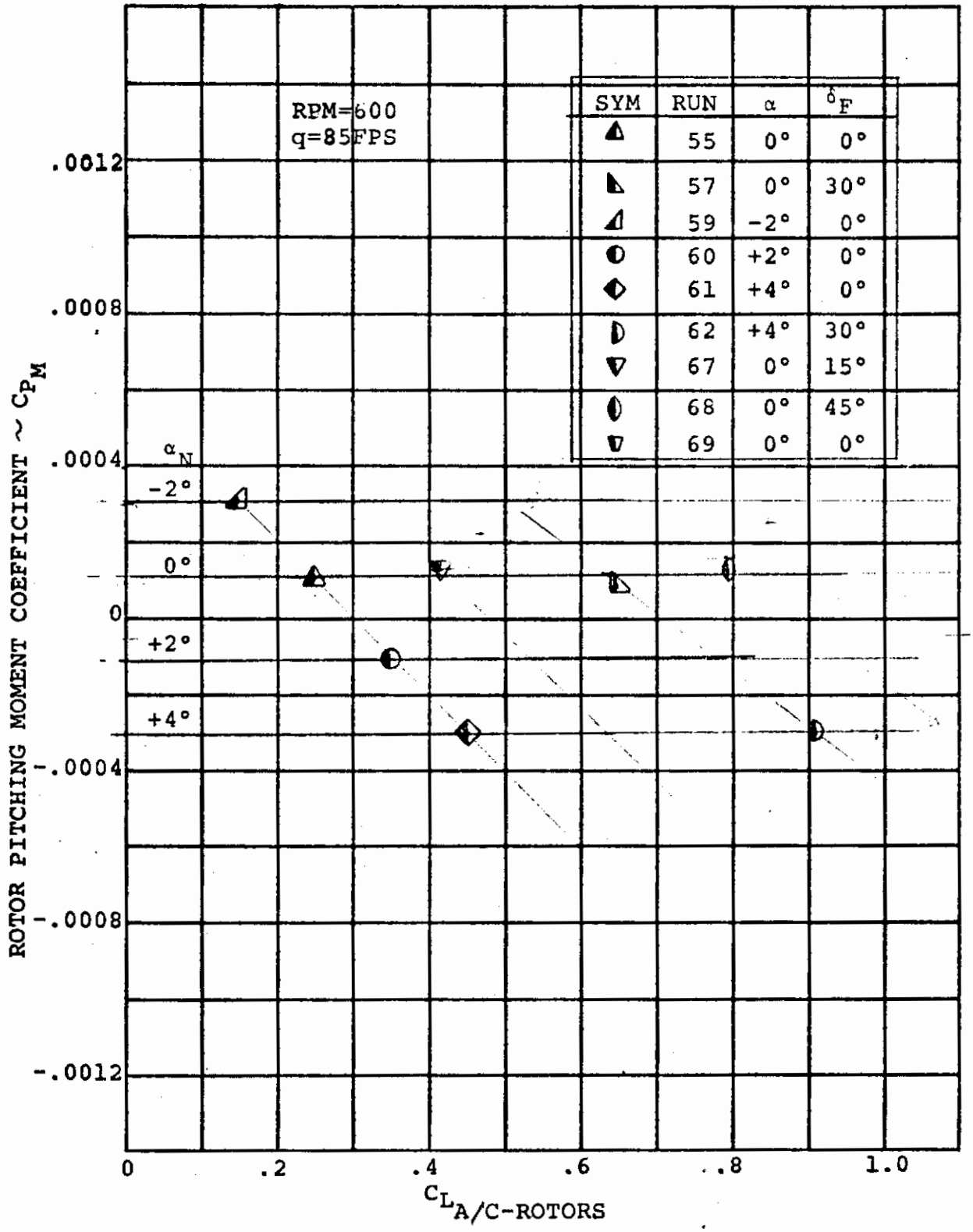

FIGURE 5.46. EFFECT OF WING LIFT ON ROTOR PITCHING MOMENT (V = 85 FPS, RPM=600)

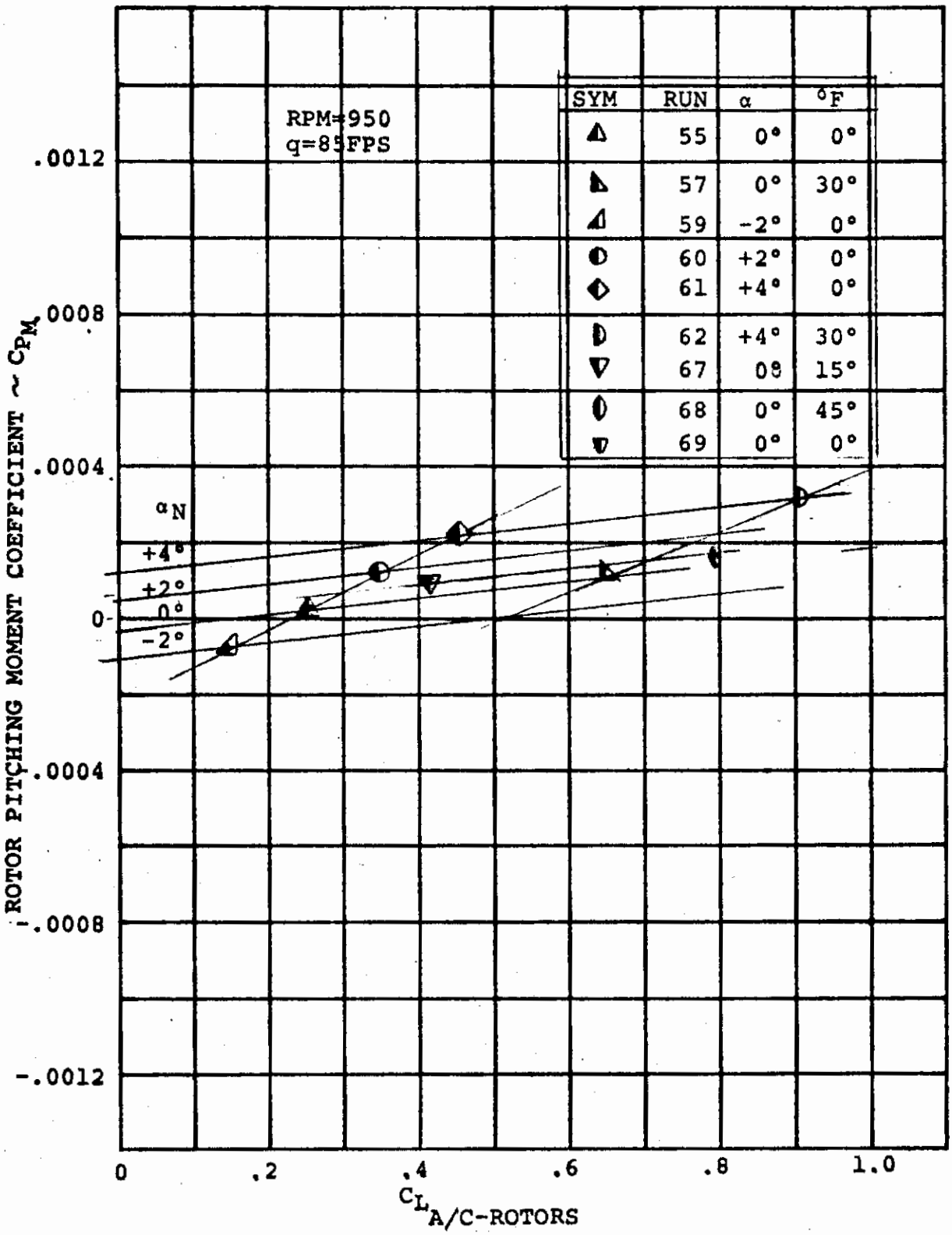

FIGURE 5.47. EFFECT OF WING LIFT ON ROTOR PITCHING MOMENT (V = 85 FPS, RPM = 950)

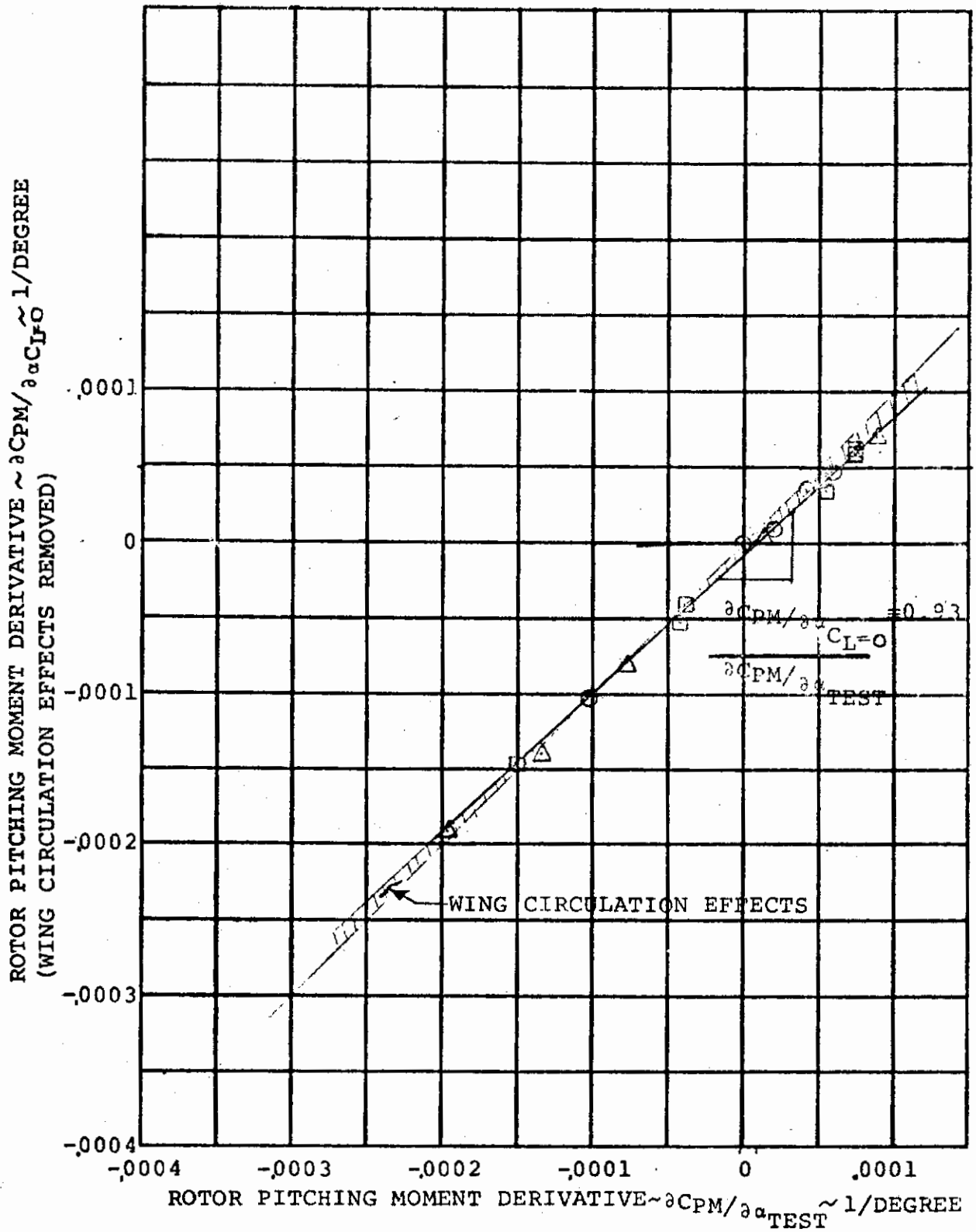

FIGURE 5.48. COMPARISON OF ROTOR PITCHING MOMENT DERIVATIVE WITH AND WITHOUT WING CIRCULATION EFFECTS
$\delta_F = 0°$

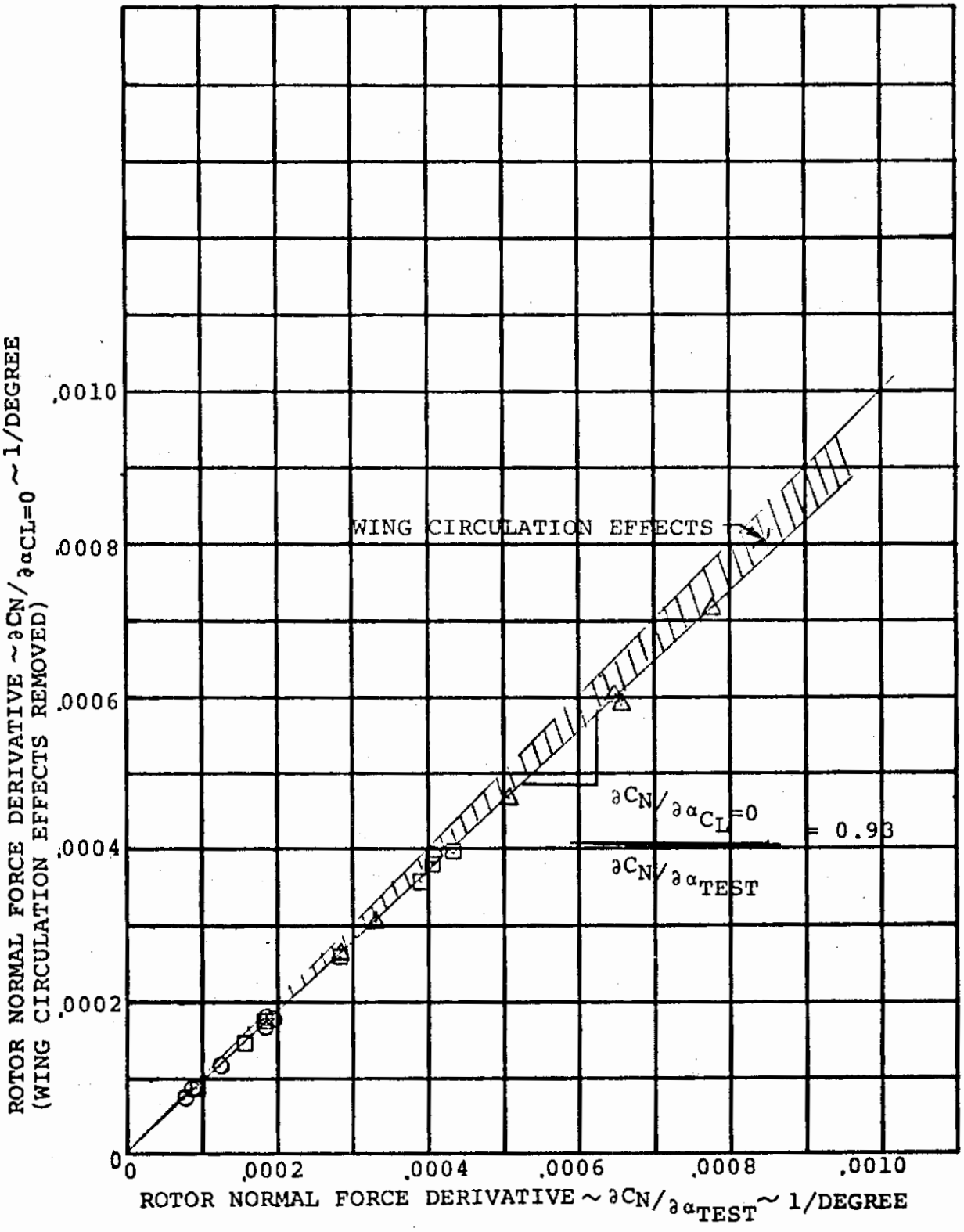

FIGURE 5.49. COMPARISON OF ROTOR NORMAL FORCE DERIVATIVE WITH AND WITHOUT WING CIRCULATION EFFECTS

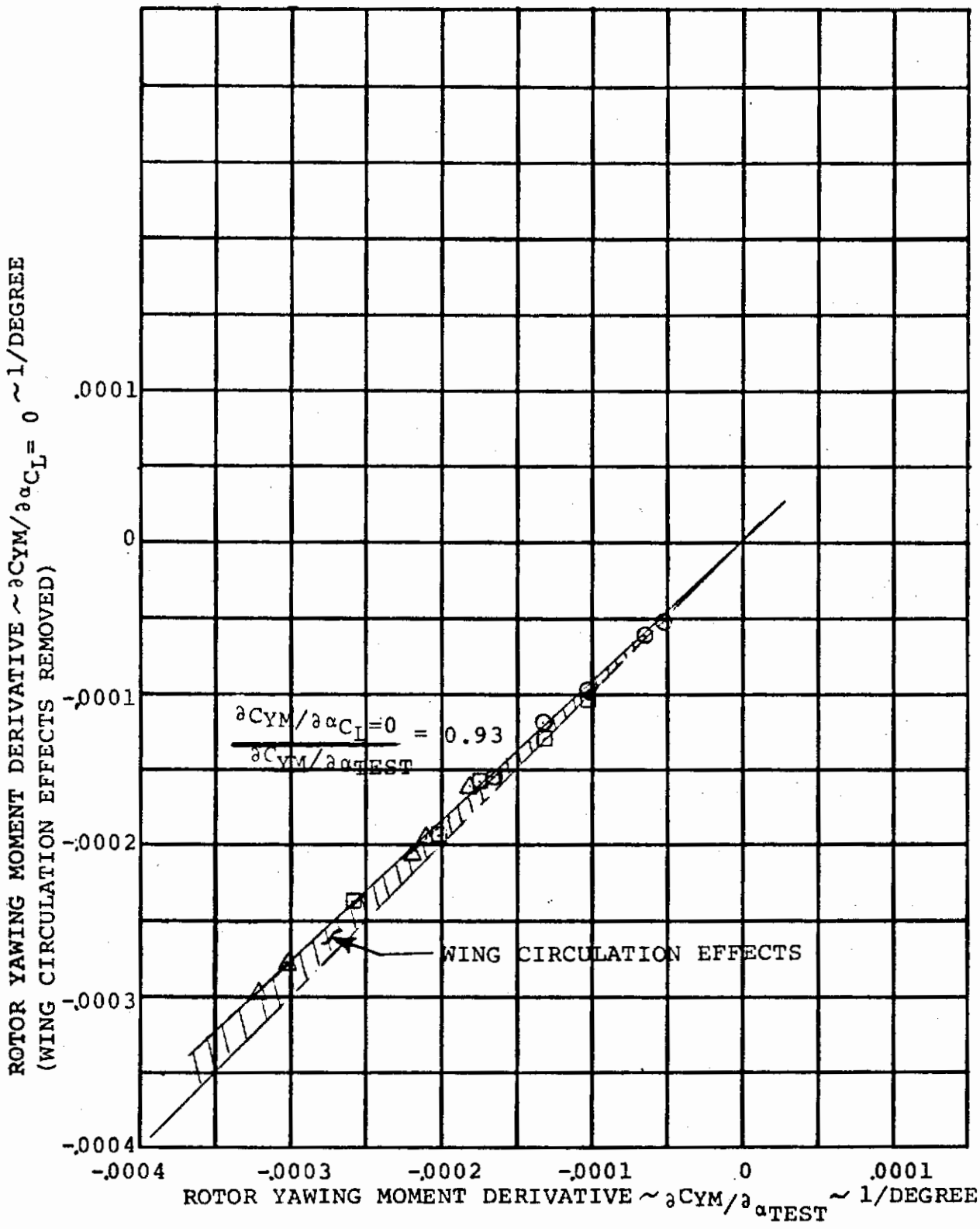

FIGURE 5.50. COMPARISON OF ROTOR YAWING MOMENT DERIVATIVE WITH AND WITHOUT WING CIRCULATION EFFECTS

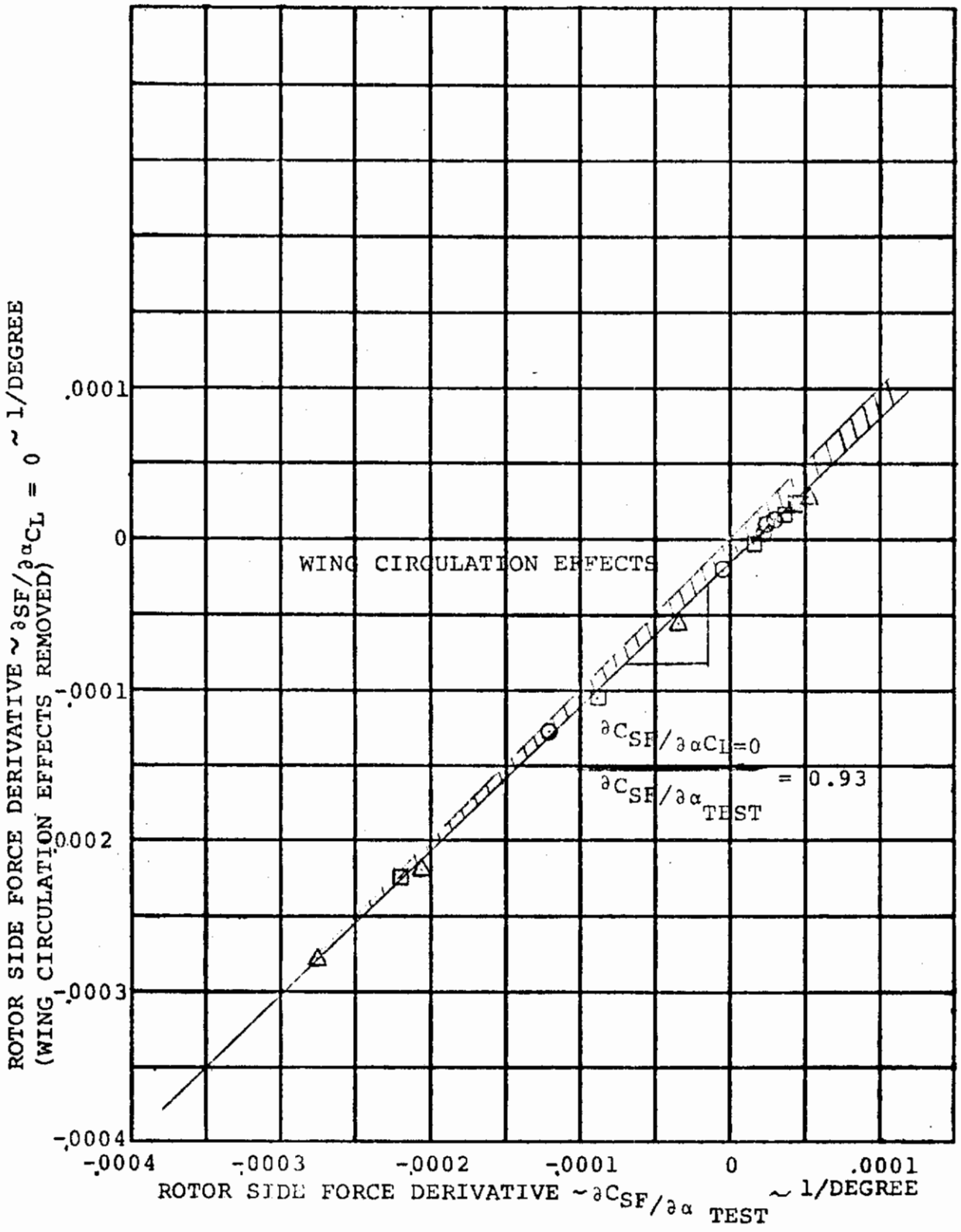

FIGURE 5.51. COMPARISON OF ROTOR SIDE FORCE DERIVATIVES WITH AND WITHOUT WING CIRCULATION EFFECTS

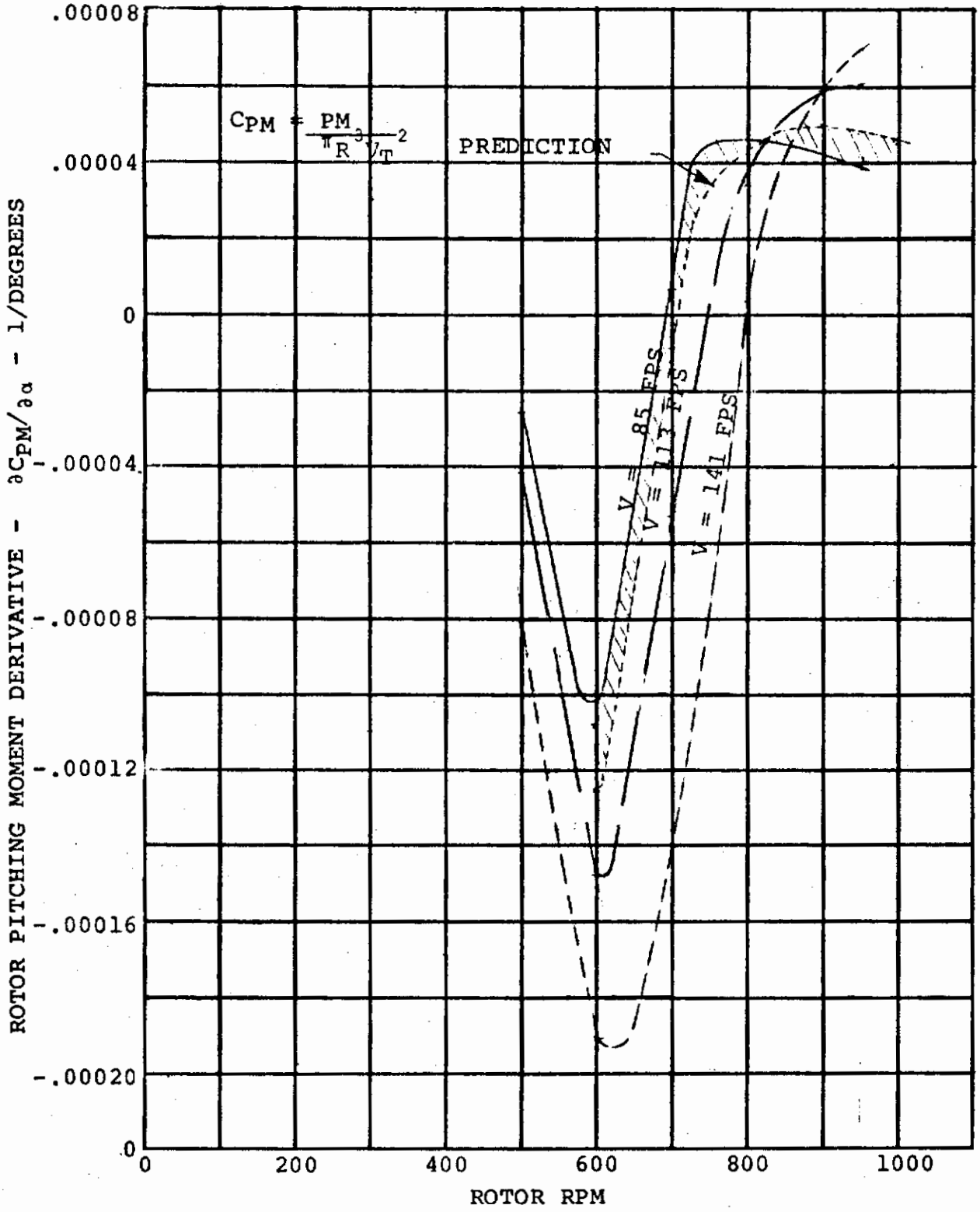

FIGURE 5.52. ROTOR PITCHING MOMENT DERIVATIVE VARIATION WITH ROTOR RPM (WING CIRCULATION EFFECTS REMOVED)

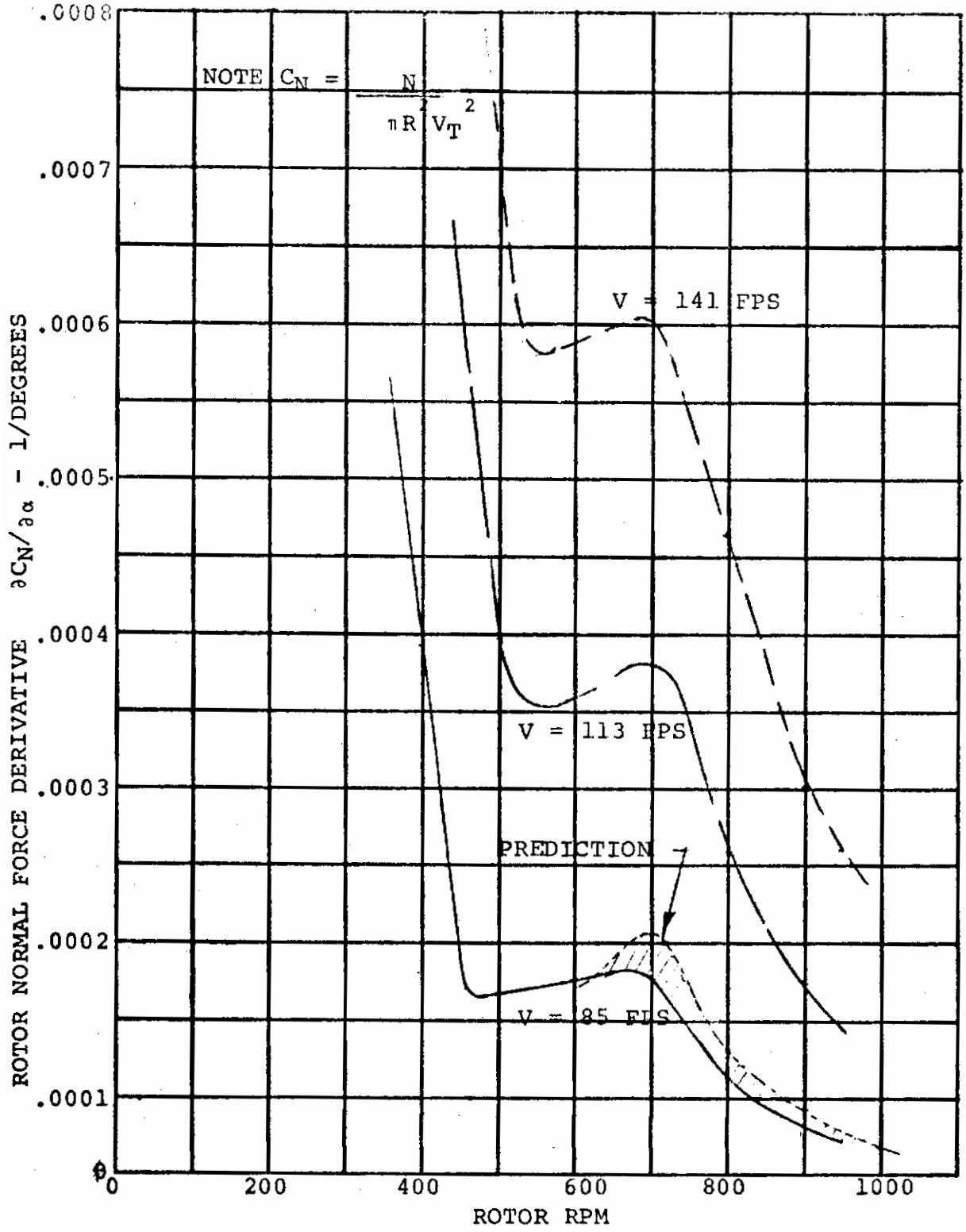

FIGURE 5.53. ROTOR NORMAL FORCE DERIVATIVE VARIATION WITH ROTOR RPM (WING CIRCULATION EFFECTS REMOVED)

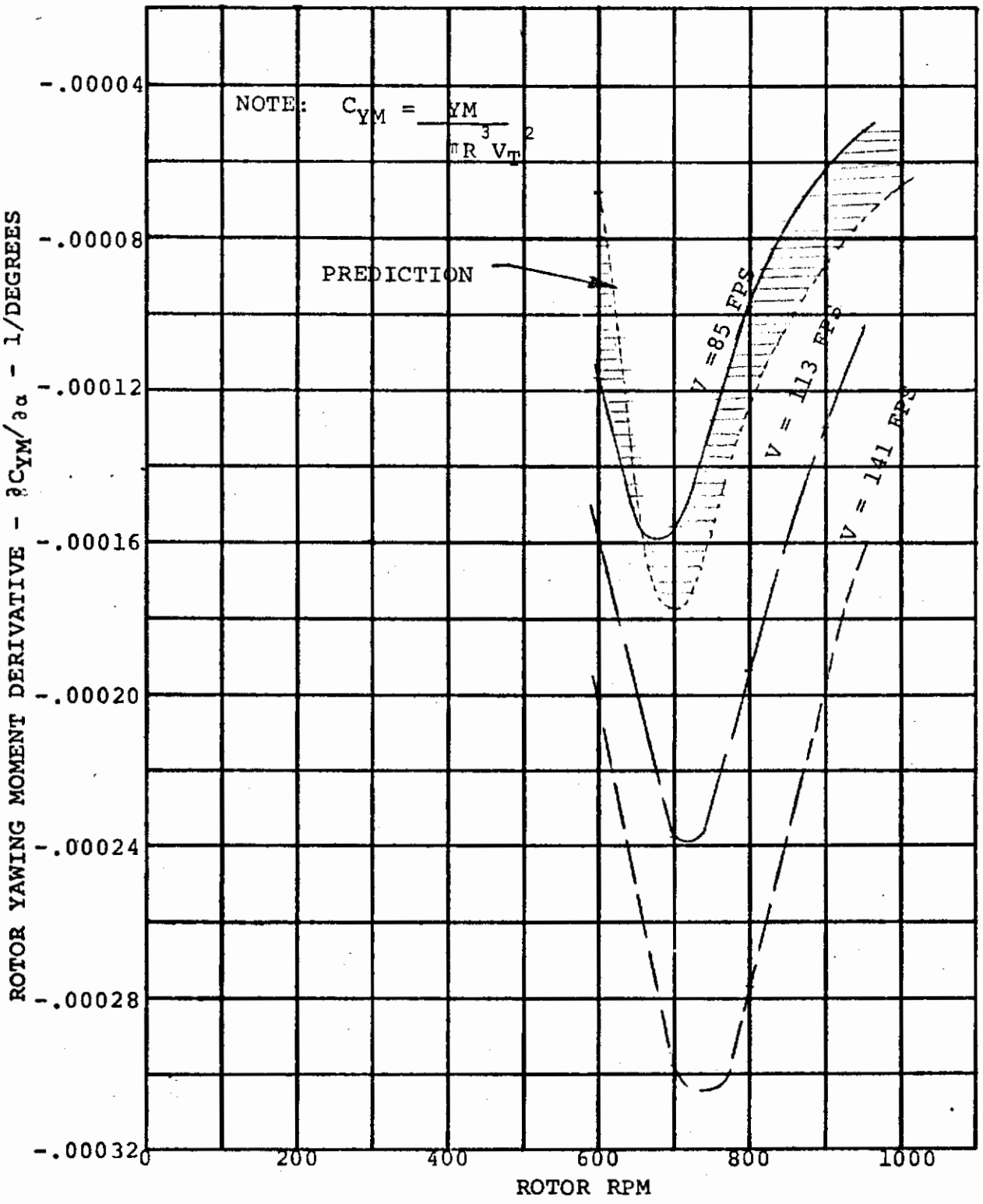

FIGURE 5.54. ROTOR YAWING MOMENT DERIVATIVE VARIATION WITH ROTOR RPM (WING CIRCULATION EFFECTS REMOVED)

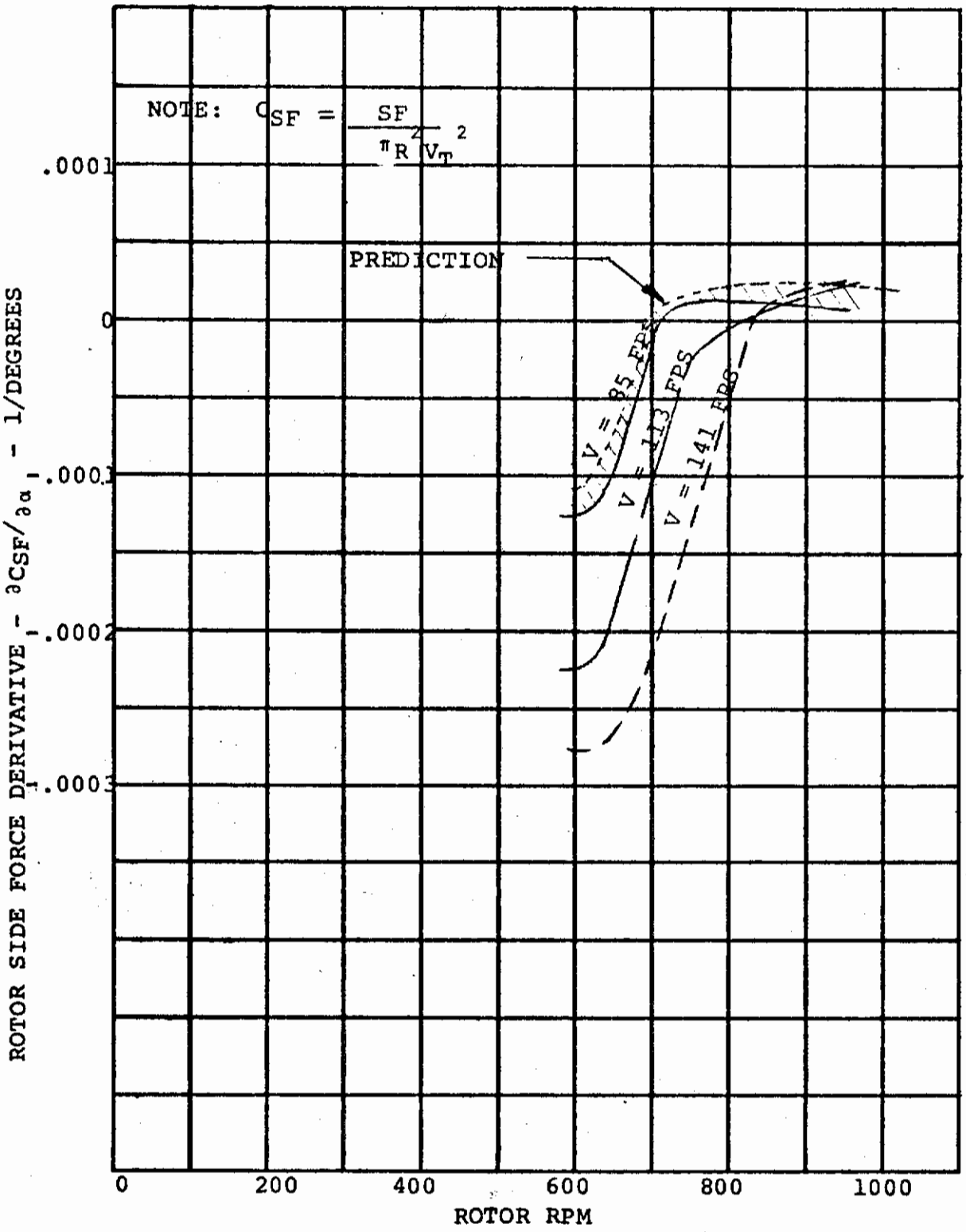

FIGURE 5.55. ROTOR SIDE FORCE DERIVATIVE VARIATION WITH ROTOR SIDE FORCE (WING CIRCULATION EFFECTS REMOVED)

is a prediction (based on Reference 3.3) of the derivatives by an analysis that accounts for the various mode shapes. The agreement is good and adequately accounts for the effects of the 1/rev first mode (lag) frequency crossover.

5.4.3 Rotor/Airframe Interference Effects

Another potential source of disturbance to the rotor flow field is the effect of one rotor on the other when in the cruise mode. The effect of this rotor/rotor interference on rotor pitching moment coefficient is illustrated on Figure 5.56 and on rotor normal force coefficient on Figure 5.57. These figures indicate no change in the derivatives and negligible change in the magnitudes of the coefficients.

The evaluation of the aircraft stability characteristics is significantly affected by the rotor forces and moments. Any influence of the rotor slipstream on the airframe is not immediately obvious. To examine the rotor effecton the horizontal and vertical tail, the contribution to aircraft stability is presented in Figures 5.58 and 5.59 for the rotors on and rotors off configuration. This indicates there is negligible effect of the rotor slipstream on the tail.

5.4.4 Total Aircraft Stability

Predictions of the airframe, the prop/rotor and tail contributions to total aircraft pitching moment characteristics were made and are compared to the test data in Figure 5.60. The airframe components were predicted by the methods defined in DATCOM, Reference 4.6. Airframe-minus-tail pitching moment prediction of $\partial C_{PM}/\partial\alpha = 0.011$ is lower than that obtained from test, $\partial C_{PM}/\partial\alpha = 0.018$. The contribution of the horizontal tail to total aircraft stability ($\partial C_{PM}/\partial\alpha$) is-0.052 per degree as predicted by the methods defined by DATCOM. Adding this increment to the airframe-minus-tail test data results in excellent agreement with the airframe test data. This indicates that the tail characteristics as well as the wing downwash are correctly accounted for. The rotor contribution was defined by the isolated rotor characteristics as discussed in Reference 4.7 increased by the empirical lift effects induced by the wing, as shown in Reference 1.5. This results in a rotor contribution of 0.043 per degree and when adding this to the airframe test data indicates good agreement with the total model aircraft data.

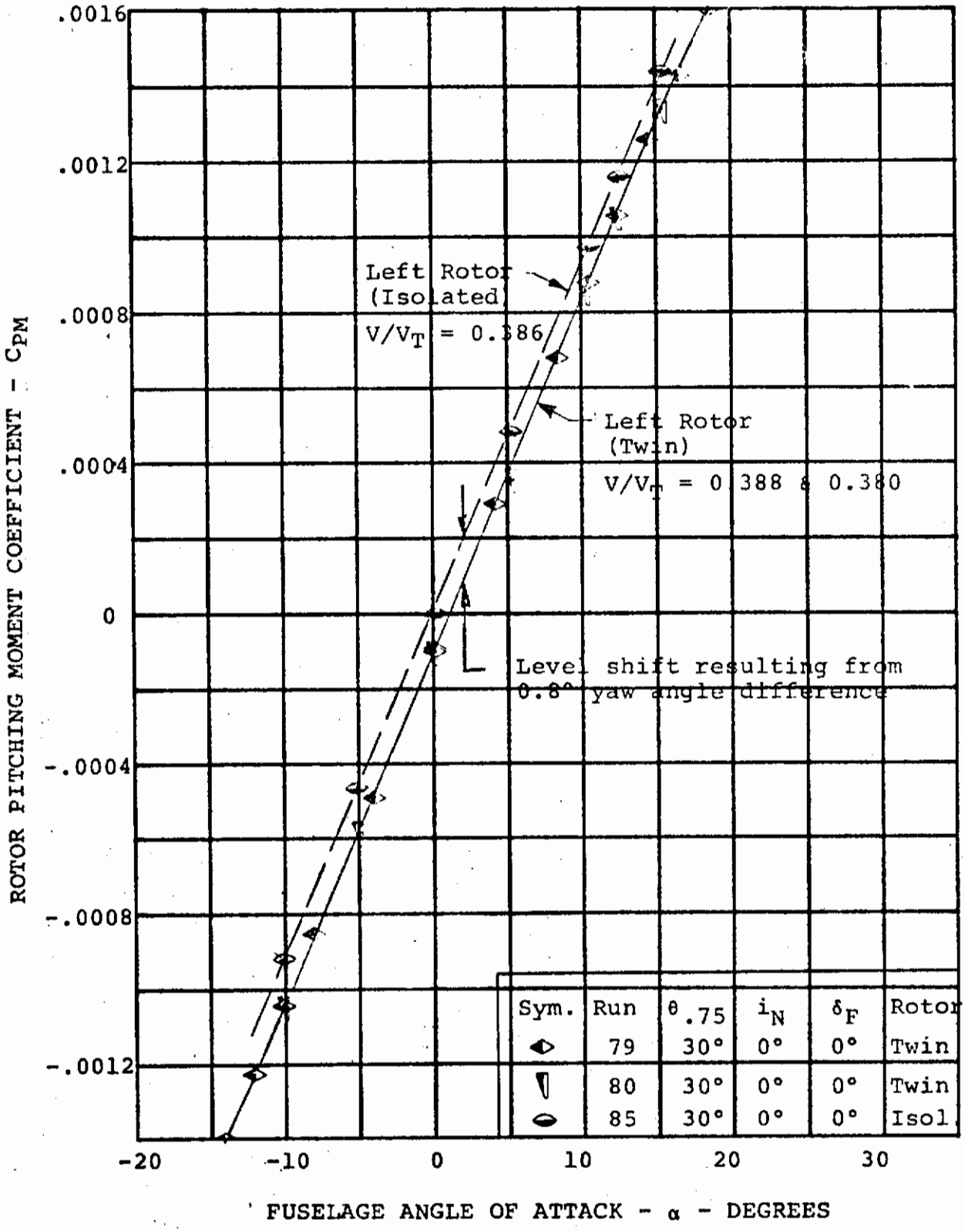

FIGURE 5.56. ROTOR/ROTOR INTERFERENCE EFFECTS ON CRUISE ROTOR CHARACTERISTICS, V/V_T = 0.386

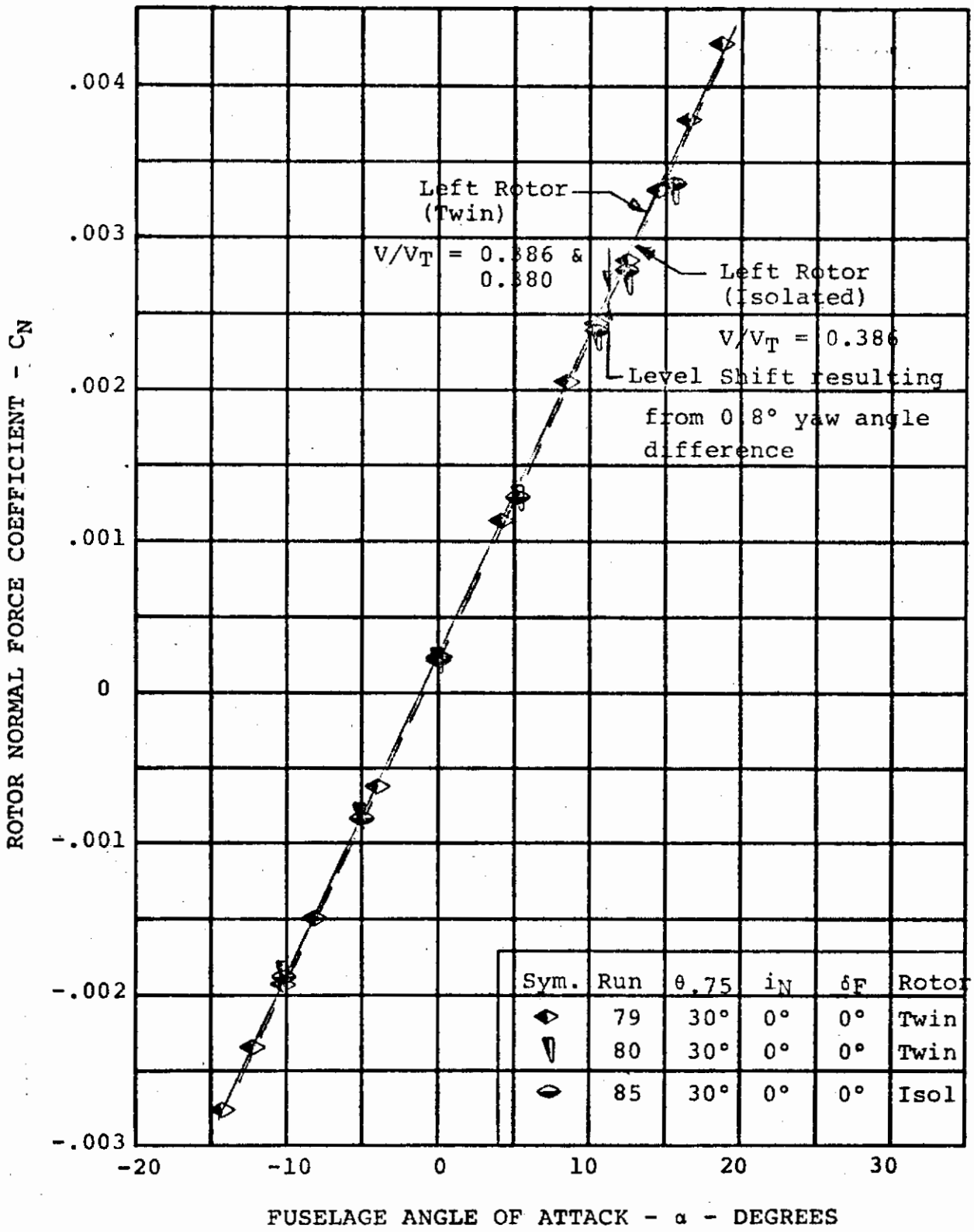

FIGURE 5.57. ROTOR/ROTOR INTERFERENCE EFFECTS ON CRUISE ROTOR CHARACTERISTICS, V/V_T = 0.386

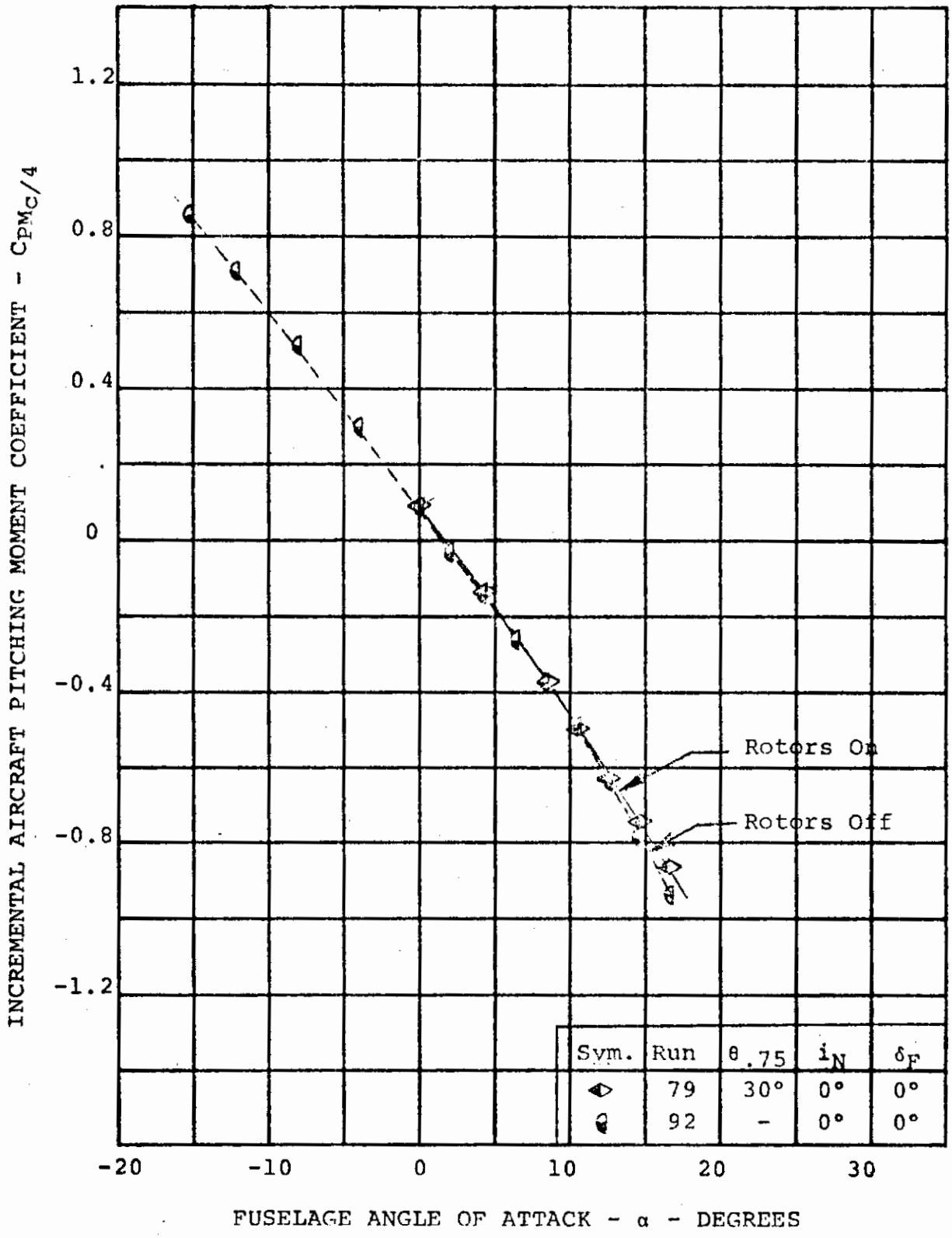

FIGURE 5.58 EFFECT OF ROTORS ON HORIZONTAL TAIL CONTRIBUTION TO AIRCRAFT PITCHING MOMENT

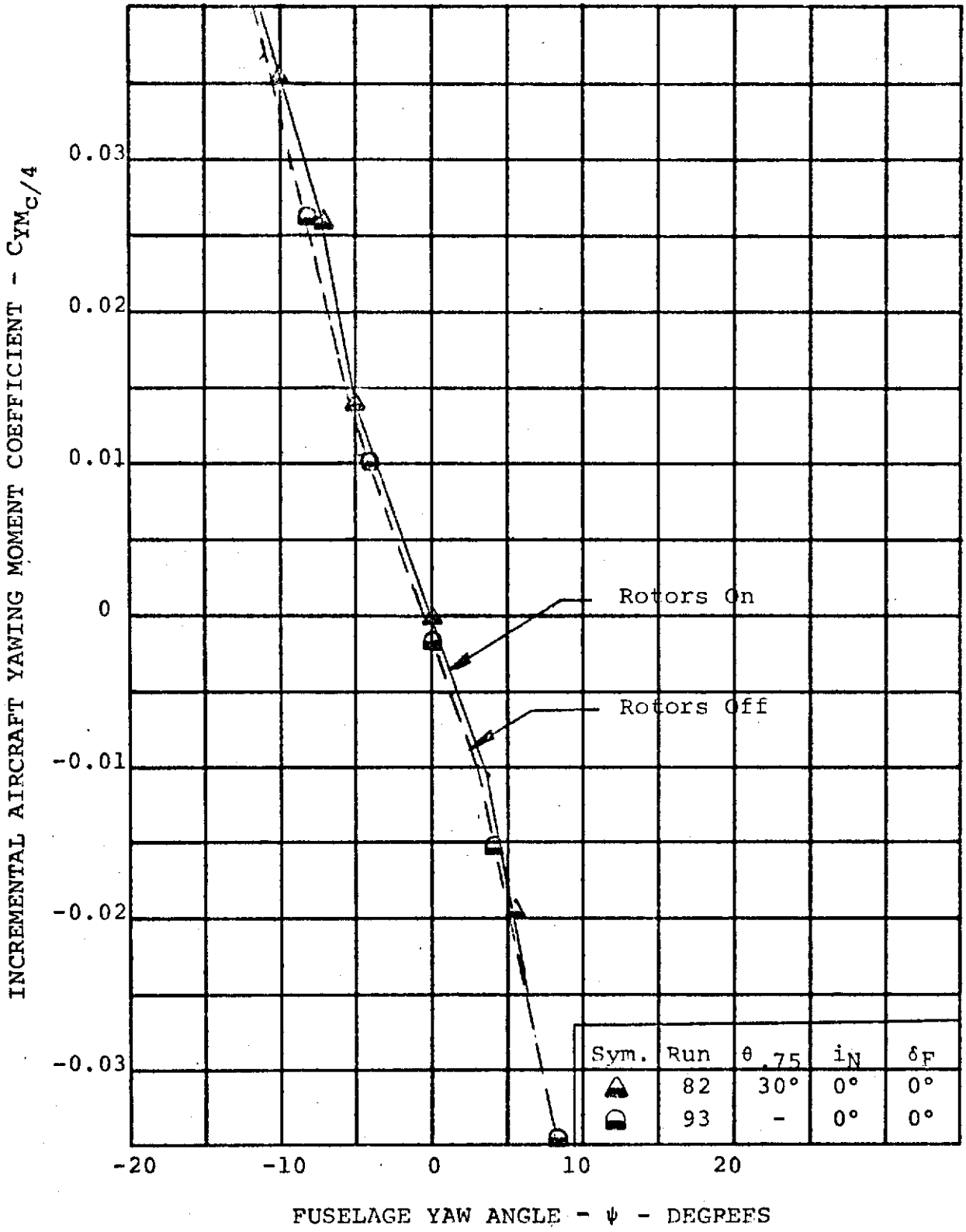

FIGURE 5-59: EFFECT OF ROTORS ON VERTICAL TAIL CONTRIBUTION TO AIRCRAFT YAWING MOMENT

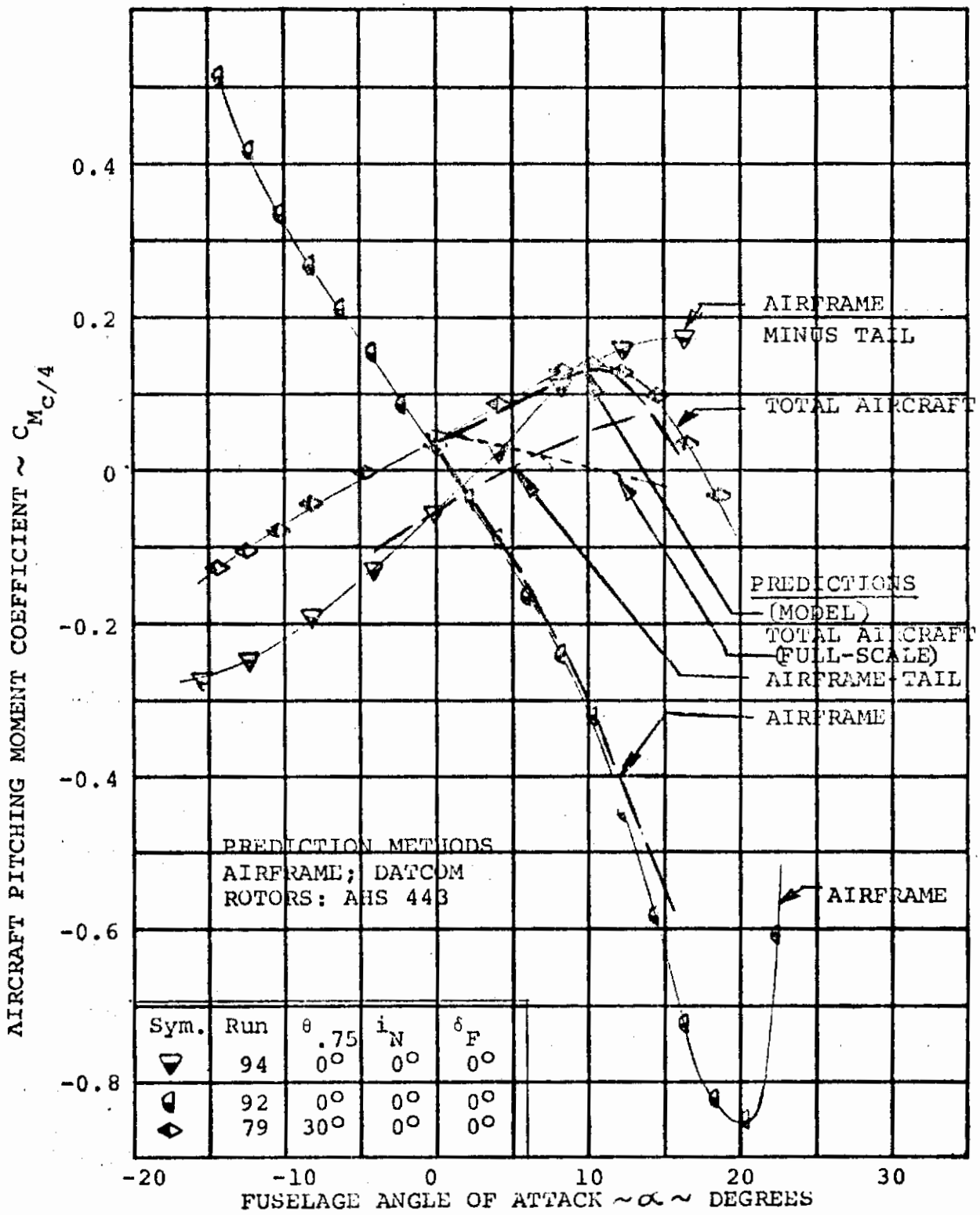

FIGURE 5.60. CONTRIBUTION OF PROP/ROTORS AND HORIZONTAL TAIL TO AIRCRAFT PITCHING MOMENT AT V/V_T = 0.386

The model nacelles are oversized to house the electric motors. Rotor characteristics for the model are such that they produce a larger destabilizing moment than would be expected from the full-scale rotor. A preliminary estimate of the increments in pitch stability associated with these two items is -0.003 per degree for the nacelles and -0.013 for the rotors. This indicates that the full-scale aircraft would have a total aircraft longitudinal stability derivative -0.016 per degree more stable than the test data. This is represented by the dotted line showing that the full scale aircraft is stable.

Figure 5.61 indicates the effects of addition of the tail and rotors on the aircraft side force coefficient. There is an increase in slope at approximately four degrees and negative seven degrees in the curve for airframe minus tail. This could be the result of flow reattachment on the aft end of the fuselage. When the vertical tail is added, the change in slope increases in the high yaw angle region indicating that the base of the tail is less separated and therefore produces less side force. The rotors provide an additional increase in slope of 0.0135 resulting from the variation of side force with yaw angle.

Yawing moment characteristics are illustrated in Figure 5.62. This figure shows the effect on yawing moment of the changes in side force mentioned above. Addition of the tail makes the aircraft stable and also makes the decreased slopes between 4 and minus 7 degrees very pronounced. This significant change in the stability increment of the tail confirms the flow reattachment and increased tail effectiveness suggested above. When the model rotors are added, the destabilizing contribution more than offsets the vertical tail contribution.

The same comments are applicable here, however, as for the longitudinal stability effects of the rotors. The contribution of the rotors to yawing moment of the full scale rotors will be significantly less because of the differences in rotor stiffness and frequencies in-plane and out-of-plane. Again, the magnitude of the difference will be such that the aircraft will be stable directionally with the rotors on.

Figure 5.63 indicates the contribution of the vertical tail and rotors to aircraft rolling moment in yaw. This figure indicates a change in slope at about 9 degrees negative yaw angle for airframe and airframe minus tail configurations in

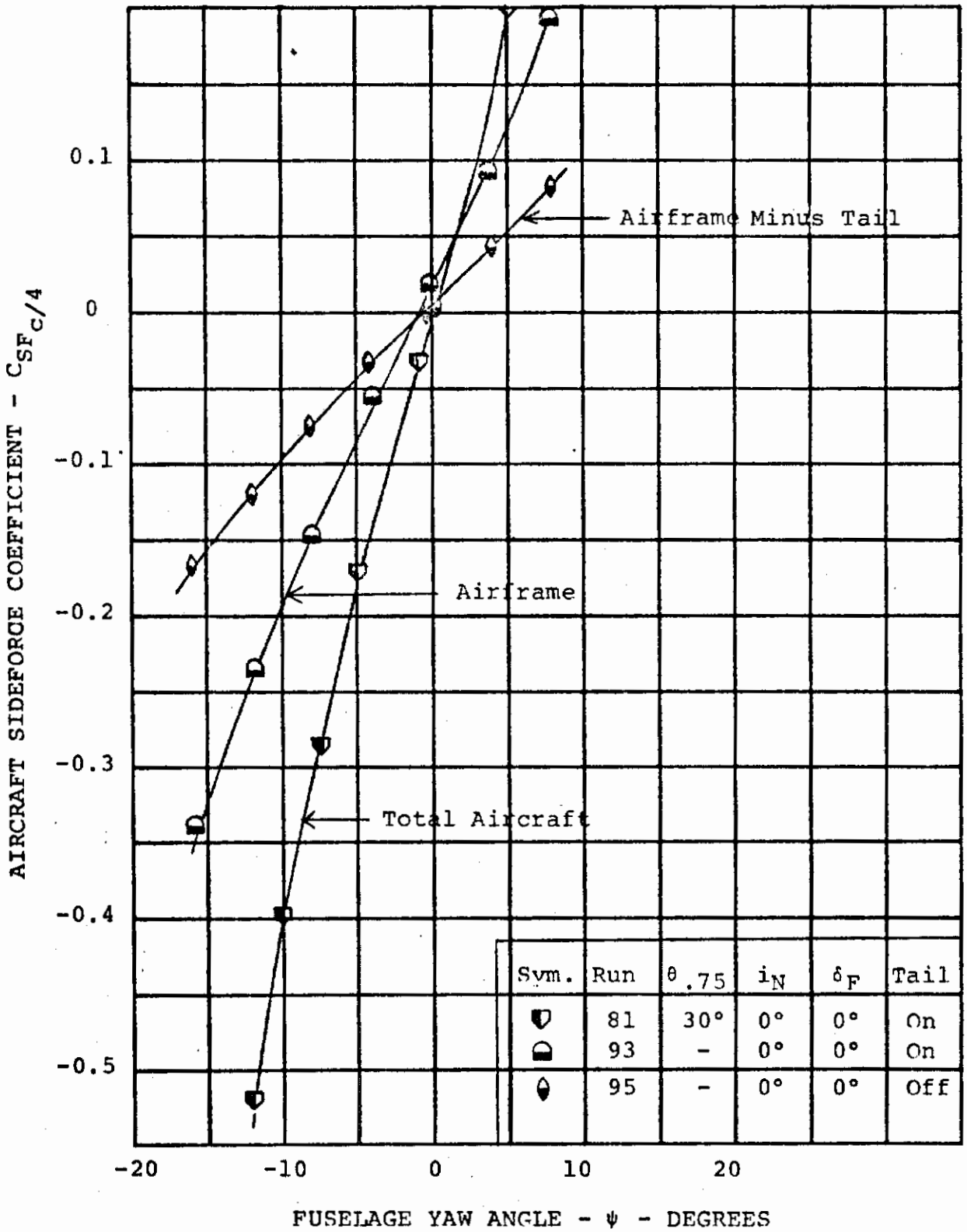

FIGURE 5.61. CONTRIBUTION OF PROP/ROTOR AND VERTICAL TAIL TO AIRCRAFT SIDE FORCE, $\delta_F = 0°$, $V/V_T = 0.382$

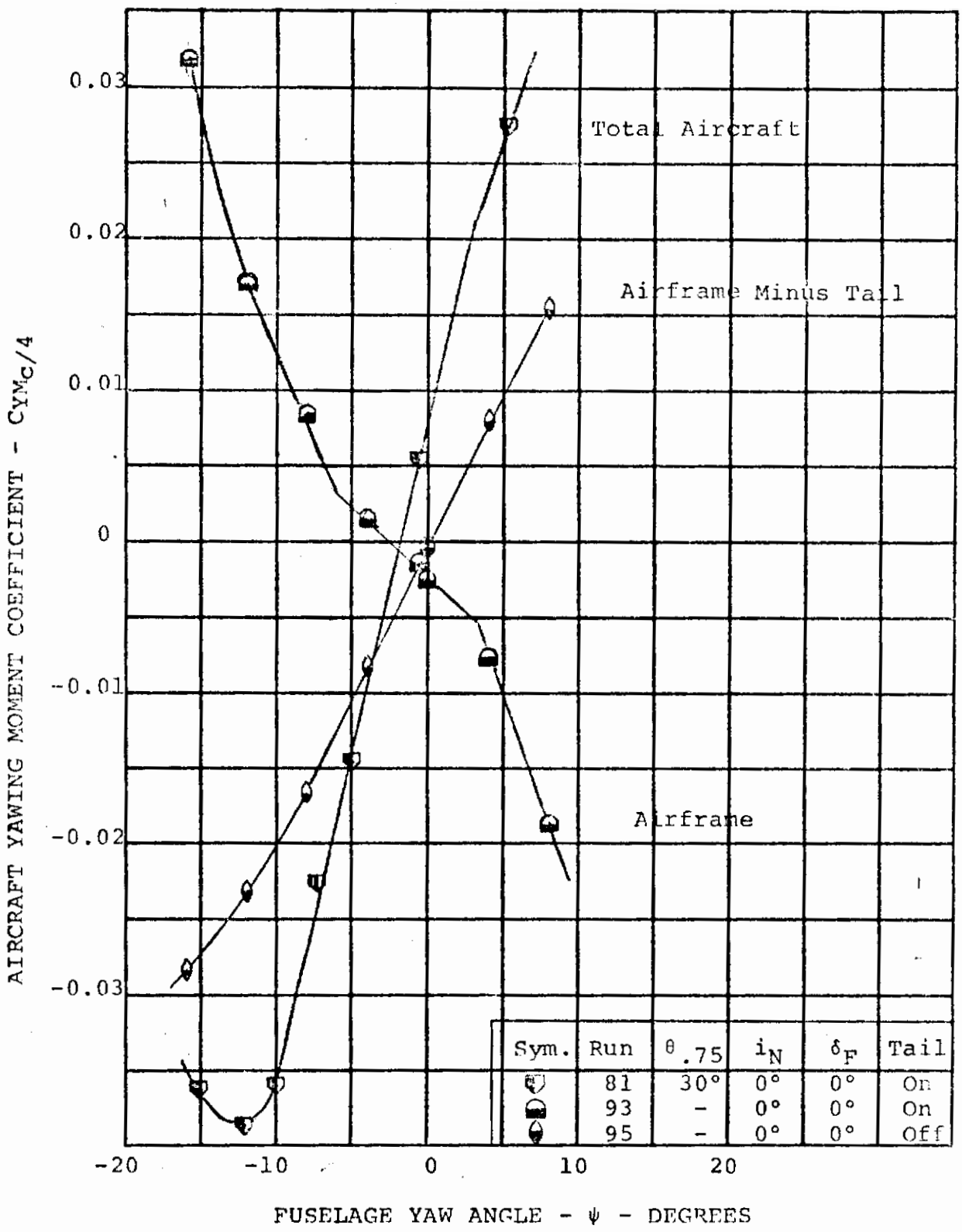

FIGURE 5.62. CONTRIBUTION OF PROP/ROTOR AND VERTICAL TAIL TO AIRCRAFT YAWING MOMENT, $\delta_F = 0$, $V/V_T = 0.382$

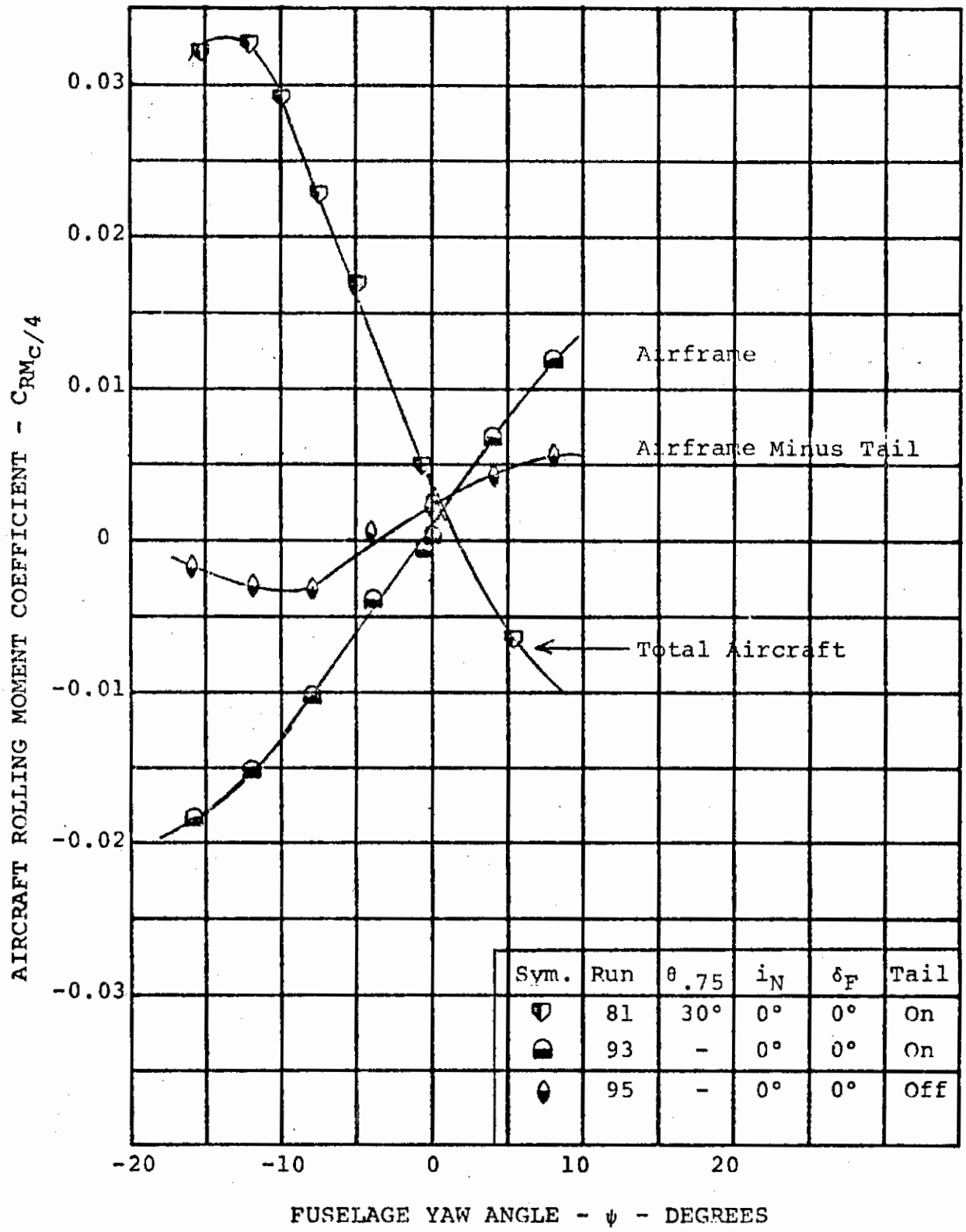

FIGURE 5.63. CONTRIBUTION OF PROP/ROTOR AND VERTICAL TAIL TO AIRCRAFT ROLLING MOMENT, $\delta_F = 0$, $V/V_T = 0.382$

the direction of decreased positive dihedral effect. It is believed that this was caused by reduction of lift just inboard of the nacelle on the leading wing. The nacelles tested on this model were quite large and slab-sided and the nacelles which will be used on the tilt/stowed rotor aircraft will be long and very slender in comparison. Thus, it is not anticipated that this slope change will be encountered on the airplane with the slimmer nacelles.

In addition, the test data for the model, with rotors on, indicates a reversal of slope, negative dihedral effect. The side force acting in the plane of the rotor disc is in the direction to increase the dihedral effect positively. Therefore, it would be anticipated that with the rotors on the aircraft should exhibit a larger positive dihedral effect. Again, the adverse effect of the large nacelles on lift, in sideslip, is believed to be accentuated with the rotors on and is responsible for the reversal in slope. Additional data is necessary to adequately define the effect of nacelle size and configuration on the dihedral effect of the tilt rotor aircraft.

The correlation between test and theory for the total aircraft has been presented for the 1/10 scale Tilt Rotor Model with stiff rotors based on test data from Reference 1.5. The correlation was good for both rotors and total aircraft. Also, the rotor derivative correlation was good between test and theory for the soft inplane rotor described in Section 5.4.2. Figure 5.64 illustrates the variation of tail lift coefficient versus airframe lift coefficient. Figure 5.65 shows that Model 213 is stable in pitch, as predicted earlier on Figure 5.60, and confirms again the tremendous impact of rotor flexibility and frequency placement on aircraft stability.

5.4.5 Control Effectiveness in Cruise - Tilt Rotor Mode

In the cruise configuration control will be provided primarily from the normal aircraft control surfaces, i.e. pitch control from the elevator or unit horizontal tail, roll control from ailerons, and yaw control from the rudder. For cruise mode operation with the rotors deployed, longitudinal cyclic, differential longitudinal cyclic and differential cyclic control could be used to supplement the normal aerodynamic controls until start of the feather operation. However, it is not anticipated that this will be required at speeds above those at which nacelle incidence is reduced to zero.

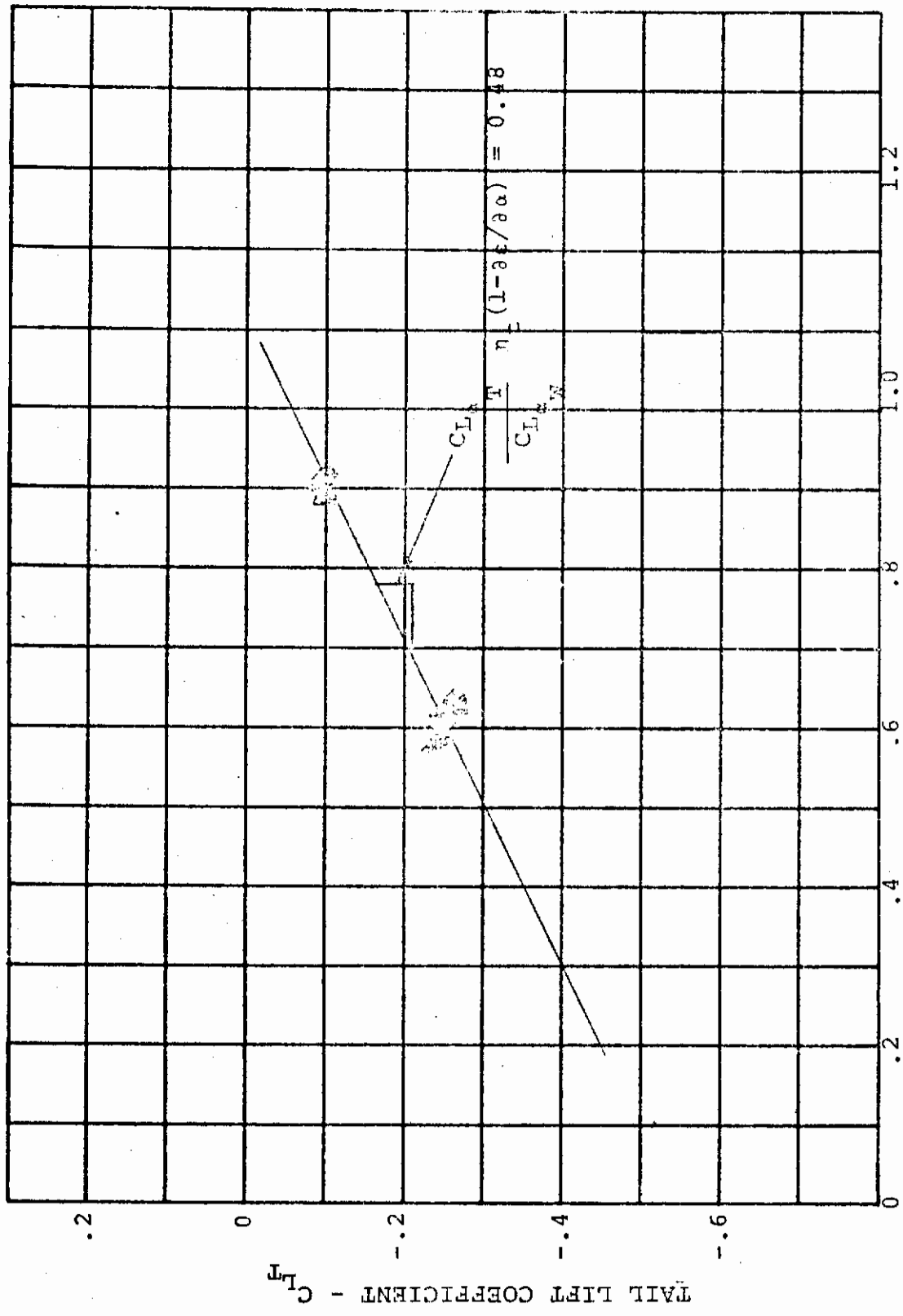

FIGURE 5.63 VARIATION OF TAIL LIFT WITH AIRFRAME LIFT DURING ANGLE OF ATTACK SWEEP FOR δ_F=30°, ROTOR STEADY WINDMILLING

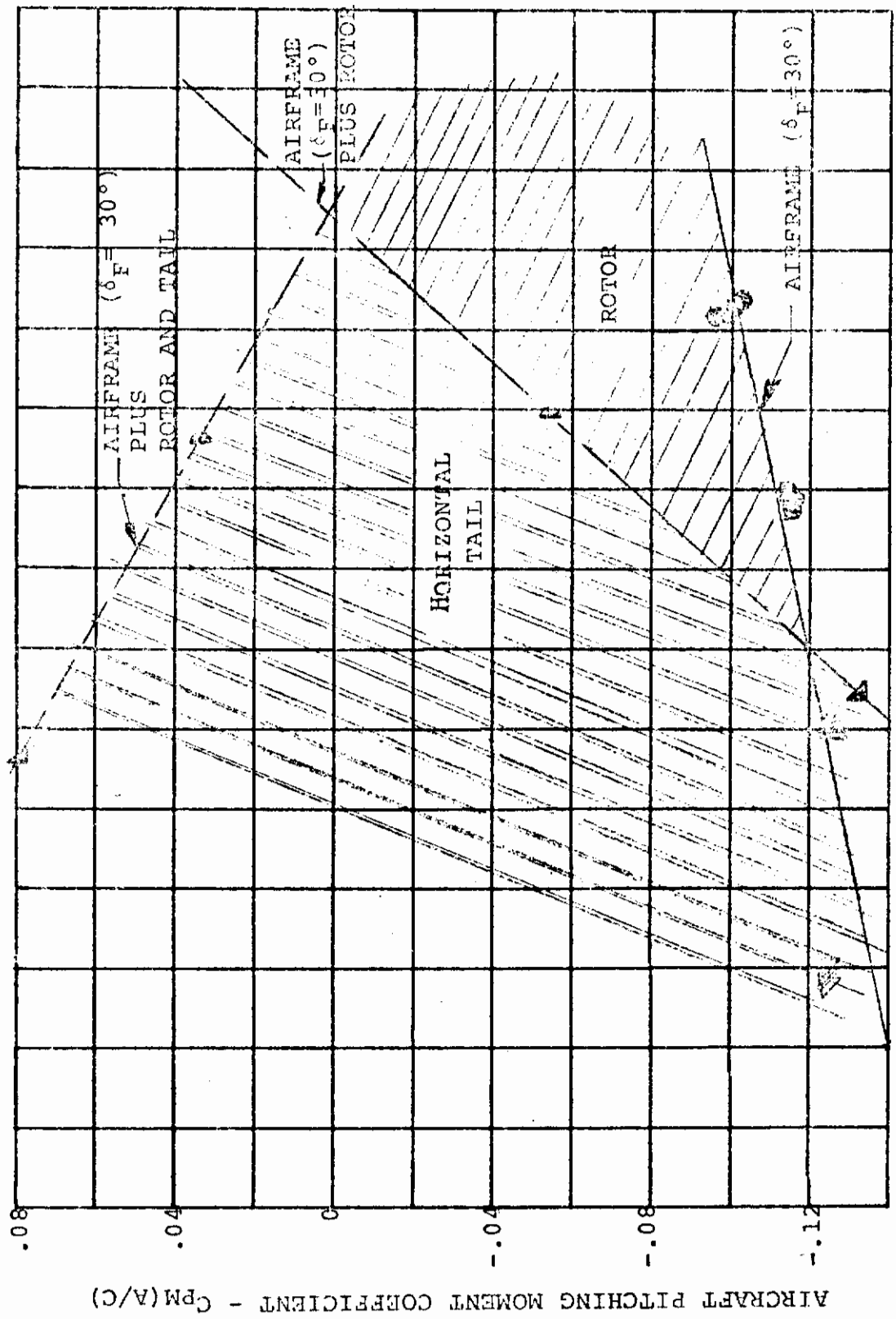

FIGURE 5.65 CONTRIBUTION OF PROP/ROTOR AND HORIZONTAL TAIL TO AIRCRAFT STABILITY FOR STEADY WINDMILLING δ_F = 30°

5.4.6 Gust Response

The requirements for the design of a rotor feedback system are discussed in Reference 5.8. Flight in the tilt rotor mode at speeds near maximum conversion speed in a gusty environment can (because of the large, relatively lightly loaded rotors) result in large aircraft accelerations which will cause a rough ride. In addition, high rotor loads and aircraft structural loads can result. These rotor and structural loads can be reduced substantially by the incorporation of a properly designed feedback system which would utilize rotor cyclic pitch and collective pitch control to reduce the aircraft and rotor responses to gusts.

Based on preliminary analyses, it is anticipated that cabin responses due to horizontal, lateral and vertical discrete (1-cosine) gusts up to 20 ft/sec amplitude will be less than the following values with the load alleviation system incorporated.

0.1 g's vertically
0.05 g's laterally
0.05 g's horizontally

5.5 CONVERSION

Conversion to and from rotor to fan-driven flight must be accomplished with minimum pilot effort and without discomfort which might result from excessive longitudinal accelerations or decelerations. Any "unusual" control switching or phasing must be accomplished automatically leaving the pilot free to operate the controls in a conventional manner to control speed, altitude, and aircraft attitude.

5.5.1 Spin-up, Feather, Fold and Deployment

The rotor contributions to aircraft stability characteristics during prop/rotor spinup and spindown were established based on the data available from Test Program III, Reference 1.6. The configuration to conversion had a zero degree fuselage angle-of-attack and a 30-degree flap setting, typical of a 200 knot conversion. The zero degree angle-of-attack condition was selected since it is the point at which the rotor contribution to lift (and pitching moment) is essentially zero. Therefore, it is expected that the change in aircraft lift and moment will be essentially zero over the range of

rpm's during spinup and spindown. The expected variations in lift and moment are substantiated by the data of Figures 5.66 and 5.67.

Rotor spinup and spindown will be accomplished with the aircraft in trim at 1.0g flight and control forces trimmed to zero. By performing the maneuver at zero degrees angle-of-attack, the net aerodynamic effects contributing to a control trim change are small as prop/rotor rpm is changed. There is a .020 change in aircraft pitching moment coefficient in the nose up direction as the rotor operating state is changed from steady windmilling to feather, Figure 5.68. As the rotors are folded at rates up to 3 seconds model scale, 9 seconds full scale, there is a -0.020 change in pitching moment coefficient, and an increase in aircraft stability with respect to the trim point. The magnitude of the stability change is a 15.4% shift in aircraft neutral point. The force feel system will be modified to compensate for the effect of changes in stability on maneuver control forces and since the trim change is small, there will be only a small effect on the conversion trim forces felt by the pilot. The requirement to modify the force feel system spring rate during the conversion maneuver does not represent an added degree of complexity. Boeing experience with tandem rotor helicopters indicates that modifications of the system as a function of airspeed to improve handling qualities between hover and cruise modes should be normal procedure and can be easily accomplished.

5.5.2 Control Scheduling

The process of bringing the rotor up to speed from the feathered condition or slowing down of the rotor from the windmilling condition is achieved by an exchange of energy between the airstream and rotor. This energy exchange results in a transient axial force, the magnitude of which is dependent on the schedule of collective blade pitch with time. Linear and parabolic collective pitch scheduling effect on the axial transient force were investigated in Test Program III with a target of holding the transient within 0.1g.

For Model 213 operating at 50,000 pounds gross weight, 0.1g translates into a transient rotor force of 2500 pounds per rotor, or 3.4 pounds for the model used in the test program. Considering the rotor spinup process, it was noted that the feathered rotor drag is 2.8 pounds (model scale) less than

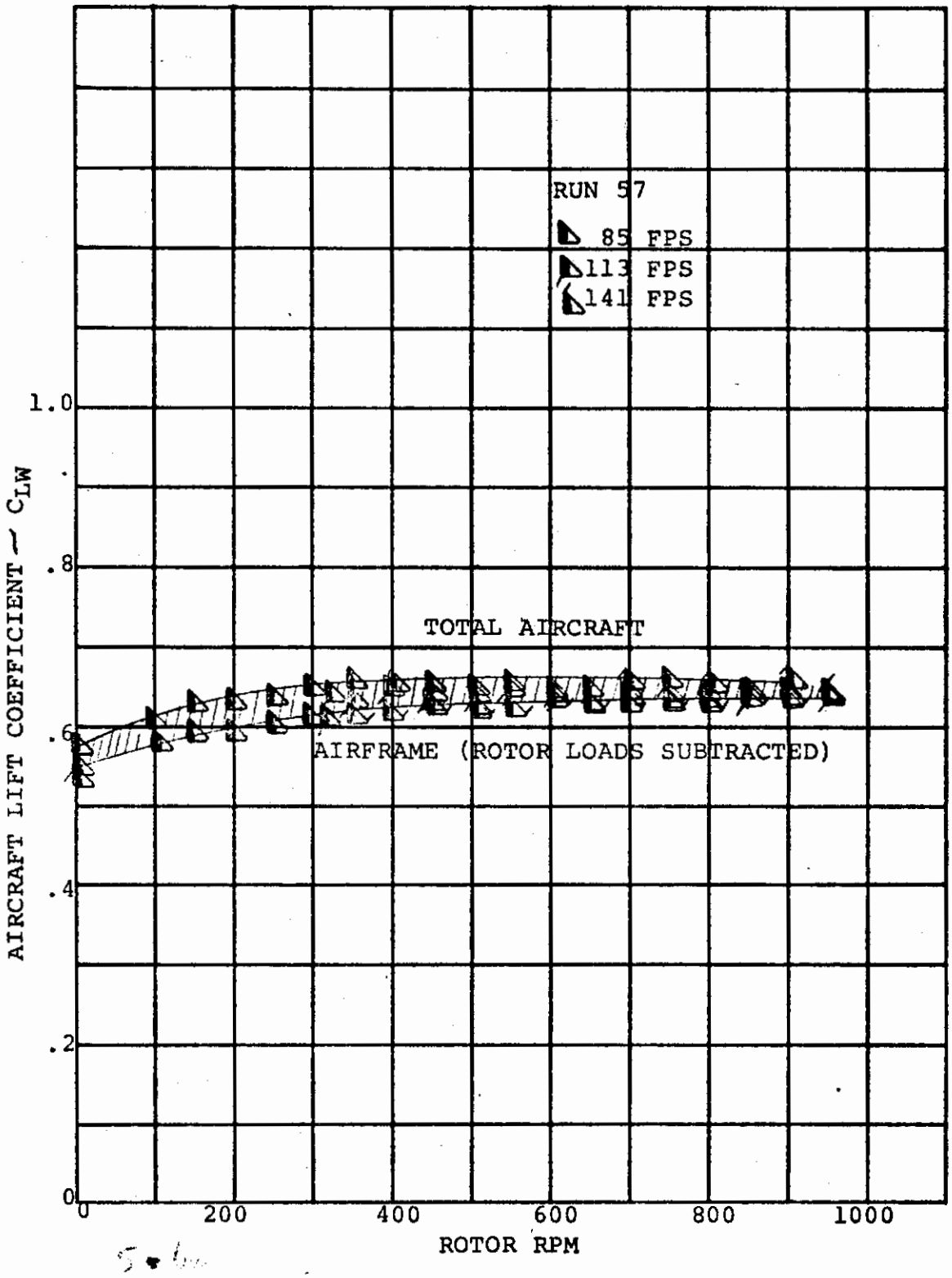

FIGURE 5.66. EFFECT OF ROTOR RPM AND FORWARD SPEED ON AIRCRAFT LIFT $\alpha=0°$ $\delta_F=30°$ (STEADY WINDMILLING)

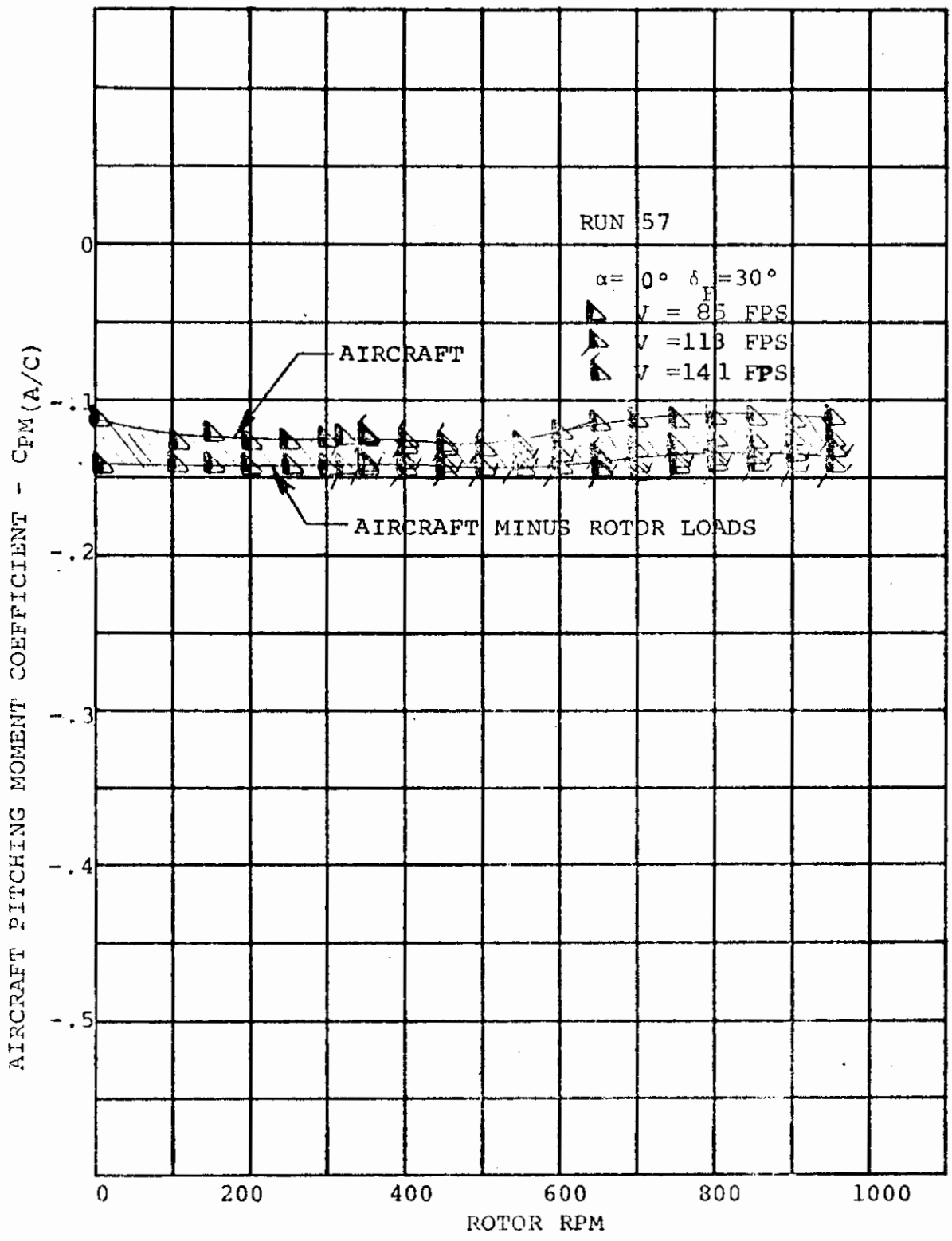

FIGURE 5.67. EFFECT OF ROTOR RPM AND FORWARD SPEED ON AIRCRAFT PITCHING MOMENT $\alpha=0°$ $\delta_F=30°$ (STEADY WINDMILLING)

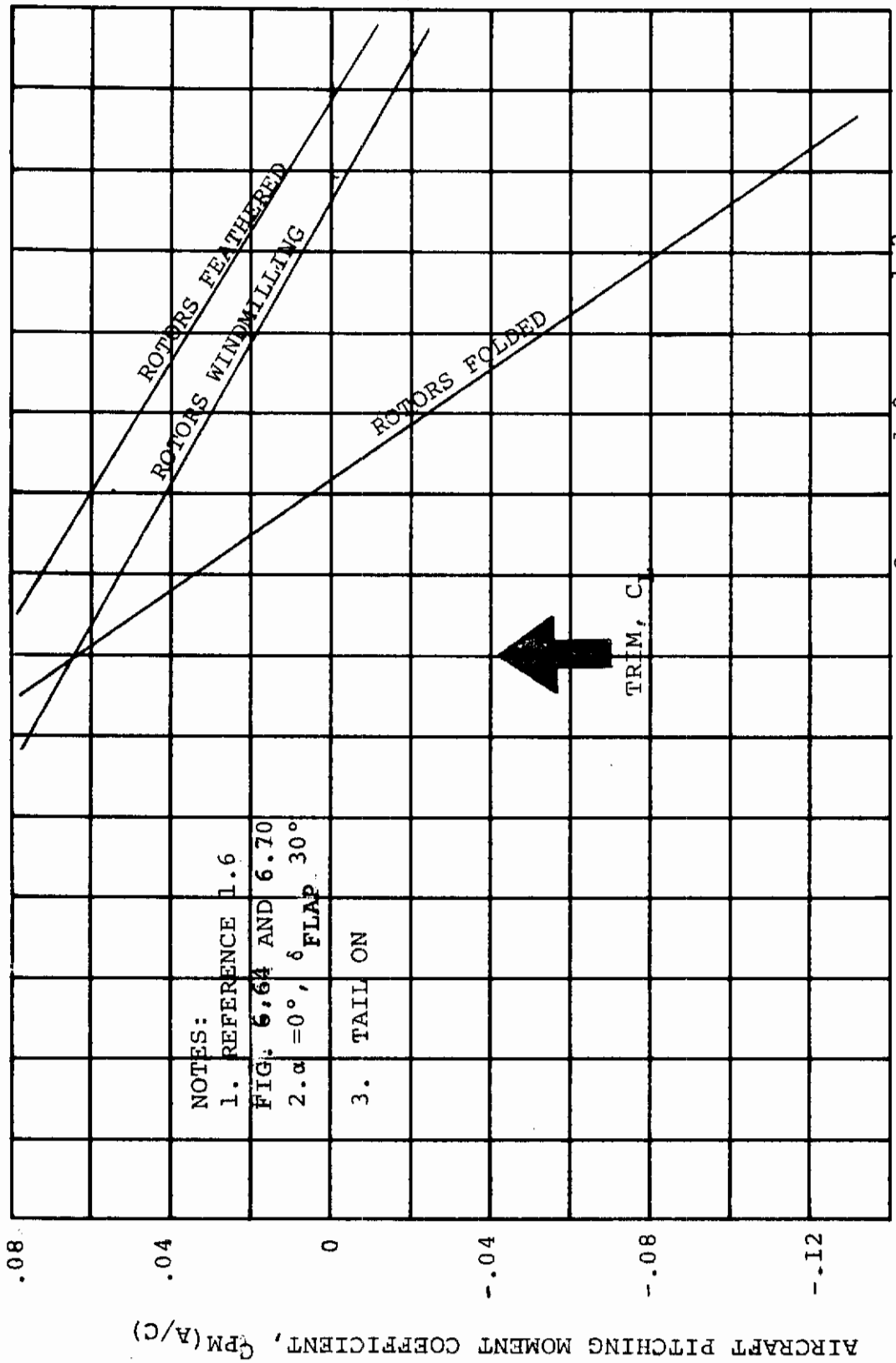

FIGURE 5.68: AIRCRAFT STABILITY DURING CONVERSION

the steady windmilling drag at the hover rpm of 1014 (338 rpm full scale). Thus, to meet the.1g target, either the transient peak must be kept down to 0.6 pound, or propulsive force must be added to balance the change in steady drag. Since the model used for the test was unpowered, it was not possible to investigate the use of fan thrust modulation to balance steady drag changes and the test program concentrated on minimizing the transient peaks.

Figure 5.69 shows that a linear schedule of approximately 10 seconds (30 seconds full scale) would be needed to meet the .1g target.

For spindown, Figure 5.70 shows that the .1g target can be met with a 10-second linear schedule (30-second full scale).

Tests in which the spinup and spindown cycles were started from 70% hover rpm, instead of 100% rpm (Figures 5.71 and 5.72), showed no difficulty in meeting the 0.1g target with 4-1/2 second linear schedule (13-1/2 second full scale) at 113 feet per second (200 knots full scale). On the full scale aircraft, simple thrust modulation of the convertible fan engines can be used to balance the change in steady trim drag between windmilling and feathered conditions thus permitting a feather and spinup from and to hover rpm in approximately 10 seconds for the full scale aircraft. It is therefore concluded that conversion can readily be completed without exceeding 0.1g longitudinal acceleration on the aircraft.

5.6 CRUISE REGIME - ROTORS STOWED

The configuration of the aircraft in cruise with the rotors stowed is very similar to that of several high wing cargo-type aircraft now operational and will have conventional flying characteristics. The anticipated flying characteristics in this configuration have been discussed previously in the Reference 1.3 report.

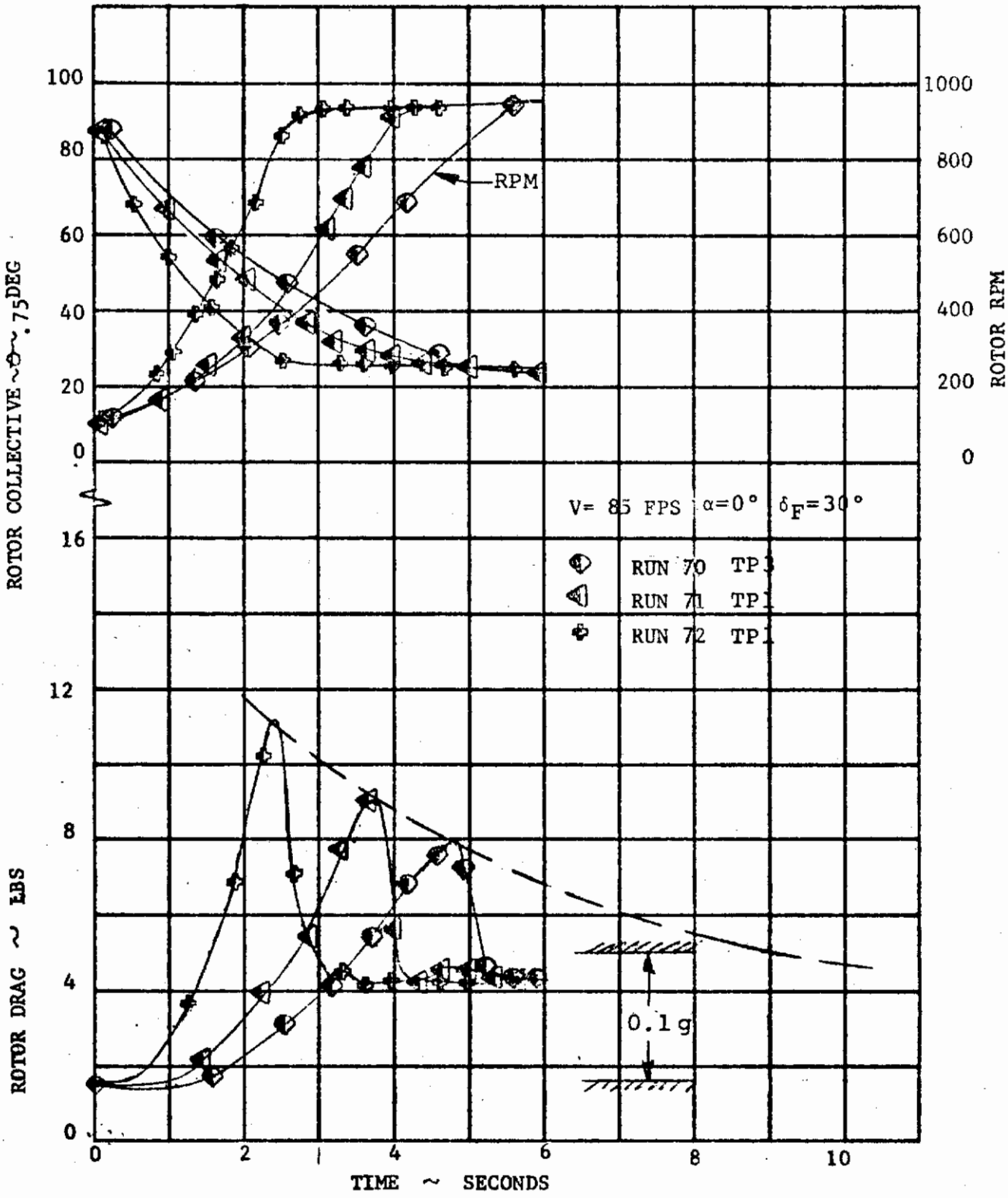

FIGURE 5.69: EFFECT OF COLLECTIVE SCHEDULING ON SPINUP RPM

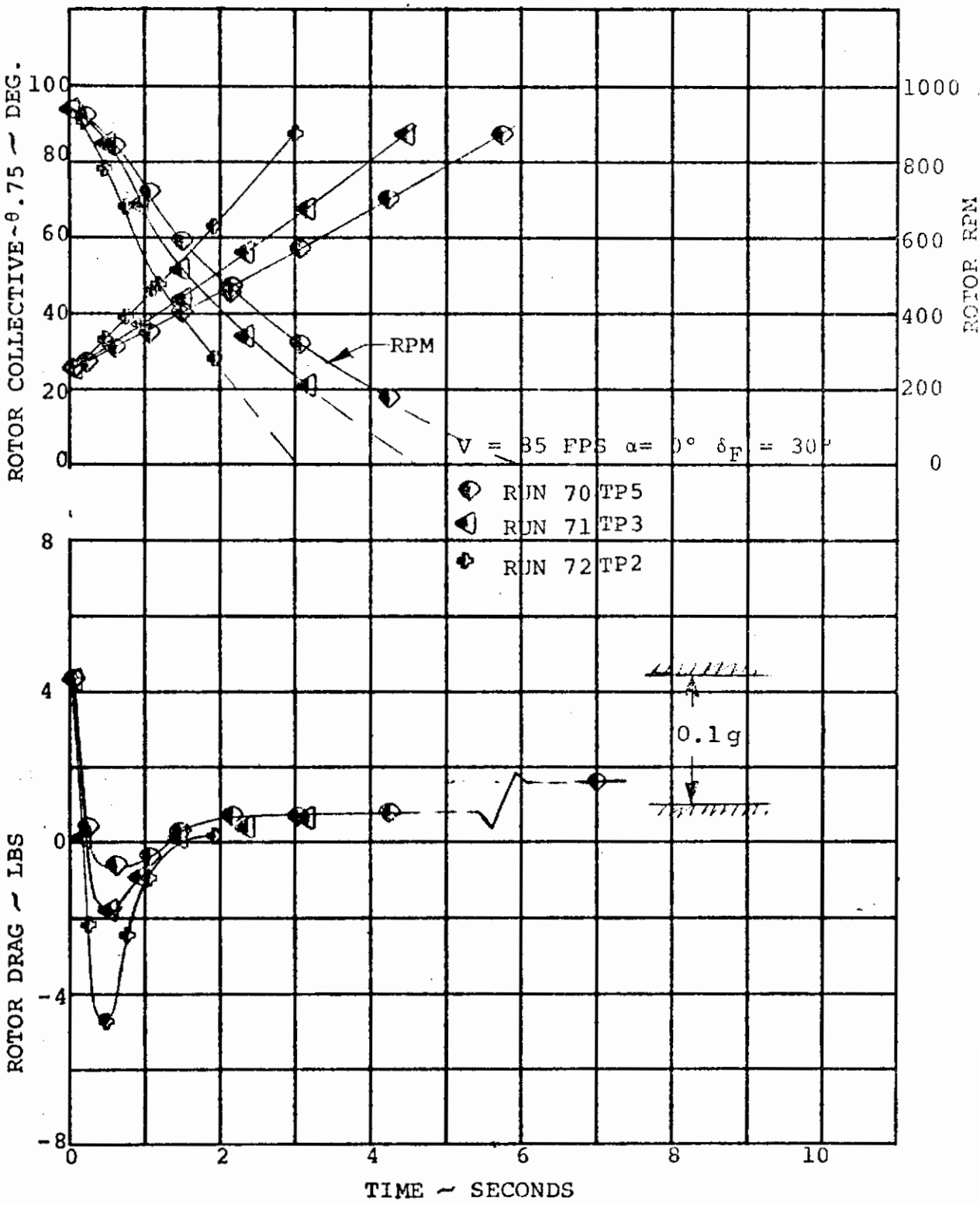

FIGURE 5.70. EFFECT OF COLLECTIVE RATE ON ROTOR DRAG DURING FEATHER AT V=85 FPS $\alpha=0°$ $\delta_F=30°$ (LINEAR COLLECTIVE RATE)

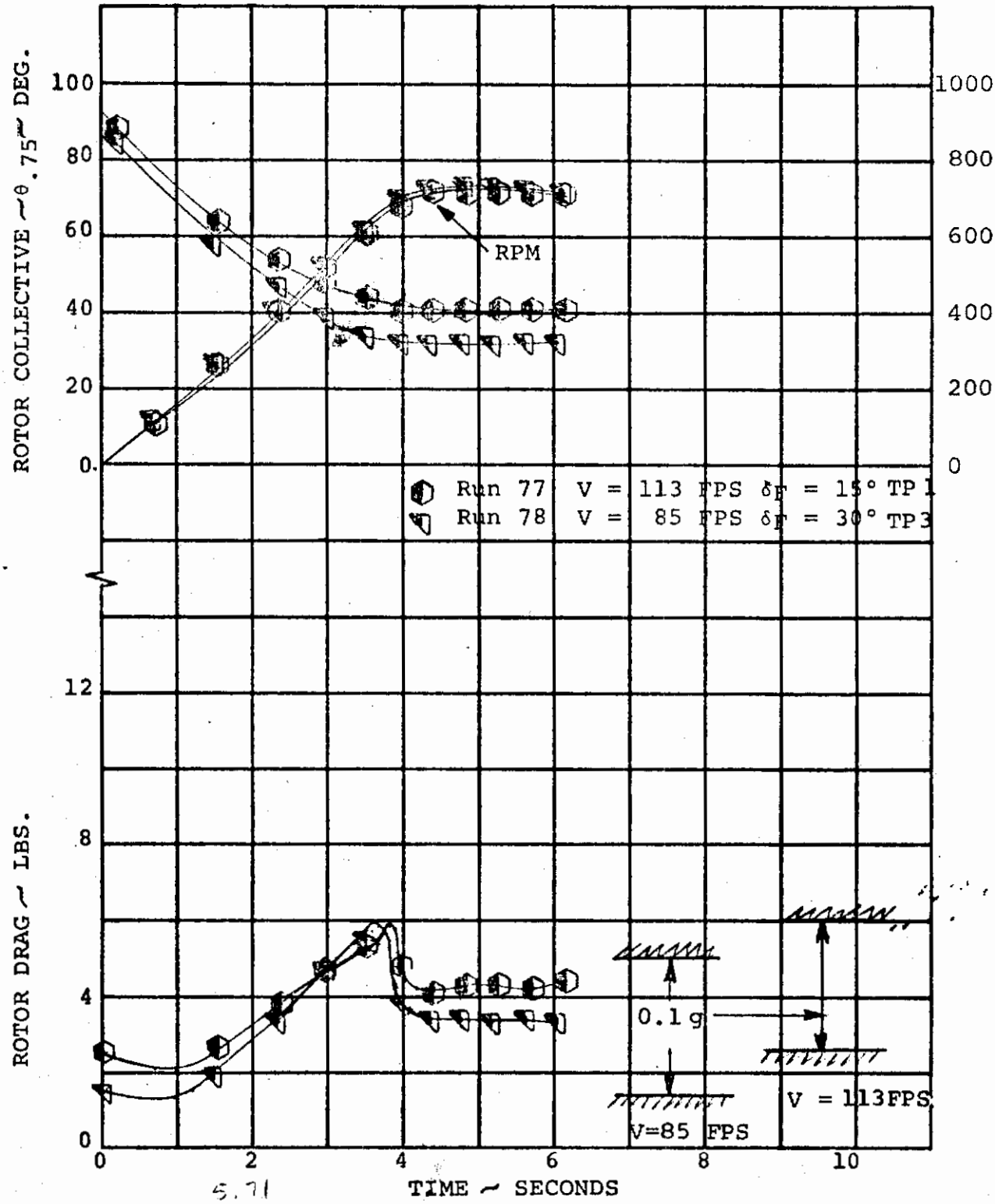

5.71

FIGURE 5.71. EFFECT OF FORWARD SPEED ON ROTOR DRAG DURING SPINUP FOR 4.5 SECOND LINEAR COLLECTIVE DATE, FINAL RPM = 715

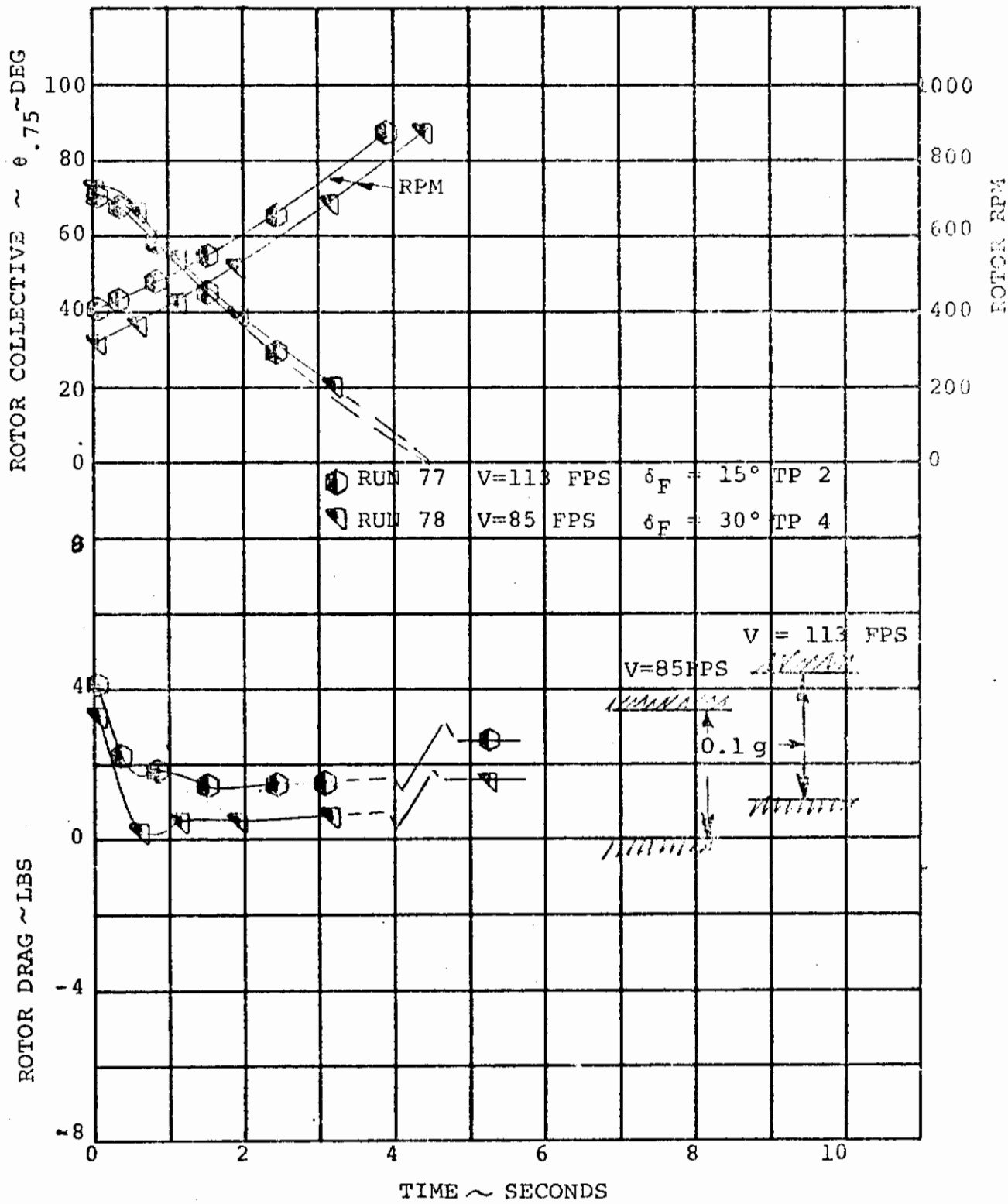

FIGURE 5.72. EFFECT OF FORWARD SPEED ON ROTOR DRAG DURING FEATHER FOR 4.5 LINEAR COLLECTIVE RATE, INITIAL RPM = 715

5.7 CONCLUSIONS

1. Skittishness in hover in-ground effect was investigated and found by a dynamic model test. It was readily stabilized by attitude stabilization.

2. Spinup, feather, fold and deploy cycles cause no stability or control problems.

3. In the tilt rotor cruise mode the soft inplane rotor has substantially less destabilizing effect than a stiff inplane rotor.

5.8 RECOMMENDATIONS

1. Additional testing is desired with a rigidly mounted dynamic rotor in transition to provide additional data for correlation and analysis development for rotor derivatives of the soft inplane rotor.

2. The total flight control system needs further study particularly in the following areas:

   a. Feedback controls for gust alleviation and blade load reduction

   b. Flight simulation

   c. System mechanization

REFERENCES

1.1 DESIGN STUDIES AND MODEL TESTS OF THE STOWED TILT ROTOR CONCEPT, VOLUME 1, PARAMETRIC DESIGN STUDIES, Fry, B.L., AFFDL-TR-71-62, Vol. I, July 1971.

1.2 DESIGN STUDIES AND MODEL TESTS OF THE STOWED TILT ROTOR CONCEPT, VOLUME II, COMPONENT DESIGN STUDIES, Fry, B.L., AFFDL-TR-71-62, Vol. II, July 1971.

1.3 DESIGN STUDIES AND MODEL TESTS OF THE STOWED TILT ROTOR CONCEPT, VOLUME III, APPENDICES, Fry, B.L., AFFDL-TR-71-62, Vol. III, July 1971.

1.4 WIND TUNNEL TEST OF THE CONVERSION PROCESS OF A FOLDING TILT ROTOR AIRCRAFT USING A SEMISPAN UNPOWERED MODEL, Magee, J.P. and Taylor, R.B., AFFDL-TR-71-62, Vol. IV, Parts I and II, Aug. 1971.

1.5 WIND TUNNEL TEST OF A POWERED TILT ROTOR PERFORMANCE MODEL, Magee, J.P., Taylor, R.B., McHugh, F.J., et al, AFFDL-TR-71-62, Vol. V, Aug. 1971.

1.6 WIND TUNNEL TEST OF THE DYNAMICS AND AERODYNAMICS OF ROTOR SPINUP, STOPPING AND FOLDING ON A SEMISPAN FOLDING TILT ROTOR MODEL, VanWagensveld, D., McHugh, F.J., DeLarm, L., et al, AFFDL-TR-71-62, Vol. VII, Aug. 1971.

1.7 WIND TUNNEL TEST OF A POWERED TILT ROTOR DYNAMIC MODEL ON A SIMULATED FREE FLIGHT SUSPENSION SYSTEM, Tomassoni, J.E., Taylor, R.B., DeLarm, L., et al, AFFDL-TR-71-62, Vol. VI, August 1971.

3.1 THE BENDING VIBRATIONS OF A TWISTED ROTATING BEAM, Targoff, W., WADC Technical Report 56-27, 1956.

3.2 INVESTIGATION OF THE PERFORMANCE OF LOW DISC LOADING TILT ROTORS IN HOVERING AND CRUISE FLIGHT, VOLUMES I AND II, Boeing Report D160-10013-1, 2, March 1971.

3.3 USER REPORT: PROP/ROTOR DYNAMIC DERIVATIVE PROGRAM C-41, Boeing Document D210-10116-1, June 1970.

4.1 ANALYSIS OF PROPELLER AND ROTOR PERFORMANCE IN STATIC AND AXIAL FLIGHT BY AN EXPLICIT VORTEX INFLUENCE TECHNIQUE, Boeing Report R-372, December 1967.

4.2 AIRFOIL CHARACTERISTICS FOR ROTOR PERFORMANCE CALCULATIONS, Boeing Document D8-0377, December 1966.

4.3 SUMMARY OF UNIVERSAL HELICOPTER MODEL WIND TUNNEL TEST RESULTS, Boeing Document D210-10077, November 1968.

4.4 A SIMPLE ANALYSIS TO COMPUTE TRANSIENT WINDMILLING PROP/ ROTOR PERFORMANCE, Boeing Reference 8-7445-2-167, July 1971.

4.5 ROTOR AIRLOADS AND PERFORMANCE ANALYSIS WITH NON-UNIFORM INDUCED INFLOW (COMPUTER PROGRAM B-67), Boeing Document D8-0312, December 1967.

4.6 USAF STABILITY AND CONTROL DATCOM, Ellison, D.E. and Malthan, L.V., Air Force Flight Dynamics Laboratory Publication.

4.7 THE PREDICTION OF STABILITY DERIVATIVES OF LARGE FLEXIBLE PROP/ROTORS BY A SIMPLIFIED ANALYSIS, Magee, J.P. and Pruyn, R.R., AHS Preprint 443, June 1970.

5.1 FLYING QUALITIES OF PILOTED V/STOL AIRCRAFT, Military Specification MIL-F-83300, December 1970.

5.2 A STABILITY AND CONTROL PREDICTION METHOD FOR HELICOPTERS AND STOPPABLE ROTOR AIRCRAFT, AFFDL-TR-69-123, VOLUMES I, II, III, IV, March 1970.

5.3 TEST RESULTS OF GROUND/AIR MECHANICAL STABILITY AND WIND TUNNEL TEST OF THE FULL-SPAN 1/10 SCALE POWERED DYNAMIC MODEL OF THE M-160 TILT ROTOR AIRCRAFT, Bean, N., Boeing Document D160-10012-1, January 1971.

5.4 WIND TUNNEL TESTS OF A POWERED AERODYNAMIC 1/10 SCALE MODEL OF THE MODEL 160 TILT ROTOR AIRCRAFT IN THE HOVER, TRANSITION AND CRUISE MODES, Taylor, R.B., and Soule, V., Boeing Document D160-10014-1, February 1971.

5.5 DYNAMICS OF FLIGHT-STABILITY AND CONTROL, Etkin, B., Wiley, 1959.

5.6 HELICOPTER FLYING AND GROUND HANDLING QUALITIES, Military Specification MIL-H-8501A, April 1962.

5.7 AIRWORTHINESS CONSIDERATIONS FOR STOL AIRCRAFT, NASA TND-5594.

5.8 CONFIGURATION DESIGN ANALYSIS OF A PROP/ROTOR AIRCRAFT, Richardson, D.A., and Liiva, J., AFFDL-TR-70-44, April 1970.

UNCLASSIFIED

Security Classification

DOCUMENT CONTROL DATA - R&D

(Security classification of title, body of abstract and indexing annotation must be entered when the overall report is classified)

1. ORIGINATING ACTIVITY (Corporate author)
The Boeing Company, Vertol Division
Boeing Center, P.O. Box 16858
Philadelphia, Pa. 19142

2a. REPORT SECURITY CLASSIFICATION
Unclassified

2b. GROUP

3. REPORT TITLE
DESIGN STUDIES AND MODEL TESTS OF THE STOWED TILT ROTOR CONCEPT
(Volume VIII - Summary of Structural Design Criteria and Aeronautic Prediction Techniques)

4. DESCRIPTIVE NOTES (Type of report and inclusive dates)
Final Report, December 1970 to July 1971

5. AUTHOR(S) (Last name, first name, initial)
Robin W. Sandford
Francis J. McHugh
Leon N. Delarm
Edward B. Schagrin
John P. Magee

6. REPORT DATE
October 1971

7a. TOTAL NO. OF PAGES
276

7b. NO. OF REFS
25

8a. CONTRACT OR GRANT NO.
F33615-69-C-1577

b. PROJECT NO.

c.

d.

9a. ORIGINATOR'S REPORT NUMBER(S)
D213-10000-8

9b. OTHER REPORT NO(S) (Any other numbers that may be assigned this report)
AFFDL-TR-71-62, Volume VIII

10. AVAILABILITY/LIMITATION NOTICES
Approved for Public Release - Distribution Unlimited

11. SUPPLEMENTARY NOTES

12. SPONSORING MILITARY ACTIVITY
Air Force Flight Dynamics Laboratory
Air Force Systems Command
Wright-Patterson Air Force Base, Ohio

13. ABSTRACT

This report presents a summary of the technical data from four wind tunnel tests on tilt and stowed rotor performance and fully dynamic models. Blade loads, dynamic stability, performance, rotor/wing interactions, and stability and control data are presented. The impact of the tests on stowed rotor aircraft design are discussed and recommendations for further technical and design work are provided.

DD FORM 1 JAN 64 1473

UNCLASSIFIED

Security Classification

UNCLASSIFIED
Security Classification

14. KEY WORDS	LINK A		LINK B		LINK C	
	ROLE	WT	ROLE	WT	ROLE	WT
Aircraft Stowed Rotor Tilt Rotor Prop/Rotor Performance Prop/Rotor Stability and Control Prop/Rotor Blade Loads Prop/Rotor Dynamic Stability Prop/Rotor Structural Criteria Transition Conversion						

INSTRUCTIONS

1. ORIGINATING ACTIVITY: Enter the name and address of the contractor, subcontractor, grantee, Department of Defense activity or other organization *(corporate author)* issuing the report.

2a. REPORT SECURITY CLASSIFICATION: Enter the overall security classification of the report. Indicate whether "Restricted Data" is included. Marking is to be in accordance with appropriate security regulations.

2b. GROUP: Automatic downgrading is specified in DoD Directive 5200.10 and Armed Forces Industrial Manual. Enter the group number. Also, when applicable, show that optional markings have been used for Group 3 and Group 4 as authorized.

3. REPORT TITLE: Enter the complete report title in all capital letters. Titles in all cases should be unclassified. If a meaningful title cannot be selected without classification, show title classification in all capitals in parenthesis immediately following the title.

4. DESCRIPTIVE NOTES: If appropriate, enter the type of report, e.g., interim, progress, summary, annual, or final. Give the inclusive dates when a specific reporting period is covered.

5. AUTHOR(S): Enter the name(s) of author(s) as shown on or in the report. Enter last name, first name, middle initial. If military, show rank and branch of service. The name of the principal author is an absolute minimum requirement.

6. REPORT DATE: Enter the date of the report as day, month, year, or month, year. If more than one date appears on the report, use date of publication.

7a. TOTAL NUMBER OF PAGES: The total page count should follow normal pagination procedures, i.e., enter the number of pages containing information.

7b. NUMBER OF REFERENCES: Enter the total number of references cited in the report.

8a. CONTRACT OR GRANT NUMBER: If appropriate, enter the applicable number of the contract or grant under which the report was written.

8b, 8c, & 8d. PROJECT NUMBER: Enter the appropriate military department identification, such as project number, subproject number, system numbers, task number, etc.

9a. ORIGINATOR'S REPORT NUMBER(S): Enter the official report number by which the document will be identified and controlled by the originating activity. This number must be unique to this report.

9b. OTHER REPORT NUMBER(S): If the report has been assigned any other report numbers *(either by the originator or by the sponsor)*, also enter this number(s).

10. AVAILABILITY/LIMITATION NOTICES: Enter any limitations on further dissemination of the report, other than those imposed by security classification, using standard statements such as:

(1) "Qualified requesters may obtain copies of this report from DDC."

(2) "Foreign announcement and dissemination of this report by DDC is not authorized."

(3) "U. S. Government agencies may obtain copies of this report directly from DDC. Other qualified DDC users shall request through _____."

(4) "U. S. military agencies may obtain copies of this report directly from DDC. Other qualified users shall request through _____."

(5) "All distribution of this report is controlled. Qualified DDC users shall request through _____."

If the report has been furnished to the Office of Technical Services, Department of Commerce, for sale to the public, indicate this fact and enter the price, if known.

11. SUPPLEMENTARY NOTES: Use for additional explanatory notes.

12. SPONSORING MILITARY ACTIVITY: Enter the name of the departmental project office or laboratory sponsoring *(paying for)* the research and development. Include address.

13. ABSTRACT: Enter an abstract giving a brief and factual summary of the document indicative of the report, even though it may also appear elsewhere in the body of the technical report. If additional space is required, a continuation sheet shall be attached.

It is highly desirable that the abstract of classified reports be unclassified. Each paragraph of the abstract shall end with an indication of the military security classification of the information in the paragraph, represented as *(TS)*, *(S)*, *(C)*, or *(U)*.

There is no limitation on the length of the abstract. However, the suggested length is from 150 to 225 words.

14. KEY WORDS: Key words are technically meaningful terms or short phrases that characterize a report and may be used as index entries for cataloging the report. Key words must be selected so that no security classification is required. Identifiers, such as equipment model designation, trade name, military project code name, geographic location, may be used as key words but will be followed by an indication of technical context. The assignment of links, rules, and weights is optional.

UNCLASSIFIED
Security Classification